Faculty of Science
Department of Applied Physics

INFLUENCE OF AGGREGATE ON THE MICROSTRUCTURE OF GEOPOLYMER

Subaer

This thesis is presented for the Degree of
Doctor of Philosophy
of
Curtin University of Technology

June 2004

Declaration

This thesis contains no material which has been accepted for the award of any other degree or diploma in any university.

To the best of my knowledge and belief this thesis contains no material previously published by any other person except where due acknowledgment has been made.

Signature: ...

Date: 25/6/04

To my parents,

ACKNOWLEDGMENTS

The work presented in this thesis was carried out under the supervision of Professor Arie van Riessen. To him I extend my deepest sense of gratitude for his perseverance and continual encouragement, guidance and suggestions throughout the progress of this work.

I also extend my special thank to my associate supervisors, Emeritus Professor Brian O'Connor and Associate Professor Craig Buckley for their encouragement, support and valuable suggestions. I am also thankful to Dr. Rob Hart for sharing his expertise and for his patience in teaching me how to operate the transmission electron microscope (TEM). Thanks to Mrs Elaine Miller for her constant help with scanning electron microscopy (SEM). Thanks also to Dr. Peter Self of The University of Adelaide, South Australia for helping with Micro-CT.

I would like to express my indebtedness to Mr Glen Lawson, Mr Geoff Carter and Mr Ashley Barker for their friendly and useful help in experimental work and technical assistance throughout the course of this study. Thanks to the Centre for Microscopy and Microanalysis at the University of Western Australia for allowing me to use their facilities in preparing TEM samples. Thanks also to Mrs Carmel McManus for her assistance in various administration tasks.

Further acknowledgments are due to my colleagues Matthew Rowles, Dr. Nigel Kirby, Hamzah Fansuri, Dr. Suminar Pratapa, Djwantoro Hardjito, Muhammad Syamsu Rosid, Irfan Syamsuddin for their friendly assistance in various ways during the course of this study.

Thanks also to all my friends that have made my stay in Australia once more a memorable and valuable experience. To list their names would make this acknowledgment unacceptably long.

My heartfelt gratitude goes to my wife Rachmatiah and my children for their understanding, patience and constant prayers for the success of my study, and to my parents for their encouragement and prayers back home.

Finally, I would like to thank the Australian Development Scholarship-AusAID for granting the scholarship award, which has allowed me to pursue a higher degree at Curtin University of Technology, Perth, Western Australia. Special thanks goes to AusAID liaison officer, Mrs Deborah Pyatt, for her understanding and help in the completion of my study.

ABSTRACT

Inorganic geopolymers or simply geopolymers based on silico-aluminate are relatively novel materials with a wide range of potential applications. The main purpose of the present study was to experimentally investigate the composition-microstructure-property relationship of these new materials. These must be understood in order to optimise the performance of geopolymers.

Geopolymers with different chemical compositions (Si:Al and Na:Al atomic ratios) were prepared by thermally assisted alkali-activation of metakaolinite at 70 °C. Metakaolinite was obtained by dehydroxylation of kaolinite at 750 °C for 6 hours. Measurements indicated that the compositions of geopolymers influence the microstructural character as well as the physical and mechanical properties of these materials. Geopolymers prepared with an atomic ratio of Si:Al = 1.04 and 1.25 are categorised as sodium-poly(sialate) (Na-PS) geopolymers. These materials were found to be composed of zeolite-A or zeolite-X in conjunction with amorphous geopolymer. These materials are relatively soft, with low density and high apparent porosity, and have low hardness and compressive strength.

Geopolymers prepared with an atomic ratio of Si:Al = 1.50, 1.75 and 2.00 are categorised as sodium-poly(sialate-siloxo) (Na-PSS) geopolymers. The structure of these geopolymers is amorphous as observed by X-ray diffraction (XRD) with no evidence of zeolite formation. A broad amorphous hump in the X-ray diffraction patterns suggests that the Na-PSS geopolymers consist of disordered frameworks with short-range order.

The thermal analysis of Na-PSS by means of thermogravitmetric-differential thermal analysis (TG-DTA) revealed that about 15 % of the initial reaction water remains in the geopolymer framework. The DTA curves for Na-PSS show a single endothermic peak around 135 °C due to water evolution. Na-PSS geopolymers exhibit substantial shrinkage and cracking after heating up to 950 °C. Geopolymers with aggregate also suffer extensive cracking due to heating although the shrinkage was less than that of geopolymers without aggregate.

Dilatometer results show that geopolymer pastes shrink about 2% below 300 °C and remain dimensionally stable up to 800 °C. The coefficient of thermal expansion of geopolymers is comparable to that of Portland cement paste. The presence of aggregate was found to reduce the shrinkage of geopolymer by 50%. Quartz aggregate, however, limits the useful working temperature range of geopolymers to below 500 °C due to a sudden expansion of quartz at 574 °C.

The thermal conductivity of geopolymers was measured using a hot-wire method. The results indicated that thermal conductivity of geopolymers was similar to those of Portland cement paste. As with Portland cement, the addition of quartz was found to increase the thermal conductivity.

The compressive strength of Na-PSS geopolymers is significantly influenced by the hardness, apparent porosity and the atomic ratio of Si:Al. It was found that geopolymers with an atomic ratio of Si:Al = 1.5, Na:Al = 0.6 have the highest compressive strength and hardness. It was also observed that the addition of aggregate (quartz and granite) has negligible effect on the strength of geopolymers.

The bond strength between geopolymer and aggregate was measured by using a tensile test. The results indicated that sandstone aggregate provides the strongest interfacial bond with geopolymer, followed by granite and quartz. The mechanical interlocking due to the rough surface of the sandstone was believed to be responsible for the relatively high interfacial bond strength.

The microstructural characterisation of Na-PSS by means of SEM (scanning electron microscopy) and TEM (transmission electron microscopy) revealed that the morphology of Na-PSS consists of aluminosilicate matrix, unreacted metakaolinite, pores and microcracks. The presence of microcracks observed by SEM and TEM are categorised as secondary microcracks formed during sample preparation. Computed Tomography Imaging (CT-Scan) results for as prepared geopolymers with and without the inclusion of aggregate did not reveal any resolvable cracks. Optical microscopy observations on polished and vacuum evacuated samples also shows the formation of cracks on the surface of geopolymers.

The presence of unreacted metakaolinite was confirmed by energy dispersive spectroscopy (EDS), X-ray mapping and electron diffraction. It was also found that Na-PSS geopolymers prepared with Si:Al = 2.0, Na:Al = 1.0 are more homogeneous (less unreacted metakaolinite) than Na-PSS geopolymers prepared with Si:Al = 1.5, Na:Al = 0.6. SEM and TEM observations revealed that the interfacial zone between geopolymer paste and aggregate has the same chemical composition as the rest of the geopolymer matrix.

As a result of this study there is a better understanding of the composition-microstructure-property relationship of geopolymers paving the way to the production of geopolymers with improved performance in a variety of applications.

Table of Contents

CHAPTER 6
CONCLUSIONS AND FUTURE WORK

List of Figures

List of Tables

List of Abbreviations used in this Thesis

CSH	Calcium Silicate Hydrate
CMM	Centre for Microscopy and Microanalysis
CT-Scan	Computed Tomography Imaging
EDS	Energy Dispersive Spectrometer
FPZ	Fracture Process Zone
FTIR	Fourier Transform Infra Red
HI	Hinckley Index
ITZ	Interfacial Transition Zone
LTGS	Low Temperature Geopolymeric Setting
MAS-NMR	Magic Angle Spinning – Nuclear Magnetic Resonance
RT	Room Temperature
SAED	Selected Area Electron Diffraction
SEM	Scanning Electron Microscopy
Na-PS	Sodium – Poly(Sialate)
Na-PSS	Sodium – Poly(Sialate-Siloxo)
SGP	Sol-Gel Process
SD	Standard Deviation
TEOS	Tetra-ethoxy orthosialate
TEM	Transmission Electron Microscopy
XRD	X-ray Diffraction

Chapter 1
INTRODUCTION

1.1 Historical Notes of Organic and Inorganic Polymers Development

Since prehistoric time, human beings have used huge amounts of *naturally occurring polymers* or *biopolymers* (polymers derived from plants and animals) known as organic polymers. These materials include wood as a construction material, wool and cotton for clothing, and starch as a glue or thickener. Organic polymers are largely linear macromolecules consisting of chains of carbon atoms as the backbone. Some biopolymers were chemically converted into other polymers in order to make them more resistant against the elements, for example, the collagen of hides into leather by tanning (Callister 1994 p.445; Elias 1997 p.4).

Biological disasters, increasing demand and wars triggered the development of *semi-synthetic* polymers. Examples of this development include the use of wood as a raw material for paper caused by the shortage of cotton, and the development of artificial silk (rayon) in response to pest infestation in silkworm. Early work on substitutes for natural materials was empirical because the macromolecular nature of these materials was unknown.

In the early 1900s, the advance of modern scientific instruments has made possible the determination of molecular structures of polymers and this paved the way for the development of numerous polymers synthesised from organic molecules. Since the end of World War II, the field of materials has been revolutionised by the advent of synthetic polymers such as plastics, rubbers and a range of fiber materials. In some applications metal and wood parts have been replaced by plastics, which have the pre-requisite properties and may be produced at a lower cost. Synthetic organic polymers, or simply polymers, have played a major role in our everyday needs although there remain a number of practical requirements they cannot fulfil (Ray 1978 p.1-2; Callister 1994 p.445; Elias 1997 p.4-8).

The primary concern about synthetic organic polymers is related to their thermal stability and oxidation resistance, including resistance to fire. The need to produce new and non-metallic materials that are able to retain their mechanical and electrical properties at higher temperatures than most organic plastics can withstand increased following the rapid growth of the aerospace industry (Ray 1978 p.3-4; Davidovits 1994a; Lyon *et* al. 1997).

In addition, various catastrophic fires and particularly the incident such as the Summerland disaster on the Isle of Man in 1973 (Ray 1978, p.2) have caused great concern about the safety of structures in which plastics are used extensively. Another drawback of plastics is their dependence on fossil carbon sources a raw material that is now becoming limited. These reasons have accelerated research into alternative materials that can be derived from the virtually unlimited mineral resources of the earth. As a result, many chemists throughout the world started to investigate the possibility of synthesising *inorganic polymers* with the required physical and mechanical properties.

The term inorganic polymer refers to a substance (polymer) composed of a network of atoms that does not have a backbone of carbon atoms. This implies that substances such as *silicates, polyphosphate, polysilanes, siloxanes, aluminosilicates, polyposphazenes, polymeric sulphur nitride* and *inorganic glasses* are inorganic polymers. Zeolite is also inorganic polymer, but it is only obtainable in small, uneconomical batch sizes or has inferior mechanical properties when compared to organic polymers. However, since the 1960s, scientists have been able to synthesise zeolites and feldpathoids similar to those found in nature by integrating silica and alumina. More recently, even cement, because its setting is a form of polycondensation, has also been regarded as a synthetic inorganic polymer (Ray 1978 p.150-153, p.4; Challa 1993, p.106-112).

An excellent summary of inorganic polymer development can be found in Ray (1978 p.19-20). The oldest synthetic inorganic polymer was a simple *alkali silicate glass* used during the Badarian period in Egypt (*c.*12000 B.C.) as a glaze that was applied to steatite after it had been carved into the shapes of amulets, beads, and scarabs. Glass appeared around 5000 B.C. and the earliest known piece of glass is the lion's amulet

originally found at Thebes, and now can be seen in the British Museum. The manufacture of glass proper began in Syria, and a clay tablet dating from 1700 B.C. was found at Tel-Umar bearing an inscription that gives the recipe for the preparation of glass.

A major discovery in the field of synthetic inorganic polymers occurred in 1833 when Thomas Graham published the first accurate description of both crystalline and amorphous *sodium polyphosphates*. In 1897, H.N. Stokes discovered the first synthetic inorganic elastomer, *polydichlorophosphazene*, and its rubber-like properties, unusual in an inorganic substance, stimulating many subsequent investigations of phosphazene polymers. In 1904, F.S. Kipping prepared *polysiloxane* the first organo-inorganic polymers. Another important discovery in the field of synthetic inorganic polymers was the discovery by V.V. Labels in 1973 that polymeric *sulphur nitride* is a metallic-type conductor, which was found by Greene *et* al. in 1975 to become superconducting at low temperature (Ray 1978 p.19-20)

Nowadays, the largest synthetic inorganic polymer industry is the manufacture of Portland cement (Ray 1978 p.150-153, Hos 2000). Various raw materials including limestone (calcium carbonate), clay, and silica are ground and fired together until partial fusion occurs at 1375-1475 ^{o}C. The final product consists of four phases whose idealised formula are Ca_3SiO_5, Ca_2SiO_4, $Ca_3Al_2O_6$, and $Ca_2(Al,Fe)_2O_5$ in proportions depending upon the final application. This process, however, releases large amount of CO_2 and given the scope of the global concrete industry, it is understood that the production of cement is the single largest contributor to industrial greenhouse gas emission, excluding the use of fossil fuels. A minor reduction of CO_2 emissions may be achieved through the blending of Portland cement with replacement materials such as coal-fly ash and iron blast furnace slag. Innovative research is clearly needed so that the cement industry will pay more attention to the development of the *greener* inorganic polymer technology. In recent years, the development of alkali-activated cementitious materials including *geopolymers* has attracted great attention as an alternative for energy saving and environmentally friendly cement (Glasser 1995; Jiang 1997; Davidovits 1987; Davidovits 1994a, 1994b).

1.2 The Need for Geopolymers

The long-term durability of ancient mortars and concretes, such as the blocks making up the pyramids, compared to those used nowadays has prompted research into the nature of these ancient compositions. Davidovits (1987) proved that the ancient products are not only physically more durable, but also more resistant to acid attack and freeze-thaw-cycles. Initially, it was thought that the main difference between the ancient products and Portland cement-based products was the presence of calcium silicate hydrates (C-S-H) gel, the main part of Portland cement. However, it was discovered that ancient concretes also contain C-S-H and consequently Davidovits (1988) paid attention to the large amount of zeolitic phases present in the ancient products. Campbell and Folk (1991) showed that the long-term durability of ancient concretes and mortars is indeed a result of high levels of zeolitic and amorphous compounds in the compositions.

As early as the 1980s Davidovits proposed a controversial theory that some of the Pyramids in Egypt were not built by mining limestone blocks and moving them into place but were cast in place and allowed to set, creating an artificial zeolitic rock. This theory, which has gained acceptance, culminated in a book "*The Pyramids An Enigma Solved*" written together with Magie Morris and published in 1988. Intensive research, initiated by Davidovits and co-workers, to prove this theory has resulted in the rediscovery of a new family of mineral polymers, which they called *alkali-activated aluminosilicate geopolymers* or simply *geopolymers*. This name was chosen because of the similarities with organic condensation polymers in regards to their hydrothermal synthesis conditions (Davidovits 1982; Davidovits & Sawyer 1985; Davidovits 1988; Davidovits 1994a).

Over the last twenty years, *geopolymers, also known as mineral polymers* or *inorganic polymer glasses*, have received much attention as a promising new form of inorganic polymer material that could substantially substitute for conventional or ordinary Portland cement, plastics and many mineral-based products. However, to date the exact mechanisms that govern geopolymerisation are still not fully understood.

In terms of the formation and chemical compositions, geopolymers can be best viewed as the amorphous equivalent of certain synthetic zeolites and would generally have similar chemical composition although the distinctive zeolitic structure is absent which makes them amorphous (van Jaarsveld, van Deventer & Lorenzen 1997). Davidovits (1982, 1988) proposed that geopolymers result from dissolution and polycondensation of polymeric aluminosilicates and alkaline silicate solution under hydrothermal condition, yielding an amorphous, three-dimensional polymeric framework. The family of these new materials is called *poly(sialates)* comprising an amorphous network of SiO_4 tetrahedra and AlO_4 tetrahedra with associated Na^+ or K^+ ions.

Research has shown that poly(sialates) geopolymer may be readily synthesised through alkali-activation of inexpensive and pure starting materials such as kaolinitic clays (Davidovits 1982; Davidovits & Sawyer 1985; Rahier *et* al. 1996; Rahier *et* al. 1997; Granizo, Blanco-Verela & Palomo; 2000; Barbosa, MacKenzie & Thaumaturgo 2000), as well as waste products such as fly ash and furnace slag (Jiang & Guan 1999; Palomo, Grutzeck & Blanco 1999; van Jaarsveld, van Deventer & Lorenzen 1997; van Jaarsveld & van Deventer 1999; Brough & Atkinson 2002; Swanepoel & Strydom 2002; Cheng & Chiu 2003). Xu & van Deventer (2000) intensively studied the geopolymerisation of 15 Al-Si minerals and reported that the mineral stilbite mixed with KOH produced geopolymer with the highest compressive strength. This study implies that there is a wide range of natural Si-Al minerals that could serve as potential precursors for synthesis of geopolymers.

As a new type of inorganic polymer material, geopolymers have a potential for a wide variety of applications, whether used pure, with fillers or reinforced. In general, these applications can be divided into two categories:

1. Structural products such as reinforced for the manufacture of moulds, tooling, cement and concrete replacements in various environments.
2. Immobilisation technology for toxic chemical and radioactive waste containment.

It is expected that in the near future these applications will also be found in automobile and aerospace industries, non-ferrous foundries and metallurgy, civil

engineering and plastic industries (Davidovits 1991; Davidovits 1994a, 1994b; van Jaarsveld, van Deventer & Lorenzen 1997; van Jaarsveld, van Deventer, & Schwartzman 1999; Xu & van Deventer 2000; Lee & van Deventer 2002; Lyon *et* al. 1997; Hermann *et* al. 1999).

1.3 Some Properties and Applications of Geopolymers

As a polymer, inorganic aluminosilicates transform, polycondense and form a dimensionally stable mass at low temperature. These geopolymers are hard, weather and chemical resistant and able to withstand high temperatures. Sand and mineral aggregates may be incorporated to make ceramic-composite materials, mortars and concretes. For geopolymer cements such as (K-Ca) poly(sialate-siloxo), the mixes undergo a low temperature rise and rapid strength gain during polymerisation with ultimate strengths similar to Portland cements. The compressive strength of this cement can reach 20 MPa only a few hours after processing and may reach 70 – 100 MPa in less than a month. In recent years, new alkali activated cementitious compositions have reached a commercial stage and marketed by the American cement manufacturer Lone Star Industries Inc. under the brand name PYRAMENT® blended cement (Davidovits 1991; Davidovits 1994a, 1994b; Palomo, Grutzeck & Blanco 1999).

The increasing attention to this new type of geopolymer cement has been triggered not only because of the abundance of alumina and silica as its raw materials but also because its manufacture is environmentally clean, as it does not directly create CO_2 emission. By contrast, the production of 1 tonne of ordinary Portland cement (made from the calcination of limestone) directly generates 0.55 tonnes of CO_2 and requires the combustion of carbon-fuel to yield an additional 0.40 tonnes of CO_2. These novel geopolymer cements, which have unique properties such as high early strength, low shrinkage, freeze-thaw resistance, sulphate and corrosion resistance could become a viable alternative to conventional cements and hence substantially reduce CO_2 emission caused by the cement and concrete industries (Davidovits 1991; Davidovits 1994a, 1994b).

The use of geopolymer matrix carbon-fiber composites for fireproof aircraft cabin interior panels, marine structural composites, and infrastructure applications has recently being evaluated (Lyon *et* al. 1997). This material made from Na- or K-poly(sialate-siloxo) did not ignite or burn at an irradiance level of 50 kW/m^2 which is typical of the heat flux in a well developed fire, and retains sixty-seven percent of its original flexural strength after a simulated large fire exposure. Most polymers, such as carbon-reinforced polyester, vinylester, epoxy, bismaleinde and engineering thermoplastic laminates ignited and released heat and smoke at this level of irradiance.

The atomic ratio of Si:Al in geopolymer structures plays an important roles in determining the properties and subsequent application. Figure 1.1 shows that materials with a low ratio of Si:Al (1, 2, 3) initiates 3 dimensional (3D)-networks that are very rigid and they are suitable for the manufacture of bricks, ceramics and fire protection while those with the composition of 20<Si:Al<35 provides polymeric character to the geopolymer and they are suitable for fire and heat resistant composites which withstand up to 1000 – 1200 °C (Davidovits 1991; Lyon *et* al. 1997, Barbosa & MacKenzie 2002).

1.4 Project Aims

Geopolymers synthesised from aluminosilicate minerals have a bulk density between 1–2 g/cm^3 and tend to be very porous. Rahier *et* al. (1996) reported that aluminosilicate inorganic polymers synthesised from metakaolinite and sodium silicate solution incorporated with sand aggregate had an apparent porosity between 21 – 26% with a compressive strength between 23 to 60 MPa. Similarly, Barbosa, MacKenzie & Thaumaturgo (2000) reported that sodium poly(sialates) geopolymers based on metakaolinite, without any inclusion of aggregate, had an apparent porosity of 37% and a compressive strength of 48 MPa.

Hos, McCormick & Byrne (2002) produced synthetic aluminosilicate inorganic polymers, exhibiting a nanoporous microstucture, from melt-quenching alumina and silica minerals. Geopolymer cement based on alkali-activated fly ash has also been

found to exhibit a high density of pores in the micrometer size range (Palomo, Grutzeck & Blanco 1999). The presence of pores in the matrix of geopolymers is intrinsic, independent of the starting materials and the processing routes while the density of pores is influenced by the ratio of starting materials.

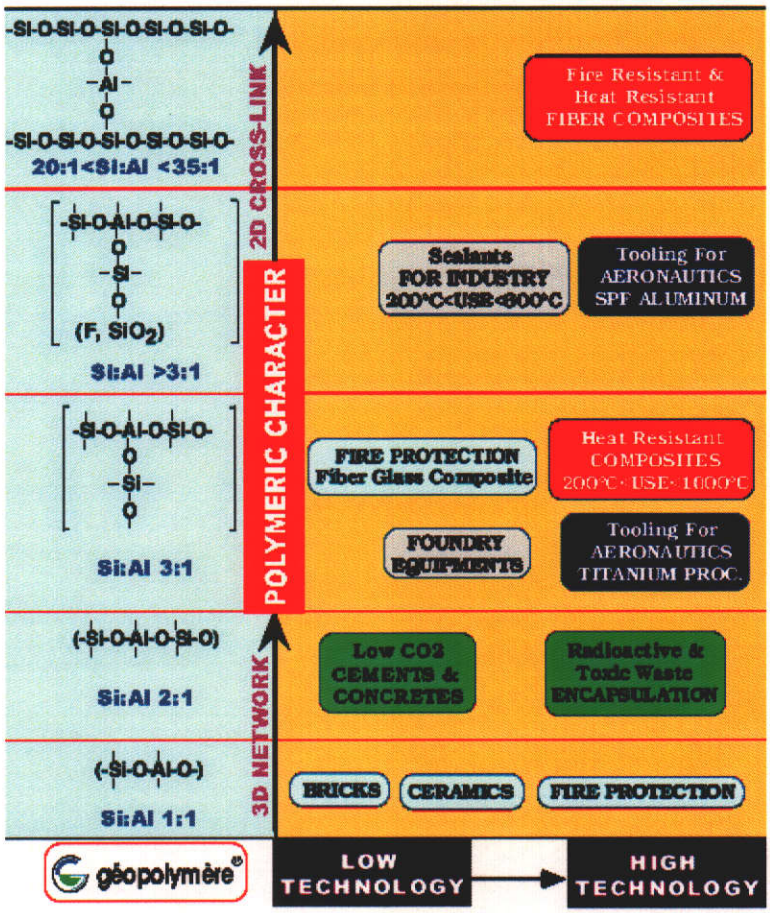

Fig.1.1 The dependence of geopolymer properties on Si:Al (after Davidovits, Geopolymer Association Website: http://www.geopolymer.org, 2000).

From a structural point of view, a stronger material would be expected to have less porosity. Various studies have investigated the surface inhomogeneities of geopolymers with the main purpose of controlling the pore structure of inorganic aluminosilicate materials as it plays an important role on the physical and mechanical properties. Jiang & Guan (1999) investigated the total porosity, pore size distribution and strength of high-volume fly ash paste. They found a linear relationship between the total porosity and compressive strength as well as the flexural strength. They also

found that the total porosity of the paste increased with increasing fly ash content and water/binder ratio.

It is expected that aggregate content, size and volume in the geopolymers network will play a major role in pore size refinement and matrix densification. It is well known in composite and cement-based materials that the addition of aggregate of a suitable particle size distribution and volume fraction will result in a low-porosity, high density material and yielding high strength. The incorporation of aggregate into a brittle matrix may have a role in increasing the toughness of the materials through two mechanisms: (a) aggregate particles acting as bridges across the crack (similar to aggregate-bridging in polycrystalline ceramics, and (b) closure of the macrocrack as a release of residual stresses and subsequent expansion (Aquino & Shah 1995; Amparano, Xi & Roh 2000; Merchant *et* al. 2001; Caliskan 2003).

Despite the growing popularity of geopolymers in various applications, limited research has been devoted to identifying the influence of aggregate on the microstructure character of geopolymer. In this study, the optimisation of processing conditions and the inclusion of aggregate will be investigated in relation to the microstructure character, the strength of interfacial bond between aggregate and the matrix as well as its overall effect on the strength of the geopolymers.

Thermal properties such as thermal expansion and thermal conductivity of geopolymers with and without the addition of aggregate will also be studied. The results gained from this study will increase our understanding of the fundamental properties of these promising new materials and pave a way to large–scale manufacture for further applications. Therefore, the main objectives of this research are:

1. To study and optimise the processing parameters in the production of geopolymers based on metakaolinite.
2. To study the effect of aggregate type, grain size and concentration on the compressive strength of the resulting geopolymers.
3. To study the microstructural character of geopolymers with and without the addition of aggregate.

4. To study the interfacial bond strength between the aggregate and the geopolymer paste.
5. To study the thermal properties of geopolymers such as thermal conductivity and thermal expansion.

1.5 Research Plan

In order to achieve the objectives of this study, experimental work was undertaken in the Department of Applied Physics, Curtin University of Technology, Perth, Western Australia. Figure 1.2 shows the schematic of the experimental steps of this study. The details of each experimental method are provided in chapter 3.

a) Selection, preparation and characterisation of the starting materials

The raw material used for producing geopolymers was metakaolinite powder. Metakaolinite was obtained by dehydroxylation of kaolinite at 750°C for several hours. The powder was activated with sodium silicate solution (alkali-activated method). The soda (Na_2O) content of sodium silicate was increased by the addition of sodium hydroxide. The geopolymers that were processed in this study have atomic ratio of Si:Al between 1 and 2, and are designated as poly(sialate) and poly(sialate-siloxo) type.

Natural sand in the form of α-quartz and granite with different size and concentration were used as aggregate. The sand and granite used in this study were similar to that used in the production of mortar and concrete. For the purpose of this study, however, the grain size of the sand and granite was limited to the range of 40 μm to 750 μm. The chemical composition and crystallographic characterisation of the starting materials were determined prior to processing of the geopolymers by the use of X-ray powder diffraction (XRD), scanning electron microscopy (SEM) as well as transmission electron microscopy (TEM).

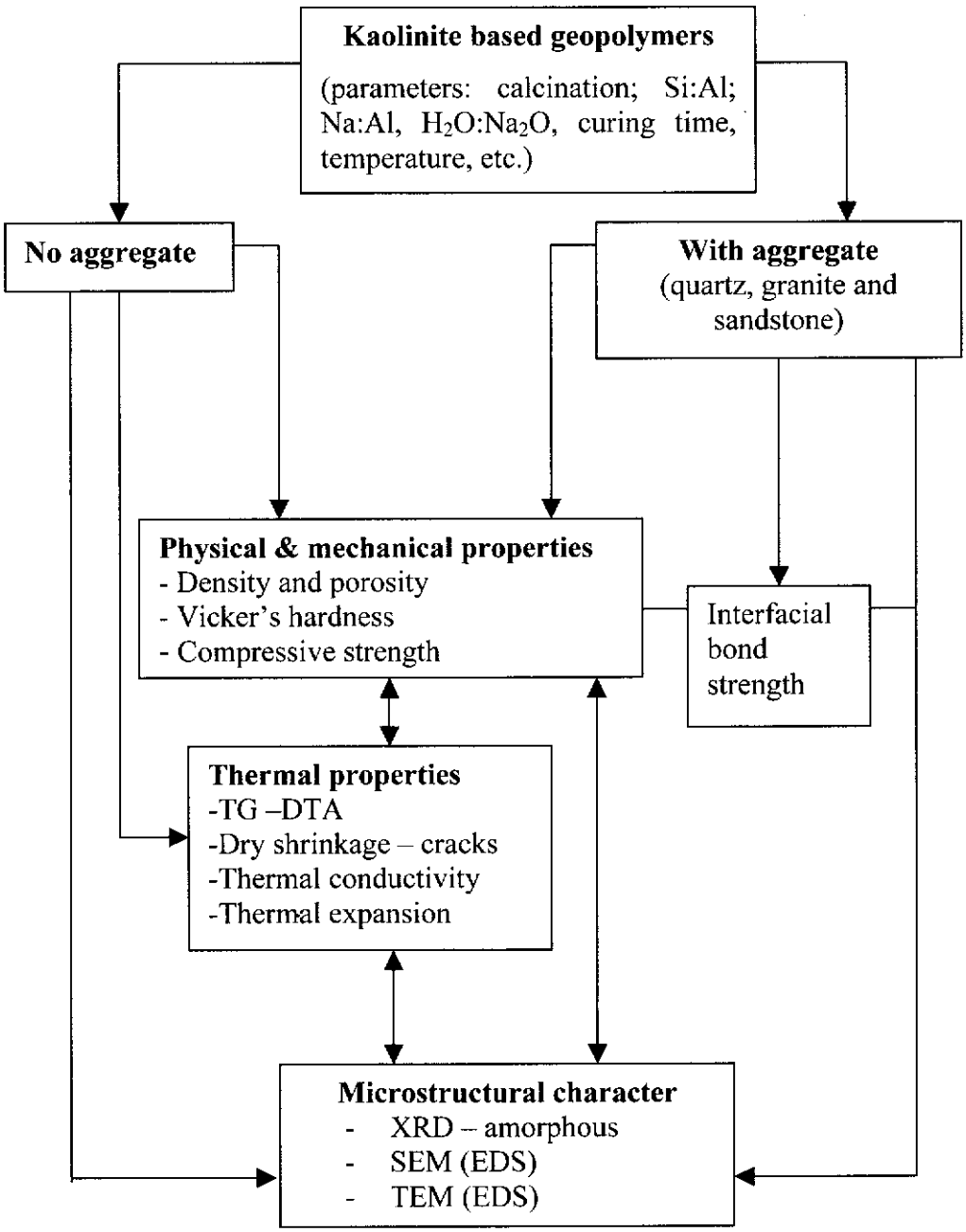

Figure 1.2 The experimental steps used in this study.

b) Material processing and characterisation

The processing of the geopolymers was based on the alkali-activated method using the starting materials mentioned above. A series of geopolymer compositions were produced by changing the ratio of Si:Al and Na:Al. The addition of aggregate was

introduced systematically to investigate the influence of aggregate grain size as well as the ratio of geopolymer paste/aggregate. These two factors were related to the total porosity, crack development and compressive strength.

c) Materials Evaluation

Characterisation of the resulting materials was conducted on specimens with and without the addition of aggregate. The bulk density and the apparent porosity were measured by using Archimedes principles. Compressive strength was related to the ratio of Si:Al and Na:Al as well as the total porosity. The strength of the interfacial bond between aggregate and the matrix was investigated by using an interfacial bond strength measurement. The bound water of the kaolinite and geopolymers was determined using thermogravimetry and differential thermal analysis (TG-DTA). The thermal conductivity of the geopolymers was measured by using a hot wire method. The thermal expansion of the geopolymers was measured by using a dilatometer.

XRD was used for phase analysis of the starting materials and to examine the crystallinity of the resulting geopolymers.

SEM and TEM were used for microstructural imaging. SEM imaging was used to examine the matrix, interfacial transition zone (ITZ) between the matrix and aggregate, porosity and crack formation. The image and diffraction patterns of the material obtained from TEM were used to gain information about the structure and constituent elements of the various features present.

1.6 Organisation of the Thesis

Chapter 2 presents some of the general theory relating to the basic concepts, structure, physical and mechanical properties of aluminosilicate inorganic polymer (geopolymer) as well as the role of aggregate in the optimisation of microstructure and mechanical strength of geopolymer.

Chapter 3 describes the chemical composition of the starting materials and processing techniques to produce geopolymers, specimen preparation and the experimental arrangements to characterise the resulting materials.

Chapter 4 presents the experimental results on the physical and mechanical properties of geopolymers. Here the physical properties and the structure of the geopolymer precursors as well as the resulting materials based on XRD is presented. The effect of atomic ratio of Si:Al and Na:Al as well as the inclusion of aggregate on the mechanical strength are shown. The effect of aggregate types on the interfacial bond strength is also presented. Results from thermal conductivity and thermal expansion measurements are also included in this chapter.

Chapter 5 presents the microstructural character of geopolymers based on SEM and TEM. SEM images show the microstructure character in the interface between the matrix and aggregate as well as the presence of pores, cracks and any impurities in the matrix. TEM images provided higher resolution information about the geopolymer microstructure.

Chapter 6 contains the conclusion of the present study and suggestions for future research.

Chapter 2
THE CHEMISTRY OF GEOPOLYMERS

2. 1 Basic Concept of Polymers

A *polymer* (Greek *poly = many* and *meros = parts)* is a substance, the molecules of which consist of a large number of low molar mass base units or monomer, which are connected by primary bonds. If A is a monomer molecule and -A- the base unit, then a polymer molecule is represented by:

$$\text{-A-A-A-A-A-} \quad \text{or} \quad [\text{-A-}]_n \tag{2.1}$$

where n is an integer, called the degree of polymerisation of this molecule.

A monomer is a compound consisting of simple small molecules that can react with each other or with another molecule. Before 1930, polymer molecules were considered as physical aggregates of unchanged monomer molecules $(A)_n$ known as "*organic colloids*" (Elias, 1997 p.4-8). However, Herman Staudinger (Nobel prize 1953) (Challa, 1993 p.13) had already postulated in 1920 that those colloidal particles were composed of a single, very long molecule or an organic macromolecule. This view paved the way for synthetic organic chemists to start building giant chain molecules in a systematic way from known monomeric compounds. Since that time, thousands of different polymers have been synthesised, some of them have reached the phase of large-scale commercial production.

Nowadays, polymers can be classified in many different ways such as by origin, chain structure, thermal behaviour, polymerisation mechanism, chain configuration and application. Based on the origin for example, polymers can be divided into: synthetic organic polymers; biopolymers; semi-synthetic polymers and inorganic polymers (Challa 1993 p.14-16).

Synthetic organic polymers, or simply polymers, are the most important class of macromolecular materials. Polymer science has developed almost entirely from

studies of organic polymers, most of which are linear macromolecules that are thermoplastic. Many organic materials are *hydrocarbon,* that is, they are composed of hydrogen and carbon. Therefore, for most organic polymers, their backbones are a string of carbon atoms. As a result of intensive commercial development, synthetic organic polymers have been able to satisfy many everyday needs.

Biopolymers are substance like protein, polynucleotides, polysaccharides (cellulose, starch), natural rubber and several gums. A biopolymer molecule is identical, monodisperse and represents a single, pure compound. Semi-synthetic polymers are macromolecular reaction products of chemical reactions applied to biopolymers. The most well-known examples are esters or ethers of cellulose or amylose and vulcanised natural rubber.

Inorganic polymers are substances made up of monomers containing inorganic elements other than carbon and linked together by mainly covalent bonds. This definition although still rather vague implies that, inorganic polymers, unlike organic polymers, can contain a wide variety of elements. Most common inorganic polymers are some natural silicates and related synthetic poly(siloxanes). Although polymer science has developed along the lines of synthetic organic polymers, a recent increase in research and development activity could facilitate the wider acceptance of inorganic polymers in the future.

2.2 Classification of Inorganic Polymers

Inorganic polymers can be further classified based on their composition or based on their network connectivity. Based on the chemical structure, inorganic polymers can be divided into three basic types (Challa 1993, p 106):

a. *homoatomic polymers*. This polymer is comprised of one kind of atom in the main chains. An example of this polymer is polymeric sulphur.

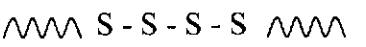

b. *heteroatomic polymers.* This type of polymer consists of more than one type of atom in the main chains.

Examples of this are (R = any hydrocarbon group):

poly(siloxanes)

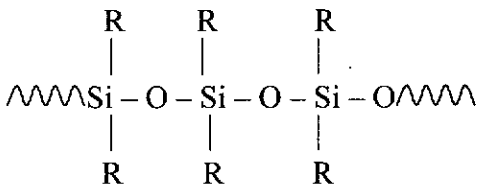

poly(sulphurnitride)

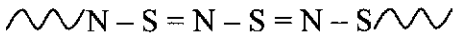

c. *hybrid heteroatomic polymers.* In this polymer inorganic atoms alternate with typical organic units, such as:

poly(phenylene sulphide)

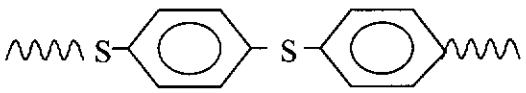

The bonds between the main chain atoms of inorganic homo– or heteroatomic polymers are predominantly covalent. Inorganic polymers often show improved properties such as better heat and chemical stability or interesting electronic properties. Some can be processed like normal organic polymers and yield ceramic fibres and coatings.

Carbon is an element that shows a strong tendency to form homoatomic chains or catenation. This tendency exists also for silicon and germanium, sulphur, selenium and tellurium. Other atoms show only a small or no tendency to catenation and can form long polymer chains through alternation with other atoms. As a result heteroatomic polymers predominate in inorganic polymer science.

Another way to classify inorganic polymers is based on network connectivity or coordination number. Each class of polymer has a real or notional parent network from which the family of polymers can be derived. All silica glasses for instance, can be viewed to be derivatives of the parent network present in amorphous silica. The

connectivity of the parent network is defined as the number of network bonds that link each repeat unit in the network. Therefore, silica with the repeat unit SiO_4 (tetrahedral) has a connectivity of 4, while boric oxide with the repeat unit BO_3 (trigonal) has a connectivity of 3 and a linear polymer such as polymeric sulphur has a connectivity of 2 (Ray 1978, p 14).

Polymers with partial substitution such as metal cation or organic ligands will have an average connectivity lower than the parent. The notion of a cross-link density is used to distinguish the actual frequency of linkages in a derived polymer from the connectivity of the parent network. The connectivity for a particular class of network polymers is considered as a constant that characterises the parent. The cross-link density is defined as a variable that describes how closely the structure of any member of the class approaches that of the parent network. As an example, an alkali silicate glass with the molar ratio of silica to soda, SiO_2:Na_2O = 3 would be classed as a derivative of silica, making it a four-connective polymer with a cross-link density of 0.667 as shown in figure 2.1 (Ray 1978. p.15).

The advantage of this type of classification is that polymers with similar physical and mechanical properties as well as areas of application can be grouped into the same class. For example, all materials formed from the two-connective (linear) polymers are soluble, with few exceptions they have low softening points, and many of them are flexible. The three-connective polymer materials are found to be insoluble, rigid solids or glasses of intermediate softening point. Materials with four-connective polymers are generally brittle, high-modulus glassy or crystalline with high softening point.

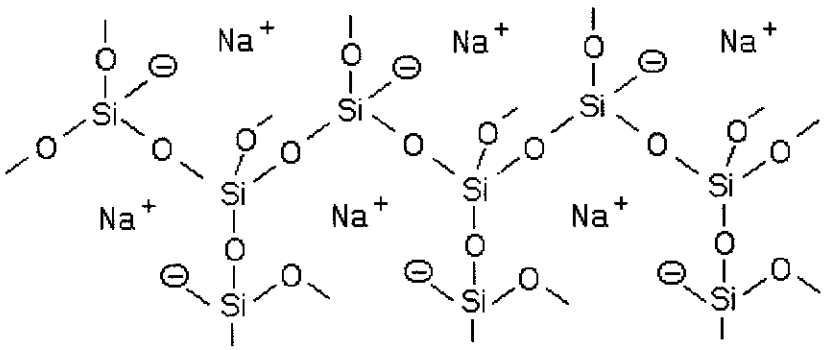

Figure 2.1 Sodium silicate as a four-connective polymer with a cross-link density of 0.667 (redrawn after the original of Ray 1978 p.15).

2.3 Synthesis of Geopolymers

Before discussing the terminology, reaction mechanism and structure formation of geopolymers, it is necessary to briefly discuss the formation of zeolites as they follow very much the same route. This view is supported by Davidovits (1982, 1994a, 1988, 1999) who stated that aluminosilicate geopolymers have a three-dimensional structure and belong to the category of zeolites and feldspathoids.

2.3.1 Zeolites

Zeolites are based on a crystalline aluminosilicate framework and are three-dimensional network inorganic polymers built up of $(Si,Al)O_4$ tetrahedra linked by sharing oxygen atoms into ring and cages. The stoichiometry of zeolites can be represented by the general formula (Bell 1999):

$$M^{n+}_{1/n}[(AlO_2)(SiO_2)_x]^-.zH_2O \qquad (2.2)$$

where x represents the atomic ratio of Si:Al. The extra lattice cation M^{n+} such as H^+, Na^+, K^+, Cu^+ and $[Fe(OH)_2]^+$ is required for charge compensation. Zeolites are found naturally but can also be synthesised hydrothermally from a caustic mixture of sodium silicate, aluminium hydroxide and an organic templating agent. The framework of zeolites is formed by corner sharing of SiO_4^{4-} and AlO_4^{5-} tetrahedra. Figure 2.2 shows the structure of faujasite which is a representative of zeolite X (Si:Al = 1) and zeolite Y (Si:Al = 2.5) in which Si or Al atom is located at the vertices and O atoms are located on the line segments joining the vertices.

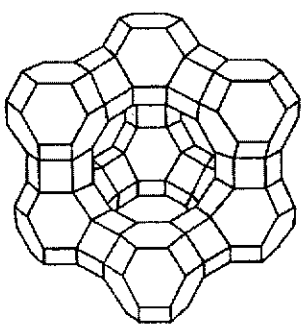

Figure 2.2 The crystal structure of faujasite, where Si or Al are at the corner of framework and these are linked by oxygen bridges represented by the lines (after Bell 1999).

Zeolite synthesis depends on the use of highly reactive starting materials, a relatively high pH, a high degree of saturation resulting in large numbers of nuclei, and a relatively low temperature. Zeolites are most commonly synthesised by sol-gel techniques. In a typical procedure, a soluble source of Al is dissolved in a highly alkaline solution of sodium silicate resulting in an amorphous aluminosilicate gel. Crystallisation is normally carried out in the temperature range of 100 – 180 °C for a few hours to a few days. During this period the amorphous gel undergoes continual dissolution and reconstruction, and the crystalline zeolite phase grows (Ray 1978 p.129-130; Bell 1999).

The silica content in zeolites is an important parameter that determines the acidity, density and the thermal resilience of zeolites. Aluminosilicate clays have been utilised to obtain high-silica zeolites. Synthesis of zeolite *A* for example is obtained from hydrothermal treatment of kaolinite (metakaolinite) in a caustic solution at 100 °C (Hos 2000):

$$Al_2O_3.2SiO_2.2H_2O + 2NaOH \rightarrow Na_2O.Al_2O_3.2SiO_2 + 3H_2O \qquad (2.3)$$

Unlike geopolymers, the science and the production of synthetic zeolites have evolved over 40 years and large-scale manufacture of ion exchange resins, molecular sieves, sorbents and catalysts are common place. The utilisation of zeolites, however, is limited due to their poor mechanical properties and sensitivity to acidic environments.

2.3.2 Terminology and formation of geopolymers

As early as the 1980s, Davidovits developed amorphous to semi-crystalline aluminosilicate inorganic polymers, now known as *geopolymers* (mineral polymers resulting from geochemistry). The geological interest of aluminosilicate is particularly based on their natural abundance in Si-Al minerals such as kaolinite ($Al_2Si_2O_5(OH)_4$). Geopolymerisation involves a chemical reaction between various aluminosilicate oxides (Al^{3+} in IV-fold coordination) with silicates under highly alkaline conditions, yielding polymeric -Si-O-Al-O- bonds (Davidovits 1982;

Davidovits 1991; Davidovits 1994a; Rahier *et* al. 1996; van Jaarsveld, van Deventer & Lorenzen 1997; Xu & van Deventer 2000).

The family of geopolymers based on aluminosilicate is called *poly(sialates)* comprising an amorphous network of AlO_4 and SiO_4 tetrahedara linked alternately by sharing all the oxygens. Sialate is an abbreviation for silicon-oxo-aluminate (-Si-O-Al-O-). The presence of positive ions, such as Na^+, K^+, Li^+, and Ca^{++}, in the framework is necessary to balance the negative charge of Al^{3+} in IV-fold coordination with oxygen. This polymeric model is similar to the formation processes of zeolites and zeolite precursors. The empirical formula of poly(sialates) is shown in equation 2.4 (Davidovits 1991):

$$M_n [(-SiO_2)_z\text{-}AlO_2]_n . wH_2O \qquad (2.4)$$

Where M_n is a cation (the alkaline element), *n* is a degree of polycondensation, $w \leq 3$ and z is 1, 2 or 3. According to Davidovits (1991) geopolymers are comprised of several fundamental poly(sialates) units as shown in figure 2.3.

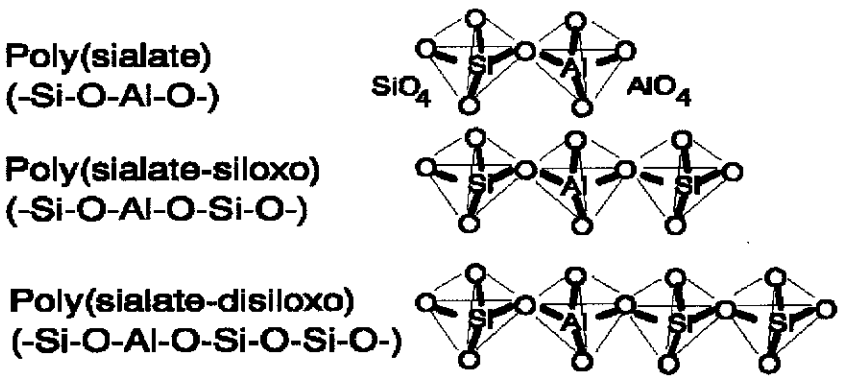

Figure 2.3 Geopolymeric molecular networks (after Davidovits 1991).

Poly(sialates) are chain and ring polymers with Si^{4+} and Al^{3+} in IV-fold coordination with oxygen and have matrices ranging from amorphous to semi-crystalline. Crystalline poly(sialate) and poly(sialate-siloxo) can be obtained from hydrothermal setting conditions, whereas hardening at ambient temperature induces an amorphous or glassy system. The degree of disorder in a geopolymer can be inferred from X-ray diffraction patterns which results in a broad hump rather than sharp diffraction peaks.

By using kaolinite as a geopolymeric precursor, hydrothermal polycondensation at 150 °C with NaOH will result in a well crystallised sodalite based Na-Poly(sialate) (Na-PS) $(Si_2O_4,Al_2O_4,2Na).3H_20$, within 20 seconds (Davidovits 1991) (Figure 2.4).

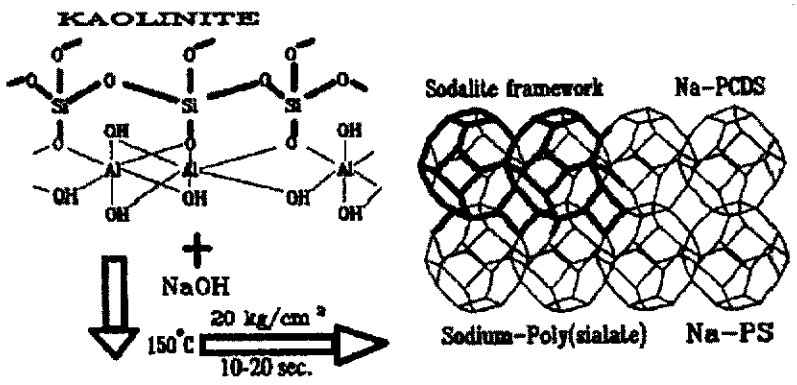

Figure 2.4. The schematic of hydrothermal polycondensation of Na-poly(sialate) (after Davidovits 1991).

The synthesis of amorphous geopolymer binders does not implement hydrothermal conditions. Geopolymerisation of aluminosilicate oxide to produce sodium or potassium poly(sialate) (Si:Al = 1.0) is shown in figure 2.5. In this example, the aluminosilicate oxide has been written as $(Si_2O_5, Al_2O_2)_n$ instead of $(2SiO_2, Al_2O_3)$ to emphasise the IV-fold coordination of Al. The fabrication of $(Si_2O_5,Al_2O_2)_n$ can be achieved by (a) calcining aluminosilicate hydroxides $(Si_2O_5,Al_2(OH)_4)$, or (b) condensation of SiO and Al_2O vapours (Davidovits 1982, Davidovits 1991).

$$(Si_2O_5,Al_2O_2)_n + nH_2O \xrightarrow{NaOH,\ KOH} n(OH)_3\text{–Si-O-Al-}(OH)_3$$

$$n(OH)_3\text{-Si-O-Al-}(OH)_3 \xrightarrow{(-)\ NaOH,KOH} (Na,K)\left(\text{- Si(O)-O-Al(O)-O- }\right)n + 3nH_2O$$

Ortho(sialate) — (Na,K)–poly(sialate)

Figure 2.5 Geopolymerisation reactions: dissolution and polycondensation of ortho(sialate) ions (after Davidovits 1991).

Figure 2.6 shows a geopolymerisation reaction to produce sodium or potassium poly(sialate-silixo) ((Na,K)–PSS, Si:Al = 2.0). Here, it has been suggested that the

syntheses are carried out through oligomers (dimmer, trimer) which provide the actual unit structures of the three dimensional macromolecular system.

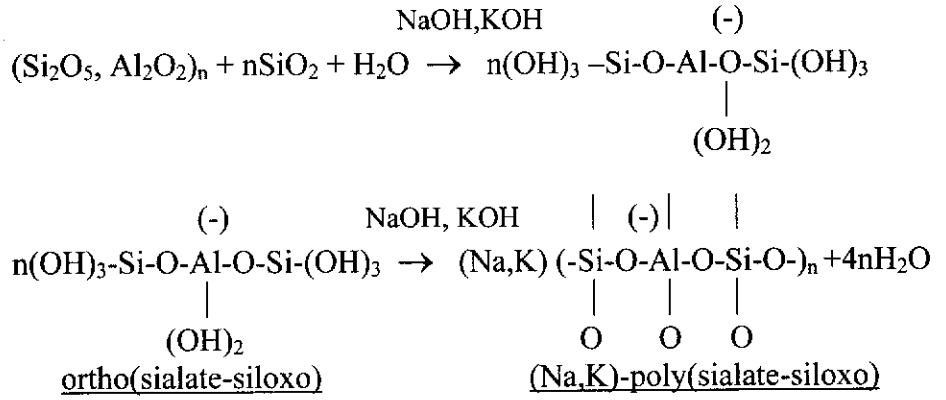

Figure2.6 Geopolymerisation reactions: dissolution and polycondensation of ortho(sialate-siloxo) anions (after Davidovits 1991).

To produce poly(sialate-disiloxo, (Si:Al = 3)), a certain amount of amorphous silica (silica fume) is added to a (Na,K)-PSS reactant mixture. This type of material is particularly useful for fire protection and heat resistance composites. For Si:Al >> 3, the polymeric structure results from cross linking of polysilicate chains or sheets with a sialate link.

Geopolymerisation is exothermic and can be considered as the dissolution and polycondensation of orthosialate ions. The exothermic reaction transforms the mixture of the starting material from a suspension into solid geopolymer and a residue, which is mainly water. During the hardening stage, however, the sample must be covered in order to avoid water evaporation.

In the processing of geopolymers, the composition of the reactant mixture, in terms of molar oxide ratios, falls within the range (Davidovits 1982; Davidovits & Sawyer 1985) (M represents Na or K):

$$0.2 < M_2O/SiO_2 < 0.48$$

$$3.3 < SiO_2/Al_2O_3 < 4.5$$

$$10.0 < H_2O/M_2O < 25$$

Some researchers, however, later discovered that these molar oxide ratios are just an indication of approximate composition and not very critical particularly when dealing with Si-Al minerals from waste materials such as fly ash. This is due to the fact that even though these molar ratios are based on chemical analyses it is highly unlikely that all of the silica and alumina actually takes part in the synthesis reaction (Rahier *et* al. 1996; van Jaarsveld, van Deventer & Lorenzen 1997; Hos 2002).

It is clear that the main differences between zeolite formation and geopolymerisation are in the concentration of the precursor species and the fact that zeolites normally form under hydrothermal conditions and geopolymers do not. Zeolites crystallise from dilute aqueous solutions where precursor species have mobility and enough time for proper orientation and alignment before bonding into a crystal structure. In contrast, setting of geopolymers mixture occurs fairly quickly, with insufficient time for the formation of a proper crystal structure (van Jaarsveld, van Deventer & Lorenzen 1997).

2.3.3 Geopolymer precursors

In the early stage of development, most geopolymers were synthesised through the *alkali-activation* of dehydroxylated kaolinite or metakaolinite below 100 °C (Davidovits 1982; Davodovits 1985; Davidovits 1994a; Rahier *et* al. 1996; Barbosa, MacKenzie & Thaumaturgo 2000; Granizo, Blanco-Verela & Palomo 2000). In recent years a wide variety of Al-Si minerals, such as fly ash, furnace slag, pozzolan and a mixture of metakaolinite/flyash or kaolinite/stilbite, have been utilised to produce geopolymers. Of particular interest is the utilisation of waste products to produce economical and environmentally friendly geopolymer cements or fireproof building materials (Palomo *et* al. 1999; van Jaarsveld & van Deventer 1999; van Jaarsveld, van Deventer & Shwartzman 1999; Xie & Xi 2001; Brough & Atkinson 2002; van Jaarsveld, van Deventer & Lukey 2002; Xu & van Deventer, 2000; Xu & van Deventer 2002).

The term alkali-activation implies that either alkalis or alkali earth ions are used as activators to simulate the pozzolanic reaction or release the latent cementitious properties of aluminosilicate minerals as well as industrial by-products such as

granulated blast furnace and fly ashes consisting essentially of silicates, aluminosilicates and calcium. The activator is a substance that dissolves the aluminosilicate allowing polycondensation to take place thus forming a geopolymer (Jiang 1997; Martinez-Ramirer & Palomo, 2001).

Kaolinite is an aluminosilicate mineral that contains chemically bound water with an ideal formula of $Al_2Si_2O_5(OH)_4$ in which the silica tetrahedral layer, represented by $(Si_2O_5)^{2-}$, is made electrically neutral by an adjacent $Al_2(OH)_4^{2+}$ layer. The crystal structure of kaolinite was first suggested by Pauling in 1930 and improved by Gruner in 1932 and revised in 1946 by Brindley and colleagues (Grim 1953). The structure is composed of a single silica tetrahedral sheet and a single alumina octahedral sheet combined in a unit so that the tips of the silica tetrahedrons and one of the layers of the octahedral sheet form a common layer (figure 2.7). All the tips of the silica tetrahedrons points in the same direction and towards the centre of the unit made of silica and octahedral sheets. The theoretical composition of kaolinite expressed in oxides is SiO_2 46.54%; Al_2O_3 39.50%; H_20 13.96%. Many samples of kaolinite contain a small amount of impurity such as quartz and have substitution of iron and/or titanium (anatase) for aluminium.

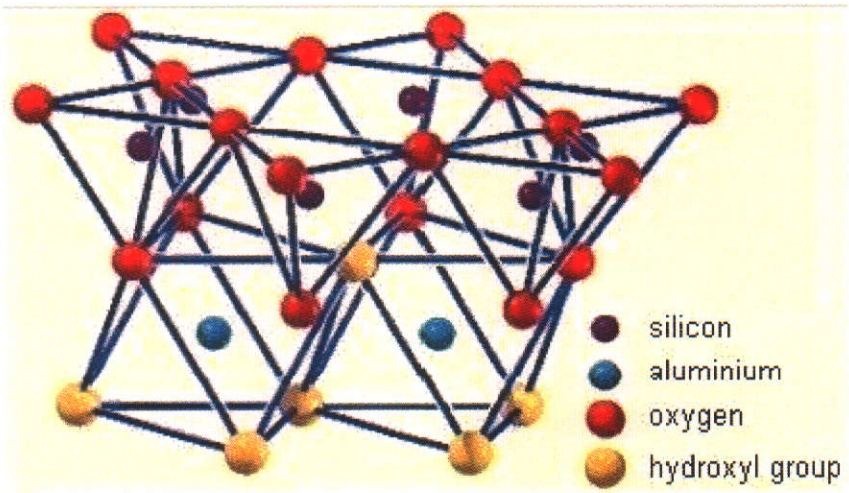

Fig.2.7 Diagrammatic sketch of the structure of kaolinite, after Rudolph (http:// www.a-m.de/englisch/lexikon/kaolinit-bild1.htm, 2003).

Metakaolinite is usually considered to be a fully dehydroxylated product of kaolinite. Dehydroxylation of most kaolinites occurs at temperatures above 500 °C and is accompanied by a weight loss of about 14%. The dehydroxylation reaction can be represented as follows (Kakali *et* al. 2001):

$$Al_2Si_2O_5(OH)_4 \rightarrow Al_2Si_2O_5(OH)_xO_{2-x} + (2-x/2)\ H_2O \qquad (2.5)$$

with a low value of x (about 10 % of residual hydroxyl groups in metakaolinite).
The thermal behaviour of kaolinite studied through Thermogravimetry and Differential Thermal Analysis (TG-DTA) show symmetrical endothermic peaks with maximum values near 550 °C and exotherms at 998 °C and 1267 °C due to the formation of a spinel phase and secondary mullite, respectively. Complete dehydroxylation is achieved at about 750°C (Temuujin *et* al. 1998; Granizo, Blanco-Varela & Palomo 2000; Kakali *et* al. 2001; Shvarzman *et* al. 2003).

Powder X-ray diffraction studies of kaolinite normally indicate an almost amorphous product after dehydroxylation but single crystal analysis indicates that some structural order is maintained. Retention of structural order is related to the particular polymorphic form of the kaolinite minerals, the degree of crystallite order and crystallite size (Brindley & Lemaitre 1987). The loss of water destroys the crystallinity of dioctahedral kaolinite and transforms the octahedrally coordinated Al layer into the more reactive tetrahedral form but the Si — O sheets of the kaolinite structure are largely conserved. It is well accepted that Al ions in metakaolinite are in four-fold coordination. This structure is considered to become unstable with the final removal of hydroxyls at higher temperatures.

Metakaolinite reacts with sodium, potassium and calcium hydroxides. The activation process of metakaolinite involves a dissolution step followed by a step of polycondensation similar to those of zeolites formed when metakaolinites are dissolved by NaOH or KOH solution. In the zeolite system, an excess activator volume is used to permit crystalline products to be separated by filtering. In metakaolinite activated geopolymer binder, a minimum activator solution volume must be used to obtain pastes with suitable plasticity and workability, resulting in practically amorphous materials. As in zeolite synthesis, the resulting materials are

controlled by several parameters, such as compositional parameters, temperature and time reaction, component mix order and siliceous source reactivity (Granizo, Blanco-Varela & Palomo 2000).

According to Davidovits (1999), the pure calcined kaolinite (which he called KANDOXI = KAolinite, Nacrite, Dickite OXIde) which is suitable for geopolymerisation should display two main resonances of ^{27}Al in the MAS-NMR spectrum, namely: 20 ± 5 ppm assigned to Al(V) and 50 ± 5 ppm assigned to Al(IV). The presence of Al(VI) at 0±5 ppm suggests incomplete dehydroxylation of aluminosilicate oxide. The author pointed out that the ideal calcination temperatures are between 700 °C and 800 °C. He reported that geopolymer processed from kaolinite calcined at 600 °C did not show any sign of exothermic behaviour during curing at 85 °C, which indicates that this material did not fully react. Geopolymer processed from kaolinite calcined at 750 °C showed strong exothermic behaviour during the curing stage.

Xu & Van Deventer (2000) proposed the ion-pair theory to explain the mechanism of Al-Si mineral dissolution as well as the mechanism of geopolymerisation. The possible chemical process for the dissolution of Al-Si minerals and silicates under alkaline solution can be expressed into a three-part reaction as follows:

$$\text{Al-Si solid particle} + OH^-(aq) \Leftrightarrow \underset{\text{monomer}}{Al(OH)^-_4} + \underset{\text{monomer}}{^-OSi(OH)_3} \qquad (2.6)$$

$$^-OSi(OH)_3 + OH^- \Leftrightarrow {}^-OSi(OH)_2O^- + H_2O \qquad (2.7)$$

$$^-OSi(OH)_2O^- + OH^- \Leftrightarrow {}^-OSi(OH)\underset{\displaystyle O^-}{\overset{\displaystyle |}{O}}{}^- + H_2O \qquad (2.8)$$

Reactions (2.6) to (2.8) are chemical hydration reactions, where OH^- anions react with Al-Si solid surface to form $Al(OH)^-_4$, $^-OSi(OH)_3$, divalent orthosilicic acid and trivalent orthosilicic acid ions.

The reactions between alkali metal cation M^+ with $Al(OH)^-_4$, $^-OSi(OH)_3$, divalent orthosilicic acid and trivalent orthosilicic acid ions, in order to balance Coulombic electrostatic repulsion, are physical electrostatic reactions shown below

$$M^+ + {}^-OSi(OH)_3 \Leftrightarrow \underset{\text{monomer}}{M^+ {}^-OSi(OH)_3} \qquad (2.9)$$

$$2M^+ + {}^-OSi(OH)_2O^- \Leftrightarrow M^{+-}OSi(OH)_2O^{-+}M \qquad (2.10)$$

$$3M^+ + \underset{\text{monomer}}{{}^-OSi(OH)O^-} \Leftrightarrow \underset{\text{monomer}}{M^{+-}OSi(OH)O^-\,M^+} \qquad (2.11)$$

$$M^+ + Al(OH)^-_4 + OH^- \Leftrightarrow M^{+-}OAl(OH)^-_3 + H_2O \qquad (2.12)$$

Reactions (2.13) to (2.16) are cation-anion pair condensation interactions based on Coulombic electrostatic attraction.

$$^-OSi(OH)_3 + M^+ + {}^-OSi(OH)_3 + M^{+-} \Leftrightarrow M^{+-}OSi(OH)_2\text{–O–}\underset{\text{dimer}}{Si(OH)_3} + MOH \qquad (2.13)$$

$$^-OSi(OH)_2O^- + M^{+-}OSi(OH)_3 + M^+ \Leftrightarrow M^{+-}OSi(OH)_2\text{–O–}Si(OH)_2O^- + MOH \qquad (2.14)$$

$$^-OSi(OH)O^- + M^{+-}OSi(OH)_3 + M^{+-}\,OSi(OH)_3 \Leftrightarrow M^+\,{}^-OSi(OH)O^-\text{–O–}\,Si(OH)_2O^- + MHO \qquad (2.15)$$

$$2 \text{ silicate monomers}^- + 2 \text{ silicate dimers}^- + 2M^+ \Leftrightarrow M^{+-} \text{ cyclic trimer} + M^{+-} \text{ linear trimer} + 2OH^- \qquad (2.16)$$

In reactions (2.12) to (2.16), the M^+ cation reacts with $Al(OH)^-_4$ and species of orthosilicic acid ions to form ion pairs of $M^{+-}Al(OH)_4$ monomer and silicate monomer, dimer and trimer ions, which reduce the amount of free $Al(OH)^-_4$ and the

species of orthosilicic acid ions, therefore shifting reactions (2.6) to (2.8) to the right hand side.

The effect of alkali-metal cations on the extent of aluminosilicate dissolution can be seen from reaction (2.10) to (2.16). It is known that cation-anion pair interaction becomes less significant as the cation size increases. The smaller cations favour the ion-pair interaction with the smaller silicate oligomers, such as silicate monomers, dimers and trimers. Because the ionic size of Na^+ is smaller than K^+, then Na^+ will be more active in reactions (2.10) to (2.16).

Rahier *et* al. (1996, 1997, 2000) reported an excellent investigation into dissolution and polycondensation of metakaolinite. The reaction below 100 °C of metakaolinite suspended in an alkali sodium silicate solution leads to an amorphous glassy aluminosilicate called *low-temperature inorganic polymer glass (LTIPG)*. The reaction stoichiometry for this polymer between a specific sodium silicate solution (with composition SiO_2/Na_2O = 1.4; H_2O/Na_2O = 10) and a specific calcined clay, metakaolinite (with composition $(Al_2O_3)(SiO_2)_2(H_2O)_{0.05}$) is as follows;

$$(Na_2O)(SiO_2)_{1.4}(H_2O)_x+(Al_2O_3)(SiO_2)_2(H_2O)_{0.05} \rightarrow (Na_2O)(Al_2O_3)(SiO_2)_{3.4}(H_2O)_z \quad \text{aq.}(<100^{\circ}C) \qquad (2.17)$$

x and z being the amount of bound water in the silicate solution and in the inorganic polymer glasses (LTIPG), respectively. By using differential scanning calorimetry (DSC), Rahier *et* al. (1996) showed that the above reaction is exothermic and a fast cure is realistic in isothermal conditions at around 60 °C. The maximum exothermic heat flow and thus the maximum reaction rate at this temperature was reached after 4 hours.

The inorganic polymer glass is formed with the ratio of silicate solution and metakaolinite equal to 1, such that the resulting material contains AlO_4^- tetrahedra with associated Na^+ ions in an amorphous network of SiO_4 tetrahedra with z = 0.4 bound water molecules. The researchers also found that the compressive strength and reaction enthalpy were maximised at this stoichiometric composition, corresponding to the complete dissolution and polycondensation of metakaolinite precursor.

A similar procedure was also used by Barbosa, MacKenzie & Thaumaturgo (2000) to produce synthetic inorganic polymer based on metakaolinite cured at room temperature and 65 °C. The work was intended to investigate the polymerisation mechanism and structure of Na^+-poly(sialate-siloxo) (Na-PSS). They reported that optimum curing and polymer properties are obtained when the Na concentration is sufficient to provide a charge-balancing mechanism for the substitution of tetrahedral Si by Al, but not in sufficient excess to form sodium carbonate by atmospheric carbonation. Polymer compositions that do not cure satisfactorily show evidence of carbonation. They also reported that the water content of the mixture is critical for satisfactory polymerisation – too little prevents adequate mixing and restricts ionic transport while excess water may dilute the reaction.

2.3.4 Sol-gel process of geopolymer precursors

As with zeolites, the production of synthetic aluminosilicates has also been studied intensively by using the sol-gel process (SGP) (Zarsycki 1988; Sinko & Mezei 1998; Pozarnsky & McCormick 1995; Hos 2000). The sol-gel process is a means of manipulating molecular precursors to form bulk oxide materials. Sol-gel processing of alkoxides has attracted intense interest because it offers non-melt routes to high-purity glasses and crystalline ceramics. Controlled hydrolysis–condensation reactions of the molecular precursors give successively: dimers, oligomers, polymers and a sol (a colloidal suspension of solid particles). In turn, the sol particles join together to form a gel, which is a highly viscous network of metal oxide bonds containing trapped solvent molecules (Gurney & Seymour 1995).

Sol-gel chemistry of tetra-alkoxy orthosilicates is based on hydrolysis and polycondensation as shown in equation 2.18 and 2.19 (Hos 2000).

$$Si(OR)_4 + 4H_2O \rightarrow Si(OH)_4 + 4ROH \qquad (2.18)$$

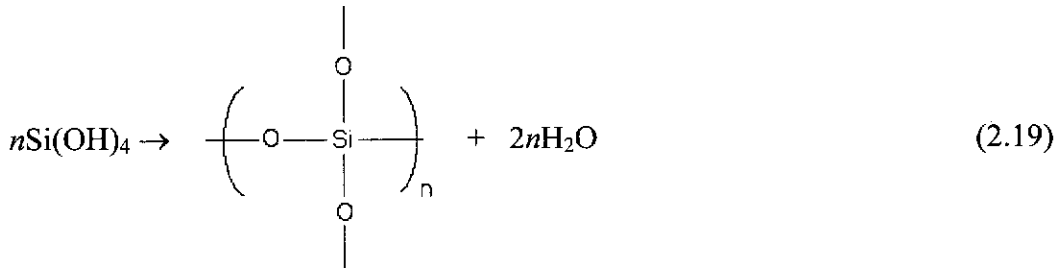

$$n\mathrm{Si(OH)_4} \rightarrow \text{(–O–Si(O)(O)–)}_n + 2n\mathrm{H_2O} \qquad (2.19)$$

Tetra-ethoxy orthosilicate (TEOS) reacts readily with water at ambient temperatures and produce amorphous gels after several hours. Transparent silica monoliths are obtained after a final calcination and sintering. Tri-alkoxy aluminium compounds hydrolyse in a similar way. Equation 2.20 shows a reaction to produce amorphous alumina from tri-alkoxy aluminium compounds

$$\mathrm{Al(OR)_3 + 3H_2O \rightarrow Al(OH)_3 + 3ROH} \qquad (2.20)$$

Reaction between aluminium tri-isopropoxide, TEOS and water will produce kaolinitic and mullitic precursors.

Theoretically, these geopolymer precursors can be used to produce amorphous aluminosilicates but the formation only works for acidic condition, not basic. As the colloidal particles grow in a basic solution, the high surface charge will cause them to repel each other and therefore inhibit the formation of a gel. This is evidenced by the fact that gels formed from high pH solutions redisperse in water, whereas those from low pH will not, which has been rationalised by the increased solubility of silica at high pH (Hos 2000).

Sinko & Mezei (1998) used similar preparation processes to produce aluminosilicate ceramics or glass materials and reported that up 70% of Al is chemically incorporated in the network. Aluminosilicate ceramics with high Al content are well known for their high chemical, electric and heat resistance and low thermal expansion.

2.4 Structure of Geopolymers

Inorganic aluminosilicate polymers or geopolymers, which result from dissolution and polycondensation of various alkali-aluminosilicates, are essentially X-ray amorphous materials. Figure 2.8 shows X-ray diffraction patterns of the starting materials (kaolinite and metakaolinite) and geopolymers of different molar oxide ratios of SiO_2/Al_2O_3, Na_2O/SiO_2, and H_2O/Na_2O.

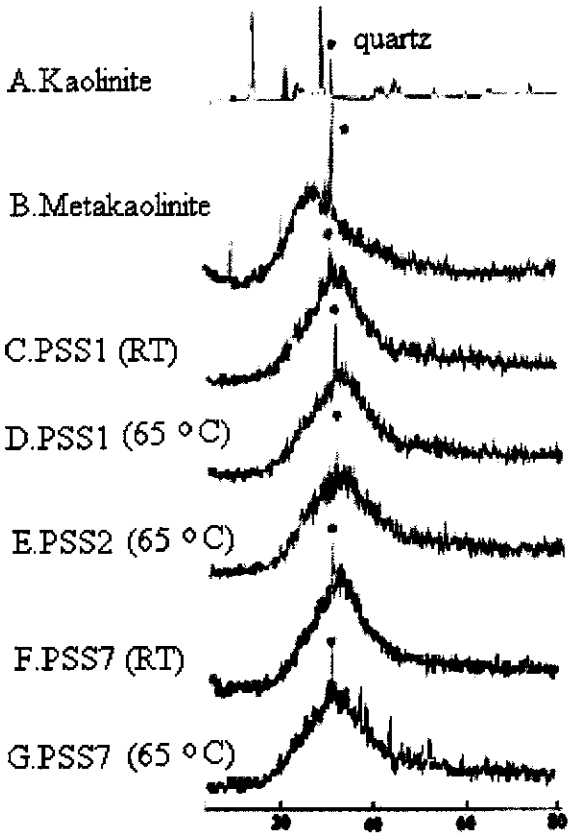

Figure 2.8 XRD patterns of the starting materials and Na-poly(sialate-siloxo, PSS) polymers (after Barbosa, MacKenzie & Thaumaturgo 2000). PSS1 (SiO_2/Al_2O_3 = 3.3, Na_2O/SiO_2=0.25, H_2O/Na_2O = 10), PSS2 (SiO_2/Al_2O_3 = 3.3, Na_2O/SiO_2 = 0.25, H_2O/Na_2O =25) and PSS7 (SiO_2/Al_2O_3 =3.8, Na_2O/SiO_2 = 0.30, H_2O/Na_2O = 17.5).

The kaolinite (figure 2.8A) shows a typical diffraction pattern of a well-ordered mineral. The quartz impurity (asterisked) remains as a sharp diffraction line after dehydoxylation at 750 °C (figure 2.8B) and polymerisation of the poly(sialate-siloxo) geopolymers with different oxide molar ratios cured at room temperature (RT) and at 65 °C (figures 2.8C to 2.9G).

The XRD patterns of all polymers show a similar amorphous character independent of curing treatment with a halo peak at about 27 – 29° 2θ. These data also suggest that the structure of all the polymers is similar to those of feldspatic glasses, consisting of randomly developed Al-Si polyhedra with a lack of periodically repeating atomic units.

Rahier *et* al. (1997) investigated the XRD patterns of Na-aluminosilicates as a function of the molar ratio of $s = SiO_2/Na_2O$. For s less than 0.8, peaks were detected suggesting that for these compositions the resulting aluminosilicates is at least partially ordered (figure 2.9).

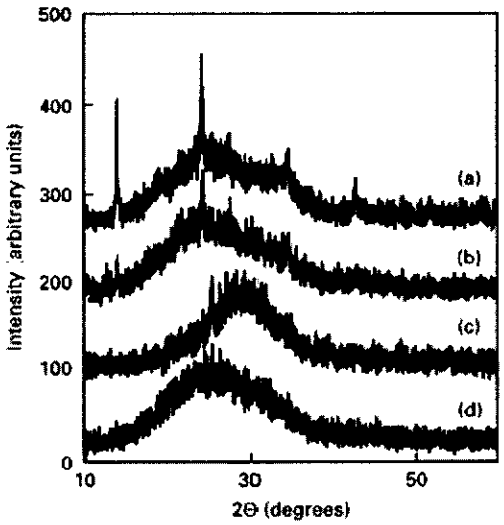

Figure 2.9 X-ray patterns of Na-aluminosilicates polymer with: (a) s = 0.0, (b) s = 0.4, (c) s = 0.8 and (d) s = 1.4 (after Rahier *et* al. 1997).

The presence of the crystalline material in the XRD patterns indicates that not all of kaolinite has been transformed into amorphous metakaolinite during the dehydroxylation process. The researchers pointed out that the reaction between kaolinite (crystalline) with NaOH yields hydroxysodalite (crystalline). When the molar ratio of $s = 0$ (pure NaOH) is reacted with metakaolinite, traces of hydroxysodalite are detected with XRD and FTIR. In order to make sure that the crystalline fraction did not originate from Na-silicate, aluminosilicates samples were prepared and heated up to 180 °C, far above the melting point of Na-silicate crystals, before further investigation by XRD. However, the same diffraction lines were still present. By comparing the height of discrete crystalline diffraction peaks with the

underlying amorphous part, they concluded that the crystalline fraction increases with decreasing *s*.

The amorphous nature of geopolymers prevents structural characterisation using XRD results alone. In order to fully understand the structure of geopolymers it is necessary to utilise Magic-Angle Spinning-Nuclear Magnetic Resonance (MAS-NMR) spectroscopy. A brief discussion about this powerful technique is given below.

Nuclear Magnetic Resonance (NMR) is a phenomenon that occurs when certain nuclei like ^{13}C and ^{19}F are immersed in a static magnetic field and exposed to a second oscillating magnetic field. Such nuclei can absorb electromagnetic radiation in the radio frequency range and are said to be *spin-active* (with quantum number spin $I \neq 0$) and *resonate*. A fundamental observation about the NMR phenomenon is that the energy difference (ΔE) between spin states is directly proportional to the magnetic field strength. The precise frequencies at which spin-active nuclei resonate can be detected and displayed by an instrument called an NMR spectrometer.

For inorganic solid-state characterisation, the NMR resolution is hampered by the direct magnetic dipolar interaction between two adjacent nuclear spins. In order to increase the resolution in NMR spectra for inorganic materials a line-narrowing technique is used. In this case, the sample is rotated about an axis that make an angle of 54.74° (the magic angle) with respect to the static B_0 field. This method is known as Magic Angle Spinning - Nuclear Magnetic Resonance (MAS-NMR). When the rate of rotation is faster than the width of the powder pattern (in Hz), the anisotropic portions of the chemical shift (δ) and dipolar interactions will disappear, leaving a narrow line at the isotropic chemical shift position. The chemical shift, δ (in ppm) reflects the magnetic shielding of a nucleus by neighbouring electron clouds and is the most commonly used NMR parameter (Fitzgerald & DePaul 1998, p.14-15).

Where present, ^{27}Al and ^{29}Si nuclei are particularly used to study the structure of inorganic solid materials and have been recently applied to geopolymers. MAS-NMR studies of aluminosilicate materials resulted in the use of the nomenclature of

Engelhardt and Hoebel known as *$Q_n(mAl)$ and $Q_n(mSi)$ notation* (*n* ranges from 0 to 4) for Al and Si environments. *$Q_n(mAl)$* notation denotes an AlO_4 tetrahedron with n bridging oxygen atoms containing *m* Al-O-Si links and *$Q_n(mSi)$ notation* describes an SiO_4 tetrahedron with *n* bridging oxygen atoms containing *m* Si-O-Al links (Davidovits 1991; Pozarnsky & McCormick 1995; Rahier *et* al.1996; Barbosa, MacKenzie & Thaumaturgo 2000; Mozgawa *et* al. 2002).

^{27}Al MAS-NMR spectra provide information on the environment of aluminium atoms in the structure. Spectra of aluminate anions showed that 4-coordinated aluminium (with respect to oxygen) resonates at 60-80 ppm, and that in aluminosilicates, 4-coordinated aluminium resonates at 50±20 ppm while 6-coordinated aluminium from $[Al(H_2O)_6]^{3+}$ resonates at about 0±10 ppm. (Davidovits 1991). The Loewenstein aluminium avoidance principle states that, whenever two tetrahedra are linked by one oxygen, only one can be occupied by Al and there can be no Al-O-Al bridge. In the absence of Al-O-Al linkages the environment of every Al atom is Al(4Si). This rule is obeyed in aluminosilicates anions. The exclusion of Al-O-Al linkages sets the number of possibilities to five $Q_n(m\text{Si})$ structural units with $m = 0, 1, 2, 3,$ and 4.

In ^{29}Si MAS-NMR studies, the silicon environment is described by $Q_n(m\text{Al})$ (written as $SiQ_n(mAl)$ in accordance to the Davidovits notation) and each one of these five environments has a corresponding range of resonances in a ^{29}Si MAS-NMR spectrum: $SiQ_4(4Al)$ from –80 to –90 ppm, $SiQ_4(3Al)$ from –85 to –95 ppm, $SiQ_4(2Al)$ from –90 to –100 ppm, $SiQ_4(1Al)$ from –95 to –105 ppm, and $SiQ_4(0Al)$ from –100 to –115 ppm.

^{27}Al MAS-NMR spectroscopy of potassium poly(sialate-siloxo) or K-PSS geopolymers showed ^{27}Al chemical shifts in the range of 55 ppm from $[Al(H_2O)_6]^{3+}$ (Figure 2.10a). The peak lies within the chemical shift range of tetrahedral Al surrounded by four SiO_4 groups. Hence, aluminium is of the $Q_4(4Si)$ type (written as $AlQ_4(4Si)$ according to the Davidovits notation). This implies that the cross-link density of Al is four (the cross-link density or connectivity is defined as the number of bridging oxygen atoms).

The spectra of ^{27}Al MAS-NMR cannot be used to distinguish between the various poly(sialate), poly(sialate-siloxo) or poly(sialate-disiloxo) structural units in geopolymers. This differentiation can be achieved with ^{29}Si MAS-NMR spectroscopy (Figure. 2.10b). The resonances found for disordered ^{29}Si in geopolymer, namely -81.5 ppm, -87 ppm and -94.5 ppm can be assigned to $SiQ_4(4Al)$, $SiQ_4(3Al)$ and $SiQ_4(2Al)$, respectively. Aluminosilicate with Si/Al > 2 generally display several ^{29}Si resonances suggesting that the Si and Al tetrahedra are not regularly ordered along polymeric chains and that different coordination environments are present. The degree of ordering can be inferred from the lineshapes and peak widths.

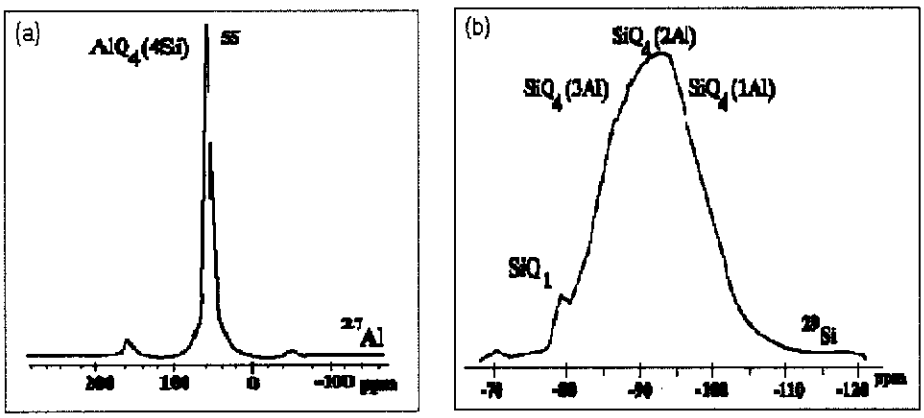

Figure 2.10 (a) ^{27}Al MAS-NMR (b) ^{29}Si MAS-NMR of geopolymers (after Davidovits 1991).

Based on the results of ^{27}Al and ^{29}Si MAS-NMR as well as XRD, Davidovits (1994) proposed a structural framework model for potassium poly(sialate-siloxo) geopolymer as shown in figure 2.11. The structure shows that Si is bound to zero (i.e. four Si centres), one, two or three Al centres through bridging oxide links. Si and Al are randomly distributed along the polymeric chains that are cross-linked so as to provide cavities of sufficient size to accommodate the charge-balancing potassium ions.

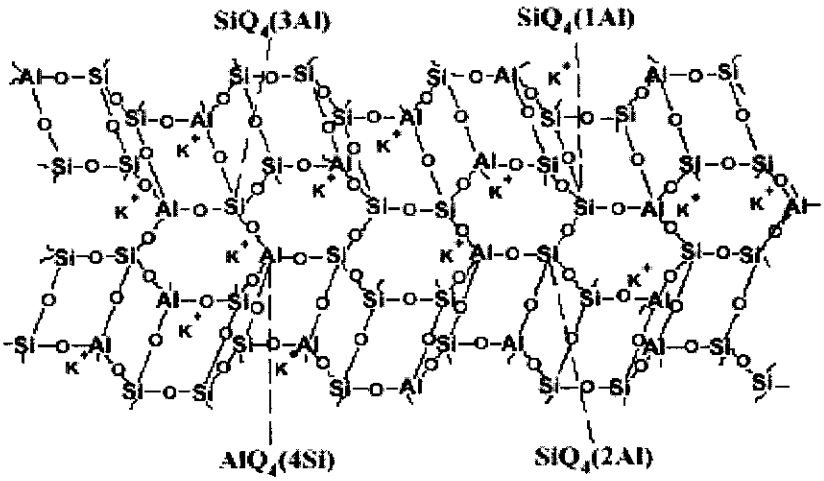

Figure 2.11 Proposed potassium poly(sialate-siloxo) geopolymer structural framework (after Davidovits 1994a).

Barbosa, MacKenzie & Thaumaturgo (2000) also utilised XRD patterns, FTIR spectra as well as ^{27}Al and ^{29}Si MAS-NMR spectra to study the structure of Na-poly(sialate-silixo) geopolymers based on metakaolinite. They proposed a structure of Na-poly(sialate-siloxo) which is similar to glasses or hydrated silicate minerals having a range of Si environments, but predominantly those of framework structures saturated in Al such as $SiQ_4(3Al)$. All of the Al is essentially in tetrahedral sites and has Si nearest neighbours, distributed randomly along the polymeric chains. These requirements lead to a structural model for Na-poly(sialate) polymer similar to figure 2.11. Their proposed structure, however, shows relatively greater disorder.

2.5 Geopolymer Cements

Alkali-activated, chemically bonded cement is considered as a special type of cement. Numerous sources of alumina and silica are potentially available to produce this cement. The production of this cement is often based on the utilisation of solid wastes and by products such as fly ash and blast furnace slag that may have pozzolanic or latent hydraulic properties. The hydraulic properties of these materials are influenced by their chemical composition, specific surface area and by the type of activation used. Extensive use has been made of glassy slag in the former Soviet Union and Finland. Blast furnace slag is usually granulated and ground to a surface area of 5000 cm^2g^{-1}, but the mix water is replaced by an equivalent volume of 10 –

30% NaOH or KOH solution. Other activators such as gypsum ($CaSO_4.2H_2O$) and its soluble anhydrate ($CaSO_4$) can also be used (Glasser 1995).

It has been mentioned that during the 1980s, Davidovits intensively studied the production of alkali-activated cement by using dexydroxylated kaolinite. The resulting cement which is now known as geopolymer cement or (K-Ca) poly(sialate-siloxo) cement was claimed to have unique properties such as high early strength, low shrinkage, freeze-thaw resistance and acid resistance. The most significant impact of geopolymer cements is its potential to contribute to environmental protection.

A (K-Ca) poly(silate-siloxo) ((K-Ca)-PSS cement, Si:Al = 2) comprises three major compounds, namely:

- Specific aluminosilicate of kaolinitic clay species, calcined at 750°C;
- Alkali-disilicates (Na_2 or K_2) $(H_2SiO_4)_2$;
- Calcium disilicates $Ca(H_3SiO_4)_2$.

Calcium disilicate, $Ca(H_3SiO_4)_2$, can be manufactured by a hydrothermal reaction between lime and silica. Geopolymerisation of these compounds based on dissolution and polycondensation reactions at low temperature (<100 °C) yield a three dimensional polymeric structure containing Si-O-Al bonds as follows:

$$2(Si_2O_5,Al_2O_2)+K_2(H_2SiO_4)_2+Ca(H_2SiO_4)_2 \rightarrow (K_2O,CaO)(8SiO_2,2Al_2O_3,nH_2O) \quad (2.21)$$

Unlike ordinary Portland cement, geopolymeric cements do not rely on lime and are not dissolved by acidic solutions. Setting of geopolymeric cement takes place through polycondensation of potassium-oligo-(sialate-siloxo) into potassium poly(sialate-siloxo) crosslinked network (figure 2.12) (Davidovits 1999).

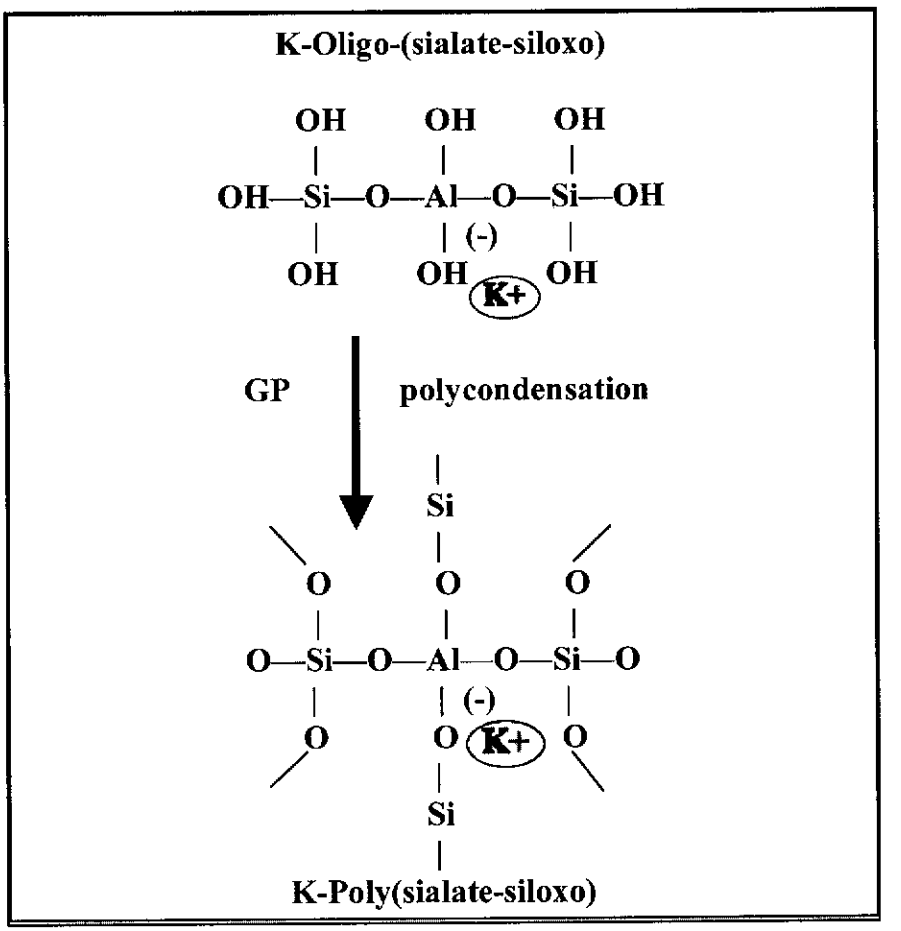

Figure 2.12 The setting process of potassium poly(sialate-siloxo) geopolymeric cement (redrawn, after Davidovits 1999).

Structural integrity and reasonable strength of the resulting material are attained in a very short time. In most cases, 20% to 30% of the final compressive strength is developed in the first few hours of setting. The high early-strength of geopolymer cement designed particularly for waste containment can be enhanced with the adjunction of microwave preheating devices in order to raise the temperature of the waste up 30-35 °C (Davidovits 1994a).

The ability to absorb toxic chemical wastes such as arsenic, mercury and lead makes geopolymer cement comparable to zeolites. Geopolymer cements immobilise hazardous elemental wastes within the matrix as well as act as a binder to convert semi-solid waste into an adhesive solid. The ability of geopolymer cements to provide immobilisation systems for toxic wastes is due largely because of their

properties such as acid resistance as well as their low permeability (table 2.1) (Davidovits 1994a).

Table 2.1 Permeability values (cm/s) (after Davidovits 1994a).

Sand	10^{-1} - 10^{-3}
Fly ash cement	10^{-6}
Clay	10^{-7}
Geopolymer cement	10^{-9}
Portland cement	10^{-10}
Granite	10^{-10}

The technology of geopolymerisation has been applied to produce some cement-related products that can be bought commercially (Davidovits 1991, Davidovits 1994a). Despite their superior properties over Portland cement, geopolymer binders have not been widely used mainly because of higher costs. If the cost of production can be reduced, geopolymer cements will eventually meet their applications in many areas such as:

- Massive concrete panels, grouts, and fiber reinforced sheets.
- Building component such as bricks and ceramic tiles.
- Structural surfaces such as floor and storage areas as well as runways.

2.6 Physical and Mechanical Properties of Geopolymers

2.6.1 The strength of geopolymers

In section 1.3, it was stated that geopolymers transform, polycondense and form a dimensionally stable mass at low temperature that is hard, weather and chemical resistant and able to withstand high temperature. Typical geopolymers made from metakaolinite have a Mohs hardness of 4 – 7 and they are stable up to 1200 °C (Barbosa, MacKenzie & Thaumaturgo 2000).

Physical as well as mechanical properties of geopolymers can be tailored by the alteration of the atomic ratio of Si:Al precursors. Geopolymers with low Si:Al (1, 2,

3) initiate a 3D-network that is very rigid which make them suitable for bricks, cements, toxic immobilisation and fire protection, while those with Si:Al > 20 provide polymeric character to the geopolymer materials and are suitable for fire or heat resistant composites for aerospace or automobile industries (Davidovits 1999; Lyon *et* al. 1997; Xu & van Deventer 2000; Hermann *et* al. 1999; Cheng & Chiu 2003).

Rahier *et* al. (1996) studied the compressive strength of aluminosilicate inorganic polymers containing sand (quartz) as a filler material with a mean particle size of 240 μm for samples with dimensions of 20x30x40 mm. The addition of sand was intended to reduce crack formation as well as to control the porosity. They reported that the compressive strength of their polymer is strongly dependent on the molar ratio of Sil/Mk = k, defined as the stoichiometric ratio of sodium in the silicate solution to aluminium in aluminosilicate materials. The optimum compressive strength is obtained at k = 1, suggesting that this strength was associated with the complete reaction of the aluminium from metakaolinite with the sodium from the silicate solution (figure 2.13).

Rahier's observations, however, are in disagreement with the data reported by Hos, McCormick & Byrne (2002). They reported that the compressive strength of their inorganic polymer synthesised from melt-quenching aluminosilicate ($Al_2O_3.2SiO_2$) pellet increased with decreasing k and achieving maximum strength at k = 0.36. In addition, the maximum compressive strength of their materials was about 360 MPa or 6 times higher than that reported by Rahier *et* al. (1996). This discrepancy probably originated from the difference of the starting material, as well as the preparation route they used.

One major problem still confronting the strength of geopolymers synthesised from aluminosilicate minerals such as metakaolinite or fly ash is porosity due to air bubbles caused by the evaporation of water during polymerisation. It is well known that porosity decreases the strength of ceramics and cementitious materials (Rahier *et* al. 1996; Zhang & Malhotra 1998).

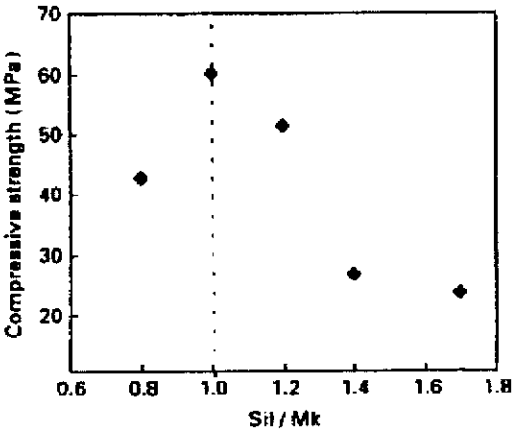

Figure 2.13 Compressive strength of aluminosilicate inorganic polymer as a function of *k* (Sil/mk) (after Rahier *et* al. 1996).

Jiang & Guan (1999) studied the effect of pore structure on the strength of high-volume fly ash paste. They reported that the relationship between the total porosity and compressive as well as flexural strength is linear. Pores with radii > 100 nm show a great effect on the reduction of the compressive strength. They also reported that the total porosity of the paste increased with increasing fly ash content and water/binder ratio.

2.6.2 Microstructural character of geopolymers

Hos, McCormick and Byrne (2002) systematically analysed the microstructure of aluminosilicate inorganic polymer. By using scanning electron microscopy (SEM) they observed the nanoporous microstructure of their materials (figure 2.14). According to the authors the nanoporous structure is a result of extensive dissolution of aluminosilicate species that occurs before polycondensation commences and consolidates the shapes of the specimen through a chaotic three-dimensional network of polysodium aluminosilicate. For specimens with low *k,* the researchers observed up to 40 % unreacted or partly reacted grains of metakaolinite. The presence of unreacted metakaolinite in the matrix creates a composite-like microstructure of geopolymers and act as *in-situ* reinforcement responsible for high strength materials.

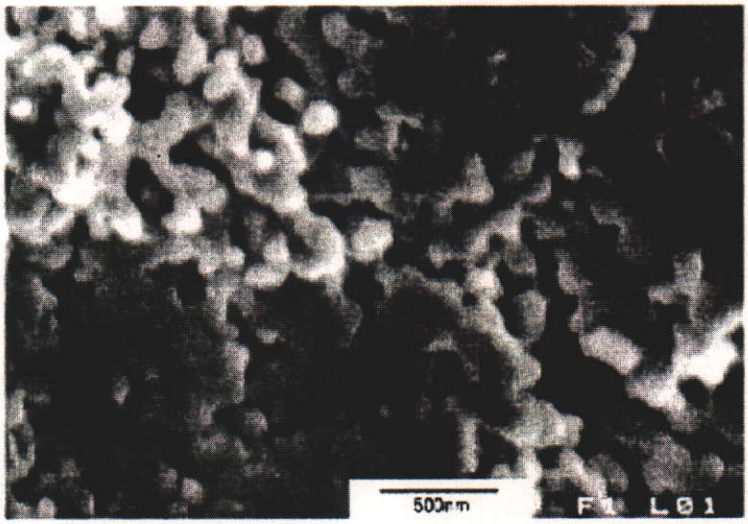

Figure 2.14 High-resolution electron micrograph of aluminosilicate inorganic polymer showing nanoporous microstructure (after Hos, McCormick & Byrne 2002).

The researchers also reported the formation of needle like-crystals of sodium carbonate on the surface of the specimen as a result of the reaction between the residual sodium silicate with atmospheric CO_2. The formation of sodium carbonate on the surface of geopolymers has also been observed by Barbosa, MacKenzie & Thaumaturgo (2000) as indicated by the band at about 1460 cm^{-1} of FTIR spectra. This suggests that excess sodium is transported by the water to the surface during evaporation to form sodium carbonate.

Alkali-activated cement based on fly ash also exhibits a high density of pores or air bubbles. Figure 2.15 shows the microstructural character of alkali-activated fly ash. The material is very porous and the microspheres (originating from fly ash grains) are surrounded by a crust of reaction product. The adherence of the crust to the spheres does not appear to be very strong and the bond between grains is produced through the necks of reaction products (figure 2.15a). Crack development is evident in the middle of the matrix and is likely to have been initiated from the pore (figure 2.15b) (Palomo, Grutzeck &Blanco1999).

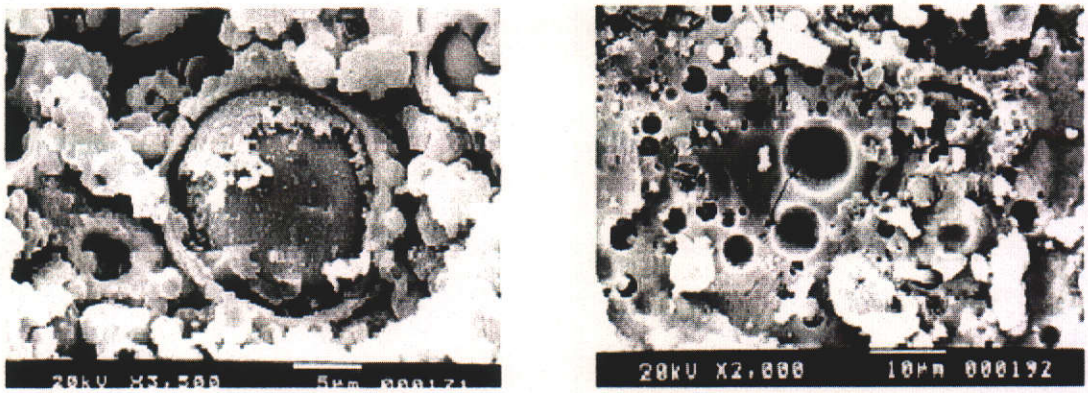

(a) (b)

Figure 2.15. Microstructure of alkali-activated flay ash (after Palomo, Crutzeck & Blanco 1999).

2.7 The Role of Aggregate

2.7.1 Influence of aggregate on strength

The inclusion of natural occurring materials such as sand (quartz), basalt, granite, sandstone and limestone as aggregate into a brittle matrix is expected to optimise the microstructure, reduce pore density as well as to reduce the risk of crack formation in geopolymers. A certain amount and a correct size of aggregate may be beneficial to the strength and fracture toughness of ceramic, composites and cement-based materials.

In the production of mortar and concrete, natural or industrially manufactured aggregate is added as a material dispersed throughout the cement paste for economic reasons. Aggregate is cheaper than the cement itself. Beside the economic reason, the inclusion of aggregate offers technical advantages as it has a higher volume stability and better durability than the cement paste alone. Therefore, the inhomogeneous structure of concrete can be described as a three-phase system consisting of hardened cement paste, aggregate and the interface between the aggregate and cement paste.

The physical and mechanical properties of aggregate such as particle size and texture, bulk density, porosity and the strength play a particular role in determining the quality of mortar or concrete. The bond between aggregate and cement paste is an

important factor in determining the compressive and flexural strength of mortar and concrete. A strong bond normally occurs due to mechanical interlocking between the aggregate and cement paste, which is controlled by the roughness of the surface, the shape, the density of pores as well as a chemical relation between aggregate and cement paste (Wasserman & Bentur 1996; Bouguerra *et* al. 1998; Neville 2000, p.117-119; Rao 2001; Husem 2003; Akcaoglu, Tokyay & Celik 2003). Alkali-aggregate reaction has been found to influence the strength and durability of concrete particularly in high-alkali cements and granite aggregate (Tasong, Lynsdale & Cripps 1998; Owsiak 2004; Mladenovic *et* al. 2004).

The ratio between aggregate and cement paste also plays an important role in determining the strength of concrete. Neville (2000. p.287-288) pointed out that when the volume of aggregate (as a percentage of the total volume) is increased from zero to 20 there is a gradual decrease in compressive strength, but between 40 and 80% there is a slight increase (figure 2.16).

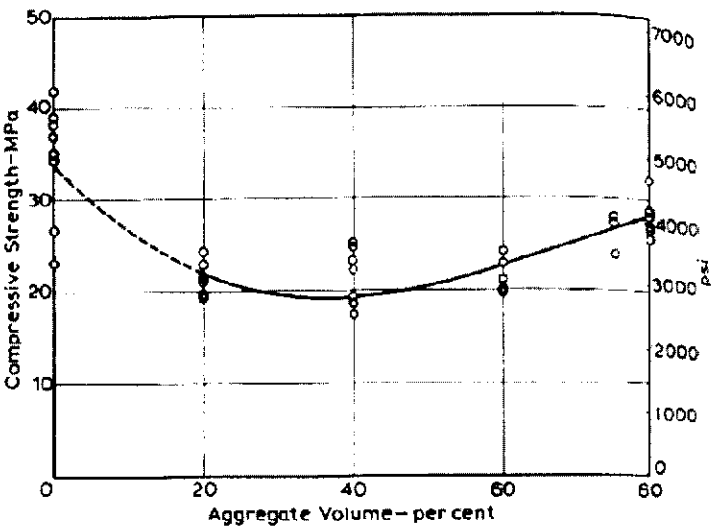

Figure 2.16 Relationship between the compressive strength and volume of aggregate at a constant water/cement ratio of 0.5 (after Neville 2000, p.288).

Based on the current literature very little work has been conducted on determining the role of aggregates (quartz and other type of aggregate materials) on the toughening mechanism, interfacial bond strength as well as the microstructure character of the interfacial bond between the geopolymer matrix and the aggregate.

Davidovits (1988) used fine quartz in the production of Na-PS-quartz block composites. In this composite, the quartz crystals are surrounded with kaolinite micelles, and the sequence of this Na-PS-quartz blockcomposite (which he called SILIFACE Q) is designated as -(Na-PS)-(SiO_2)n-(Na-PS)-SiO_2)n-. The siloxane link (Si-O-Si) on the surface of quartz is hydrolysed into silanol (Si-OH). These silanols polycondense with the sialates or polysialates from the surrounding kaolinite (figure 2.17).

SILIFACE Q has been successfully fabricated into industrial ceramics and mortars and it is known as a low temperature geopolymeric setting (LTGS) ceramic (processed in temperature range between 50 °C and 500 °C). The bulk density of these ceramics is about 1.9 gcm^{-3} with an apparent porosity of about 30 %. The compressive strength of these LTGS ceramics have reached about 40 MPa (Davidovits & James 1988).

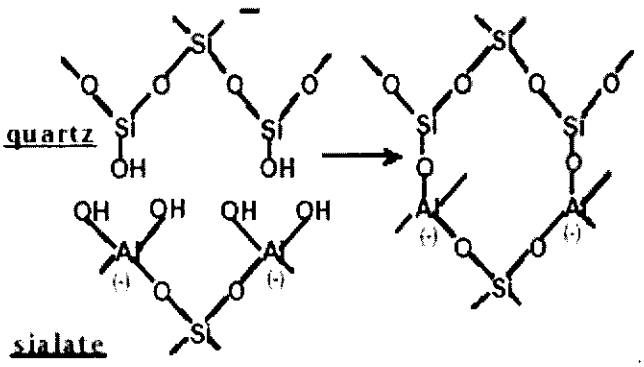

Figure 2.17 Polycondensation of quartz silanols Si-OH with poly(sialate) Al-OH or silanol Si-OH (after Davidovits 1988).

As mentioned in section 2.6, work by Rahier *et* al. (1996) used specimens for mechanical testing containing sand with a mean particle size about 240 μm. The objective of their study, however, was specifically aimed to minimise the porosity as well as to prevent self-cracking of the specimen after demoulding. There were no cracks observed in these specimens and the apparent porosity for all the specimens was almost constant at about 26%. The compressive strength of these materials ranged from 23 MPa to 60 MPa depending on *k* ratio as shown in figure 2.13. The

researchers, however, did not attempt to compare the strength of their materials with those prepared with no sand aggregate.

Hos, McCormick & Byrne (2002) also used sand as aggregate in their materials with a mean particle size of 200 μm to prevent the tendency of cracking of aluminosilicate inorganic polymers particularly for samples with $k > 0.8$. Samples with lower values of k did not exhibit any cracking with or without the addition of silica aggregate. They reported that the addition of sand particles appeared to have a negligible effect on the compressive strength of the specimens. There was no explanation given by the researchers regarding their findings. Qualitatively, according to Davidovits (Curtin's geopolymer workshop, October 2002) the bond between sand (quartz) and geopolymer matrix is relatively weak and hence the incorporation of sand as an aggregate will not significantly increase the compressive strength of geopolymers although it can be used to prevent self-cracking before demoulding.

More recently, Barbosa and MacKenzie (2003) reported the thermal behaviour and the strength of geopolymer composites. The composites consisted of sodium polysialate geopolymers as the matrix and 10 – 20 vol % of 6 different inorganic fillers (crushed brick, granite, kaolinite, iron sand, α-alumina and β-sialon) as aggregate. They reported that the strength of all composites was much less than the strength of unfilled geopolymer matrix.

2.7.2 Interfacial Transition Zone (ITZ)

The region in which the presence of inclusions affects the properties of the cement paste (matrix) is known as the Interfacial Transition Zone (ITZ). The morphology, composition, density and other features in the ITZ differ from those of the matrix (Akcaoglu, Tokyay & Celik 2003). In this zone the porosity is greatest near the aggregate and decreases with increasing distance from the aggregate (Lutz, Monteiro & Zimmerman 1997; Elsharief, Cohen & Olek 2003).

According to Shi & Xie (1998) there are several mechanisms contributing to the formation of a porous zone around the aggregates:

- Formation of a water layer on the non-porous aggregate surface at the beginning of the mixing, inhibiting anhydrous grains from coming into contact with the interface.
- Flocculation of cement grains in contact with the aggregate, resulting in high local porosity.
- Inadequate intergrain filling due to the wall effect, resulting in high local porosity.

Apparently, the microstructure at the interfacial zone plays important roles in the mechanical properties and durability of cement-based materials such as mortar and concrete, and this has been a subject of numerous studies in the field of cement and concrete (Aquino *et* al. 1995; Zhandarov & Pisanova 1997; Shie & Xie 1998; Tasong, Lynsdale & Cripps 1998; Wong *et* al. 1999; Diamond & Huang 2001; Rao 2001; Rocco, Guinea & Elices 2001; Guinea *et* al. 2002; Rao & Prasad 2002; Caliskan 2003; Elsharief, Cohen & Olek 2003).

The inclusion of aggregate can be beneficial in enhancing the toughness and fracture resistance of cement based materials and composites. The enhancement of fracture resistance due to the presence of aggregate can be explained by several mechanisms (Amparano, Xi & Roh 2000; Merchant *et* al. 2001):

- Microcrack shielding which causes a reduction in stress within the fracture process zone (FPZ);
- Crack bridging which provides closing pressure in the FPZ;
- A crack becomes pinned when it meets an array of impenetrable obstacles.

The ability of aggregate to act as a crack-bridging agent depends upon the ability of the aggregate particle to anchor the matrix on both sides of a crack so that crack face separation is inhibited. According to Merchant *et* al. (2001) if the aggregate particle is fully bonded to the matrix there is no guarantee that the toughness of the material is increased. This is due to the crack detaching early and not allowing the formation of a bridge. If the aggregate particle is too weak, crack propagation may occur through the aggregate particle and therefore no bridging occurs.

Tasong, Lynsdale & Cripps (1998) noted that the bond behaviour between the aggregate and the cementitious matrix (ordinary Portland cement) depends on three different mechanisms. These are: the mechanical keying of the hydration products of cement with the rough surface of the aggregate (often covered with fine cracks); the epitaxial growth of hydration products at some aggregate surface; and the physical-chemical bond between the hydrated cement paste and the aggregate, due to a chemical reaction. By using a single aggregate pull-out method, the researchers studied the aggregate-cement paste (ordinary Portland cement) interface using three different aggregates (basalt, limestone and quartzite). They pointed out that the interfacial bond strength increases with increasing surface area available for bonding (i.e. increasing roughness), however, the aggregate must be mechanically strong enough at its bonded surface to withstand this increase in bond strength. The researchers observed that quartzite aggregate provides higher bond strength than limestone and basalt aggregate. They also noted that a pozzolanic reaction between Si^{4+}, leached out from quartzite, and the CH may possibly be the reason for this high bond strength.

Similarly, Caliskan (2003) investigated the interfacial bond strength between aggregate and mortar made from Portland cement (plain mortar and 20% silica fume mortar) using an aggregate push-out experiment. He reported that sandstone aggregate was found to provide the highest interfacial bond strength in Portland cement-based mortar, followed by granite and limestone aggregate. This can be related to the coarse texture of sandstone, which provides extra strong mechanical interlocking between the matrix and the aggregate. He also observed that the interfacial bond strength increases as the aggregate size decreases, irrespective of the type of aggregate and mortar matrix.

Chapter 3

EXPERIMENTAL METHODS

3.1 Sample Preparation

Geopolymers prepared in this study were prepared by alkali-activation of dehydroxylated kaolinite. Kaolinite is one of the main sources of naturally occurring alumino-silicates. At least 55 % of the volume of the Earth's crust is composed of siloxo-sialates (Davidovits, 1999) and it was deemed important to explore and optimise the use of this abundant material for the production of geopolymers.

3.1.1 Starting materials (kaolinite and metakaolinite)

Kaolin (Chinese *Kauling* = *high ridge*) is a fine, white clay mineral that has been traditionally used by Chinese people in the manufacture of porcelain and other ceramic materials. Kaolinite is the mineralogical term that is applicable to clay minerals. It is defined as a hydrated aluminium disilicate, $Al_2Si_2O_5(OH)_4$ resulting from continental weathering where solutions percolate and are purified over time. Kaolinite cannot develop in sedimentary basins where solutions accumulate and are enriched (Chen, Lin & Zheng, 1997).

The kaolinite used in this study was paint/filler Grade Kaolin Clay (Kingwhite 65) supplied by Unimin Australia Limited. The particle size distribution of the material is: 0.05 % > 53 μm screen residue, 8.0 % > 10 μm, 24 % > 2 μm (and < 10 μm) and 68 % < 2 μm. The pH (20% suspension) is 7.0 and specific gravity is 2.6. The mineralogical analysis, performed by the supplier, showed that the material contained 99 % kaolinite and a trace of quartz (see Table 3.1).

Sodium silicate solutions were used as activators and the soda content was increased by the addition of sodium hydroxide (NaOH) pellets. Tap water was used through out the processing of the materials. Sodium silicate solution and sodium hydroxide

were supplied by Sigma Chemical Ltd. Australia. The chemical composition of the sodium silicate is presented in table 3.1.

Table 3.1 Chemical composition of the starting materials

Component (%)	Kaolinite	Sodium silicate
Al_2O_3	37.8	-
SiO_2	46.4	30.1
K_2O	0.21	-
Na_2O	0.01	9.4
CaO	0.08	-
MgO	0.15	-
Fe_2O_3	0.8	-
TiO_2	0.8	-
LOI (1000°C)	13.8	-
H_2O	-	60.5

Metakaolinite was obtained by dehydroxylation of kaolinite at 750 °C. Dehydroxylation was performed using a low temperature furnace (Kiln Manufacture of W.A.) with a heating rate of about 10 °C/minute. The temperature was maintained at 750 °C for about 6 hours to ensure a complete dehydroxylation of the kaolinite.

The processing of Na-Poly(sialate) and Na-Poly(sialate-siloxo) was performed by adopting the range of molar oxide ratios suggested by Davidovits (1982) and Davidovits & Sawyer (1985). Chemical compositions of the activation solution in terms of the molar oxide ratio used in this study were divided into 3 groups as shown in table 3.2. In each group, the nominal Si:Al ranged from 1 to 2 while varying Na:Al from 0.6 for group A, 0.8 for group B and 1.0 for group C.

Table 3.2 Molar oxide ratios used in the production of geopolymers.

Group	SiO_2:Al_2O_3	Na_2O:SiO_2	H_2O:Na_2O
A	2.00	0.30	10
	2.50	0.24	10
	3.00	0.20	10
	3.50	0.17	10
	4.00	0.15	10
B	2.00	0.40	10
	2.50	0.32	10
	3.00	0.27	10
	3.50	0.23	10
	4.00	0.20	10
C	2.00	0.50	10
	2.50	0.40	10
	3.00	0.33	10
	3.50	0.28	10
	4.00	0.25	10

Throughout this project, the oxide molar ratio of H_2O:Na_2O was kept at a value of 10. At this value the water content of the sodium silicate mixture was adequate to facilitate geopolymerisation without deterioration of the mechanical properties of the geopolymer. It has been recognised that the water content of the mixture is ultimately important in facilitating ion exchange and controlling the polymerisation process (Rahier *et* al. 1996; Barbosa, MacKenzie & Thaumaturgo 2000).

The sodium silicate solution, sodium hydroxide pellets and water were mixed and hand-stirred until dissolution occurred. Initially the temperature of the mixture was quite high, so it was left until it reached room temperature before proceeding. Geopolymer resins were obtained by the addition of metakaolinite powder to this solution followed by hand mixing or using a shake mixer to ensure homogeneity. The mixing normally took place between 5 – 10 minutes depending on the volume of the starting materials. The pH of the sodium silicate solution and geopolymer resins were measured using a digital pH meter from Dick Smith Electronics (Q1416), with pH resolution of 0.01. A standard buffer solution with a pH of 10 was used for pH electrode calibration.

Natural sand in the form of α-quartz with different particle size was used as aggregate and poured directly into the geopolymer resin. The sand used in this study was similar to that used for standard mortar and concrete production. The sand was sieved, washed with water and left to dry overnight before processing. The grain size and concentration of sand aggregate used were 40 μm, 125 μm, 212 μm, 500 μm and 750 μm, and 10 wt %, 20 wt %, 30wt % and 50 wt %, respectively. Another type of aggregate used was granite (known as blue metal), which was crushed and sieved to attain a grain size of 300 μm and 600 μm. For measurement of interfacial bond strength sandstone was included as a third "aggregate".

The resulting geopolymer resin was poured into polycarbonate cylindrical moulds (30 ml container, 2.50 cm in diameter and about 6.00 cm in height), compacted manually using a spatula and vibrated for a few minutes to release air bubbles and allowed to mature at room temperature for 30 - 60 minutes. Curing was undertaken at 70 °C for 2 hours followed by drying at room temperature before demoulding. During the curing stage the water, that is essential for polymerisation, was retained by sealing the top of the moulds.

Figure 3.1 shows a photograph of the resulting geopolymers, with and without the addition of sand aggregate. The samples with a height of 5.00 cm and 2.50 cm in diameter were prepared for compression tests. The 1.00 cm high samples were used for hardness testing as well as for density and apparent porosity measurements.

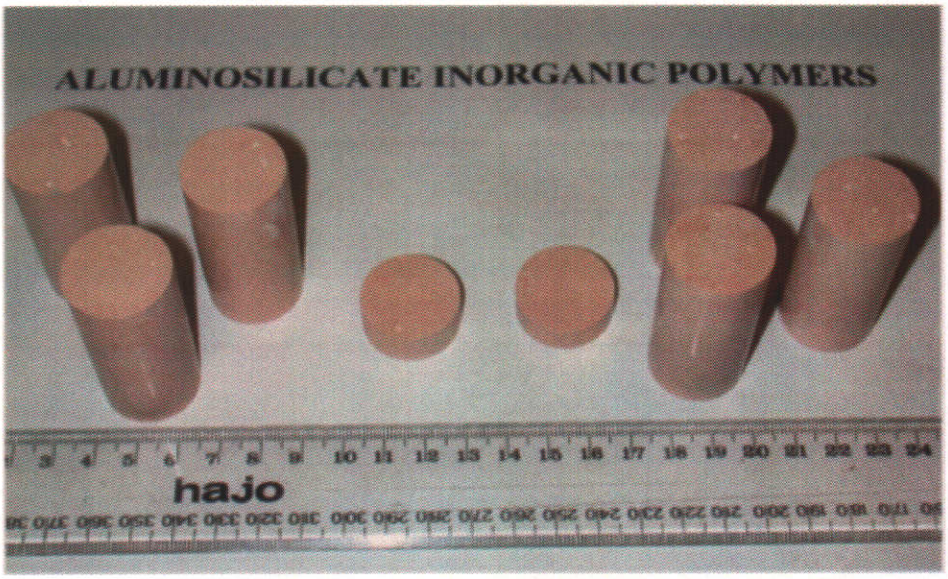

Figure 3.1 Geopolymer samples prepared in this study.

3.2 Materials Evaluation

This section describes the experimental techniques used to characterise the resulting materials during the course of this study.

3.2.1 Density and porosity measurements

Density and porosity measurements were performed to evaluate the quality of the resulting geopolymers. The bulk density of a sample is the total mass per total volume of the sample including porosity. Porosity is a *phase* present in materials, which can be characterised by its volume fraction, size and distribution, compared with other phases. One method of characterising porosity is to measure apparent porosity, namely those pores connected to the surface of a material.

The values of bulk density (D_b) and apparent porosity (P_a) of geopolymers in this study were determined using the Archimedès principle according to ASTM Standard (C-20) with deionised water as the immersion medium. The bulk density (D_b) and apparent porosity (P_a) were calculated using the following formulae:

Bulk density, $$D_b = \frac{m_d}{m_s - m_i} \times D_i \qquad (3.1)$$

Apparent porosity, $$P_a = \frac{m_s - m_d}{m_s - m_i} \times 100\% \qquad (3.2)$$

Where m_d is the mass of the dried sample, m_i is the mass of the samples saturated with and suspended in water, m_s is the mass of the sample saturated and suspended in air and D_i is the density of water at room temperature.

For bulk density and apparent porosity measurements samples were sectioned with a diamond saw to obtain a specimen 0.50 cm high and 2.50 cm in diameter. After sectioning the samples were cleaned with water and compressed air and then dried. The mass of the samples (dry samples, saturated and suspended in water) was determined by using a digital balance (Denver Instrument Company AA-200). The

samples were placed in water and boiled for 2 hours. During the boiling period, the samples were kept entirely covered with water, and prevented from contacting the heated bottom of the container. After the boiling period, the samples were left in the container covered with water for a minimum of 12 hours before weighing. Each measurement was performed on three samples and the measurement uncertainty was taken as the standard deviation.

3.2.2 Vickers microhardness

Hardness is a measure of a material's resistance to localised plastic deformation. Hardness testing is a method commonly used to evaluate the quality of materials, particularly metals and ceramics. This test is based on forcing an indenter into the surface of the material by dynamic or static loading and determining the response in terms of the size of indentation (Sridhar & Yovanovich 1996; Igarashi, Bentur & Mindes 1998).

In this study the hardness testing was conducted using a ZWICK microhardness tester with a Vickers diamond pyramid indenter. Samples used for the indentation test were cut using a Struers Minitom diamond saw and the test surface was polished using a Struers Pedamat polisher finishing with 1 μm grade diamond. The size of the samples was about 1.00 cm in height and 2.50 cm in diameter. Based on the standard test method for microhardness of materials (ASTM E384), the test loads used in this study were between 300 – 1000 g. The indentation diagonal lengths were measured directly using a micrometer attached to the sample stage or using an optical microscope.

Vickers hardness number, H_v is a number related to the applied force (P) and the surface area of the permanent impression made by a square-based pyramidal diamond indenter having included face angles of 136^o (figure 3.2).

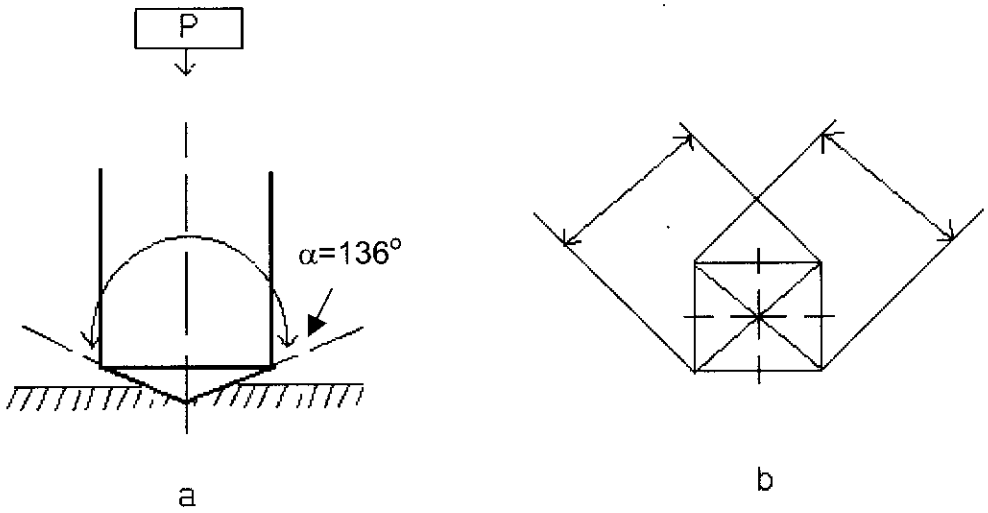

Figure 3. 2 Vickers indentation, (a) side view of diamond indenter (b) plan view of indent, d is diagonal of indentation.

The Vickers hardness (H_v) in MPa is calculated using the following formula

$$H_v = \frac{P}{A_s} = 2P\frac{\sin\left(\alpha/2\right)}{d^2} = 1.8544\frac{P}{d^2} \qquad (3.3)$$

where:

P = load (N)

A_s = surface area of indentation (mm^2).

d = mean diagonal of indentation (mm) and

α = face angle of indenter (136°).

Microhardness tests for samples containing aggregate were performed in the vicinity of an aggregate grain. This zone can extend to distances of about 50 μm from the geopolymer-aggregate interface and is referred to as the interfacial transition zone (ITZ) (Igarashi, Bentur & Mindess 1996; Sridhar & Yovanovich 1996).

3.2.3 Compressive strength

Compression tests were conducted to investigate the ultimate strength of aluminosilicate geopolymers with and without aggregate. The compressive tests were conducted after ageing the specimen at 1, 3, 7 and 28 days. These tests were performed using a Wykeham Farrance 50 ton compression test machine with a loading rate of 0.33 mm/minute. The test specimens were cylindrical in shape, 5.00 cm in length and 2.50 cm in diameter and hence the length to diameter ratio (2:1) fulfils the standard requirement for compression test ASTM C773. Each measurement was conducted on 3 samples. The compressive strength of a sample was calculated using the following formula:

$$C = \frac{P}{A} \tag{3.4}$$

where C = compressive strength (MPa), P = total load on the sample at failure (N) and A = calculated area of the bearing surface of the specimen (m^2).

3.2.4 Aggregate-geopolymer interfacial bond strength

This test was performed to measure the interfacial bond strength between aggregate and the geopolymer matrix. The bonding strength in the interfacial transition zone (ITZ) is one of the most important properties of ceramics and cementitious materials for various applications such as coatings, joins or junctions (Diamond & Huang 2001; Caliskan 2003).

For interfacial bond strength measurements a sample was prepared as 20 mm x 20 mm x 100 mm and shown schematically in Figure 3.3. The specimen arrangement was designed to enable the uniaxial tensile bond strength to be measured by pulling apart the aggregate-geopolymer matrix composite. This arrangement is similar to that used by Tasong, Lyndsdale & Cripps (1998) to measure the interfacial bond strength

between aggregate and Portland cement matrix. A special perspex mould was designed to prepare the specimen.

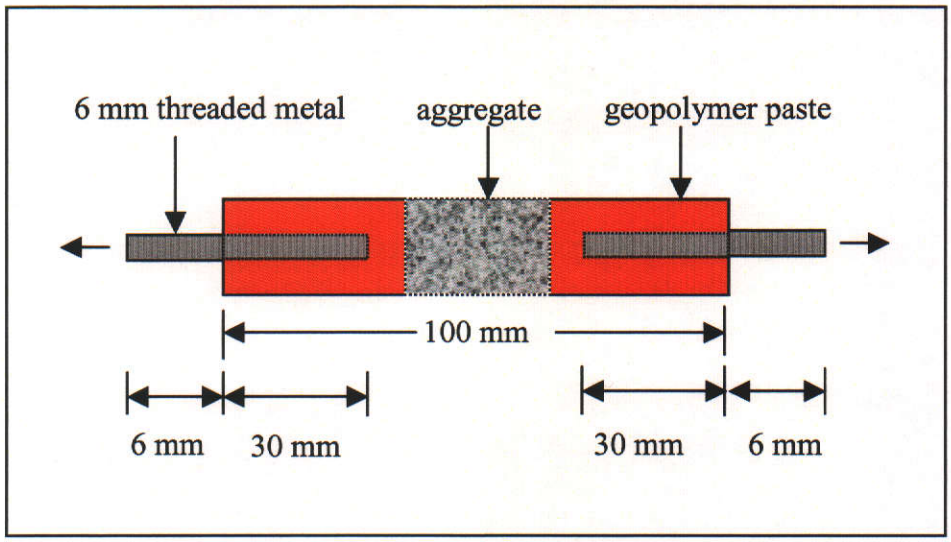

Figure 3.3 Schematic representation of arrangement for interfacial bond strength measurement.

Three types of aggregate were used in this experiment, namely quartz, sandstone and granite. The aggregate was cut with a diamond saw to 20 mm cubes. Two 40 mm long threaded metal rods were inserted into the perspex mould. The aggregate was then placed in the centre of the mould and finally geopolymer paste was added. All specimens were cured at 70 °C for about 2 hours and stored for at least 7 days after demoulding. Interfacial bond strength was conducted using a Hounsfield Tensometer with a maximum load capacity of 250 kg using an extension rate of 0.253 +/-0.005 mm/s.

3.2.5 Thermal conductivity

Thermal conductivity and thermal diffusivity are thermophysical properties associated with steady state heat transfer and play an important role in determining the performance of ceramics and cementitious materials. Thermal conductivity (k) is defined as:

$$k = \frac{q/A}{\Delta T/\Delta L} \qquad (k \text{ in } Wm^{-1}K^{-1}) \qquad (3.5)$$

Where q (in watt) is the amount of heat passing through a cross section, A (in m^2) and causing a temperature difference, ΔT (in K), over a distance of, ΔL (in m). Thus q/A is the heat flux causing the thermal gradient, $\Delta T/\Delta L$.

The thermal conductivity (k) and the thermal diffusivity (α) are related by the expression:

$$\alpha = \frac{k}{\rho C_p} \qquad (\alpha \text{ in } m^2/s) \qquad (3.6)$$

where ρ is the density of the specimen (in kgm^{-3}) and C_p is the heat capacity of the specimen (in $J\,kg^{-1}K^{-1}$).

The measurement of thermal conductivity involves the measurement of the heat flux and temperature difference. In this study the experimental technique used to measure the thermal conductivity and the thermal diffusivity of geopolymers was a transient hot wire method. Hot wire methods are most commonly used to measure the thermal conductivity of refractories such as insulating bricks and powder or fibrous materials. Because it is basically a transient radial flow technique, isotropic specimens are required. The sample is cylindrical in shape with a length of 25 cm and a radius of 5 cm. A 0.25 mm diameter nickel-chromium wire imbedded along the axis of the sample was used as a line heat source. The temperature rise was measured by using an imbedded thermocouple (figure 3.4).

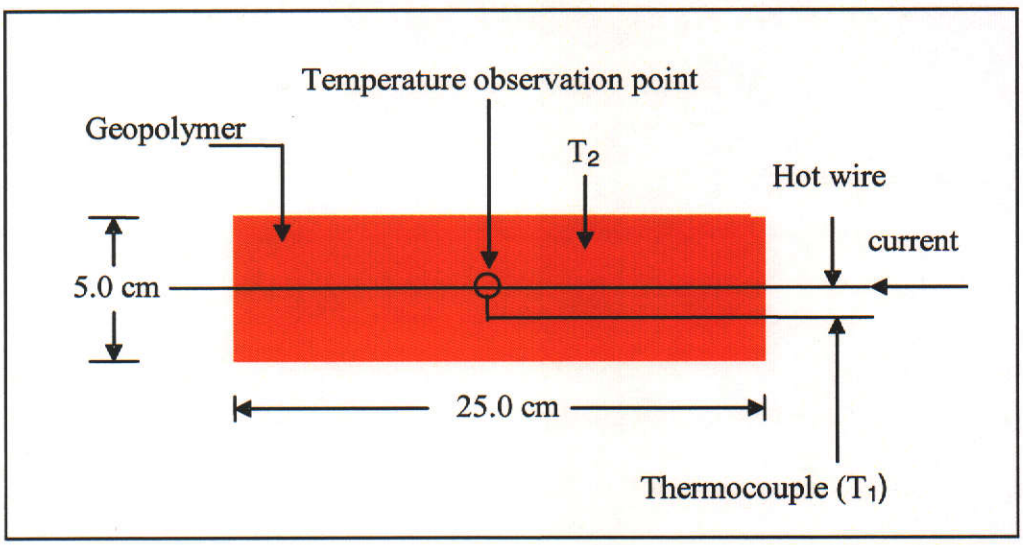

Figure 3.4 Schematic diagram of arrangement for measurement of thermal conductivity.

The mathematical principle for the hot wire method is based on an infinite line heat source imbedded in an infinite medium. The time dependent conduction equation in cylindrical coordinates with temperature varying only in the radial direction is given by (Parrott & Stuckes 1975 p.19-20; Glatzmaier & Ramirez 1988; Tavman 1996; Griesinger, Heidermann & Hahne 1999; ASTM D5930):

$$\frac{\partial T}{\partial t}=\alpha\frac{1}{r}\frac{\partial}{\partial r}\left(r\frac{\partial T}{\partial r}\right) \tag{3.7}$$

where r is radial distance from the line source where the temperature is measured. The solution of equation (3.7) for a medium with a constant initial temperature, T_0, and a heat input q per unit length of line source is:

$$T-T_0=-\frac{q}{4\pi k}E_i\left(\frac{-r^2}{4\alpha t}\right) \tag{3.8}$$

where t is the time after the start of heating. The function $E_i(-r^2/4\alpha t)$ is known as an exponential integral, and for $r^2/4\alpha t \ll 1$, equation (3.8) can be expressed as (Glatzmaier & Ramirez 1988);

$$\Delta T = T - T_0 = \frac{q}{4\pi k} \ln\left(\frac{4\alpha t}{r_w^2 C}\right) \tag{3.9}$$

where: r_w = radius of wire

$C = e^y$ where $y = 0.5772$.

Differentiating equation (3.9) with respect to ln t and solving for *k* yields:

$$k = \frac{q/4\pi}{d\Delta T/d\ln t} \tag{3.10}$$

Substituting equation (3.10) into equation (3.9) gives:

$$\alpha = \frac{r_w^2 C}{4t} \exp\left(\frac{\Delta T\, d\ln t}{d\Delta T}\right) \tag{3.11}$$

In order to obtain the values of thermal conductivity (*k*) and thermal diffusivity (α) from experimental data, the temperature rise is recorded as a function of ln t and is fitted using a linear least squares regression. If *a* is a slope and *b* is the y-intercept of the fit, then the equation for *k* and α are given by:

$$k = \frac{q}{4\pi a} \tag{3.12}$$

$$\alpha = \frac{C r_w^2}{4} \exp(b/a) \tag{3.13}$$

During the measurement, a constant current between 0.5 to 1.0 A was supplied to the heater. The power dissipated by the heater was obtained by precise measurement of the potential difference across the heating wire and the current.

3.2.6 Thermal analysis

The thermogravimetric and differential thermal analysis (TG-DTA) measurement was performed to measure the loss of the bound water from kaolinite as well as the resulting geopolymers. TG-DTA measurement was performed on a SDT Q600 V3.4 Texas Instrument. In all cases the heating rate was 10 °C/min measured with a Pt/Pt 10 %Rh thermocouple. Approximately 10 mg of sample was placed in a platinum crucible and heated up to 900 °C with an empty reference.

3.2.7 Thermal expansion

Cylindrical samples with 4 mm diameter and 25 mm length were prepared to study the thermal expansion and shrinkage behaviour. A DI-24 Adamel Limohargy dilatometer was used to characterise the densification behaviour of geopolymers. The measurements were conducted over the range of 20 – 900 °C with a heating rate of 2 °C/minute.

3.2.8 X-ray diffraction (XRD)

X-ray diffraction (XRD) measurements were performed for phase analysis of the starting materials and to investigate the crystallinity of the resulting geopolymers. Random powder samples of kaolinite and metakaolinite were prepared by lightly pressing powder samples into aluminium holders. Samples from the resulting geopolymers were prepared either in a powder form or by cutting 0.5 mm thick slices of specimen and mounting in aluminium holders.

Diffraction patterns were acquired on a Siemens D500 Bragg-Brentano Diffractometer. Operating conditions were 40 kV and 30 mA, Cu-Kα wavelengths: 1.54060 and 1.54439 Å. In collecting data sets, the 2θ step size was 0.02°, the

counting time per step was 1.2 s, and the 2θ range between 10 – 70°. The software MDI–Jade (version 5) for peak identification and automated search and match was used to analyse the results of diffraction patterns.

3.3 Microstructural Characterisation

3.3.1 Optical Microscopy

Optical microscopy was used routinely to observe the microstructure of geopolymers produced during this investigation. For low magnification work a Nikon SMZ800 stereo microscope with oblique illumination was used. When more detail was required a Nikon ME600 optical microscope with reflected illumination was utilised. In both instances images were acquired with a Spot Insight CCD camera.

3.3.2 Scanning electron microscopy (SEM)

SEM was performed to investigate the microstructures of pastes (including porosity and crack formation) and the paste-aggregate interface in the matrix of the samples. The SEM imaging was conducted on a Philips XL-30 using secondary as well as backscattered electron detectors. The microscope was coupled with an Oxford Instruments energy dispersive X-ray spectrometer (EDS) for elemental analysis. Analysis of EDS spectra was performed using Inca-Analyser software.

Microstructural analysis was performed on polished as well as on fractured specimens. Sample preparation for SEM investigation was as follows: The samples were cut using a diamond saw to a size of 2.00 to 4.00 mm in height and 10 to 25 mm in diameter. Samples were polished to a 1 μm finish using diamond paste. The samples were then cleaned to remove any polishing residue using an ultrasonic bath. The samples were oven dried at about 60 °C for at least 1 hour. Following drying the samples were gold coated for imaging and carbon coated for EDS work. Samples were mounted on the SEM sample stage with conductive, double-sided carbon tape.

3.3.3 Transmission electron microscopy (TEM)

The TEM used was a Jeol 2011 operated at 200 kV, to observe the microstructures of kaolinite and the resulting geopolymers at higher resolution than is possible with the SEM. The microscope is also coupled with Oxford Instrument EDS X-ray unit and Inca-Analyser software.

The crystal structures of kaolinite and geopolymers were determined from the diffraction patterns using selected area electron diffraction (SAED). The interplanar distances (d) of the assigned indexed crystals planes were calculated using the formula (Gard 1976):

$$d = \frac{L\lambda}{R} \tag{3.14}$$

where :

L = the effective distance from the specimen to the photographic plate = 150 cm

λ = the wavelength of electron beam = 0.00252 nm, and

R = the distance between a pair of spots equidistant from direct beam spot.

Crushed and dispersed samples as well as thin films were prepared for TEM examination. Samples from suspension were prepared for TEM examination to investigate the microstructure character and chemical composition of kaolinite and metakaolinite as well as geopolymers. A dilute suspension of the material was prepared in deionized water. Drops of the suspension were placed on carbon films supported by copper grids and dried at room temperature.

Thin film specimens of geopolymers for TEM examination were prepared at the Centre for Microscopy and Microanalysis (CMM), University of Western Australia. Sections about 0.5 mm thick and 2.5 cm in diameter were cut with a diamond saw. From these sections, several 3 mm diameter discs were cut using an ultrasonic disc cutter (Gatan model 601). These sections (maximum 3) were then mounted on the sample holder of a disc grinder (Gatan model 623) and polished using 1000, 2000 and 4000 grit silicon carbide paper down to about 40 μm.

A dimple grinder (Gatan 656) was then used to grind the centre of the disc down to approximately 20 μm. The dimple grinding was accomplished by progressively grinding the sample with 1 and 0.25 μm size diamond pastes.

After dimple grinding the disc was glued (5 minutes araldite) onto a 50 mesh copper grid. The sample was then mounted on the sample holder of an ion beam-milling machine (Precision Ion Polishing System (PIPS), Gatan Model 691). The chamber of the PIPS was purged with Ar for 30 minutes before inserting the sample into the chamber. Thinning was achieved by impinging 5 – 6 keV Ar ions on both sides of the thinned region of the disc. During thinning the sample was rotated at 3 rpm. The intensity of the beam was controlled by regulating the Ar flow rate to maintain a pressure of 5×10^{-4} torr. These conditions resulted in gun currents of 8 – 13 μA. The thinning process was monitored by periodic examination of the sample using an optical microscope. The thinning was terminated when some regions appeared to be perforated. Ion milling of dimpled samples normally took place between 4 – 5 hours depending on the initial thickness of the sample.

3.3.4 Microtomography

In order to determine if cracks in the geopolymers arose during production or sample preparation microtomography was undertaken on as-prepared specimens. A CT-Scan, also known as Micro-CT (Skyscan-1072 Desk-Top-X-Ray Microtomograph) was used for this purpose. The size of the samples was 10 mm in length and 4 mm in diameter.

Chapter 4

PHYSICAL AND MECHANICAL PROPERTIES OF GEOPOLYMERS

4.1 Introduction

This chapter presents the experimental results on the physical and mechanical properties of geopolymers synthesised from metakaolinite activated with sodium silicate solution. The structure of the resulting geopolymers based on X-Ray diffraction (XRD) results is also presented and discussed in this chapter.

It is important to characterise the physical and mechanical properties of geopolymers such as bulk density, porosity, Vickers hardness, compressive strength, interfacial bond strength, thermal expansion and thermal conductivity for two main reasons; (i) the influence of process variables such as Si:Al, Na:Al, Na_2O:H_2O, curing temperature and time need to be determined and optimised and (ii) it allows direct comparison with the properties of ordinary Portland cement which it may replace or substitute.

4.2 Microstructure of kaolinite

The raw kaolin material used to prepare geopolymers in this study was a paint/filler-grade kaolinite (Kingwhite 65). Some properties of this kaolinite, including its chemical composition, have been described in section 3.1. In this section, the microstructure of kaolinite investigated using scanning electron microscopy (SEM) as well as transmission electron microscopy (TEM) are presented and discussed. Both microscopes were equipped with an energy dispersive X-ray spectrometer (EDS), which allowed elemental analysis to be performed.

Figure 4.1 shows a typical SEM micrograph of the Kingwhite kaolinite. The micrograph reveals platy shaped kaolinite particles stacked parallel to each other.

The image indicates that the kaolinite has approximately hexagonal flakes with poorly defined edges that would indicate imperfect crystallisation. Some SEM images showed the presence of tubular–like particles typical of halloysite. The presence of ancillary minerals such as TiO_2 was confirmed using backscattered electron imaging and EDS.

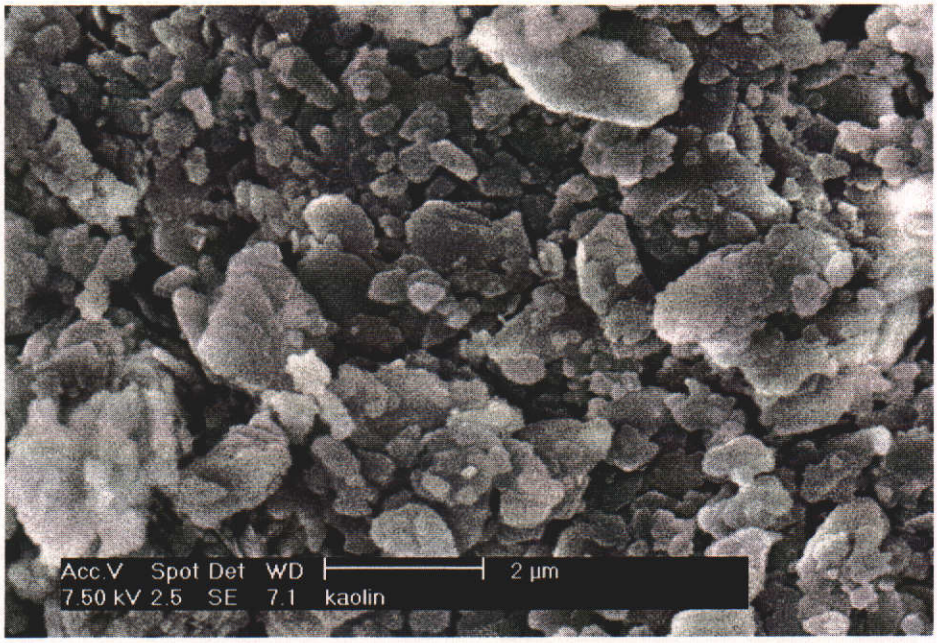

Figure 4. 1 SEM micrograph of Kingwhite 65 kaolinite.

TEM observations allowed examination of the kaolinite microstructure at higher magnifications. Figure 4.2 shows a representative TEM image of kaolinite. The image shows that the kaolinite is composed of layers of small platy flakes less that 1 µm in width and with slightly distorted hexagonal edges. Both TEM and SEM images reveal that while most crystals are euhedral some kaolinite crystals are anhedral (no euhedral faces) with elongated, rounded or ill-defined morphologies.

The size distribution of kaolinite crystals was determined from several TEM images based on their width (w) (figure 4.3) that is parallel to the (001) plane. The size of kaolinite crystals will be related to the microstructure character of the resulting geopolymers. The size distribution of the kaolinite crystals is depicted in figure 4.4.

Some of the larger kaolinite crystals may have been excluded by the TEM sample preparation process, which will slightly bias the results shown in figure 4.4.

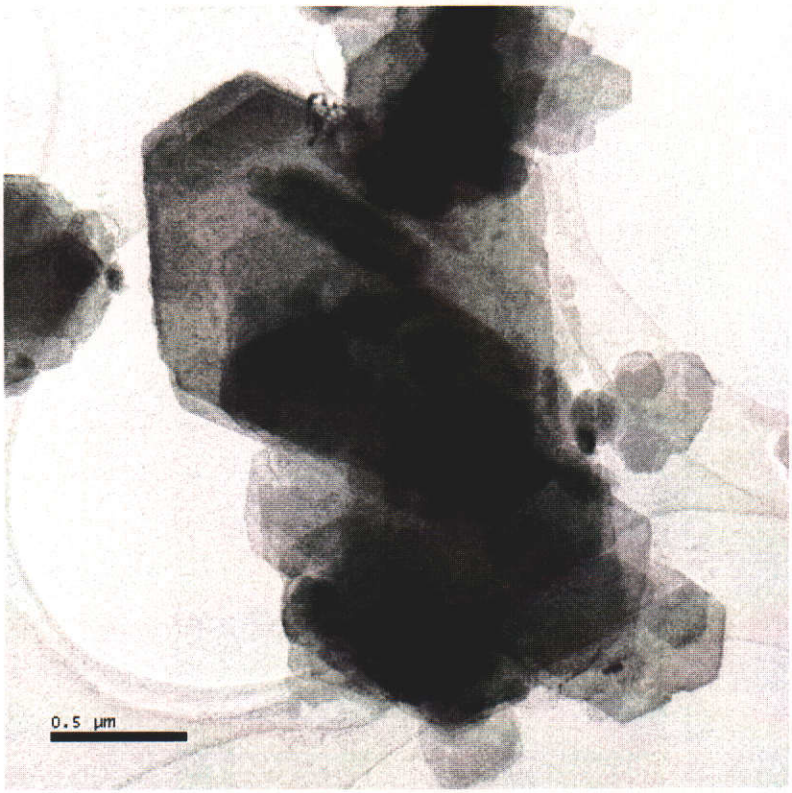

Figure 4. 2 TEM image of Kingwhite 65 kaolinite.

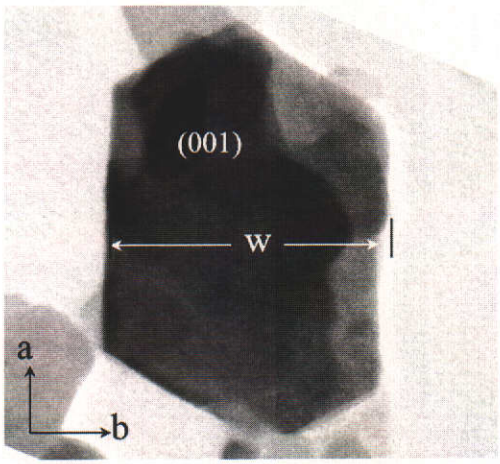

Figure 4.3 The size of kaolinite crystals was determined by measuring 'w' which is parallel to (001) plane.

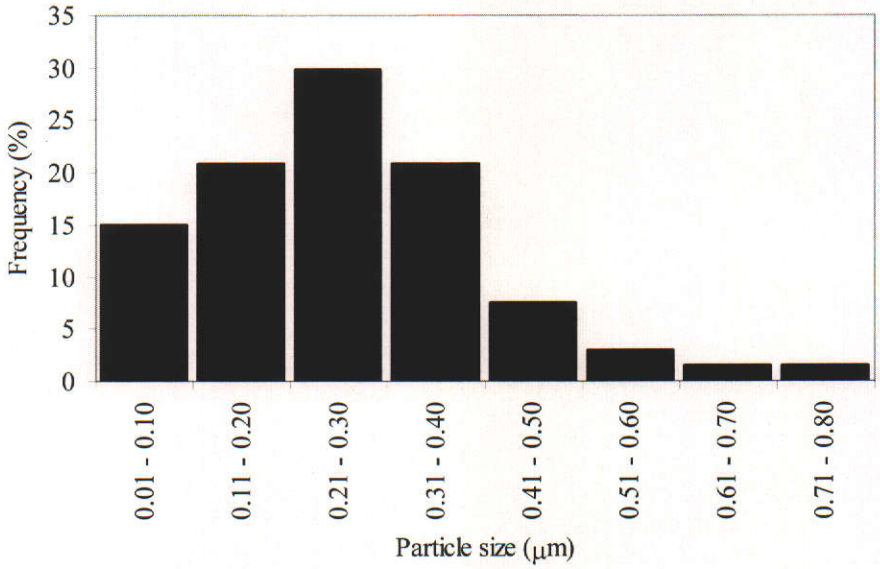

Figure 4.4 Size distribution of kaolinite crystals determined from TEM images.

Selected area electron diffraction (SAED) of kaolinite crystals typically produced diffraction patterns as shown in figure 4.5. Indexing the patterns indicates that the c-axis of the crystals is almost parallel to the electron beam.

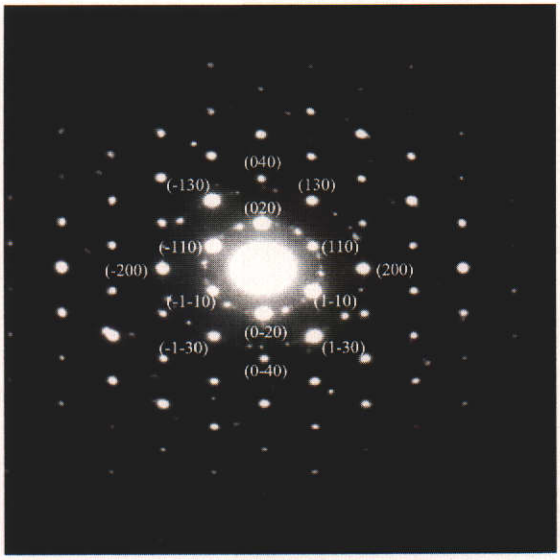

Figure 4.5 A typical SAED of Kingwhite 65 kaolinite showing the regular hexagonal grid and symmetry of the intensity distribution possessed by the reciprocal lattice plane perpendicular to the c-axis.

X-ray diffraction patterns for kaolinite were recorded over the 2θ angle range 10° to 80° counting for 1 second per 0.02° step. The low angle range (<10° 2θ) contains no kaolinite diffraction peaks and so was not measured. Figure 4.6 shows the XRD pattern of Kingwhite 65 kaolinite used in this study. All the observed reflections match those from PDF#14-0164.

The structure of kaolinite is highly complex due to the large number of stacking faults that may appear during its formation and growth (Aparicia & Galan 1999). These structural defects can be estimated by using an index known as the Hinckley index (HI) (Hinckley 1963). The HI essentially measures the definition of the closely spaced (020) and (111) diffraction lines in the diffraction pattern of a kaolinite sample as a measure of the degree of disorder in the crystal structure. The HI is the ratio of (a) the sum of the heights of the reflections $(1\bar{1}0)$ and $(11\bar{1})$ measured from the inter-peak background, and (b) the height of $(1\bar{1}0)$ peak measured from the general background (Plancon, Giese & Snyder 1988).

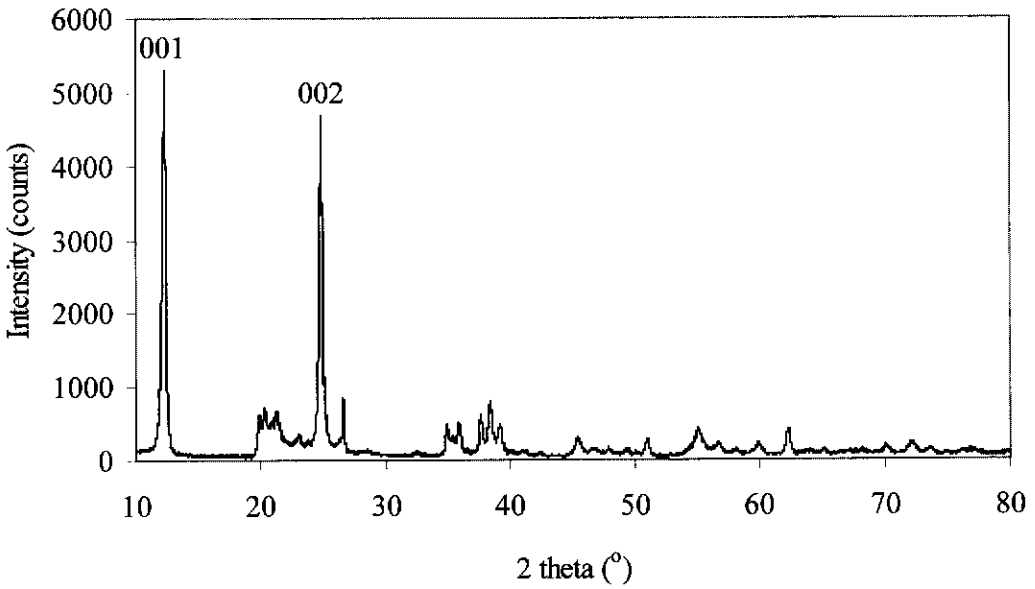

Figure 4.6 XRD pattern of Kingwhite 65 kaolinite.

Figure 4.7 shows an expanded region of the diffraction pattern from figure 4.6 to enable the HI to be determined. Close inspection of the region (18.0° to 28° 2θ) revealed the presence of several peaks from α-quartz (SiO_2). The major peaks of

quartz are found at 4.26 Å (20.86° 2θ) and 3.34 Å (26.64° 2θ)(PDF#46-1045) although the latter peak is superimposed on a kaolinite reflection (111) at 3.35 Å (26.58° 2θ) (PDF#14-0164). Based on intensity measurements taken from figure 4.7 the HI is calculated as follows:

$$HI = \frac{A + B}{C} = 0.88.$$

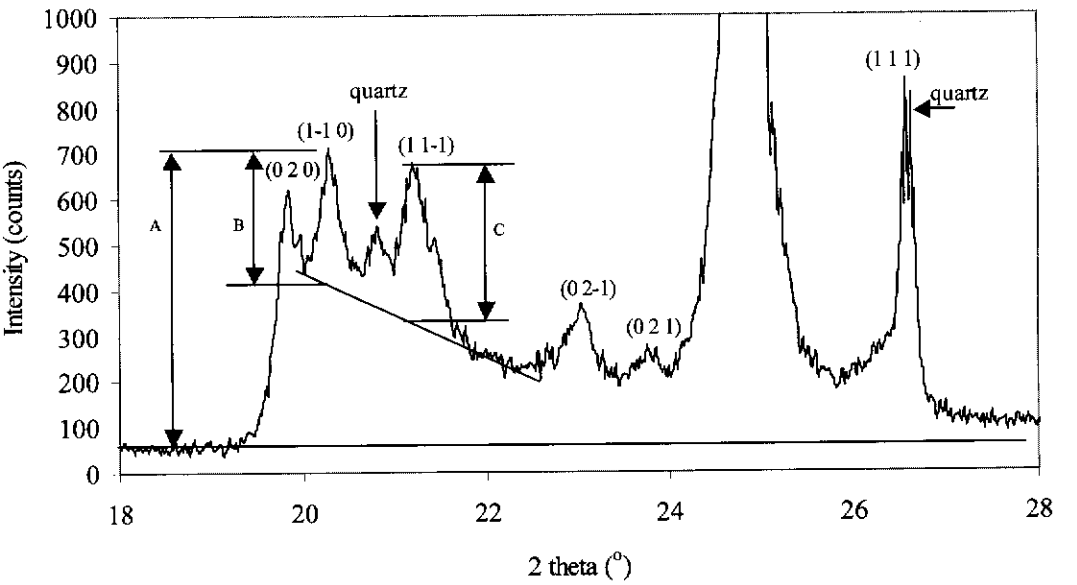

Figure 4.7 XRD pattern showing parameters measured for determination of the Hinckley index for Kingwhite 65 kaolinite.

The HI normally varies between 0.2 and 1.5 where the larger the value of the index the greater the crystallinity or the lower the number of defects in kaolinite crystal structure. The HI of Kingwhite 65 kaolinite suggests a medium-defect kaolinite. Dehydroxylated kaolinite (metakaolinite) was assumed to have high reactivity when activated with sodium silicate solution. Kakali *et* al. (2001) pointed out that the pozzolanic activity of metakaolinite is strongly related to the crystallinity of the original kaolinite. Well ordered kaolinite is transformed into less reactive metakaolinite.

4.3 Microstructure of metakaolinite

Geopolymers produced in this study were synthesised from metakaolinite. The kaolinite was transformed into amorphous metakaolinite by calcination

(dehydroxylation) at 750 °C in air for 6 hours. Davidovits (1999) and Shvarzman *et* al. (2003) pointed out that the reactivity of metakaolinite depends on calcination parameters such as temperature and time as well as the type of the kiln used. The ideal calcination temperatures are between 700 °C and 800 °C for about 6 hours. Calcination of kaolinite at lower than 700 °C as well as a rapid calcination in rotary kilns yields a deficit in IV-V coordinated Al in the metakaolinite which does not react readily with sodium or potassium silicate.

The exact temperature at which dehydroxylation of kaolinite take place was determined using TG-DTA (figure 4.8). The DTA trace is typical of kaolinite, showing a dehydroxylation endotherm at 513 °C and an exotherm at 989 °C indicating the formation of spinel.

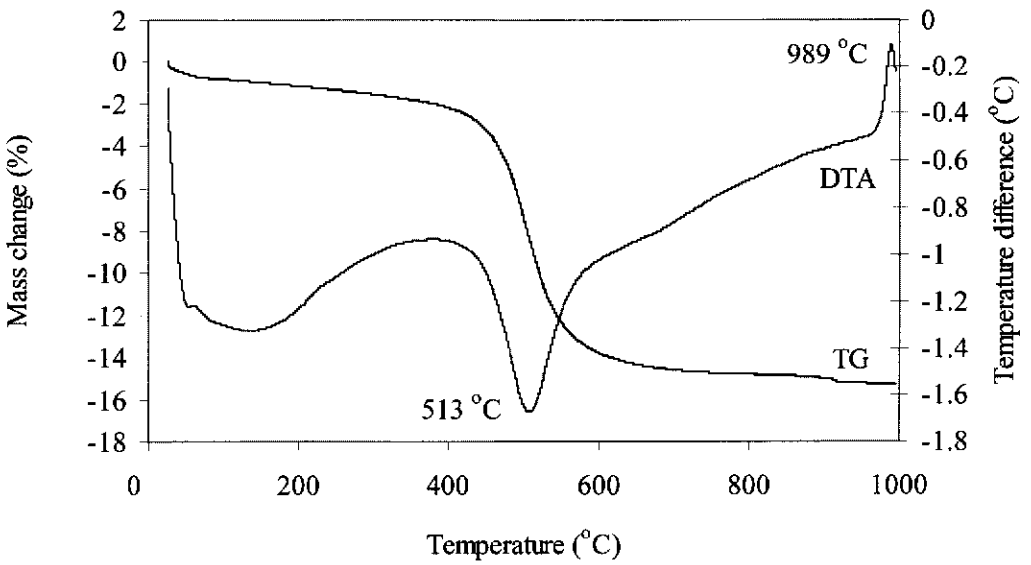

Figure 4.8 TG-DTA curves for Kingwhite 65 kaolinite. Heating rate 10 °C/minute in air.

The TG curve indicates that at temperature < 400 °C the weight loss can be attributed to a pre-dehydration process, which occurs due to reorganisation in the octahedral layer. The loss of OH lattice water starts to take place at 400 °C and the dehydroxylation is essentially complete at 650 °C. This result is in good agreement with dehydroxylation of other types of kaolinite (Ray *et* al.1995; Temuujin *et* al. 1998; Granizo, Blanco-Varela & Palomo 2000; Kakali *et* al. 2001, Shvarzman *et* al. 2003). Cioffi, Maffucci & Santoro (2003) pointed out that the loss of lattice water

causes the crystalline structure of kaolinite to collapse and changes the coordination number of Al from VI to IV.

XRD of metakaolinite indicates that all the kaolinite reflections have been eliminated (figure 4.9) leaving an amorphous pattern with ancillary peaks due to α-quartz (SiO_2) (PDF#05-0490) and anatase (TiO_2) (PDF#21-1272).

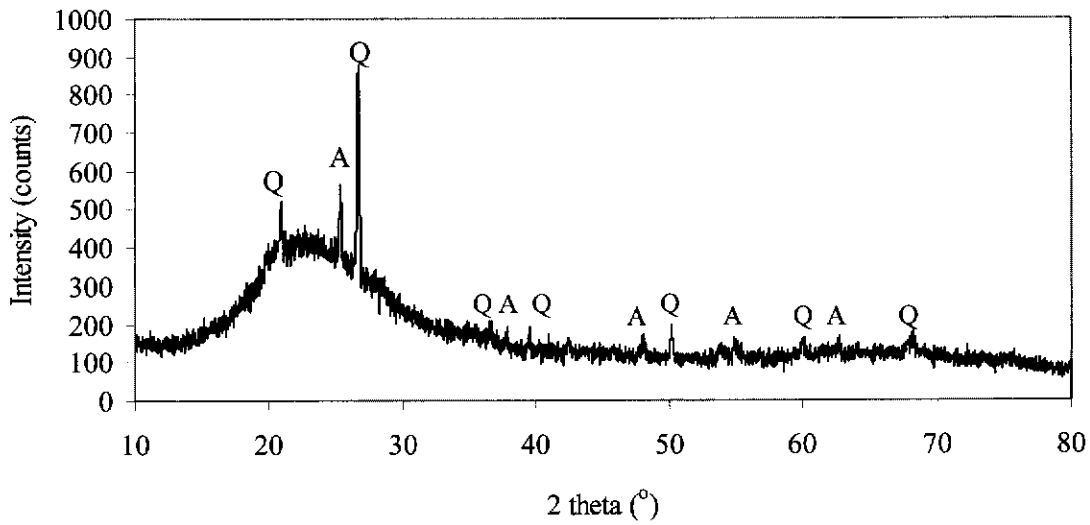

Figure 4.9 XRD pattern of metakaolinite, A = anatase (TiO_2) and Q = α-quartz (SiO_2).

Microstructural examination of metakaolinite by TEM revealed that the morphology of the original kaolinite is maintained as depicted in figure 4.10(a) although SAED shows the material to be amorphous (fig.4.10(b)). This observation is in good agreement with results reported by Zhang & Malhotra (1995). The loss of water during dehydroxylation of kaolinite destroys dioctahedral kaolinite and tranforms the octahdedrally coordinated Al layer into the tetrahedral form but the Si — O sheets of the kaolinite structure are largely conserved (Brindley & Lemaitre 1987).

Akolekar, Chaffee & Howe (1997) suggested that metakaolinite may contain 11% to 12% of the original kaolinitic structural water, associated with approximately 8% to 10% of aluminium atoms that remain in undistorted sites. Some areas of the metakaolinite specimens indicated the presence of crystallinity, but most of areas were amorphous (figure 4.10(b)).

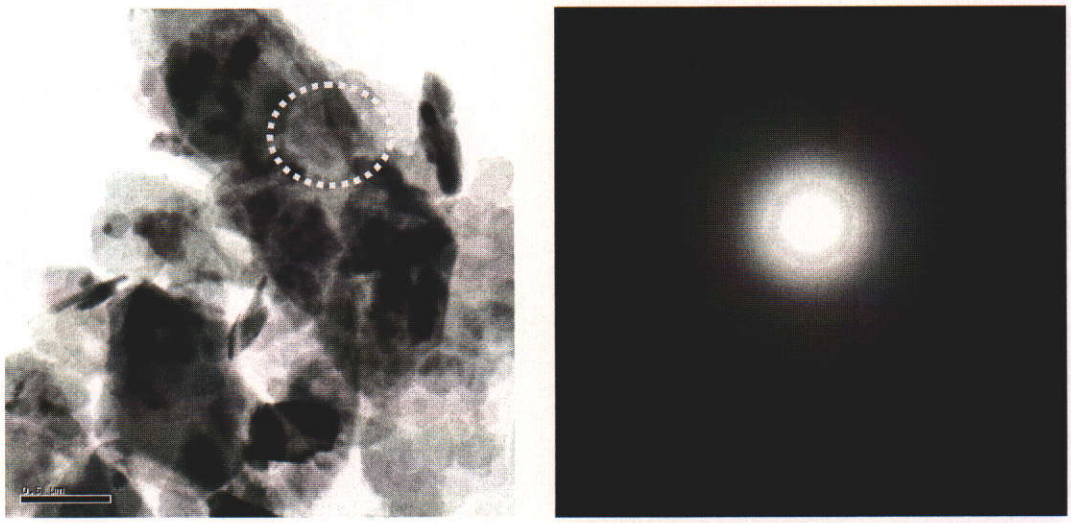

(a) (b)

Figure 4.10 TEM image of (a) metakaolinite showing that the original morphology of kaolinite has been retained (b) electron diffraction from the circled area.

4.4 Synthesis of Geopolymers

The processing procedure and chemical composition of the starting materials used in the production of geopolymers have been described in detail in section 3.1. In this section the geopolymerisation reaction as well as the structure of the resulting geopolymers based on XRD patterns are presented and discussed.

4.4.1 Geopolymerisation

Metakaolinite used in the production of geopolymers contains only a small quantity of calcium oxide (0.08%) and alkalis, and therefore it does not have the capacity to hydrate itself. Thermally assisted curing of the mixture of geopolymer precursors plays an important role in determining the rate of polycondensation, setting time and hence the physical and mechanical properties of the resulting geopolymers.

Figure 4.11 shows a geopolymerisation thermograph for metakaolinite mixed with sodium silicate solution. The sample used in this experiment was prepared using the atomic ratio of Si:Al = 1.50 and Na:Al = 0.6. The mixture was poured into three

polycarbonate cylindrical moulds and left to mature at room temperature for 1 hour. The mass of each sample was kept the same at about 50 grams. During the observation the oven temperature was set constant at 45 °C for sample A, 70 °C for sample B and 85 °C for sample C. The temperature of the samples was monitored using a thermocouple embedded in the sample.

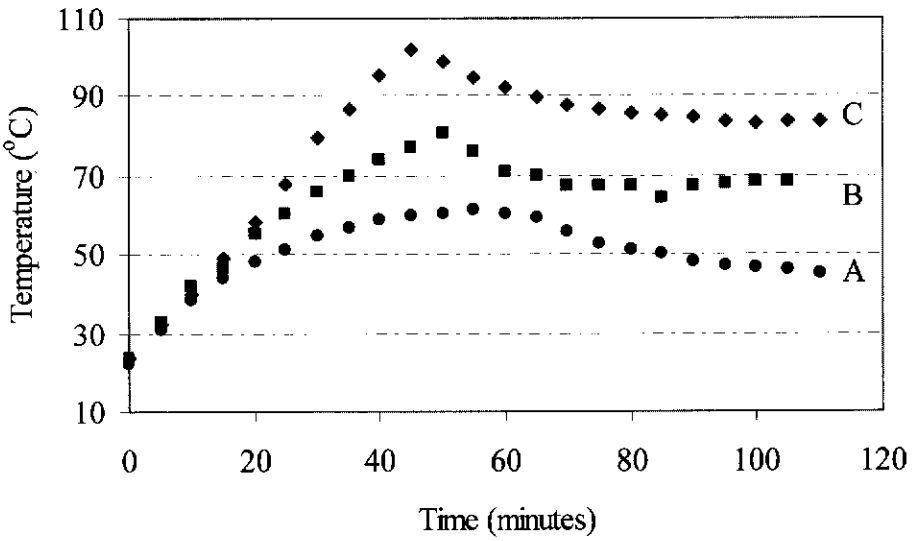

Figure 4.11 Geopolymerisation thermograph for a mixture of metakaolinite and sodium silicate solution at three different curing temperatures. Sample A cured at 45 °C, sample B cured at 70 °C and sample C cured at 85 °C.

Each curve shows that the sample temperature increases rapidly to a maximum value, which is higher than the oven temperature, then slowly decreases to an equilibrium temperature. The maximum of each curve is an indication that the geopolymerisation is essentially complete. The reaction by product, mainly water, is expelled and resides on the surface of the geopolymer.

Figure 4.11 also shows that the exothermic peak is reached later as the curing temperature decreases. For sample A, the geopolymerisation reaction was completed after 60 minutes while for sample C the reaction was complete after 45 minutes. The curves also indicated that the metakaolinite used in the processing of geopolymers has a high reactivity.

Throughout this study, the curing temperature was set to 70 °C so that the geopolymerisation temperature was kept below 100 °C to avoid evaporation of reaction water. TG-DTA results (section 4.5.1) showed that at this curing temperature more than 75% of reaction water was expelled from the structure without creating any cracks on the surface of the sample. Samples for thermal conductivity measurements, which were larger than compression test samples, were also cured at 70 °C but for 2 hours in order to ensure that the whole sample was completely cured. There was no post curing treatment conducted after the sample was removed from its mould.

4.4.2 X-ray diffraction of the geopolymers

Geopolymers prepared in this study were divided into three groups based on the nominal ratio of atomic Si:Al and Na:Al (table 4.1)

Table 4.1 Groups of geopolymers based on atomic ratio of Si:Al and Na:Al

Group	Si:Al					Na:Al
A	1.04	1.25	1.50	1.75	2.00	0.6
B	1.04	1.25	1.50	1.75	2.00	0.8
C	1.04	1.25	1.50	1.75	2.00	1.0

The resulting geopolymers from all groups, with Si:Al = 1.04 and 1.25 are designated as *sodium-poly(sialate) (Na-PS)* type, and geopolymers with Si:Al = 1.50, 1.75 and 2.00 are designated as *sodium-poly(sialate-siloxo) (Na-PSS)* type. All geopolymers prepared in this study were chemically activated with sodium silicate solution. The pH of the sodium silicate solution used in these experiments for all mixtures ranges between 13 to 14, providing optimal conditions for geopolymerisation (Phair & Van Deventer 2001, 2002).

Na-PS type of geopolymer (The formation of zeolite-A and zeolite-X)

Geopolymers with composition of Si:Al = 1.04 and Na:Al = 0.6 were prepared from metakaolinite and activated solely by NaOH solution. The addition of sodium silicate solution to the reacting materials was unnecessary because the atomic ratio of Si:Al of the raw metakaolinite is 1.04. The amount of water was determined based on a molar oxide ratio of H_2O:Na_2O = 10. This amount of water was enough to facilitate mixing and with sufficient NaOH to dissolve the metakaolinite, although the workability of this mixture is poor. The mixture was then poured into a polycarbonate mould, left for an hour to mature and then cured at 70 °C. The resulting geopolymers were quite soft and brittle although there were no cracks visible on the surface.

Figure 4.12 shows a typical XRD pattern of a geopolymer with a composition of Si:Al = 1.04 and Na:Al = 0.6. The diffraction pattern shows amorphous metakaolinite and zeolite-A (PDF#38-0241) in addition to several peaks from quartz and anatase impurities.

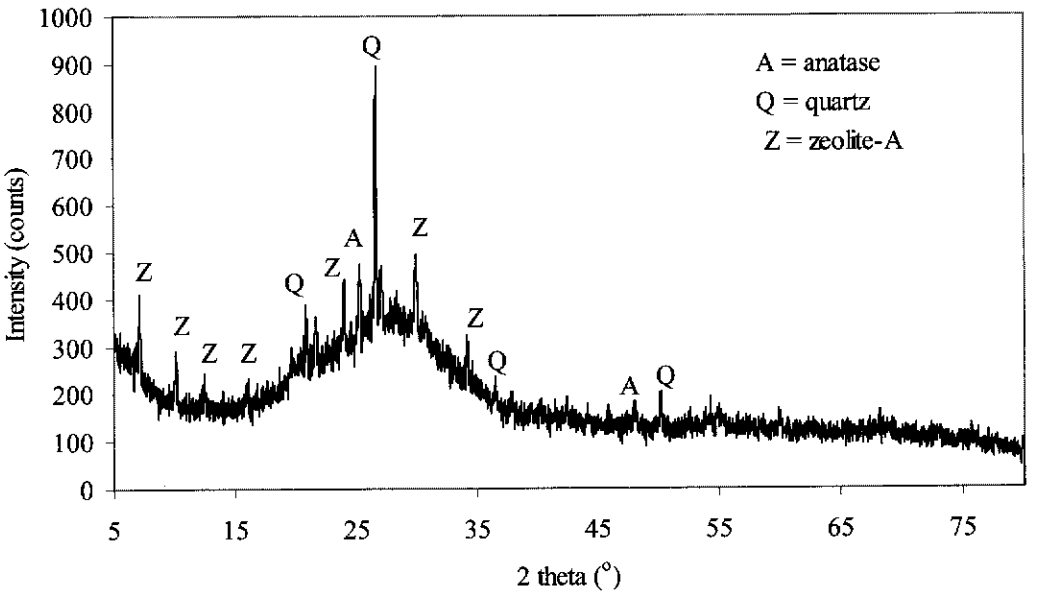

Figure 4.12 XRD pattern of a geopolymer sample showing the formation of zeolite-A (Si:Al = 1.04, Na:Al = 0.6).

For some time, it has been recognised that one of the most important aluminosilicate raw materials for fabrication of zeolite (low-silica zeolite) is calcined kaolinite (metakaolinite) (Davidovits 1988; Akolekar, Chaffe & Howe, 1997; Chandrasekhar *et* al. 1997, Chandrasekhar & Pramada 2001). However, the processing route applied in the production of geopolymers is different from those usually applied in the production of zeolite. In the fabrication of zeolite, the mixture is constantly stirred while applying heat for several hours and water is added intermittently to compensate for evaporation loss.

Davidovits (1988) reported that hydrothermal polycondensation at 150 °C and 5 – 10 MPa on a mixture of calcined kaolinite and NaOH with a reaction time between 10 – 15 minutes results in a ceramic paste comprising a mixture of zeolite A and hydrosodalite. With longer reaction time, 45 – 60 minutes, only a denser hydrosodalite is formed. Davidovits (1988) discovered that the surface area of zeolite- A is greater than that of hydrosodalite and therefore requires a longer reaction time to collapse the open structure of zeolite A to form hydrosodalite. In geopolymer terminology synthetic hydrosodalite is designated as Na-Polysialate (Na-PS) $(Si\text{-}O\text{-}Al\text{-}O)_n$ or sodalite type of geopolymer.

Figure 4.13 shows an XRD pattern of a geopolymer sample prepared with Si:Al = 1.04, and Na:Al = 0.8. The molar ratio of H_2O:Na_2O was held constant at 10 which provided good workability of the mixture. The diffraction pattern shows the presence of more zeolite-A for the higher Na:Al ratio.

A similar XRD pattern to that of figure 4.13 was also obtained for a sample prepared with a chemical composition of Si:Al = 1.04, Na:Al = 1.0. The amorphous component in the framework of these high Na:Al samples is significantly lower than that for the sample shown in figure 4.12. This suggests that the chemical composition used to prepare the sample with Na:Al = 0.6 is inadequate for the complete formation of zeolite-A.

Geopolymer prepared with Si:Al = 1.25, Na:Al = 1.0 required the addition of sodium silicate solution to achieve the correct Si:Al ratio of the starting materials. This composition results in the formation of zeolite-X (PDF#38-0237) (figure 4.14).

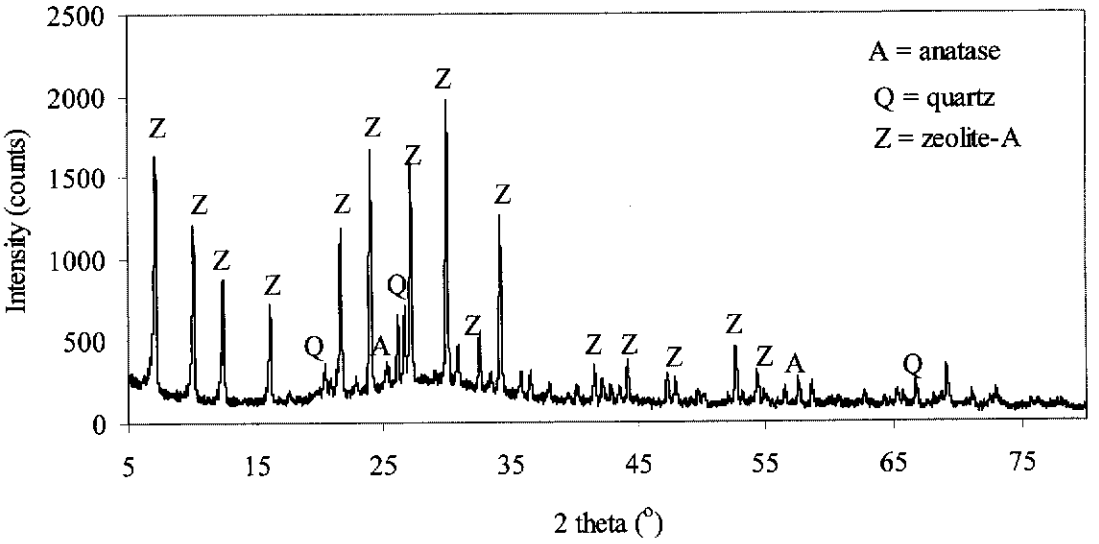

Figure 4.13 XRD pattern of a geopolymer sample showing the formation of zeolite-A (Si:Al = 1.04, Na:Al = 0.8).

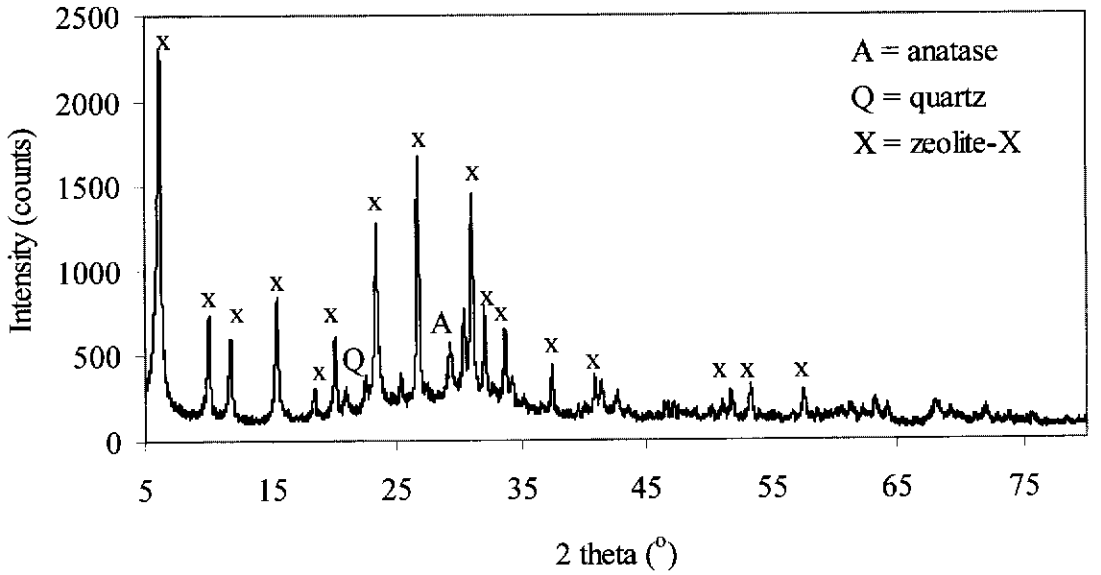

Figure 4.14 XRD pattern of a geopolymer sample showing the formation of zeolite-X (Si:Al = 1.25, Na:Al = 1.0).

Table 4.2 tabulates the starting materials that formed zeolite.

Table 4.2 The chemical compositions of the starting materials that formed zeolite.

Si:Al	Na:Al	Zeolite Type
1.04	0.6	A
1.04	0.8	A
1.04	1.0	A
1.25	0.8	A
1.25	1.0	X

The formation of zeolite-A and zeolite-X from the geopolymer processing route was also observed by Rowles & O'Connor (2003). The use of silica fume mixed with sodium hydroxide solution as an activating agent enabled them to observe a wider range of compositions forming zeolite-A and zeolite-X. They also reported that the formation of zeolite from the geopolymer route occurs with either low Si:Al or high Na:Al ratios. Similarly, Grutzeck, Kwan & DiCola (2004) reported the formation of zeolite in alkali-activated cement based on fly-ash.

The mechanical properties of the zeolites prepared for this project are shown in table 4.3.

Table 4.3 Mechanical properties of zeolites formed in this study. Standard deviations calculated from results of three measurements are shown in parentheses.

Sample ID (Si:Al; Na:Al)	Bulk density (g cm^{-3})	Apparent porosity (%)	Vickers hardness (GPa)	Compressive Strength (MPa)
1.04; 0.6	1.42 (0.06)	33.2 (2.0)	0.06 (0.02)	4.4 (1.5)
1.04; 0.8	1.44 (0.10)	30.5 (4.5)	0.10 (0.03)	12.4 (1.2)
1.04; 1.0	1.26 (0.00)	36.6 (1.5)	0.16 (0.02)	4.51 (0.6)
1.25; 0.8	1.25 (0.09)	26.4 (4.8)	0.21 (0.01)	29.1 (1.5)
1.25; 1.0	1.40 (0.02)	35.6 (3.3)	0.18 (0.03)	6.9 (0.5)

One of the main objectives of this study was to investigate the influence of aggregate on the compressive strength of geopolymers. Table 4.3 indicates that the apparent porosity of these materials is very high. It is well known that the porosity affects the strength of ceramic and cementitious materials. The strength of the materials listed in table 4.3 is too low for useful mortar or concrete applications. Preliminary

investigations showed that incorporation of aggregate in these materials did not significantly increase their strength and therefore this group of geopolymers did not receive further consideration.

Na-PSS type of geopolymers

Sodium-Poly(sialate-siloxo) (Na-PSS) geopolymers were formed by increasing the Si:Al atomic ratio from 1.50, 1.75 and 2.00 for Na:Al atomic ratios of 0.6, 0.8 and 1.0. For these compositions the XRD patterns indicated that the structure of the resulting geopolymers were essentially amorphous. Figure 4.15 shows the XRD patterns of a series of Na-PSS geopolymers formed with a Na:Al atomic ratio = 0.6.

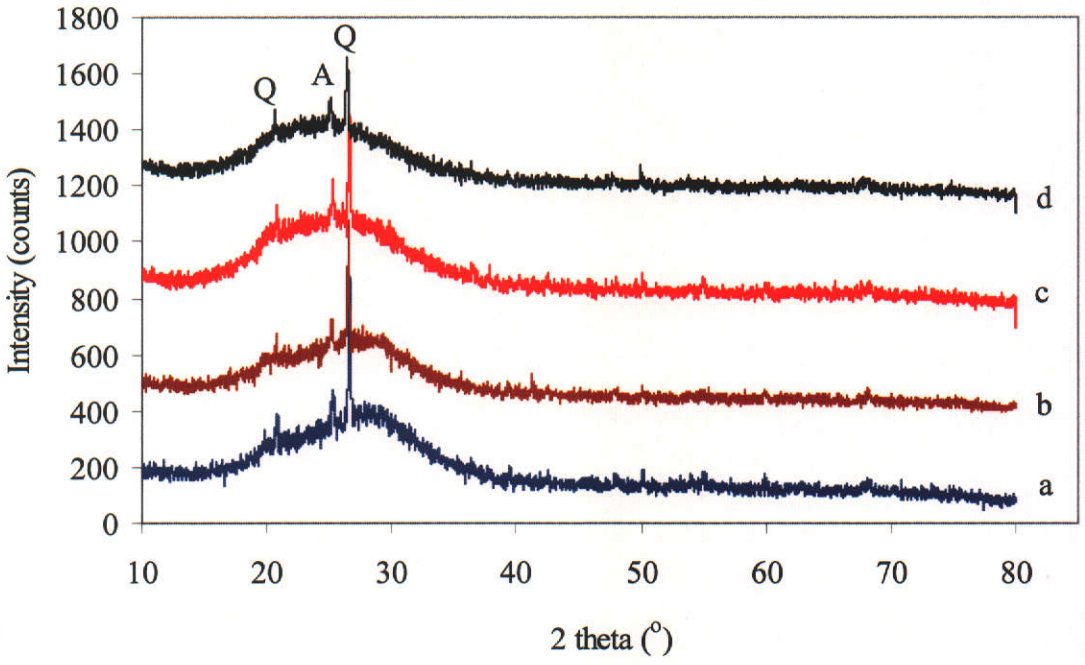

Figure 4.15 XRD patterns of geopolymers prepared with Na:Al molar ratio of 0.6. (a) Si:Al = 1.25, (b) Si:Al = 1.50, (c) Si:Al = 1.75 and (d) Si:Al = 2.0. The sharp diffraction peaks are anatase (A) and quartz (Q). Each pattern has been offset for clarity.

The diffraction patterns of these geopolymers, like the pattern of the original metakaolinite, have a broad amorphous hump in the region 20° – 38°(2θ). This suggests that the Na-PSS geopolymers consist of disordered frameworks with short-

range order, with structures similar to those of feldspatic glasses (Davidovits 1991; Barbosa, MacKenzie & Thaumaturgo 2000).

Figure 4.15 also shows that the peak of the amorphous hump shifts to higher values of 2θ as the Si:Al ratio decreases. The shift of the peak of the amorphous hump for metakaolinte can be attributed to the change of Al coordination to predominantly tetrahedral Al when metakaolinite is activated with sodium silicate solution during geopolymerisation as observed in ^{27}Al MAS-NMR (Rahier *et* al. 1997; Barbosa, MacKenzie & Thaumaturgo 2000). The geopolymer network consists of SiO_4 and AlO_4 tetrahedra linked alternatively by sharing all the oxygens. Each AlO_4 unit introduces one negative charge that is compensated by a Na^+ cation. The ^{27}Al MAS-NMR results also showed that a small resonance of octahedral Al remains in all geopolymers indicating the presence of undissolved metakaolinite. Evidence of undissolved metakaolinite in geopolymer will be presented in chapter 5.

Geopolymers with Na:Al = 0.8 and Na:Al = 1.0 were found to have similar diffraction patterns to geopolymers with Na:Al = 0.6 and the increase of Na atoms did not significantly change the shape or the position of the amorphous hump. By using ^{29}Si MAS-NMR, Rahier *et* al. (1997) observed that the ^{29}Si resonance position shifts to a higher field with increasing concentration of Si atoms suggesting the average Al bonding to Si decreases in the geopolymer network. Barbosa, Mackenzie & Thaumaturgo (2000) also observed that poly(sialate-siloxo) type of geopolymers generally display several ^{29}Si resonances indicating that the Si and Al tetrahedra are present in several different sites. Based on XRD and MAS-NMR results, the researchers pointed out that the structures of geopolymers are similar to glasses or hydrated silicate minerals with a wide range of Si linkages, but predominantly those of framework structures saturated in Al.

4.5 Thermal Properties of Geopolymers

This section presents the thermal properties of Na-PSS based on TG-DTA, shrinkage and thermal conductivity measurements. Thermal properties of geopolymers with or

without the inclusion of aggregate at elevated temperature are of interest because of their potential for high temperature applications such as fire-protection, thermal insulation or heat-resistance substitutes for flammable organic materials (Liefke 1999; Barbosa & MacKenzie 2003). Lyon *et* al. (1997) pointed out that geopolymers with high Si:Al are suitable for fire-proof aircraft cabin interior panels and marine structural composites.

4.5.1 Zeolitic water and shrinkage

Thermal analysis by means of TG-DTA of crushed geopolymer samples produced in this study was performed from room temperature to 900 °C at 10 °C/min. Figure 4.16 shows the TG-DTA curves of geopolymer with nominal atomic ratios of Si:Al = 1.5 and Na:Al = 0.6.

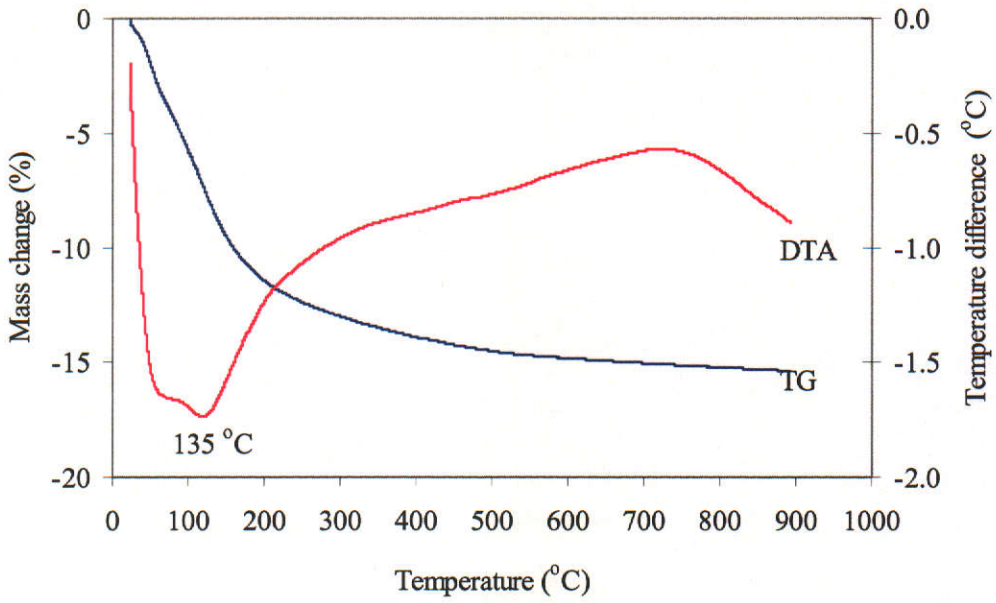

Figure 4.16 TG-DTA curves for a geopolymer prepared with an initial composition of Si:Al = 1.5 and Na:Al = 0.6.

The TG curve shows that the sample cured at 70 °C has about 15% water in the structure, of which 8.5% was lost before about 135 °C. The remainder was either bound tightly or less able to diffuse to the surface, and continued to evolve gradually from about 135° up to 900 °C. The DTA curve is typical for poly(sialate-siloxo)

geopolymers showing a single endothermic peak at 135 °C due to dehydration (water evolution).

Figure 4.17 shows TG-DTA curves for a geopolymer with initial composition of Si:Al = 2.0 and Na:Al = 1.0 and cured at 70 °C. It should be noted that more water was initially added to this sample than was added to the sample shown in figure 4.16. The TG curve indicates that this sample incorporated about 20 % of the reaction water in its structure. The TG curve also indicates that up to 140 °C about 11.5% of the initial weight was lost and between 140° and 500 °C a further 8 % was lost. The DTA curve shows an endothermic peak around 140 °C along with unexplained peak at 80 °C.

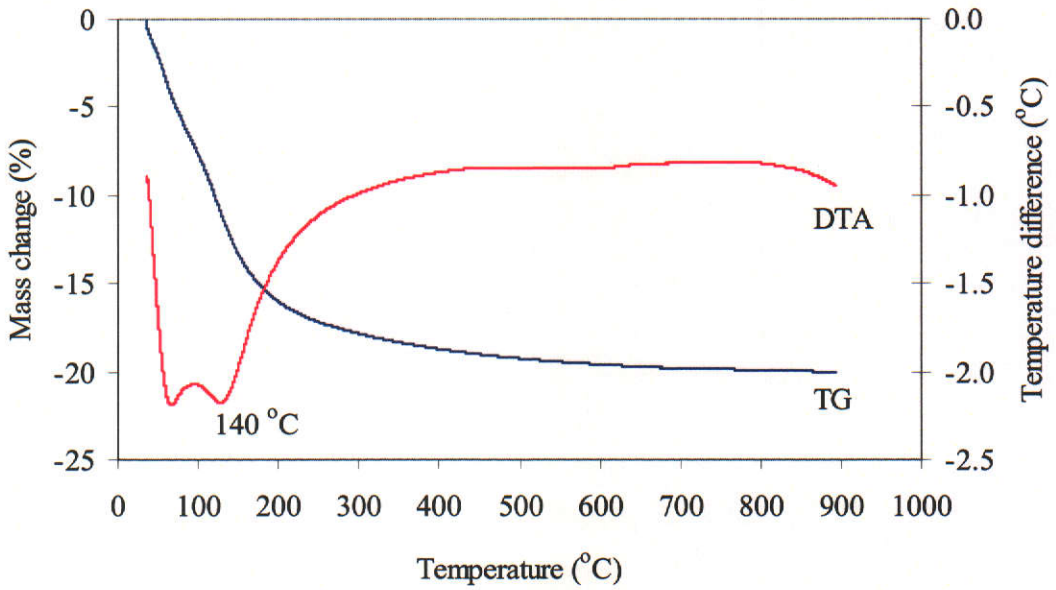

Figure 4.17. TG-DTA curves for a geopolymer with an initial composition of Si:Al = 2.0 and Na:Al = 1.0.

In Portland cement, the DTA curve normally displays three zones. Zone one (100 – 300 °C), which is attributed to dehydration of C-S-H where about 8% of H_2O is lost. Zone two (300 – 350 °C) characterises the decomposition of calcium aluminate silicate hydrate, calcium aluminate hydrate and calcium chloroaluminate and the third zone (450 –500 °C) is referred to as $Ca(OH)_2$ dehydration (Ray *et* al. 1995; Silva, Mathias & Thaumaturgo 1999; Vedalakshmi *et* al. 2003).

Based on the geopolymerisation reaction shown in figure 2.6, it can be seen that some of the reaction water remains within the geopolymeric framework as *zeolitic water* (Davidovits 1988). The loss of zeolitic water from the geopolymer framework could induce cracks to form due to shrinkage when drying the samples at temperatures higher than 100 °C.

The influence of dehydration on the shrinkage of geopolymers was investigated on samples without aggregate as well as samples containing quartz and crushed granite. The initial length of the samples was about 5.00 cm and 2.50 cm in diameter. The samples were heated in an oven up to 950 °C with a heating rate of 10 °C/minute. The change in length of the sample was measured with a digital vernier calliper and the mass loss of the sample was measured with a digital balance placed adjacent to the oven. The measurements were performed subsequently after the samples were heated at 70, 150, 250, 500, 750 and 950 °C.

Figure 4.18 shows some samples before and after they were heated at 950 °C. Sample A and C contain no aggregate with compositions of Si:Al = 1.5, Na:Al = 0.6 and Si:Al = 2.0, Na:Al = 1.0, respectively. Sample B contained crushed granite (20 wt %) with Si:Al = 1.5, Na:Al = 0.6.

Figure 4.19 shows weight loss and shrinkage for a sample prepared with Si:Al = 1.5 and Na:Al =0.6. It was observed that at about 150 °C extensive cracks appeared on the surface of the sample. At this temperature the weight loss was about 3.69% and the relative shrinkage of the sample was about 2.67%. At 950 °C the shrinkage reached 17% with the sample remaining intact and dimensionally stable although extensive cracks had appeared.

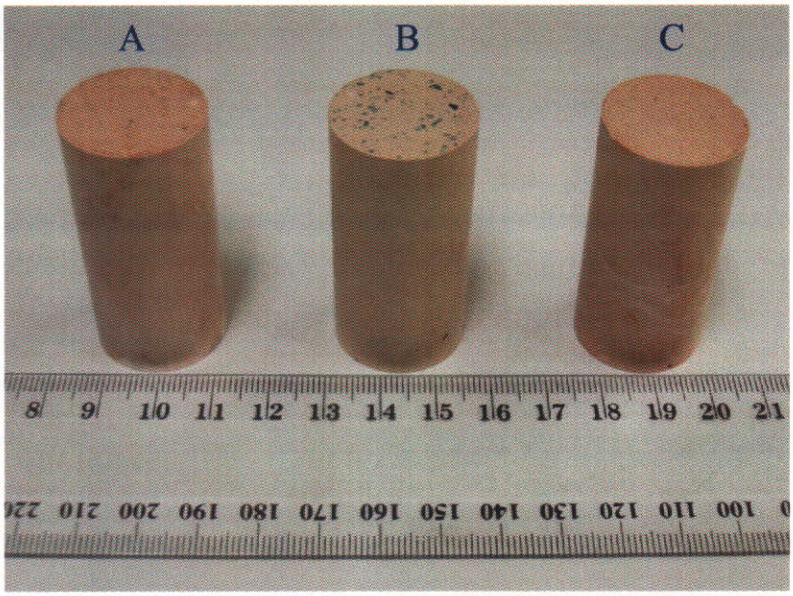

Figure 4.18A Samples prepared for dry shrinkage measurements before heating. (A) Si:Al = 1.5, Na:Al = 0.6; (B) Si:Al = 1.5, Na:Al = 0.6 with granite; (C) Si:Al = 2.0, Na:Al = 1.0.

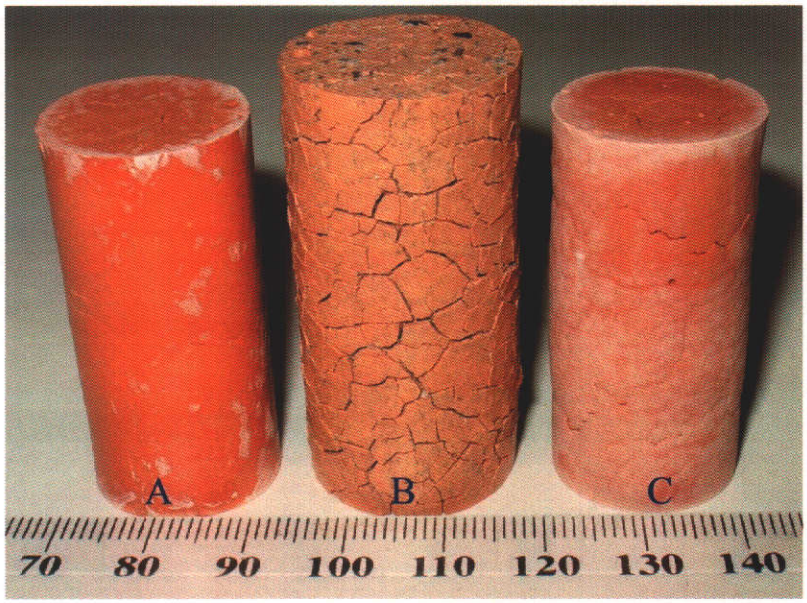

Figure 4.18B Samples after heating to 950°C. (A) Si:Al = 1.5, Na:Al = 0.6; (B) Si:Al = 1.5, Na:Al = 0.6 with granite; (C) Si:Al = 2.0, Na:Al = 1.0.

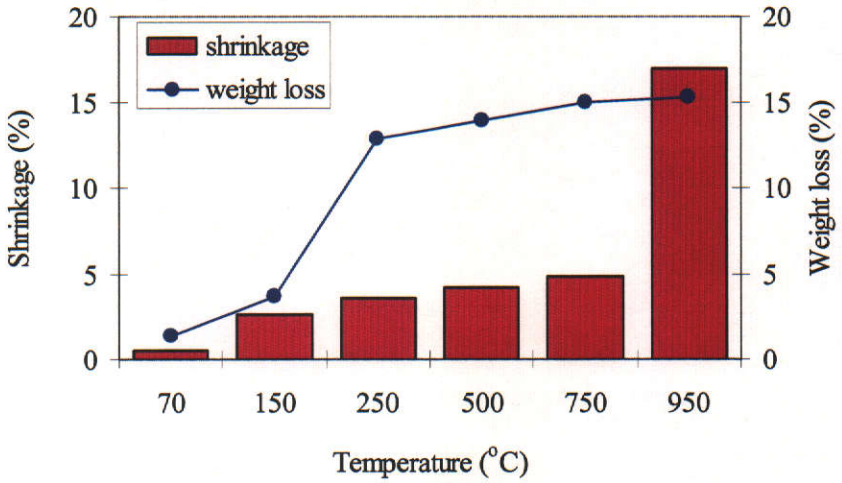

Figure 4.19 Shrinkage and weight loss for a geopolymer with Si:Al = 1.5, Na:Al = 0.6.

Figure 4.20 shows the shrinkage and water loss of geopolymer with an initial composition of Si:Al = 2.0, Na:Al = 1.0. The percentage weight loss as well as the relative shrinkage of this sample was higher than that of the sample with Si:Al = 1.5; Na:Al = 0.6 (figure 4.19) believed to be due to a higher content of reaction water. Crack development of this sample was significantly more extensive than that of the sample in figure 4.19. This suggests that the structural integrity at elevated temperatures of geopolymer with Si:Al = 1.5, Na:Al = 0.6 is likely to be higher than geopolymer with Si:Al = 2.0, Na:Al = 1.0.

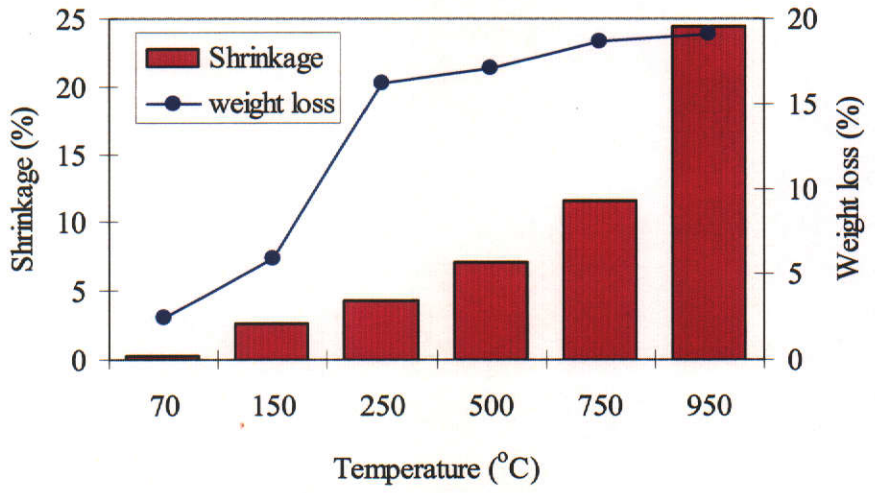

Figure 4.20 Shrinkage and weight loss for a geopolymer with Si:Al = 2.0, Na:Al = 1.0.

X-ray diffraction was performed on samples heated to 950 °C for 1 hour to determine if any structural change had occurred due to heating. Figure 4.21 shows the XRD pattern of the sample in figure 4.19 (Si:Al = 1.5; Na:Al = 0.6) along with the pattern of an unheated sample for comparison. The XRD pattern showed that up to 950 °C, the geopolymer remains amorphous and the peaks of quartz and anatase are also undisturbed. The most significant change in the diffraction pattern is the shift of the amorphous hump towards a lower 2θ indicating a change in bonding configuration in the geopolymer network. Apart from this change, heating the sample up to 950 °C, did not change the structure of geopolymer which displayed a high degree of thermal stabililty and retained its amorphous character. Barbosa & MacKenzie (2003) pointed out that the change in the bonding configuration of heated geopolymer is largely due to the movement of Na^+.

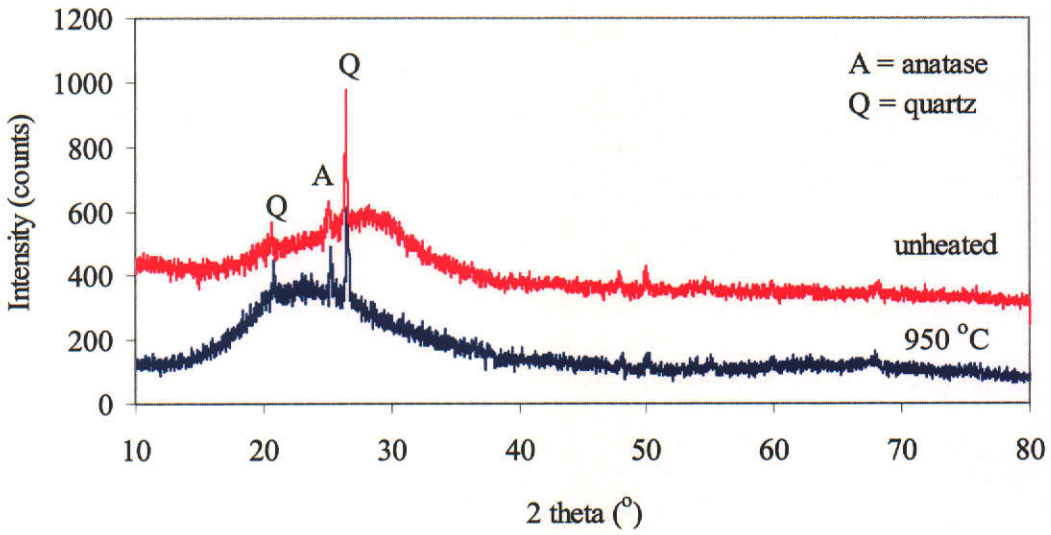

Figure 4.21 XRD patterns of unheated sample and sample heated to 950 °C (Si:Al = 1.5, Na:Al = 0.6).

Figure 4.22 shows the XRD patterns of sample with Si:Al = 2.0, Na:Al = 1.0 before and after heating to 950 °C. The diffraction pattern of this sample indicated that the amorphous nature of geopolymer is largely conserved but additional peaks have appeared at 4.21 Å (21.1° 2θ) and 2.57 Å (34.8° 2θ) due to the formation of sodium aluminium silicate ($Na_6Al_4Si_4O_{17}$) (PDF#10-0033). The formation of sodium

aluminium silicate is likely to occur through solid-state transformation of any excess sodium and unreacted metakaolinite.

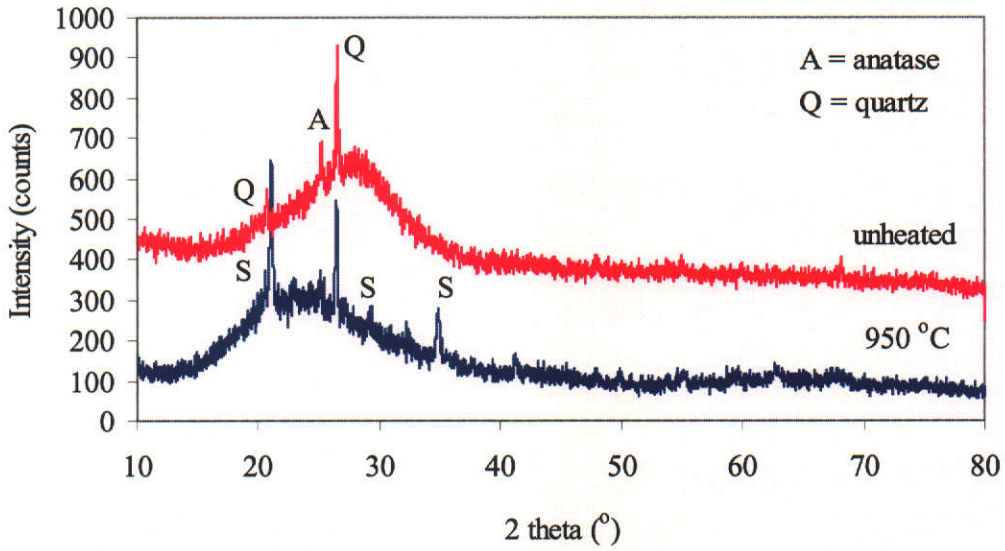

Figure 4.22 XRD patterns of unheated sample and sample heated to 950 °C (Si:Al = 2.0, Na:Al = 1.0). Note additional peaks (S) due to the formation of $Na_6Al_4Si_4O_{17}$.

Figure 4.23 shows shrinkage and weight loss for the geopolymer with a composition of Si:Al = 2.0, Na:Al = 1.0 and 20 wt % quartz aggregate. The curve shows that the percentage weight loss due to dehydration is very similar to that of the geopolymer by itself (figure 4.20). The presence of the aggregate, however, reduced the shrinkage by 60%.

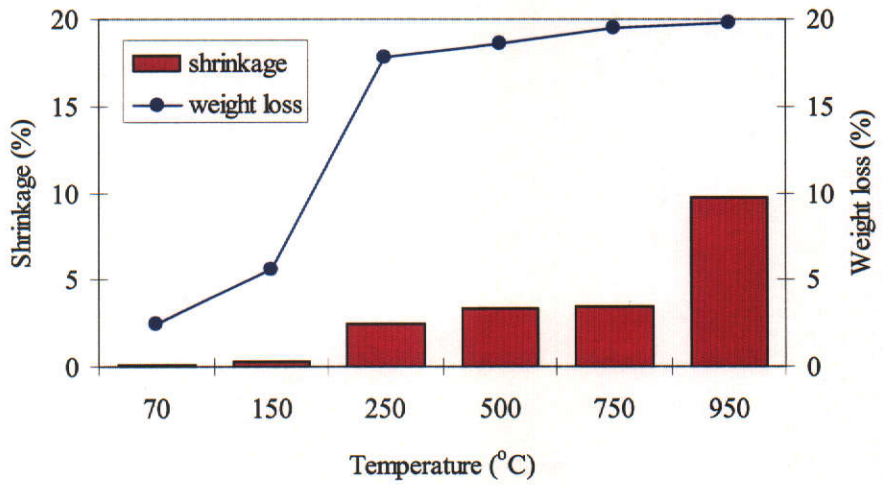

Figure 4.23 Shrinkage and weight loss for geopolymer with Si:Al = 2.0, Na:Al = 1.0 and 20 wt % quartz aggregate.

Figure 4.24 shows shrinkage and water loss for a sample with Si:Al = 1.5, Na:Al = 0.6 containing 20 wt % granite aggregate.

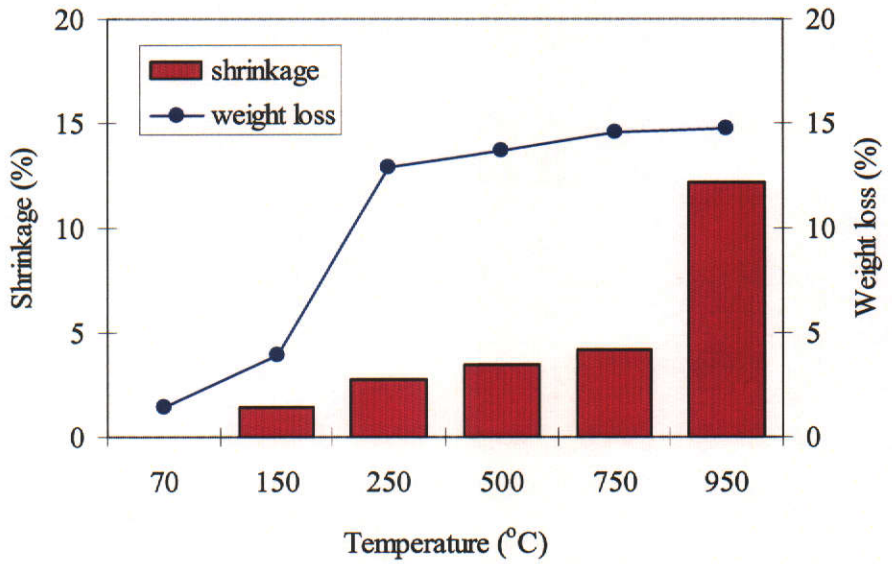

Figure 4.24 Shrinkage and weight loss for geopolymer with Si:Al = 1.5, Na:Al = 0.6 and 20 wt % granite aggregate.

Notwithstanding the different Si:Al and Na:Al the shrinkage for samples containing granite and quartz aggregate is similar. Both samples suffered extensive cracking extending from the surface through to the bulk of the materials (figure 4.17B), which made it impossible to cut a section for XRD characterisation. The development of extensive cracks on these samples is probably due to the differential shrinkage as a result of the difference in the coefficient of thermal expansion between the geopolymer matrix and the aggregate.

4.5.2 Thermal expansion

The thermal expansion and shrinkage behaviour of geopolymers was measured using a DI-24 Adamel Limohargy dilatometer. The measurements were calibrated by using a Pyros standard. Table 4.4 shows that the measurements were performed on geopolymers prepared with a composition of Si:Al = 1.5, Na:Al = 0.6 and Si:Al = 2.0, Na:Al = 1.0. Geopolymers prepared with these compositions were found to have

the highest compressive strengths as well as structural integrity at elevated temperature.

Table 4.4 Geopolymers prepared for thermal expansion measurements.

Sample ID (Si:Al, Na:Al)	Length (L_0) mm	Treatment
(1.5, 0.6)	25.95	as prepared
(2.0, 1.0)	25.50	as prepared
(1.5, 0.6)	25.30	preheated at 125 °C
(2.0, 1.0)	25.10	preheated at 125 °C
(1.5, 0.6) + 20 wt % quartz	25.70	as prepared
(1.5, 0.6) + 20 wt % quartz	26.16	preheated at 125 °C
(2.0, 1.0) + 20 wt % quartz	25.28	as prepared
(1.5, 0.6) + 20 wt % granite	25.20	as prepared
(1.5, 0.6) + 40 wt % quartz	25.02	as prepared

Geopolymer prepared with Si:Al = 2.0, Na:Al = 1.0 suffered substantial shrinkage (about 6 % below 200 °C) which was beyond the capabilities of the dilatometer and thus could not be measured. Figure 4.25 shows the dilatometer curve of an as prepared geopolymer with Si:Al = 1.50, Na:Al = 0.6 measured from about 23 °C to 900 °C with a heating rate of 2 °C/minute.

The curve shows that the water loss (about 15 wt %, see section 4.5.1) from room temperature up to 250 °C is associated with about 2 % shrinkage. Between 250 and 800 °C the geopolymer is essentially dimensionally stable indicating that this may be a useful working temperature range. Further substantial shrinkage from about 800 °C to 900 °C occurs due to densification within the sample bulk and was beyond the range of the dilatometer. The shrinkage behaviour of geopolymer reported in this study is in good agreement with the results reported by Barbosa & McKenzie (2003).

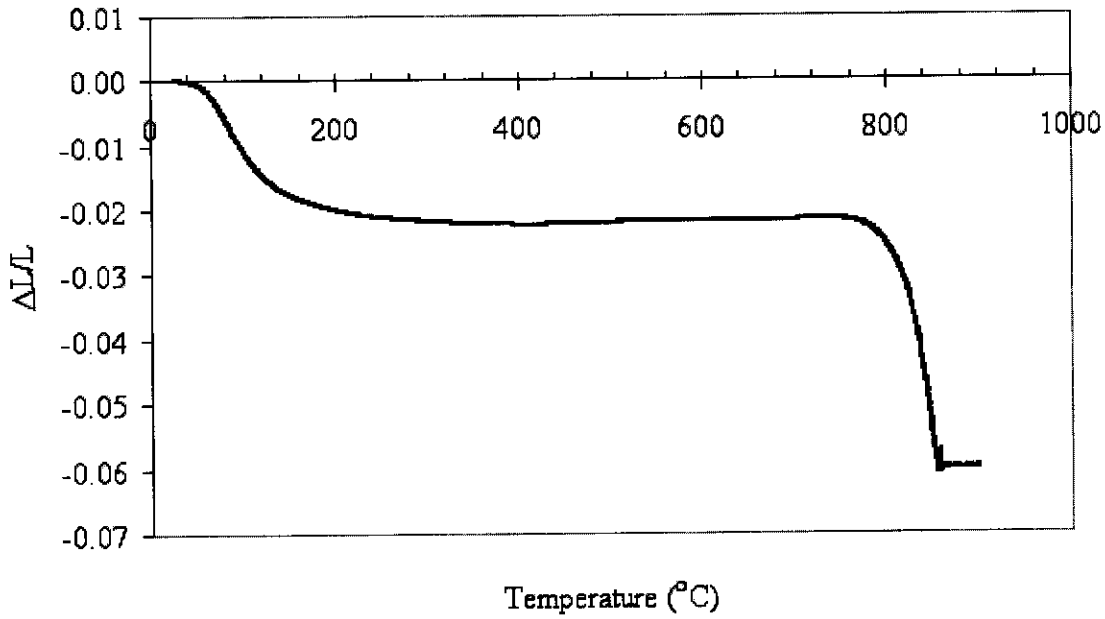

Figure 4.25 Dilatometer curve for geopolymer with Si:Al = 1.5, Na:Al = 0.6. ΔL is the change in length.

The coefficient of thermal expansion (α) based on dilatometer measurements was calculated by using the following formula:

$$\alpha = \left[\frac{1}{L_T}\right]\left[\frac{dL}{dT}\right]_T \qquad (4.1)$$

where:

L_T = the length of the sample at temperature (T) (mm)

$dL = L_0 - L_T = \Delta L$ = the change of the length as a function of temperature (mm)

dT = the change of temperature (°C).

Figure 4.26 shows the change of the length versus temperature for geopolymer with Si:Al = 1.5, Na:Al = 0.6 in the temperature range between 100 and 750 °C. A fifth degree of polynomial was used to fit the experimental results. The polynomial expression is differentiated to obtain dL/dT and the result divided by the value of L_T to obtain α_T at each temperature.

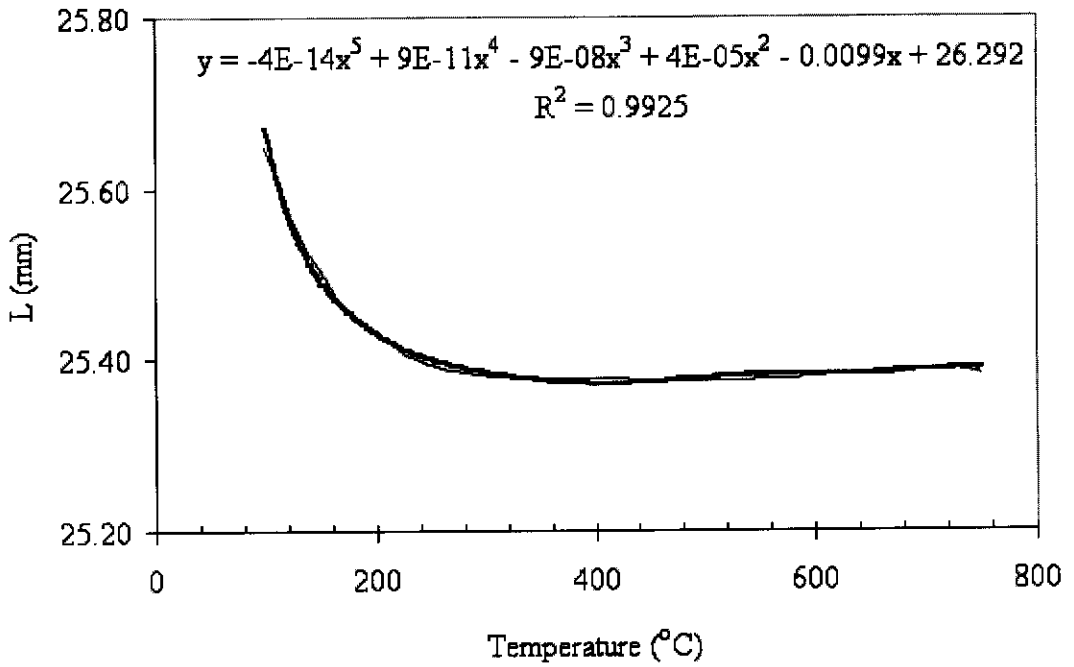

Figure 4.26 The relationship between sample length (L) and temperature for as prepared geopolymer with Si:Al = 1.5, Na:Al = 0.6.

The plot of α_T versus temperature for geopolymer with Si:Al = 1.5, Na:Al = 0.6 is provided in figure 4.27. Figure 4.27 shows that the coefficient of thermal expansion of geopolymer is negative and decreases rapidly from 100 °C (α = - 2 x 10^{-4} $°C^{-1}$) to 250 °C (α = - 0.76 x 10^{-4} $°C^{-1}$) and gradually increases from 300 °C to 750 °C (α = - 5.2 x 10^{-4} °C).

According to Neville (2000, p. 378) the coefficient of thermal expansion for Portland cement paste is positive and varies between 1.1 x 10^{-5} $°C^{-1}$ and 2.0 x10^{-5} $°C^{-1}$. The author, however, does not mention the temperature range of these values.

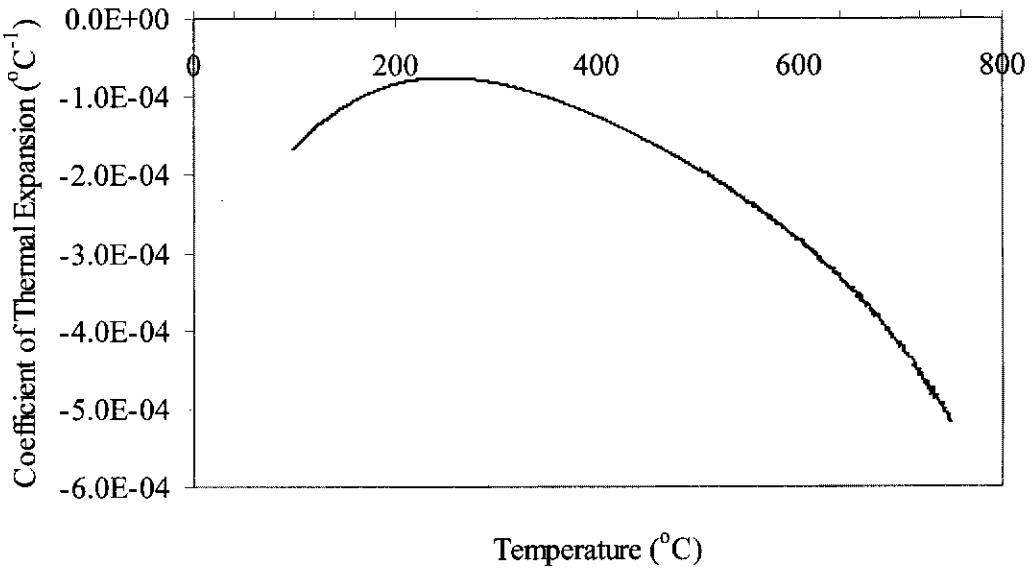

Figure 4.27 The coefficient of thermal expansion as a function of temperature for geopolymer with Si:Al = 1.5, Na:Al = 0.6.

Figure 4.28 shows dilatometer curves for geopolymers containing quartz and granite aggregate. For geopolymer with Si:Al = 1.5, Na:Al = 0.6 the presence of 20 wt% aggregate was found to reduce the shrinkage to about 1 % in the temperature range between 23 and 500 °C. Increasing the aggregate content to 40 wt % for the same geopolymer composition further reduced the shrinkage. An even greater reduction in shrinkage occurred when quartz aggregate was added to geopolymer with Si:Al = 2.0, Na:Al= 1.0, albeit with severe cracking.

Geopolymers containing quartz aggregate show an abrupt expansion between 500 – 540 °C followed by further shrinkage as the temperature is increased. This is believed to be due to quartz undergoing a phase change. Raz, Girsperger & Thompson (2004) pointed out that the thermal expansion of quartz is divided into two regions: the first region shows the thermal expansion of quartz increasing rapidly up to the low-high quartz transition (at 574 °C) and the second region which occurs above 574 °C where the quartz shows negative thermal expansion. It is apparent that there is a discrepancy between our observed quartz transition temperature and the reference temperature. In an attempt to determine the cause of this discrepancy the dilatometer thermocouple was re-calibrated and data was collected for a pure quartz sample that confirmed that

the quartz transition temperature was 574 °C. The next step was to collect additional TG-DTA and differential scanning calorimetry (DSC) data. These data revealed the presence of an exothermic reaction in the region 400 to 500 °C that is believed to result in the interior of the sample becoming hotter than the exterior during the dilatometry experiments leading to an apparent incorrect lower transition temperature being recorded. Geopolymer containing granite aggregate does not exhibit this transition and is dimensionally stable up to 800 °C.

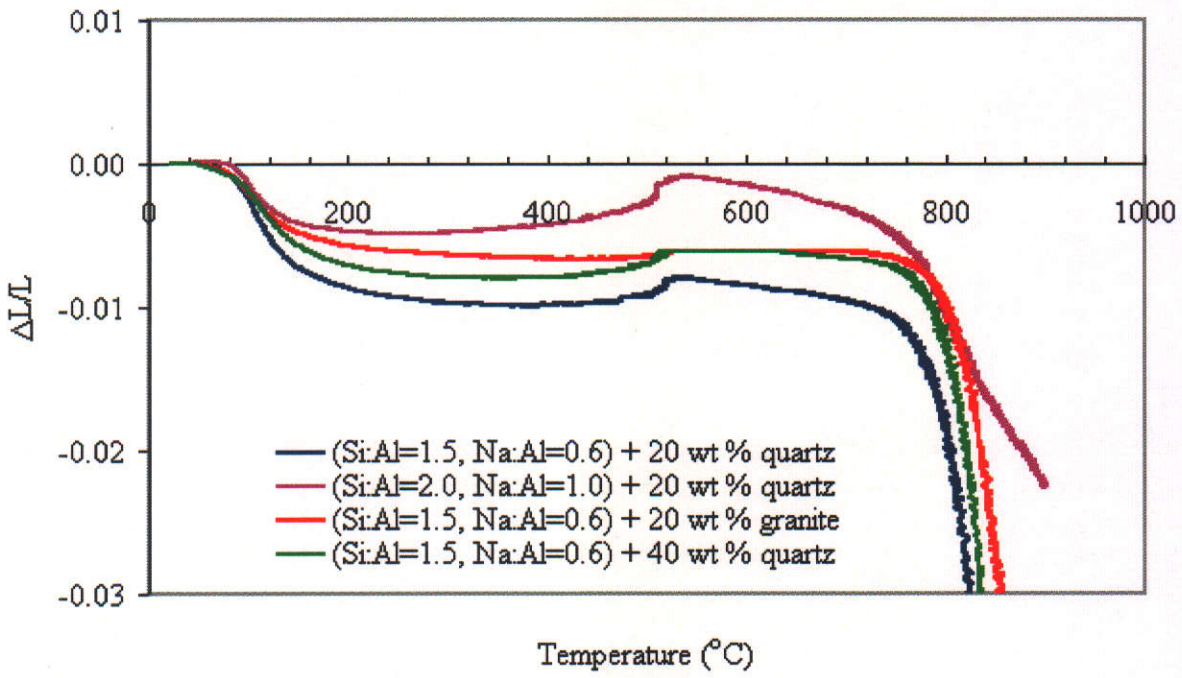

Figure 4.28 Dilatometer curves for geopolymers containing quartz and granite aggregate.

Figure 4.28 indicates that although the inclusion of quartz has a significant effect in reducing the shrinkage of geopolymers at elevated temperatures, the useful upper working temperature is restricted to 500 °C to maintain the sample below the quartz transition temperature. For this reason, fire-resistant concrete based on Portland cement is never made with quartz aggregate (Neville, 2000 p.149).

The TG-DTA results (section 4.4.1) suggest that geopolymers incorporated about 15% of the initial reaction water in the structure, of which 8.5% was lost before about 135 °C. The following measurements were performed to separate the effect of

water loss on subsequent shrinkage behaviour. The samples were first dried in an oven at 125 °C for 1 hour (preheated) and then air cooled to room temperature before undertaking thermal expansion measurements.

Figure 4.29 shows the dilatometer curves for geopolymers with Si:Al = 1.5, Na:Al = 0.6 for both as prepared and preheated samples. The curve shows that the preheating has a significant effect on reducing the shrinkage between 23 and 350 °C. The curve also shows that the preheated geopolymer has a lower densification temperature (750 °C) than the as prepared geopolymer (800 °C).

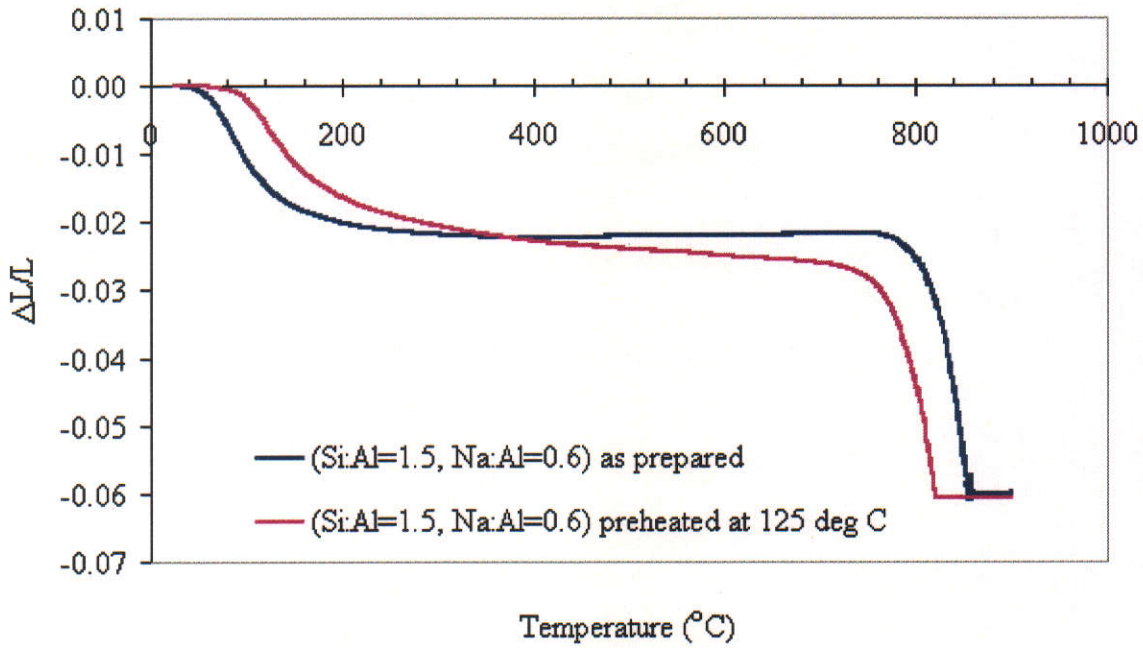

Figure 4.29 Dilatometer curves for as prepared and preheated geopolymers with Si:Al = 1.5, Na:Al = 0.6.

Preheating a geopolymer containing quartz aggregate was also found to reduce the shrinkage as shown in figure 4.30. The dilatometer curve for preheated geopolymer containing aggregate shows, that between 23 and 500 °C, the shrinkage is about 0.5%. The results indicate that geopolymers with or without aggregate require a post-thermal treatment to minimise the shrinkage as a function of temperature before it can be put in service, particularly for fire-resistance applications.

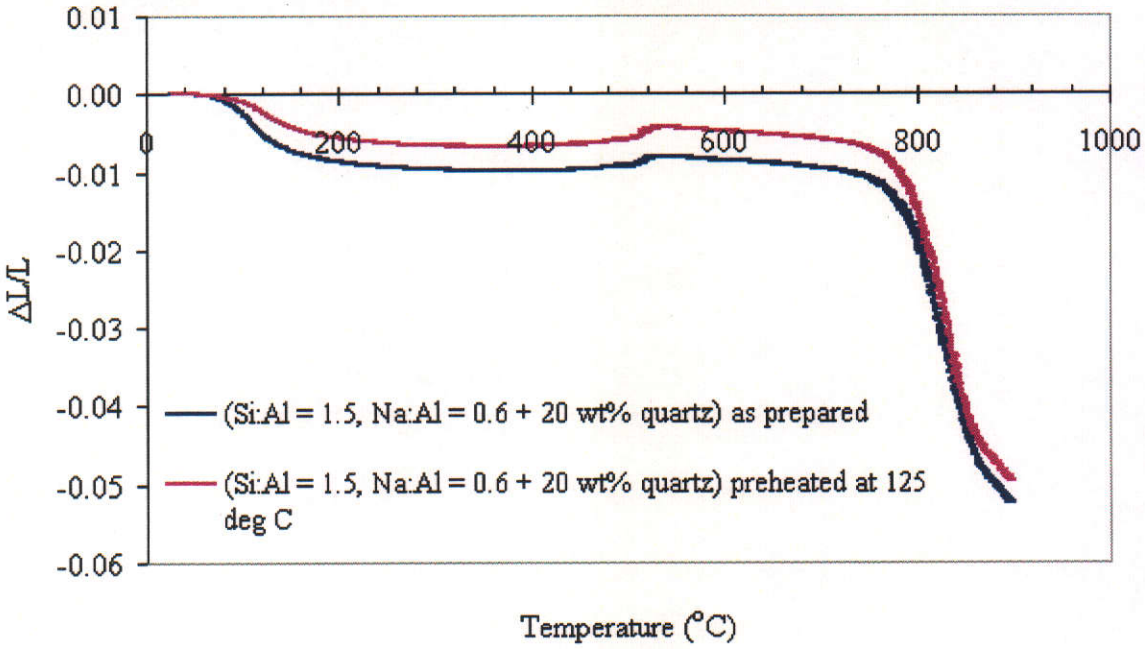

Figure 4.30 Dilatometer curves for geopolymers with Si:Al = 1.5, Na:Al = 0.6 containing 20 wt% quartz aggregate. The measurements were performed on as prepared and a sample preheated to 125 °C.

4.5.2 Thermal conductivity

Aluminosilicate geopolymers have been recognised as a potential substitute material for ordinary Portland cement as well as being suitable for insulation purposes. For both applications, thermal conductivity is one of the important parameters to be determined if the material is to perform adequately. Xu and Chung (2000) reported that the typical value of thermal conductivity of ordinary Portland cement paste is (0.53 ± 0.03) W m^{-1} K^{-1} while Demirboga (2003) reported that the thermal conductivity of cement paste was (0.76 ± 0.05) W m^{-1} K^{-1} and (1.19 ± 0.05)W m^{-1} K^{-1} for mortar. Santoyo *et* al. (2001) reported that the thermal conductivity of cements for geothermal applications was between 0.5 – 0.8 W m^{-1} K^{-1}.

The technique employed to measure the thermal conductivity of geopolymers in this study was a hot-wire method (see chapter 3 for details). In this method, the temperature as a function of time consists of two distinct regions (figure 4.31) (ASTM D5930). In the first region, the temperature will rapidly rise and contact resistance due to the interface between the specimen and the measuring device

results in a nonlinearity in the initial portion of the transient. As the heat begins to soak in, the rate of rise becomes constant (region two). This state typically is achieved after about 10 and 20 s after the current starts flowing.

A series of preliminary measurements was performed in order to optimise the current passing through the heating wire. The preliminary results indicated that the power applied to the wire should be between 2.0 – 3.0 watt, which caused the sample's temperature to rise approximately 6 – 7 °C. Figure 4.32 shows the temperature as a function of time for a sample having a length of approximately 12.00 cm and diameter of 2.00 cm. The results indicated that the heat front reached the edge of the sample in a very short time, degrading the linearity of region 2. The thermal conductivity can be calculated from the linear portion of the curve using equation 3.16.

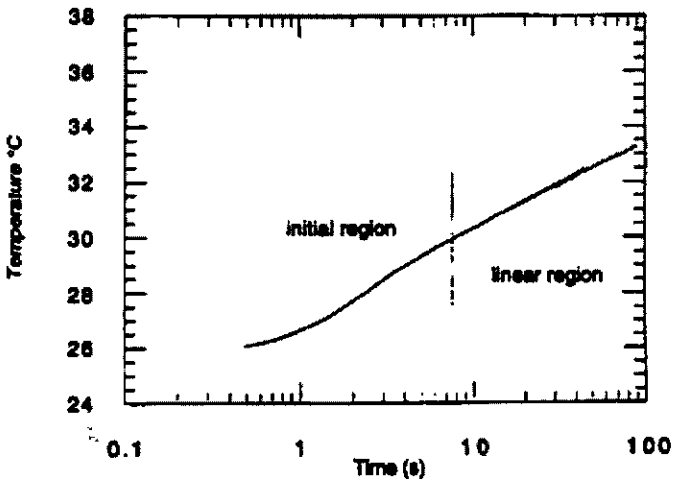

Figure 4.31 Temperature as a function of time from hot-wire method (ASTM D5930).

In order to minimise the effect of contact resistance as well as to improve the linearity of region 2, the size of the specimen should be large enough to allow a sufficiently long measurement time to be performed. Figure 4.33 shows the temperature rise as a function of time for a larger specimen (L = 23.10 cm, d = 5.00 cm). The curve shows that effect of contact resistance has been reduced significantly and the linearity of region 2 is very high. The slope used in the calculation of thermal conductivity was determined by using a linear least square regression.

The thermal conductivity of each sample was measured at least 3 times keeping the voltage and current relatively constant. After each measurement, the sample was left for several hours before the next measurement so that the initial sample temperature was the same. Table 4.5 shows the thermal conductivity values of geopolymers measured in this study. The values of the thermal conductivity of the sample TC-03 (Si:Al = 2.0; Na:Al = 1.0) is slightly lower than that of TC-01 (Si:Al = 1.5, Na:Al = 0.6) and TC-02 (Si:Al = 1.5, Na:Al = 0.8). The difference in thermal conductivity for these samples is believed to be due to the differences in their bulk density. Equation 3.10 shows that for a typical sample the thermal conductivity is related (proportionally) to its bulk density.

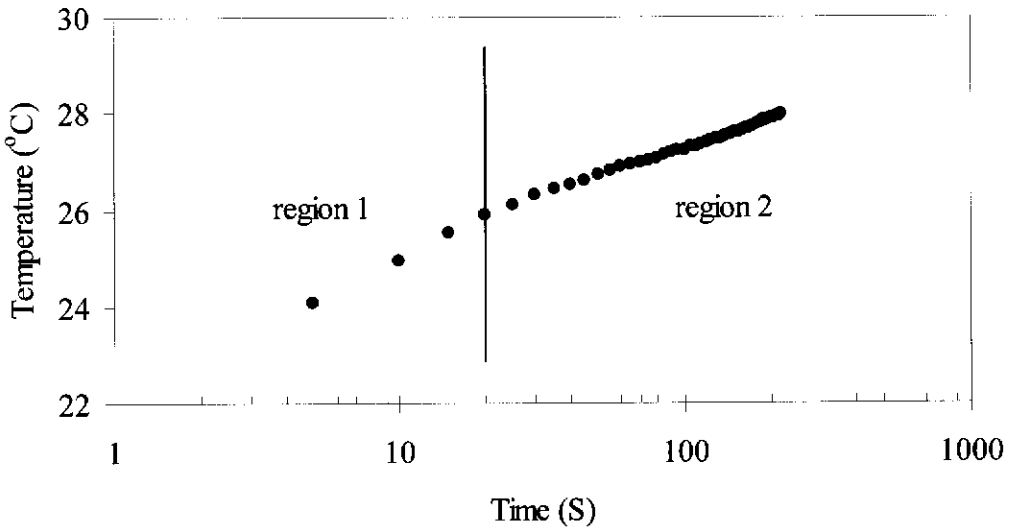

Figure 4.32 Temperature as a function of time measured on a small sample (L =12.00 cm; d = 2.00 cm), showing two distinct regions.

Table 4. 5 Density and thermal conductivity of geopolymers.

Sample ID	Density (g cm^{-3})	Thermal conductivity (W m^{-1} K^{-1})
TC-01 (Si:Al = 1.5, Na:Al =0.6)	1.68 (0.09)	0.65 (0.04)
TC-02 (Si:Al = 1.5, Na:Al =0.8)	1.62 (0.05)	0.64 (0.03)
TC-03 (Si:Al = 2.0, Na:Al =1.0)	1.43 (0.01)	0.55 (0.03)
TC-04 (Si:Al = 1.5, Na:Al = 0.6 40 wt% quartz aggregate)	1.89 (0.02)	0.91 (0.07)

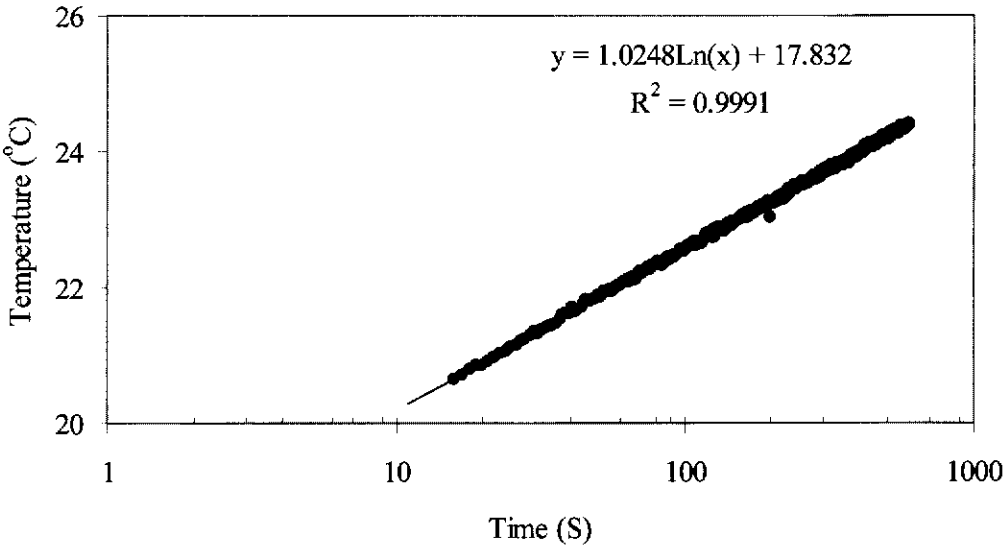

Figure 4.33 Temperature as a function of time for geopolymer with composition Si:Al = 1.5, Na:Al = 0.8. Note only region 2 is shown.

The addition of 40 wt% of quartz aggregate increased the thermal conductivity by about 40%. This was expected since the presence of quartz in the structure of geopolymer increases the density by 12.5 % and hence will increase the thermal conductivity. The higher value of thermal conductivity of geopolymer containing quartz aggregate makes this material suitable as a structural material for buildings and bridges. It is known that a high value of thermal conductivity can be desirable due to the associated ability to reduce temperature gradients and hence the thermal stress (Xu & Chung 2000).

Davidovits (2000) reported that the average value of thermal conductivity for geopolymers paste is about 0.7 W m^{-1} K^{-1}. This value, however, can be tailored in accordance to its intended application. Liefke (1999) produced geopolymer foam for thermal insulation having a thermal conductivity of 0.037 W m^{-1} K^{-1} (with a density between 0.1 – 0.8 g cm^{-3}).

The value of thermal conductivity of geopolymer paste obtained in this study is slightly higher than the thermal conductivity of ordinary Portland cement reported by Xu & Chung (2000) and Demiborga (2003), but within the range of thermal conductivity reported by Santoyo *et* al (2001). In addition, Xu & Chung (2000) reported that the addition of sand into the cement paste increases its thermal

conductivity by 22%. This suggests that the increase of thermal conductivity due to the presence of quartz aggregate in geopolymer (40%) is much higher than the increase of thermal conductivity observed in Portland cement plus quartz (12%) as reported by Xu and Chung (2000).

4.6 Physical and Mechanical Properties of Geopolymers.

This section presents the physical and mechanical properties of the geopolymers prepared in this project. The properties measured are bulk density and apparent porosity, Vickers hardness, compressive strength, and the interfacial bond strength between the geopolymer matrix and the aggregate. The relationships between each parameter is established and discussed in order to gain insight into the nature of the physical and mechanical properties of geopolymers.

4.6.1 Bulk density and apparent porosity

Figure 4.34 shows the bulk density and the apparent porosity of geopolymers as a function of Si:Al atomic ratio with a fixed atomic ratio of Na:Al = 0.6. The apparent porosity of the specimens ranges from about 33 to 24 %, decreasing as the initial Si:Al atomic ratio of increases. The highest apparent porosity occurred for a Si:Al = 1.04 where zeolite-A was formed in conjunction with amorphous geopolymer.

The bulk density of the specimens ranged from about 1.40 to 1.70 g cm^{-3} with a maximum at Si:Al = 1.50. The apparent density and hence the bulk density of the specimen with Si:Al = 2.0, Na:Al = 0.6 could not be measured since the sample disintegrated during the boiling process.

Figure 4.35 shows the bulk density and the apparent porosity of samples with Si:Al = 1.04 – 2.00 and Na:Al = 0.8. The curve shows that the apparent porosity of the specimens decreases from Si:Al = 1.04 to 1.50 and increases slightly as the Si:Al increases. The bulk density of the specimens shows a slight increase up to Si:Al = 1.5 and then remain constant for higher ratios. The large measurement uncertainties associated with both parameters, however, makes it difficult to identify any trend.

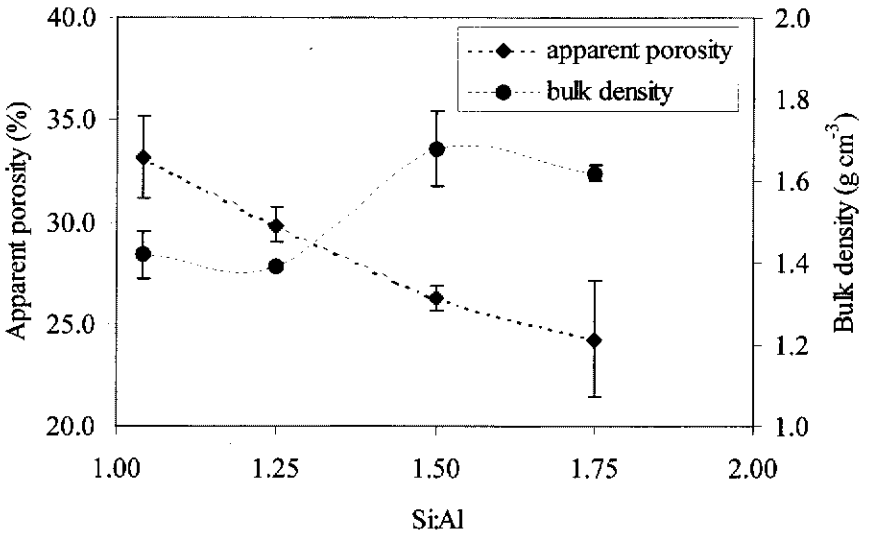

Figure 4.34 Bulk density and apparent porosity as a function of Si:Al (Na:Al = 0.6). Error bars represent 2SD.

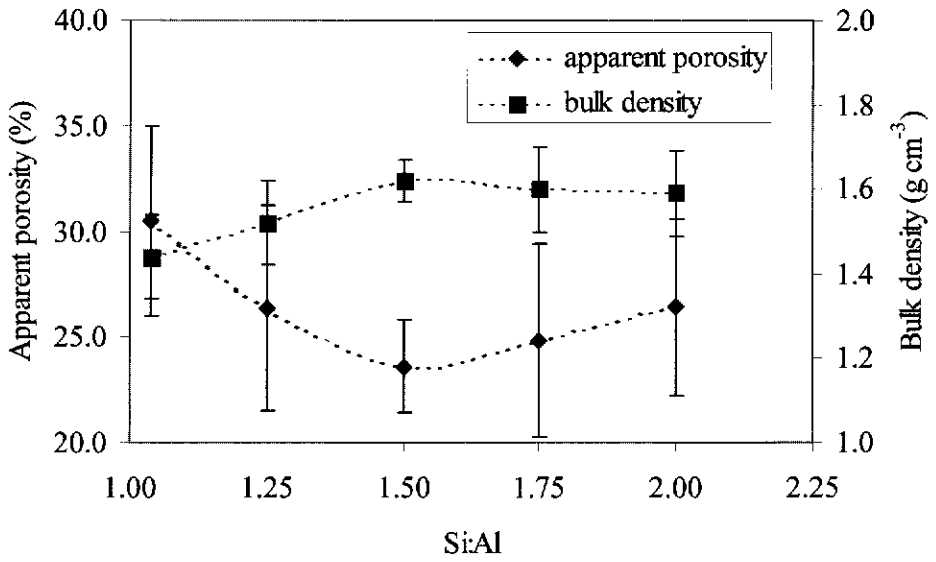

Figure 4.35 Bulk density and apparent porosity as a function of Si:Al (Na:Al = 0.8). Error bars represent 2SD.

Figure 4.36 shows the bulk density and the apparent porosity of geopolymers with Si:Al = 1.04 – 2.00 and Na:Al = 1.0. There is a large variation of apparent porosity as a function of Si:Al, in contrast with the value of bulk density, which shows only a

small change. The apparent porosity of the sample with Si:Al = 1.04, Na:Al = 1.0 is about 37 % representing the highest apparent porosity of all the samples produced.

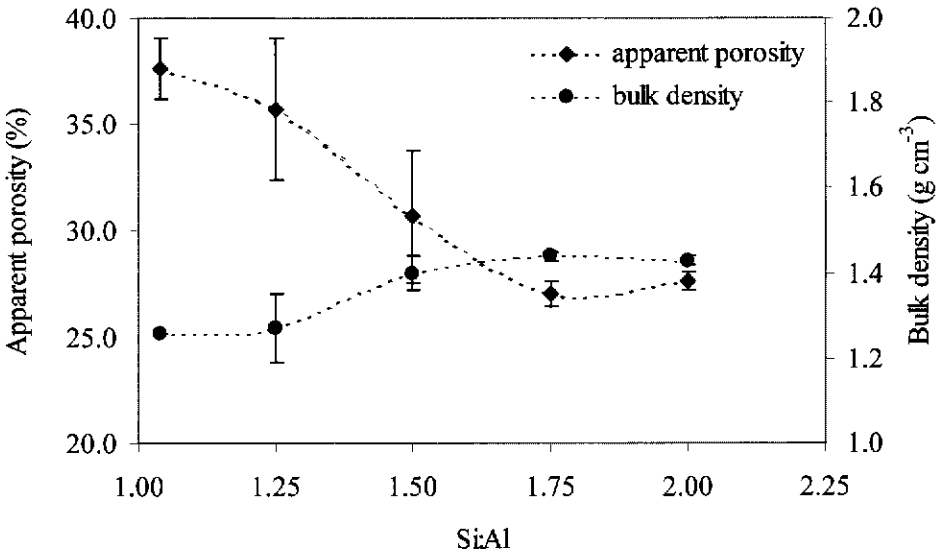

Figure 4.36 Bulk density and apparent porosity as a function of Si:Al (Na:Al = 1.0). Error bars represent 2SD.

4.6.2 Vickers hardness

Vickers hardness tests were performed to measure the geopolymers' resistance to plastic deformation. As a cementitious type of material, geopolymers do not have a very high hardness and therefore the applied load should be in the range 0.1 to 1.5 kg, referred to as low load hardness (Igarashi, Bentur & Mindess 1996). In this study, the applied load was varied between 0.3 – 1.0 kg which provided a reasonable indent for hardness determination.

A series of preliminary measurements were made to investigate the influence of the applied load (kg) on hardness. Figure 4.37 shows a plot of the applied load versus the hardness of geopolymer prepared with nominal composition Si:Al = 1.5, Na:Al = 0.6 and Si:Al = 1.75, Na:Al = 0.8. The curves show that the hardness of the material slightly decreases as the load increases indicating that the material is not homogeneous. Microstructural examination reveals that the material consists of a large number of grains (unreacted metakaolinite) surrounded by the geopolymer

matrix as well as a large number of pores. The presence of these grains as well as the pores affects the size of the indentation, which in turn influences the hardness value.

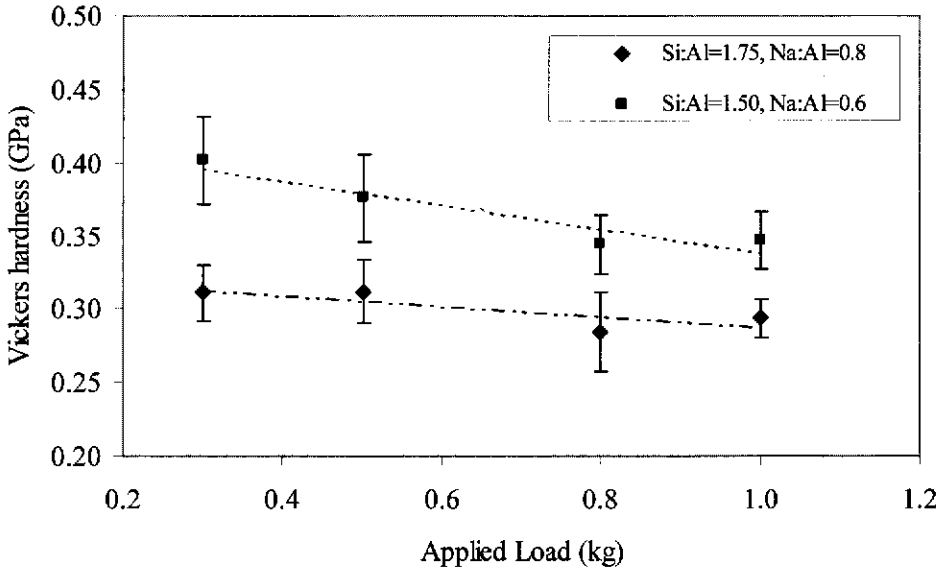

Figure 4.37 Dependence of hardness on the applied load with linear lines of best fit. Error bars represent 2SD.

Figure 4.38 shows the relationship between the applied load and the resulting indentation size (d) for geopolymer samples shown in figure 4.37. The results indicate that the indentation size is related to the applied load (P) as shown by the best-fit lines.

The widely used model to describe the relationship between the applied load and the indentation size is the Meyer law (Quinn & Quinn 1997):

$$P = \beta d^{n} \tag{4.2}$$

where P is the applied load, d is the length of the diagonal indentation, β and *n* are constants which can be derived from curve fitting of the experimental data.

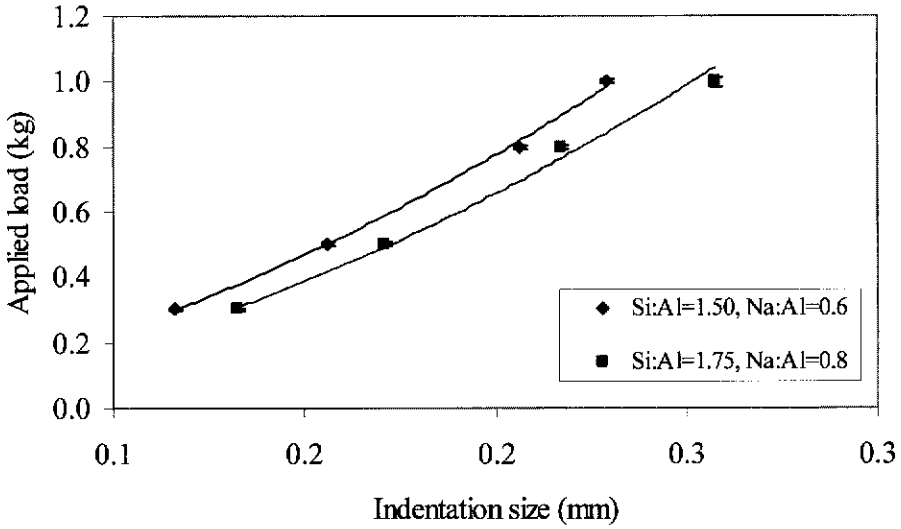

Figure 4.38 Indentation size (d) as a function of applied load for geopolymer samples shown in figure 4.37. The lines indicate the best-fit satisfying equation 4.2.

Sangwal (2000) pointed out that the Meyer index (n) can be used to express the indentation size effect (ISE): (i) $n < 2$, the hardness is dependent on load and (ii) $n = 2$, the hardness is independent of load. The application of equation 4.1 to the geopolymer samples is shown in figure 4.37. The best-fit values of the parameters β and n for each sample are shown in table 4.6.

Table 4.6 Variation of β and n parameters derived from equation 4.1 for geopolymer samples shown in figure 4.38.

Sample ID	β (N/mm)	n	Correlation
Si:Al=1.50, Na:Al =0.6	12.970	1.7507	0.9991
Si:Al=1.75, Na:Al=0.8	12.687	1.8404	0.9939

Based on this result (n<2), the determination of Vickers hardness for geopolymers as a function of Si:Al and Na:Al atomic ratios was performed using a 1 kg load applied for about 20 s. With this load, the indent diagonals can be determined with high accuracy under the optical microscope.

Figure 4.39 and 4.40 are SEM micrographs showing typical indentations for a 1 kg load. Figure 4.39 shows the indentation of geopolymer with Si:Al = 1.04 and Na:Al = 0.6 which has the lowest hardness and figure 4.40 shows the indent of geopolymer Si:Al = 1.5 and Na:Al = 0.6 which has the highest hardness.

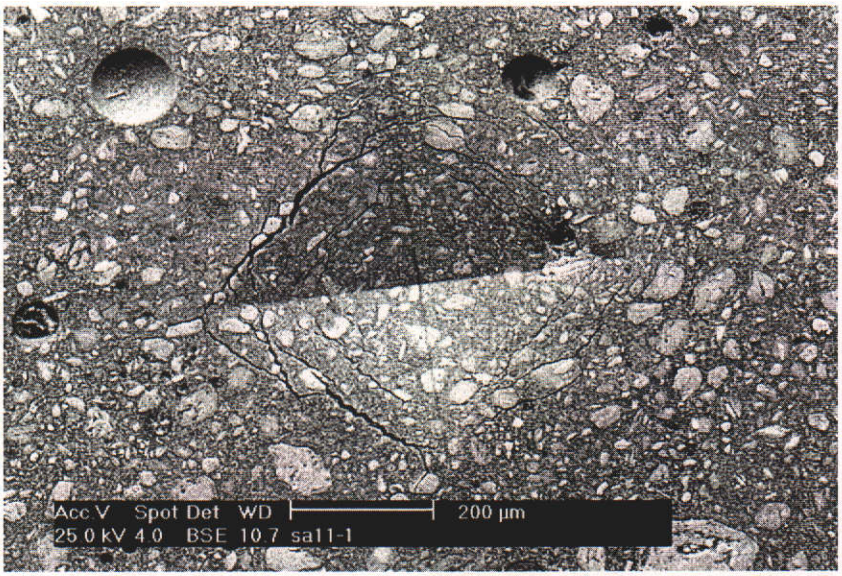

Figure 4.39 SEM micrograph of Vickers indentation of Si:Al = 1.04, Na:Al = 0.6 (load = 1 kg).

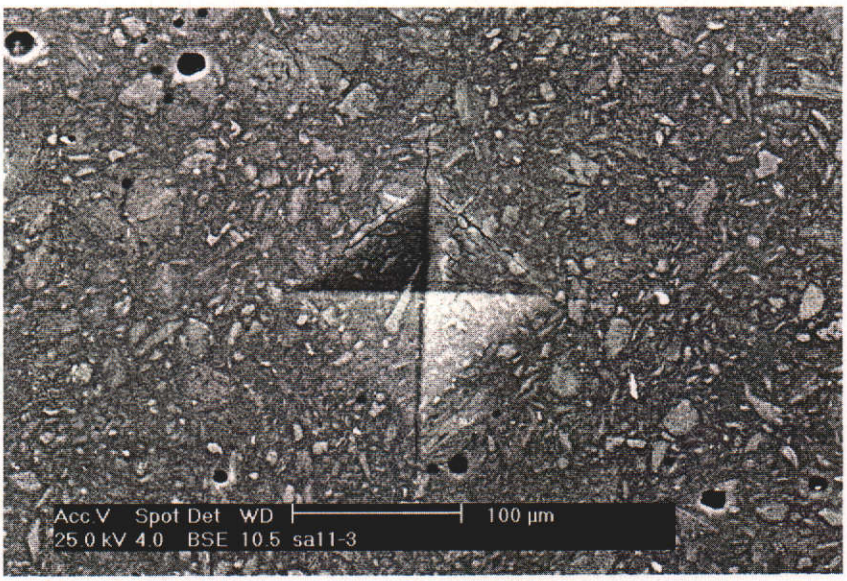

Figure 4.40 SEM micrograph of Vickers indentation of Si:Al = 1.5, Na:Al = 0.6 (load = 1 kg).

The value of Vickers hardness as a function of Si:Al is presented in figure 4.41. The hardness of all specimens increases in an almost linear fashion as the Si:Al increases except for the sample with Si:Al = 1.50, Na:Al = 0.6. The relationship between the hardness and the compressive strength of the geopolymers is presented in the next section.

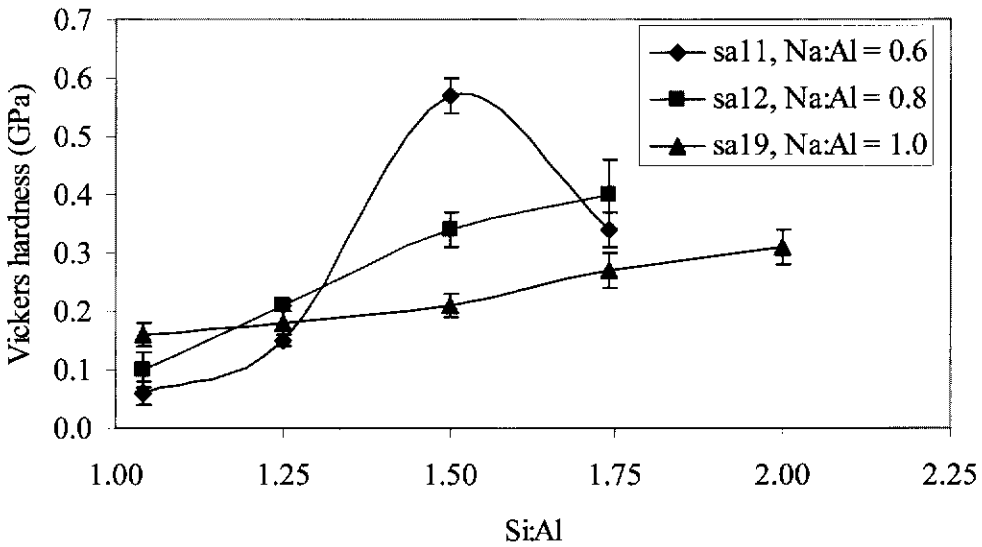

Figure 4.41 Vickers hardness as a function of Si:Al for three different values of Na:Al. Error bars represent 2SD.

4.6.3 Compressive strength

Compressive strength is a critical characteristic required for many of the proposed applications for geopolymers. It has been recognised that the compressive strength of mortar or concrete is an important parameter in structural design while flexural strength is of interest for the design of highway and airfield slabs where shear strength and crack resistance is more important (Neville 2000 p.308 –309).

In compression testing geopolymer sample were tested to failure to obtain an overall view of geopolymer quality as it is related to structure of the geopolymer paste.

Strength development

It has been recognised that geopolymers have high-early strength with maximum strength being achieved after several days (Davidovits 1994a; Zhang & Malhotra 1995). In order to examine the influence of chemical composition as well as the inclusion of aggregate on the strength of the geopolymers, it was first necessary to determine the strength-time relationship.

Figure 4.42 shows the compressive strength development of geopolymers (Si:Al = 1.75 and Na:Al = 0.6) with and without aggregate. The samples with aggregate were prepared by adding of 20 wt % α-quartz with a particle size < 212 μm to the geopolymer resin prior to curing. Each compression strength test was conducted on cylindrical samples, 50 mm in length and 25 mm in diameter, achieving a length to diameter ratio of 2 as required by ASTM C 773. All the values presented in the graphs are the average of three separate tests, with error bars equal to 2 SD (standard deviation).

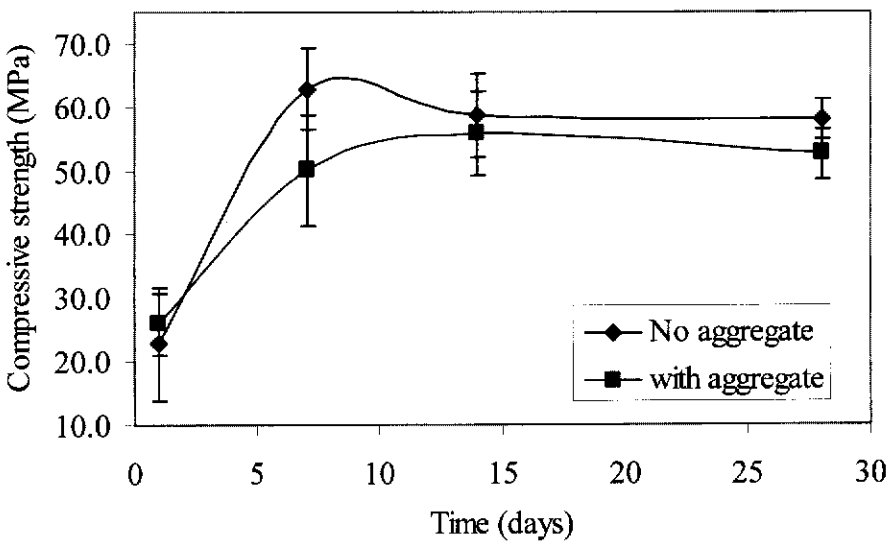

Figure 4.42 Strength development of geopolymer (Si:Al = 1.75, Na:Al = 0.6) with and without α-quartz aggregate. Error bars represent 2 SD.

The curves show that the strength of the geopolymers increases rapidly with time, reaching a maximum after 7 days. When the error bars are taken into account, the curves indicate that samples containing α-quartz aggregate have essentially the same

compressive strength as the specimens without aggregate. Further results on the strength of geopolymers with aggregates will be presented and discussed in the next section.

Strength vs Si:Al

Figure 4.43 is a plot of compressive strength as a function of Si:Al for three different series of samples measured after ageing the samples between 7 to 14 days. A Si:Al ratio of 1.5 (Na:Al = 0.6) was found to produce the highest compressive strength (86 ± 16 MPa). It is notable that for samples with a Na:Al = 1.0, the maximum strength occurred at Si:Al = 1.75 and Si:Al = 2.0. The trend in the measured compressive strength observed in this study is in good agreement with the results reported by Hos, McCormick & Byrne (2002). However, the maximum strength they reported is 5 times higher than that observed in this study. The difference in the strength is probably due to the preparation method as the researchers prepared their samples from melt-quenching a sintered $Al_2O_3.2SiO_2$ pellet.

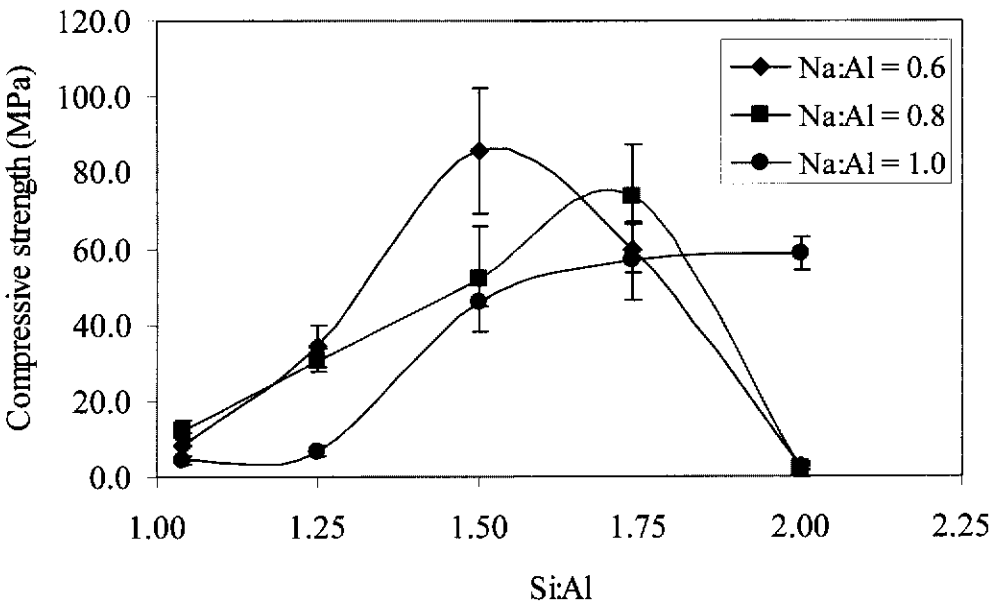

Figure 4.43 Compressive strength of geopolymers prepared with different initial ratios of Si:Al and Na:Al. Error bars represent 2SD.

Escalante-Garcia and Sharp (2001) measured the compressive strength of ordinary Portland cement paste hydrated at various temperatures. They reported that for conditions similar to this study (age = 7 days, curing temperature = 60 °C) a maximum compressive strength of 40 Mpa was obtained. The result of this study indicates that the compressive strengths of geopolymers with Si:Al ≥1.5, Na:Al ≥ 0.6 exceed those for Portland cement pastes.

In this study, all Na-poly(sialate) type of geopolymers showed low compressive strength. Similar results are also reported by Davidovits (1988) and Rowles & O'Connor (2003). It is believed that the low compressive strength is due to the formation of zeolite or sodalite in the geopolymer network. In the formation of these geopolymers, there is insufficient OH^- to completely dissolve Si^{4+} and Al^{3+} as well as insufficient Na^+ to allow a complete geopolymerisation of the network. As a result, the resulting geopolymers cannot form large enough polymer networks that have high structural integrity (Rowles & O'Connor 2003).

The dependence of compressive strength on the sample composition is clearly demonstrated in figure 4.43. It is important, however, to also examine the dependence of strength on the porosity of each composition. It has been shown in section 4.5.1 that the apparent porosity of geopolymers decreases as the Si:Al ratio increases. Figure 4.44 shows the relationship between the porosity and the compressive strength of the samples shown in figure 4.43. As expected, the strength of the material decreases as the porosity increases.

The curve-fit of the data presented on figure 4.44 was obtained by a power function shown in table 4.7.

Table 4.7 Variation of the power function for curve-fit shown in figure 4.44.

Sample ID	Power function	Correlation
Na:Al = 0.6	$y = 9.97^{14x^{-9.40}}$	0.8852
Na:Al = 0.8	$y = 6.30^{10x^{-6.53}}$	0.8646
Na:Al = 1.0	$y = 6.83^{12x^{-7.72}}$	0.9914

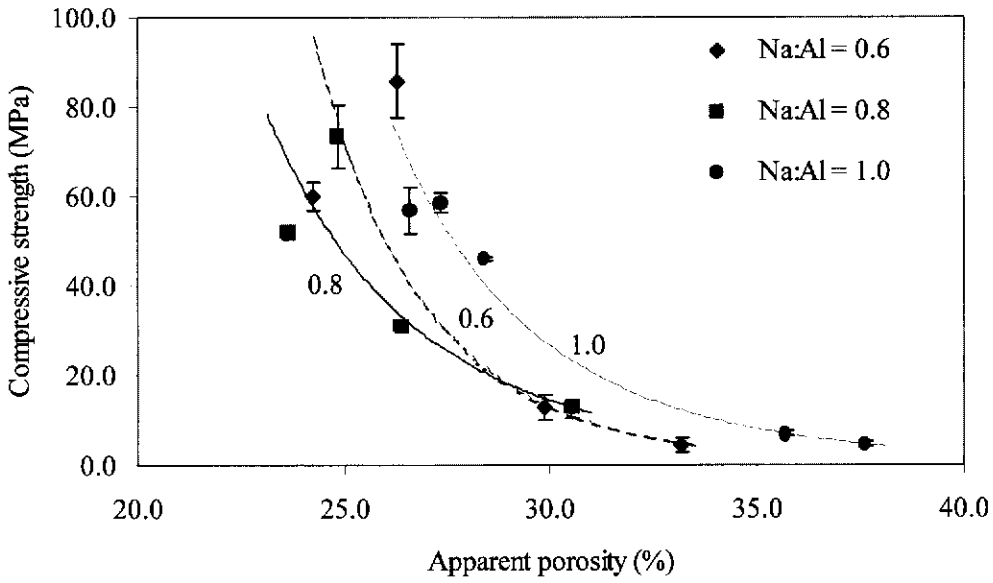

Figure 4.44 Compressive strength as a function of apparent porosity for different Si:Al ratios.

The dependence of strength on pores is not a unique property of geopolymers or Portland cement but is also found in other materials in which water leaves behind pores (Mosquera, Benitez, & Perry 2002; Matusinovic, Sipusic & Vrbos 2003; Kumar & Battacharjee 2003; Salgueiro *et* al. 2004). Neville (2000, p. 280) pointed out that the influence of pores on strength of concrete can be expressed by a power function of the type:

$$f_c = f_{c,o}(1-p)^n \tag{4.3}$$

where :

p = porosity, the volume of voids expressed as a fraction of the total volume of concrete,

f_c = strength of concrete with porosity p

$f_{c,o}$ = strength at zero porosity, and

n = a coefficient, which need not be constant.

Tests on pressed and heat-treated cement, as well as on ordinary cement paste have been shown to produce a large deviation from equation 4.3 (Neville, 2000 p. 280). The power function shown in table 4.7 does not fulfil equation 4.3.

The strength of geopolymers is also dependent on the hardness. Figure 4.45 shows the graph of Vickers hardness as a function of the compressive strength. The curve showed a linear relationship between compressive strength and hardness. Generally, strength is proportional to hardness (Igarashi, Bentur & Mindes 1996):

$$\sigma = H_v C \tag{4.4}$$

where, σ = Strength (MPa), H_v = Vickers hardness (GPa) and C = a constant.

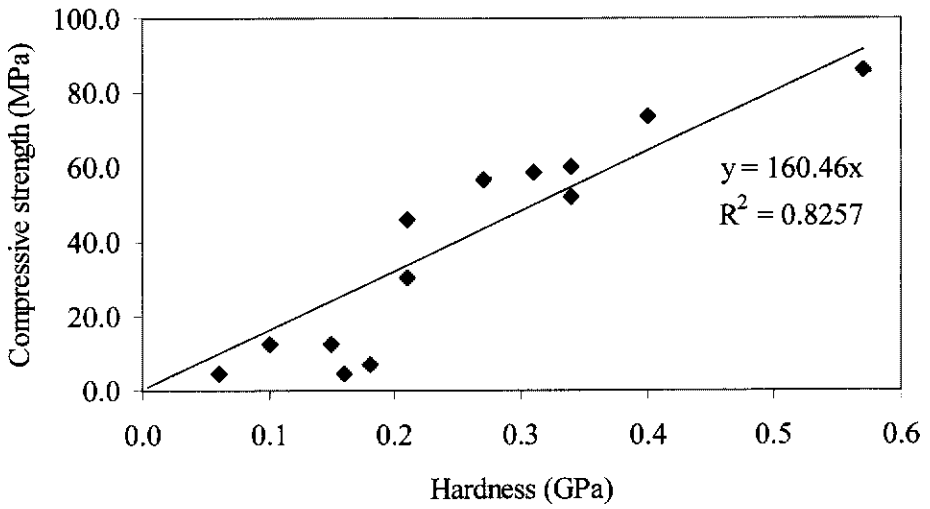

Figure 4.45 Vickers hardness versus compressive strength of geopolymers for all atomic ratios of Si:Al and Na:Al without aggregate.

Figure 4.45 clearly indicates that the compressive strength depends on the hardness of geopolymer paste. Similar results were reported by Feldman and Cheng-Yi (Igarashi, Bentur & Mindes 1996) who investigated the influence of silica fume on the compressive strength and microhardness of Portland cement paste. They also found that the addition of silica fume increased the microhardness of cement paste.

The role of aggregate on the compressive strength of geopolymers

The incorporation of aggregate into the geopolymer paste was aimed particularly at increasing the strength of the resulting materials through the densification of the matrix. The geopolymer can be considered to be a composite consisting of two materials with different physical and mechanical properties. Two types of aggregates, α-quartz and crushed granite, were investigated as these materials are most commonly used in the production of mortar or concrete. It should be pointed out that aggregate was only incorporated in Na-poly(sialate-silixo) geopolymer paste with compositions Si:Al = 1.5, 1.75 and 2.0; Na:Al = 0.6, 0,8 and 1.0. These compositions were found to produce high strength with no tendency to crack after curing.

It has been shown (figure 4.42) that the strength development with time of geopolymer with and without aggregate follows the same trend. To further examine the influence of aggregate on the strength of geopolymers, a suite of samples was produced with Si:Al = 1.5 but with different Na:Al ratios (Figure 4.46).

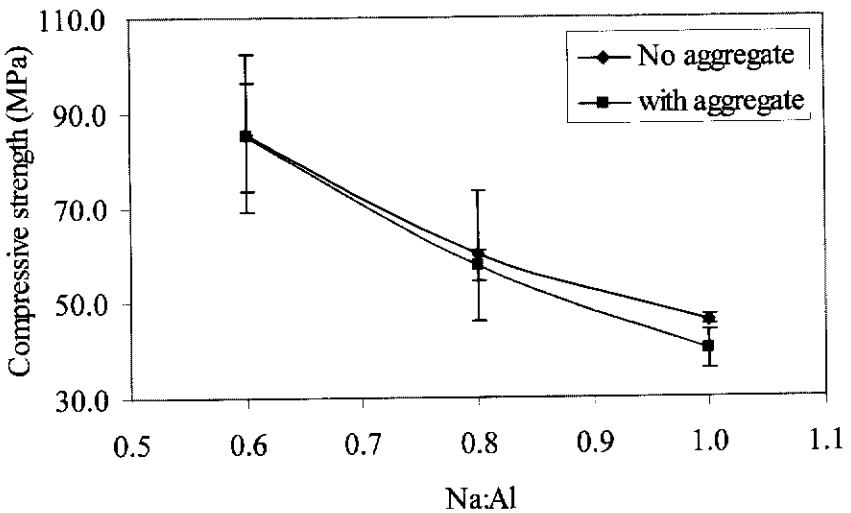

Figure 4.46 Compressive strength as a function of Na:Al ratio (Si:Al = 1.5) for samples with and without aggregate. Error bars represent 2 SD.

The curves show that for constant Si:Al ratio, the strength of geopolymers with and without aggregate are essentially the same for the same Na:Al ratio. Compressive strength is observed to decrease with increasing Na:Al ratio although large uncertainties restrict the confidence with which this can be stated.

The next step was to vary the aggregate content incorporated into the geopolymer paste, keeping the aggregate size constant (figure 4.47). The curve shows a sharp decrease in compressive strength for aggregate content greater than 40 wt%. This is believed to be due in part to the fact that as the amount of aggregate increases the workability of the mixture decreases preventing thorough mixing which may lead to reduced bond strength between aggregate and geopolymer paste. Also, as the aggregate content increases, the amount of geopolymer available to deflect and absorb cracks decreases that ultimately limits the strength of the material. Similar results were also reported by Hos, McCormick and Byrne (2002).

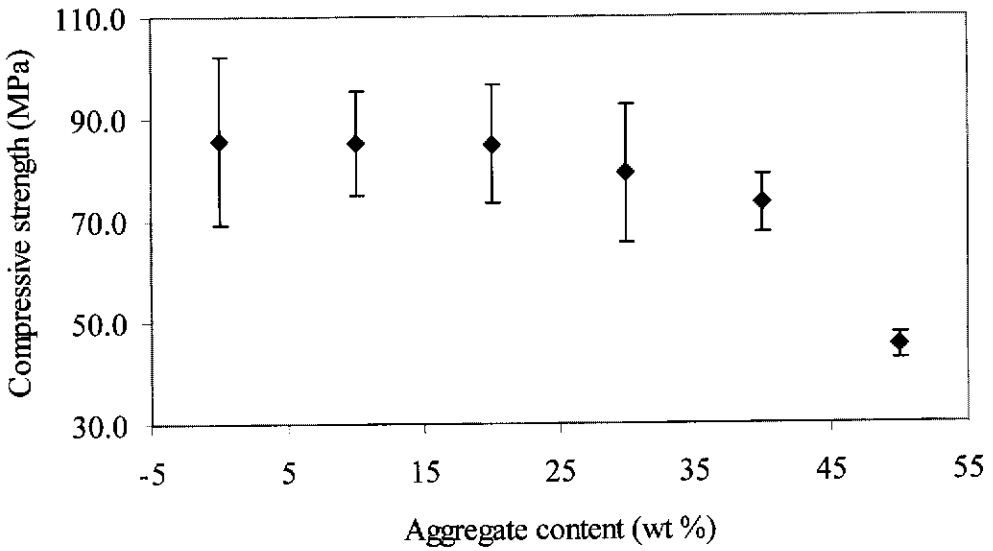

Figure 4.47 Compressive strength as a function of quartz aggregate (< 212 μm) content (Si:Al = 1.50, Na:Al = 0.6). Error bars represent 2 SD.

Further investigation was performed to establish a relationship between the strength of geopolymer and the size of aggregate (figure 4.48). In this study, the size of

aggregate was limited to <1000 μm and referred to as *fine aggregate* in the production of concrete (Neville 2000, p. 108-109).

For quartz aggregate there is no significant variation in compressive strength as aggregate size is varied. From the limited data it would appear that geopolymer with granite has a lower strength than geopolymer with quartz aggregate. More data is required before the influence of granite aggregate size can be determined with confidence. Barbosa & MacKenzie (2003) measured the reduction of compressive strength of geopolymers containing 6 types of inorganic aggregates. The most significant reduction in the strength was observed for geopolymers containing alumina and β-sialon. The researchers, however, did not vary the Si:Al ratio of their geopolymers.

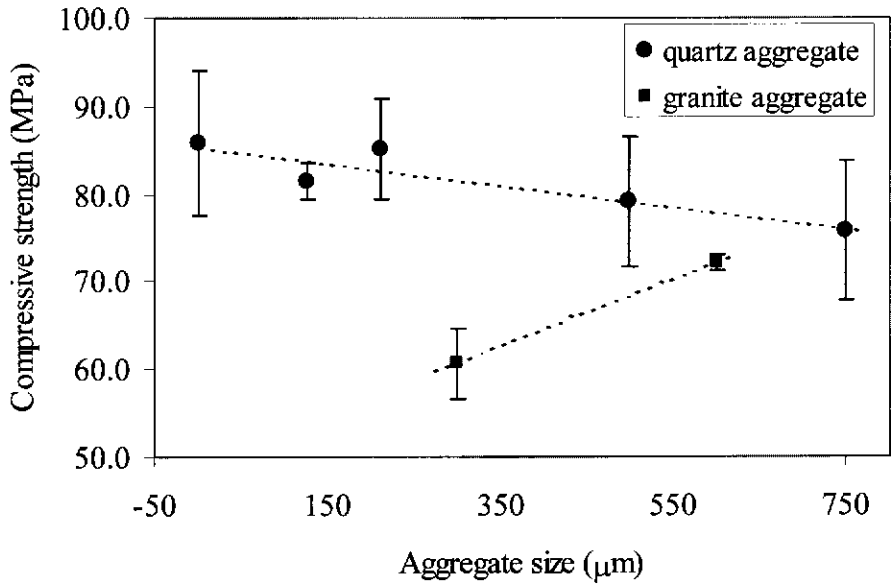

Figure 4.48 Compressive strength as a function of aggregate size (Si:Al = 1.5, Na:Al = 0.6). Error bars represent 2 SD.

Donza, Cabrera & Irassar (2002) studied the influence of fine aggregate (natural sand and crushed granite) on the compressive strength of concrete made from Portland cement. They reported that the 28-day compressive strength of their sample was 65 MPa and 58 MPa for concrete containing crushed granite and natural sand, respectively. The strength of their samples increased significantly after one year. They pointed out that the higher strength of concrete containing crushed granite

compared to concrete containing natural sand are related to the strong paste-fine aggregate interface and the intrinsic strength of granite particles. It should be noted the size of crushed granite used by Donza, Cabrera & Irassar (2002) was < 2.36 mm which is much larger than the crushed granite used in this study.

In chapter 5, the microstructure character of the geopolymers containing aggregate as well as the morphology of the interfacial transition zone (ITZ) between the aggregate and the geopolymer matrix will be presented and discussed.

4.7 Interfacial Bond Strength

The tensile mechanical bond strength between aggregate and geopolymer matrix was measured by applying a force perpendicular to the interface. Details of the experiment as well as the sample preparation are given in section 3.2.4. Three types of aggregates were used namely, quartz, granite and sandstone (commercial samples of rose quartz, granite and sandstone). In this experiment, sandstone was included as one type of common aggregate although its compressive strength is considerably lower than the strength of quartz and granite (Neville 2000, p.120 – 121).

The aggregates were sectioned into 2 cm x 2 cm x 2 cm pieces with a diamond saw with their surfaces left as cut. For the interfacial bond strength test two compositions of geopolymer matrix were prepared namely Si:Al = 1.5, Na:Al = 0.6 and Si:Al = 2.0, Na:Al = 1.0. Geopolymers prepared with these compositions have high compressive strength while the amount of silicate solution used in the processing varied considerably.

Observations using optical microscopy were performed to examine the interfacial bond between the aggregate and the geopolymer. Samples from the same batch were sectioned into 0.5 cm x 0.5 cm x 0.5 cm pieces comprising aggregate and geopolymer. The samples were then impregnated with a low viscosity resin and polished to a finish of 20 μm. Figure 4.49 shows an optical image of the interfacial zone between quartz and geopolymer. The image does not show an intimate bond between the aggregate and geopolymer.

SEM images of the interfacial zone between aggregate and geopolymer were not taken, as it was difficult to prepare a specimen without incurring shrinkage of the geopolymer during evacuation in the coating unit.

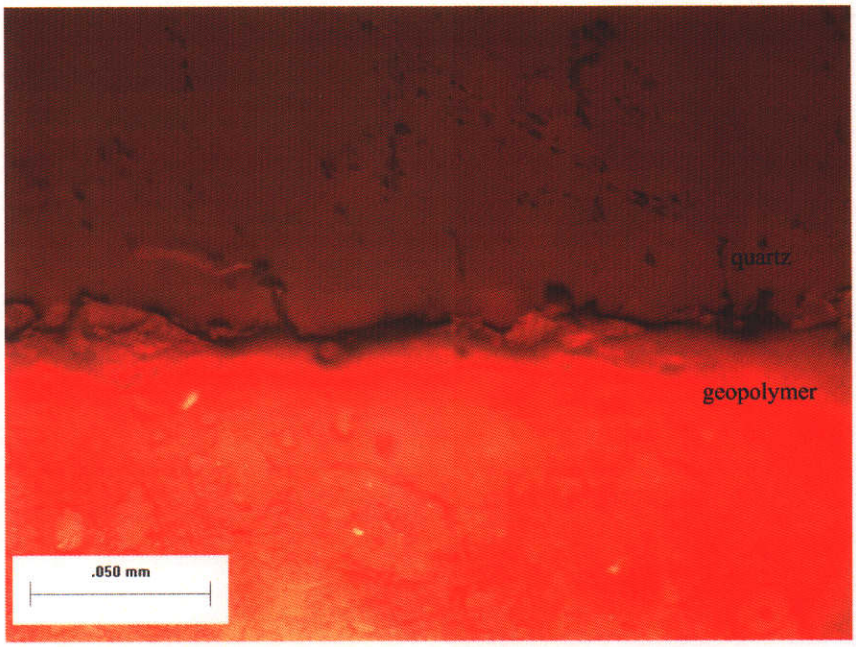

Figure 4.49 An optical microscope image of the interfacial zone between quartz and geopolymer.

Figure 4.50 shows an image of the interfacial zone between granite and geopolymer. As with the quartz aggregate the bond between geopolymer and granite is not intimate suggesting a weak bond. Figure 4.51 shows an image of the interfacial zone between sandstone and geopolymer. This bond appears more intimate suggesting a stronger bond.

The quantitative measurements of the bond strength using a tensometer were performed after ageing the specimens for more than 7 days at room temperature. It was found that all of the quartz-geopolymer samples for all compositions failed at the interfaces as soon as the force was applied and no useful bond strength value could be obtained. The same result was obtained for specimens prepared with Si:Al = 2.0, Na:Al = 1.0 bonded to granite.

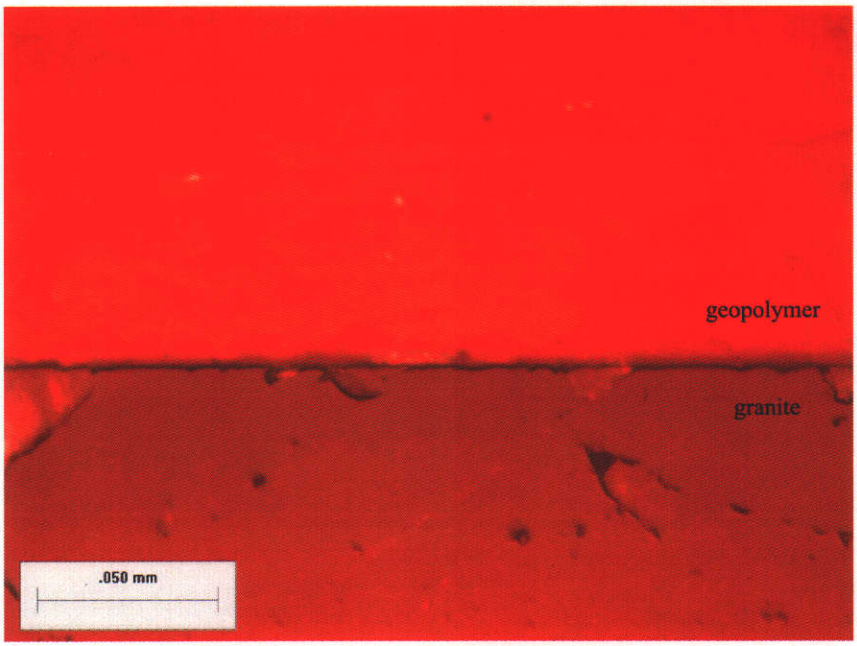

Figure 4.50 An optical microscope image of the interfacial zone between granite and geopolymer.

Figure 4.51 An optical microscope image of the interfacial zone between sandstone and geopolymer.

Useful information about the bond strength was only obtained from specimens with Si:Al = 1.5, Na:Al = 0.6 bonded to granite and sandstone, as well as specimens with

Si:Al = 2.0, Na:Al = 1.0 bonded to sandstone. Figure 4.52 shows the photographs of the specimens after testing.

All geopolymer-granite samples failed at the interfacial zone while all specimens with sandstone failed within the aggregate. The results indicated that interfacial bond between the sandstone and the geopolymer matrix is stronger than the tensile strength of the sandstone itself. It also indicated that the tensile strength of the geopolymer is stronger than the sandstone.

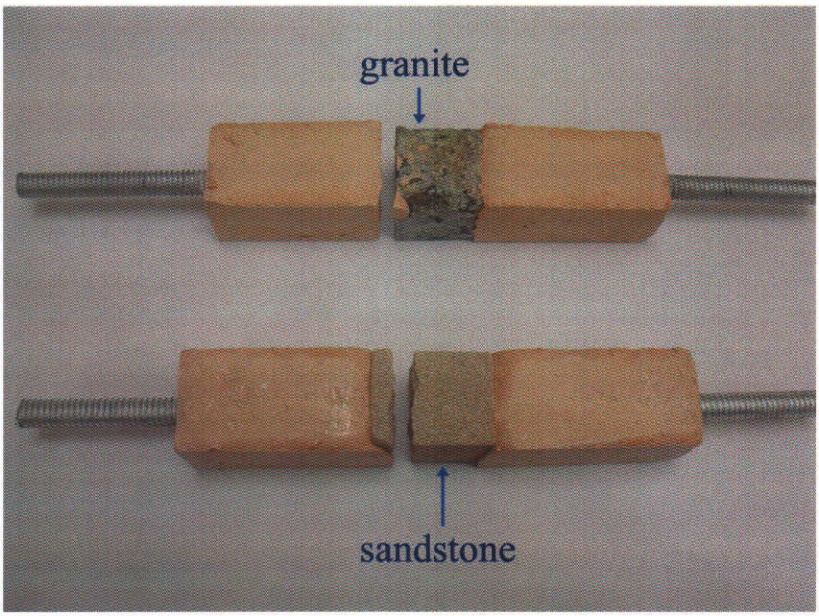

Figure 4.52 Specimens after interfacial bond strength test showing the failure at the interface (granite) and within the aggregate (sandstone).

The mean values of interfacial bond strength between aggregate and geopolymer are presented in table 4.8. It should be noted that value of strength for sandstone is not actually the interfacial bond strength but rather the tensile strength of the sandstone.

Table 4.8 Interfacial bond strength between geopolymer matrix and aggregates.

Type of aggregate	Bond strength (MPa)
quartz	0.00*
granite	0.49 (0.05)
sandstone	> 2.42 (0.75)

* Values too low to register and are assumed to be 0 MPa.
Uncertainties (SD) shown in brackets.

The strong interfacial bond between the sandstone and the geopolymer is most likely due to the mechanical interlocking between the matrix and sandstone as the surface of sandstone is porous compared to the surface of quartz and granite. The cut surface of quartz and granite is smooth and free from any pores preventing penetration of the geopolymer matrix to mechanically interlock with the aggregate.

Lee and Van Deventer (2004) studied the interfacial strength between natural aggregates (basalt and siltstone) and geopolymer mortar manufactured from a mixture of fly ash and kaolinite. They reported that the concentration of activation solution (sodium silicate) influences the magnitude of the interfacial strength between aggregate and geopolymers. The highest interfacial strength (1.27 MPa) was achieved for a sandwich between basalt and geopolymer mortar using a high concentration of sodium silicate.

Rao & Prasad (2002) investigated the influence of the surface roughness of aggregate (rock) on the interface bond strength of mortar made from Portland cement. They reported that the bond strengths between rough rock and mortar were between 0.34 to 0.56 MPa. Similarly, Caliskan (2003) studied the interfacial strength between aggregates (sandstone, limestone and granite) and Portland cement mortar. He reported that sandstone aggregate provided the highest interfacial bond strength (1.3 MPa), followed by the granite (1.2 MPa) and then limestone (1.1 MPa). The researcher pointed out that the coarse texture of sandstone provides extra strong mechanical interlocking between the mortar matrix and aggregate. Caliskan also reported that the interfacial bond strength between all aggregates and cement increases significantly by the inclusion of 20 % of silica fume.

4.8 Summary

- Microstructural characterisation by means of SEM and TEM revealed that the Kingwhite 65 kaolinite crystals have approximately hexagonal morphology with poorly defined edges. A small amount of halloysite and ancillary minerals such as quartz and anatase are present in the kaolinite.

- XRD analysis showed that the Hinckley index (HI) of Kingwhite kaolinite is 0.88 suggesting a medium-defect kaolinite.

- Dehydroxylation at 750 °C in air for 6 hours has transformed a crystalline kaolinite into amorphous metakaolinite.

- TG-DTA results indicate the loss of OH lattice water occurred at 400 °C and that dehydroxylation is complete at 600 °C.

- Microstructural characterisation by means of TEM revealed that while most of the kaolinite particles have been transformed into amorphous metakaolinite some particles retain their original structure as well as crystallinity.

- The curing temperature of the mixture of geopolymer precursors (metakaolinite plus sodium silicate) plays an important role in determining the rate of geopolymerisation and setting time.

- Geopolymers synthesised in this study have been divided into two groups based on their nominal Si:Al atomic ratio: *sodium-poly(sialate)(Na-PS)* (Si:Al = 1.04 – 1.25) and *sodium-poly(sialate-siloxo) (Na-PSS)* (Si:Al = 1.50 – 2.00).

- The XRD patterns of Na-PS geopolymers showed the formation of Zeolite-A and Zeolite-X in conjunction with amorphous geopolymer paste.

- The mechanical properties of Na-PS geopolymers have common features: low density, high apparent porosity and low compressive strength.

- XRD patterns revealed that the Na-PSS geopolymers were amorphous except for traces of quartz and anatase.

- TG-DTA of Na-PSS showed the presence of a single endothermic peak at 135 – 140 °C suggesting the loss of the initial reaction water incorporated in the geopolymeric framework.

- Extensive shrinkage and cracking occurred when geopolymers were heated up to 950 °C. Geopolymer prepared with Si:Al = 1.5, Na:Al = 0.6 was found to have less cracks than geopolymer prepared with Si:Al = 2.0, Na:Al = 1.0. Severe cracking occurred for geopolymers containing aggregate (quartz and granite).

- The cracks and shrinkage of geopolymers are associated with mass loss as high as 15% for geopolymer prepared with Si:Al = 1.5, Na:Al = 0.6 and about 19% for geopolymer prepared with Si:Al = 2.0, Na:Al = 1.0. The mass loss of geopolymers containing aggregate (quartz and granite) is less than 15%.

- Dilatometer measurements of geopolymer pastes indicate that initial shrinkage of geopolymers (about 2%) occurs before 300 °C. Between 300 and 800 °C geopolymer is essentially dimensionally stable indicating that this may be the useful working temperature of geopolymer paste.

- The coefficient of thermal expansion of geopolymers is comparable to that of Portland cement paste.

- The addition of aggregate was found to reduce the shrinkage of geopolymers.

- Quartz aggregate was found to limit the useful upper temperature of geopolymer to below 500 °C.

- The hot wire method has been successfully employed to measure the thermal conductivity of geopolymers.

- The chemical composition (Si:Al and Na:Al) of geopolymers was found to influence the bulk density, apparent porosity, Vickers hardness and compressive strength.

- The compressive strength of geopolymers reaches maximum after 7 days.

- Vickers hardness and apparent porosity were found to be linearly related to the compressive strength of geopolymers.

- The inclusion of aggregate (quartz and granite) was found to have negligible effect on the strength of geopolymers.

- Sandstone was found to have the highest interfacial bond strength between geopolymer and the aggregate followed by granite and quartz.

CHAPTER 5
MICROSTRUCTURAL CHARACTER OF GEOPOLYMERS

5.1 Introduction

Davidovits (1994a) reported that geopolymer binders manufactured from kaolinite or calcined kaolinite are amorphous to poorly ordered three dimensional aluminosilicate polymers. Xu & van Deventer (2002) pointed out that most geopolymers synthesised from different starting materials such as fly ash are mixtures of crystalline aluminosilicate particles and amorphous aluminosilicate gel.

As a mixture of amorphous and crystalline phases, the physical and mechanical properties of geopolymers should be the resultant of both the amorphous gel phase as binder and the cystalline aluminosilicate particles as fillers. Therefore, an understanding of the microstructure character of geopolymers is important in the development of improved geopolymers.

This chapter presents and discusses the microstructure character of geopolymers synthesised from dehydroxylated kaolinite with and without the inclusion of aggregate based on scanning electron microscope (SEM) and transmission electron microscope (TEM) observations. The details of sample preparation for SEM and TEM investigations have been described in chapter 3. The energy dispersive X-ray spectrometer (EDS) was used for point analysis as well as X-ray mapping to investigate the chemical compositions of the resulting geopolymers.

5.2 The morphology of geopolymer paste

As mentioned in chapter 4 geopolymers prepared in this study have been divided into two groups, Na-poly(sialate) (Na-PS) and Na-poly(sialate-siloxo) (Na-PSS) geopolymers. X-ray diffraction (XRD) patterns showed that Na-PS geopolymers contain crystalline zeolites in conjunction with amorphous geopolymer, while the structure of Na-PSS is amorphous. In addition to the information presented in the next two sections supplementary SEM micrographs and EDS spectra have been provided in Appendix C.

5.2.1 The morphology of Na-PS geopolymers

All Na-PS geopolymers prepared in this study had similar physical and mechanical properties; they were soft, brittle and porous. The XRD patterns of these samples showed the formation of crystalline zeolite-A or zeolite-X in conjunction with amorphous geopolymer. As mentioned in chapter 4 no attempt was made to incorporate aggregate in these materials.

Figure 5.1 shows an SEM image of Na-PS prepared with Si:Al = 1.04 and Na:Al = 0.6. The image shows the presence of grains of various sizes and pores as well as cracks around the central grain. During polishing grains were readily pulled out from the surface of the specimen limiting the quality of surface polish that could be attained even though the sample was impregnated with a resin.

Figure 5.1 SEM image of Na-PS geopolymer prepared with Si:Al = 1.04 and Na:Al = 0.6.

It is likely that the grains in figure 5.1 are a mixture of crystalline zeolite-A and unreacted (undissolved) metakaolinite. Akolekar, Chaffee and Howe (1997) observed similar grains in the well-developed crystalline zeolite-A made from metakaolinite and referred to them as zeolitic grains. The presence of unreacted metakaolinite, predominantly found in Na-PSS geopolymers, is described in section 5.2.2. Needle-like crystals observed on the surface of the specimen are sodium

carbonate formed from a reaction of residual sodium hydroxide with atmospheric CO_2.

Figure 5.2 shows how a crack has propagated around a grain. It is not clear whether these cracks are primary cracks or a mix of primary and secondary cracks. Secondary cracks are cracks introduced during the cutting and polishing process as well as forming due to shrinkage during the evacuation in the coating chamber. The development of secondary cracks was investigated using optical microscopy, and will be described in section 5.2.2. In this study, a crack with a width less than 10 μm is referred to as a microcrack. This arbitrary definition is much smaller than that defined by Bisschop & van Mier (2001) where a microcrack is referred to as a crack with a width of less than 50 μm.

Figure 5.2 Enlarged image of sample shown in figure 5.1. Note the crack running around the large grain.

Figure 5.3 and 5.4 show SEM images of a sample prepared with Si:Al = 1.25 and Na:Al = 0.8. Based on the XRD results, a greater amount of zeolite-A was formed in this sample than in sample shown in figure 5.1. From figure 5.3 and 5.4 the average grain size is 7.5 μm.

Figure 5.3 SEM image of a geopolymer sample with Si:Al = 1.25, Na:Al = 0.8.

Figure 5.4 SEM image showing spots used for EDS analysis (Si:Al = 1.25, Na:Al = 0.8).

EDS investigation on spots shown in figure 5.4 revealed that most of the grains consist of the original constituents of metakaolinite plus sodium from the sodium hydroxide and sodium silicate solution. Elemental analysis (quantitative analysis) across the surface of the specimen showed that the average atomic ratio of Si:Al = (1.23 ± 0.05) and Na:Al = (0.57 ± 0.12). The atomic ratio of Na:Al of the sample is slightly lower than its nominal ratio of 0.8. It is possible that some of Na has leached away from the surface during the cutting and polishing process.

The XRD pattern of the sample prepared with Si:Al = 1.25, Na:Al = 1.0 showed the formation of zeolite-X in conjunction with amorphous geopolymer. As with other Na-PS samples, this material was also difficult to polish due to grain pull out preventing achievement of a high quality polish for SEM investigation. Figure 5.5 shows an SEM image of a sample with Si:Al = 1.25, Na:Al = 1.0. The sample appears more dense than the sample shown in figure 5.1. Large voids on the surface of the sample are believed to be due to the grain pullout during polishing.

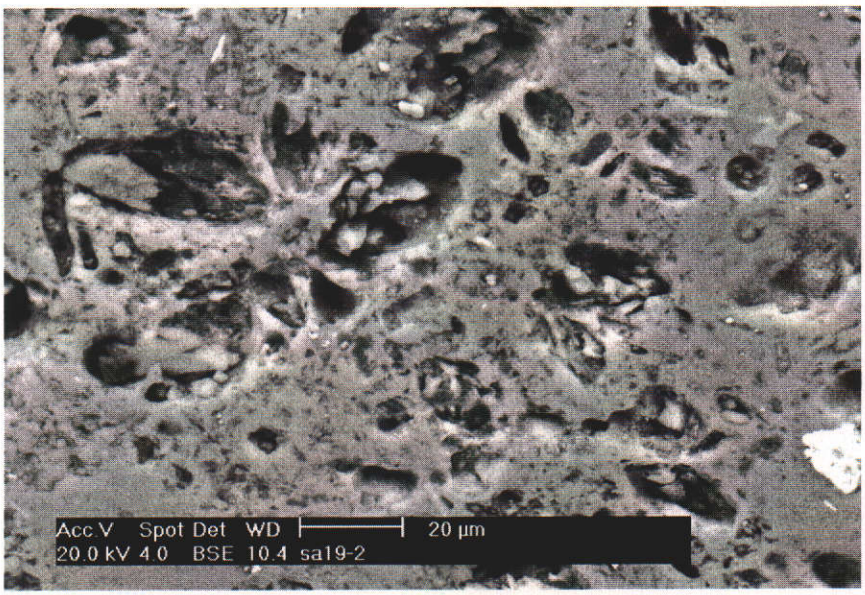

Figure 5.5 SEM image of geopolymer sample with Si:Al = 1.25, Na:Al = 1.0.

The SEM images of all Na-PS geopolymers suggest that these materials have a common microstructure consisting of grains of crystalline zeolite and/or unreacted metakaolinite, substantial pores as well as cracks.

The presence of unreacted metakaolinite particles and pores in the structure of K-PS geopolymer was also observed by Wei *et* al (2003) using environmental scanning electron microscopy (ESEM) with a chamber pressure of 4.2 Torr and a 80 % RH environment. The use of ESEM enabled them to observe the hydration process of K-PS as well as the evolution of the microstructure as a function of time. The researchers observed that initially a lot of metakaolinite particles were packed loosely resulting in substantial voids. As the geopolymerisation proceeded, gel appeared and gradually precipitated on the surface covering most of the unreacted metakaolinite and filling the pores. After 4 hours, the hydration process was

completed and a hardened-geopolymer paste was produced. As the hydration process took place at room temperature it required longer to complete. The 28-day compressive strength of their K-PS geopolymer was about 12 MPa, which is similar to the compressive strength of Na-PS geopolymers produced in this study.

5.2.2 The morphology of Na-PSS geopolymers

The XRD patterns of all Na-PSS geopolymers (section 4.3.1) show that the structure of these materials is amorphous with no evidence of zeolite. The physical and mechanical properties of these materials are significantly different to those of Na-PS geopolymers. The compressive strength of these materials is between 40 – 90 MPa with a Vickers hardness between 0.2 – 0.6 GPa depending on the chemical composition of the sample.

Na-PSS geopolymer with Si:Al = 1.5, Na:Al = 0.6

Figure 5.6 shows an SEM image of a geopolymer prepared with Si:Al = 1.5, Na:Al = 0.6. The image shows that the surface of the sample consists of the grains of unreacted metakaolinite (lighter phase) surrounded by geopolymer matrix, pores and extensive microcracks. The grains of unreacted metakaolinite appear to be aggregates and previous TEM sizing of kaolinite (section 4.2).

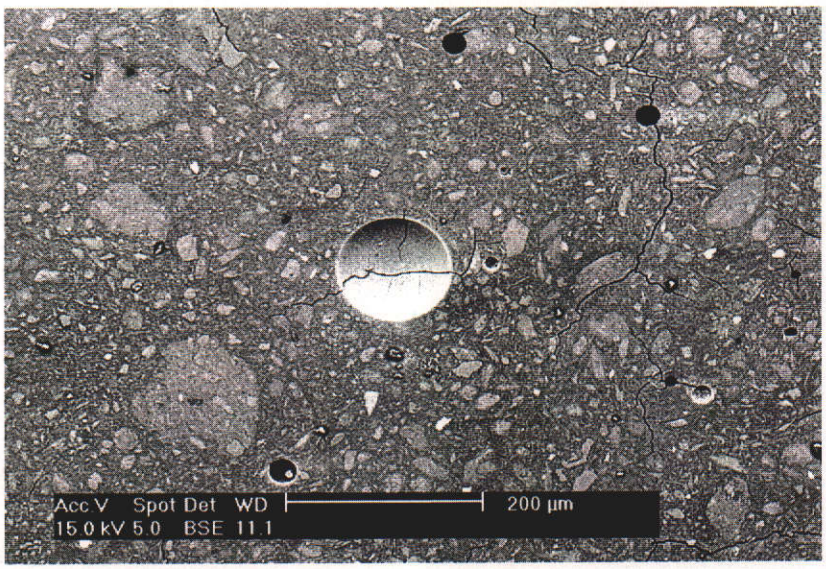

Figure 5.6 SEM image of Na-PSS geopolymer sample (Si:Al = 1.5, Na:Al = 0.6).

Computed Tomography Imaging (CT-Scan)

The presence of microcracks shown on figure 5.6 was assumed to be due to cutting, polishing and vacuum evacuation in the coating unit during sample preparation. In order to ensure that this assumption is correct, a non-destructive imaging technique which does not involving cutting, polishing and coating of the sample was performed to examine the microstructure of as prepared geopolymers. A CT-Scan, also known as Micro-CT (skyscan-1072 Desk-Top-X-Ray Microtomograph) was used for this purpose. The size of the samples was 10 mm in length and 4 mm in diameter.

Figure 5.7 shows a representative of CT-Scan image for as prepared Na-PSS geopolymer (Si:Al = 1.5, Na:Al = 0.6). The image was taken at a magnification where the whole sample fitted into the field of view, which gives the voxel size of 6.477 μm by 6.477 μm by 6.477 μm. This parameter was kept constant to capture and reconstruct the cross section for all samples so that the intensities of cross sections which are linearly related to x-ray absorption density can be compared qualitatively.

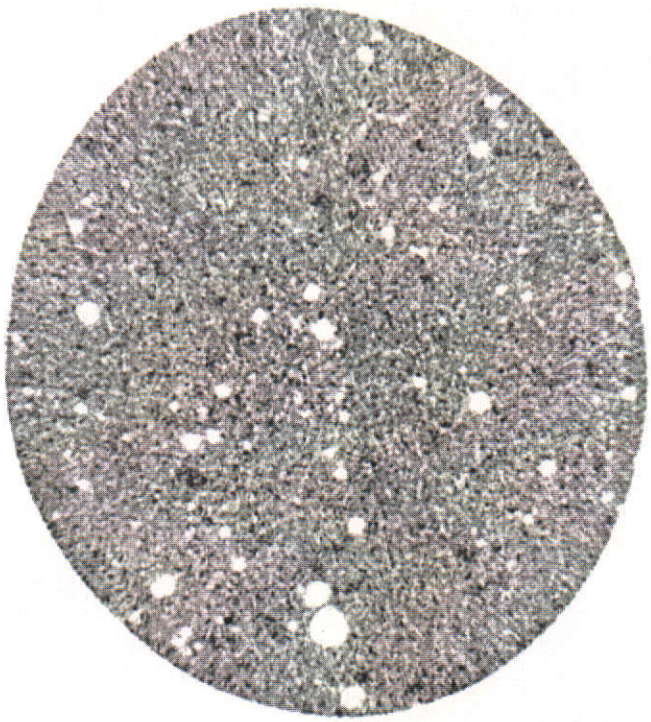

Figure 5.7 A representative CT-Scan image of as prepared Na-PSS geopolymer (Si:Al = 1.5, Na:Al = 0.6). Magnification 22 times.

The image shows that there are no resolvable cracks formed within the sample. The bright circles are pores similar to those observed on SEM. This result indicates that cracks observed on SEM are cracks formed as results of cutting, polishing and vacuum evacuation. These types of cracks are categorised as secondary cracks.

Figure 5.8 shows the CT-Scan image of as prepared Na-PSS geopolymer (Si:Al = 1.5, Na:Al = 0.6) containing 20 wt % quartz aggregate. The image also shows that the as prepared Na-PSS geopolymer sample containing quartz aggregate is free of cracks. The sample also contains substantial pores and air bubbles despite the presence of aggregate.

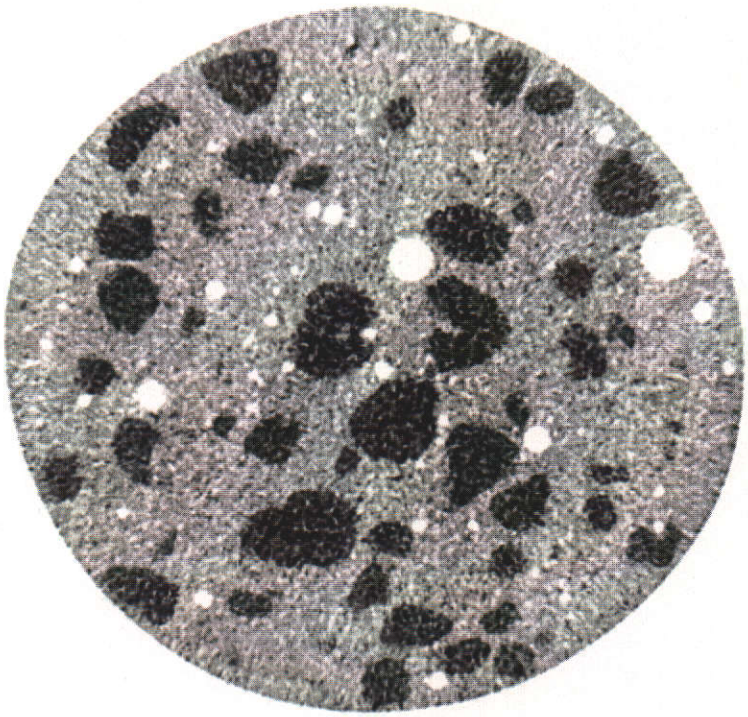

Figure 5.8 A representative CT-Scan image of as prepared Na-PSS geopolymer containing 20 wt% quartz aggregate (Si:Al = 1.5, Na:Al = 0.6). Magnification 24 times.

These results indicate that CT-Scan or Micro-CT is a powerful technique to examine the microstructure of geopolymer or other cement–based materials without introducing any cracks due to sample preparation technique.

Optical Microscopy

Another sample of the same composition was prepared for optical microscope observation to examine crack development on the surface of the sample which was assumed to be due to shrinkage as a result of moisture loss when the sample was evacuated in a vacuum chamber for gold or carbon coating. Figure 5.9 shows an image of the polished sample with no evidence of cracks on the surface of the sample.

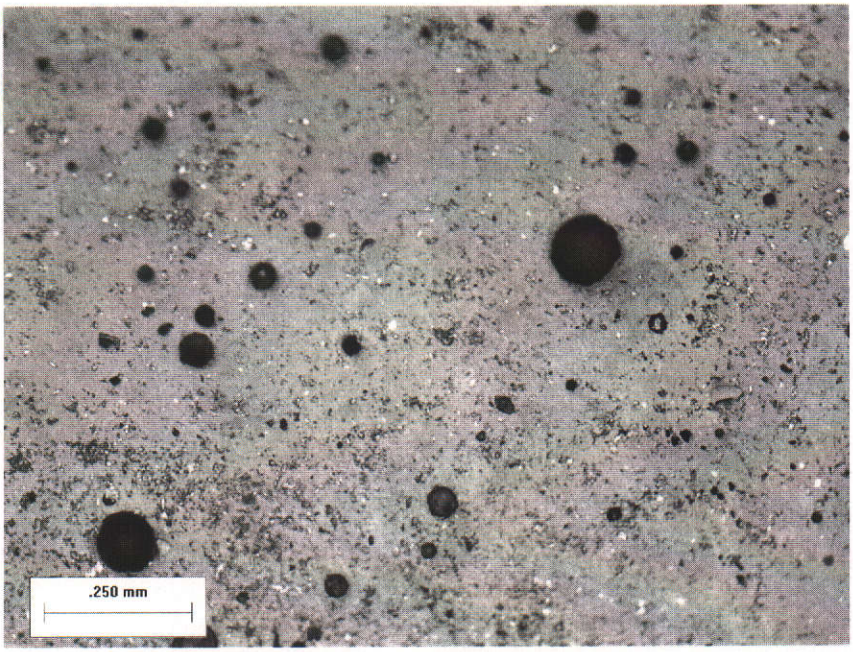

Figure 5.9 An optical image of a geopolymer sample (Si:Al = 1.5, Na:Al = 0.6). The black circular features are pores.

Figure 5.10 shows an image of the sample after it was evacuated in a vacuum chamber with a pressure of 0.1 Torr for 30 minutes. Figure 5.10 clearly shows the development of cracks due to moisture loss. It appears that when moisture is lost from the specimen, a moisture gradient develops across the specimen causing differential shrinkage, leading to generation of cracks. In hardened cement-based material, this will be accompanied by tensile stresses parallel to the drying surface causing cracks perpendicular to this surface (Bisschop & van Mier 2002). The cracks propagate in a non-linear fashion usually extending from the edge of a pore. This

type of crack is known as a secondary crack and is commonly observed in cement-based material, such as Portland cement. The optical microscopy examinations suggest that extensive microcracks on the surface of samples as observed by SEM (figure 5.6) are mostly secondary microcracks. The existence of primary microcracks could not be resolved by the optical microscopy used in the present study.

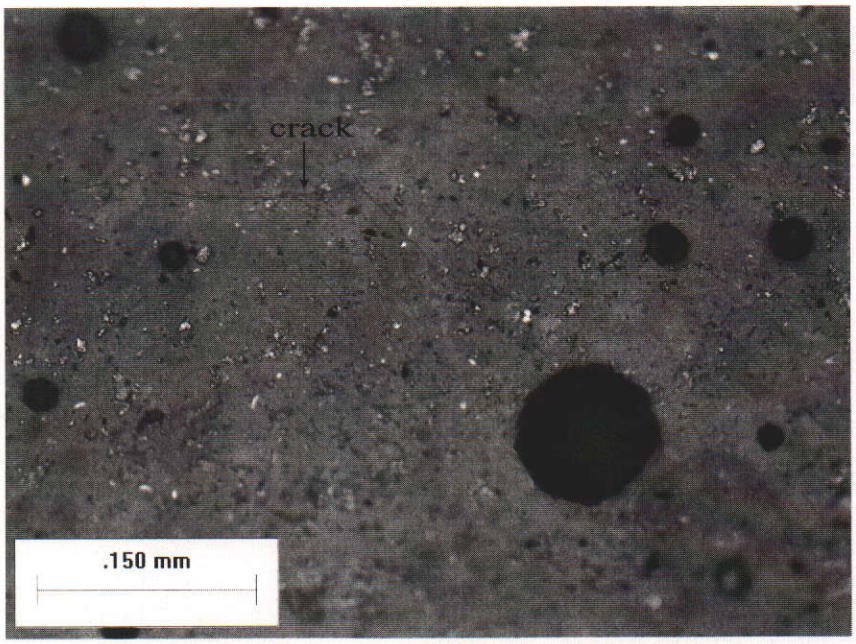

Figure 5.10 An optical image of the geopolymer sample shown in figure 5.7. Note that the magnification and the field of view have been adjusted to enhance the position of the crack.

Figure 5.11 is a higher magnification image of that shown in figure 5.6 to allow closer examination of the morphology as well as allow the chemical composition of unreacted metakaolinite and the geopolymer matrix to be determined by EDS.

Figure 5.11 SEM image of a geopolymer sample with Si:Al = 1.5, Na:Al = 0.6 showing grains of unreacted metakaolinite bonded with the geopolymer matrix.

Figures 5.12 and 5.13 show examples of EDS spectra from the grains and the geopolymer matrix for a sample with a nominal atomic ratio of Si:Al = 1.5, Na:Al = 0.6.

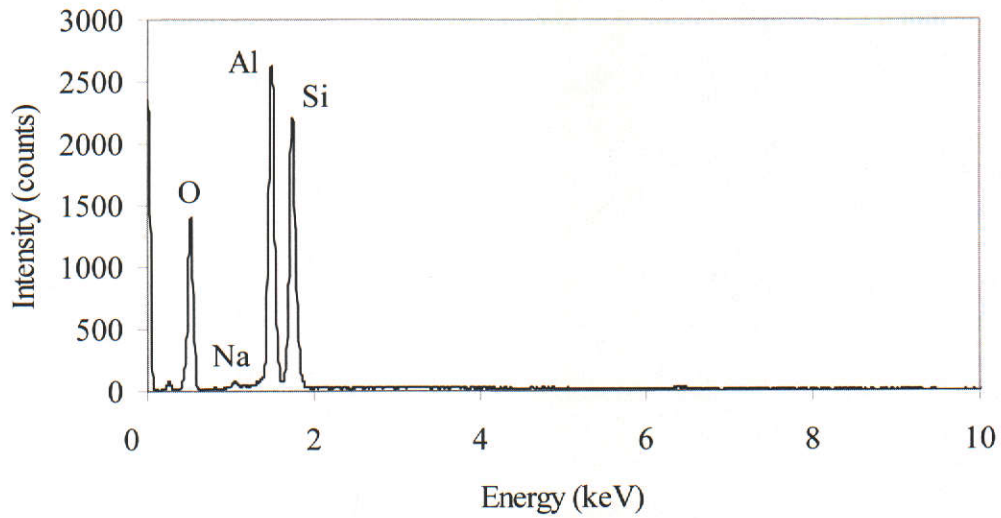

Figure 5.12 A representative EDS spectrum from a grain (unreacted metakaolinite) in the geopolymer matrix (Si:Al = 1.5, Na:Al = 0.6). Spectrum collected at 25 kV.

The EDS spectrum from a grain (figure 5.11) shows a typical elemental composition of the original metakaolinite in addition to a small amount of Na. The presence of low levels of Na in the grains indicates an incomplete reaction between the activation solution and the metakaolinte. The EDS spectrum of the geopolymer matrix (figure

5.13) shows that atomic ratio of Si:Al and Na:Al has changed to be closer to their nominal atomic ratios.

Table 5.1 shows the average of Si:Al and Na:Al atomic ratios of the grains and the geopolymer matrix as obtained from elemental analysis for a sample prepared with a nominal atomic ratio of Si:Al = 1.5, Na:Al = 0.6. It can be seen that there is a difference in the atomic ratios of Si:Al and Na:Al measured from the grains and from the matrix of geopolymer. The atomic ratio of Na:Al from the matrix is well below its nominal value of 0.6.

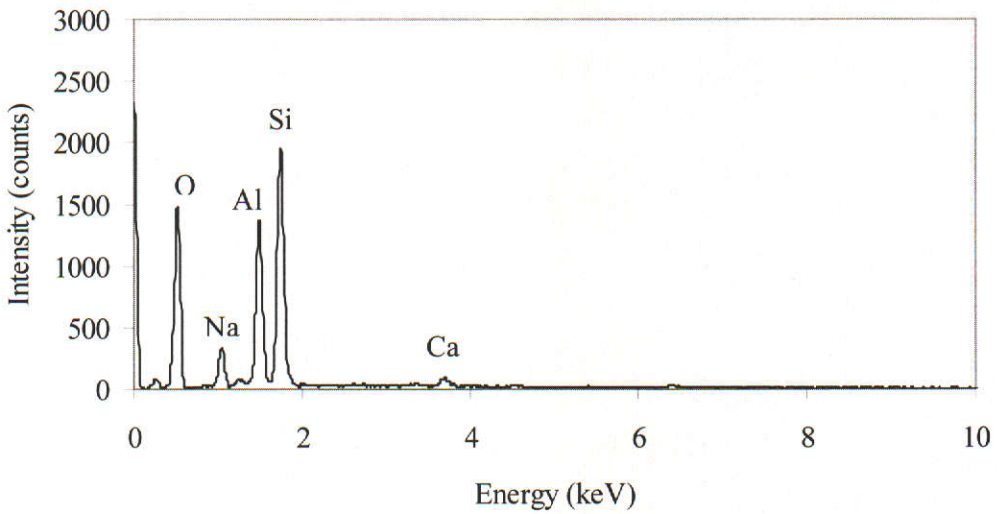

Figure 5.13 A representative EDS spectrum from the geopolymer matrix (Si:Al = 1.5, Na:Al = 0.6). Ca is an original constituent of kaolinite (CaO = 0.08%). Spectrum collected at 25 kV.

Table 5.1 Average atomic ratios of Si:Al and Na:Al for a geopolymer sample prepared with Si:Al = 1.50, Na:Al = 0.6. Standard deviations (2SD) are shown in parentheses.

Phase	Si:Al	Na:Al
grain	1.1 (0.3)	0.1 (0.1)
matrix	1.5 (0.3)	0.3 (0.1)

Further elemental analysis was performed around and on unreacted metakaolinite grain as shown in figure 5.14. The EDS was performed on 6 different spots representing the geopolymer matrix and unreacted metakaolinite.

Table 5.2 shows the EDS results from 5 different spots shown in figure 5.14. The results show that spot 2, 3 and 4 are sodium-deficient where the atomic ratio of Si:Al is close to the composition of the original metakaolinite (Si:Al = 1.04).

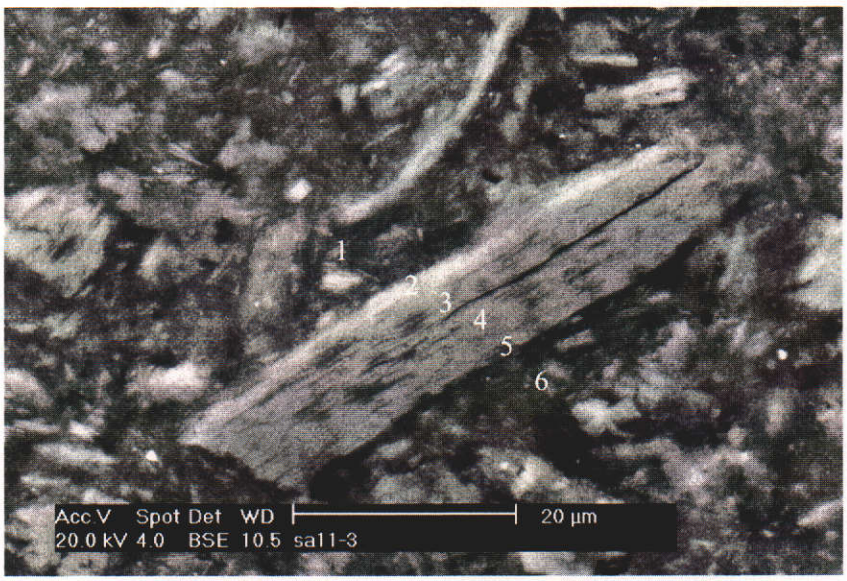

Figure 5.14 SEM image of unreacted metakaolinite grain in geopolymer matrix (Si:Al = 1.5, Na:Al = 0.6). The numbers show the spots where EDS analysis was undertaken.

Table 5.2 EDS results from 5 different spots around and on the unreacted metakaolinite. Results in atomic percent and normalised to 100%.

Spectrum Label	O	Na	Al	Si	Ca	Fe
1	66.17	4.33	10.21	18.46	0.55	0.27
2	68.65	2.83	12.53	15.84	0.15	
3	64.64	2.07	15.31	17.78		0.20
4	63.39	1.65	15.65	19.06		0.24
5	64.46	2.90	14.09	18.07	0.18	0.29
6	64.28	3.50	12.49	19.12	0.39	0.23

X-ray mapping (figure 5.15) was also performed to examine the distribution of sodium, aluminium and silicon in geopolymer with a Si:Al = 1.5 and Na:Al = 0.6.

(a)

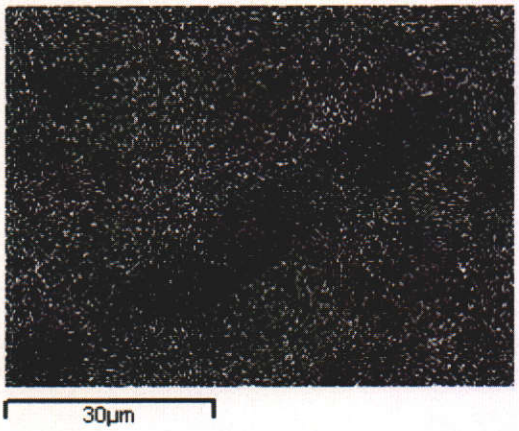

(b) Na map

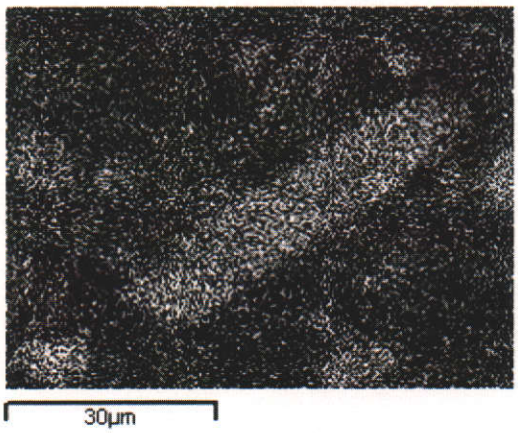

(c)Al map

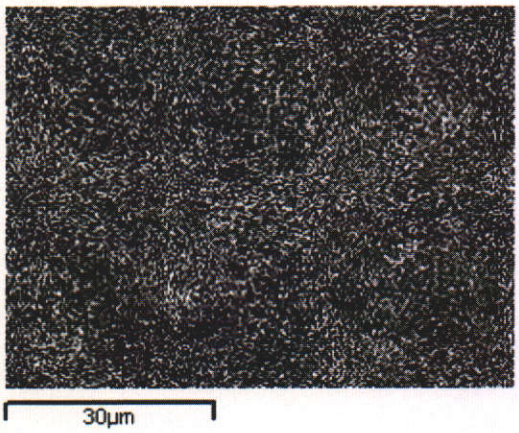

(b) Si map

Figure 5.15 (a) SEM image of geopolymer sample (Si:Al = 1.5, Na:Al = 0.6) for collection of X-ray elemental maps: (b) sodium, (c) aluminium, and (d) silicon.

The SEM image shows a number of grains, which are suspected to be unreacted metakaolinte surrounded by a geopolymer matrix. The elemental maps show clearly the presence of aluminium-rich regions, corresponding to particles of unreacted metakaolinite (bright phase) bonded within a geopolymer matrix. Na is distributed across the surface of the sample except on the grain of unreacted metakaolinite. This result provides further evidence that some of the metakaolinite particles did not fully dissolve during geopolymerisation.

TEM examination was performed for further microstructural characterisation of the Na-PSS geopolymer including the determination of the crystallinity of unreacted metakaolinite. Details of sample preparation for TEM examination is provided in chapter 3. Figure 5.16 shows a representative TEM image for a geopolymer sample with Si:Al = 1.5, Na:Al = 0.6.

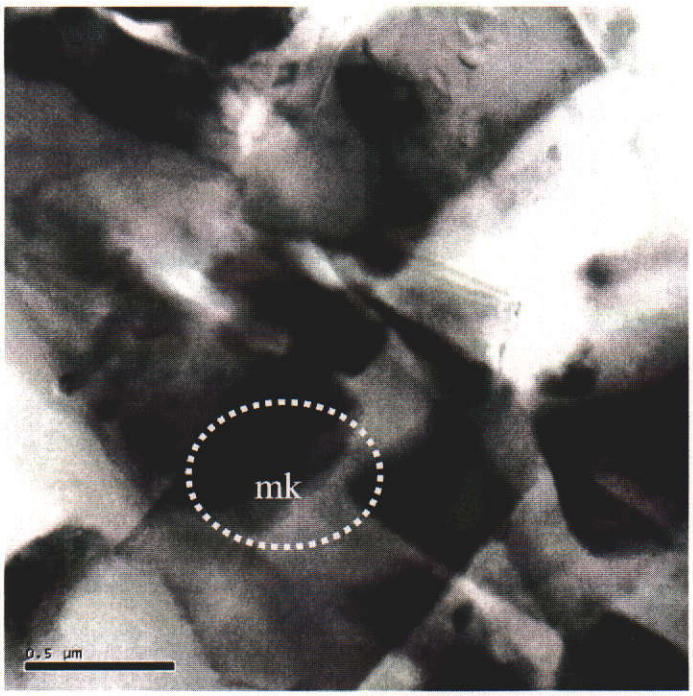

Figure 5.16 TEM image of geopolymer with Si:Al = 1.5, Na:Al = 0.6. SAED and EDS analysis was performed in the circled area, mk = metakaolinite.

The image reveals grains with the original morphology of metakaolinite bonded to a geopolymer matrix similar to that observed in SEM images. The boundary between the unreacted metakaolinite and the matrix is continuous indicating a strong intimate bond. Some areas of the specimen appear brighter than the others indicating that the thickness of the specimen is not uniform which may be a result of differences in density.

Selected area electron diffraction (SAED) from the circled area reveals that some degree of crystallinity still exists (figure 5.17). This suggests that unreacted metakaolinite retains the morphology of the original kaolinite and in some instances also maintains a degree of crystal order. The poor quality of the diffraction pattern,

however, prevented the accurate determination of d-spacing. This type of diffraction pattern was also observed in other samples with similar composition.

Figure 5.17 SAED from the circled area of figure 5.14 showing some retained crystal order of the unreacted metakaolinite.

Figure 5.18 shows the EDS spectrum of the circled area shown in figure 5.16. The spectrum is similar to the SEM-EDS spectrum in figure 5.12 which provides further evidence of the presence of unreacted metakaolinite.

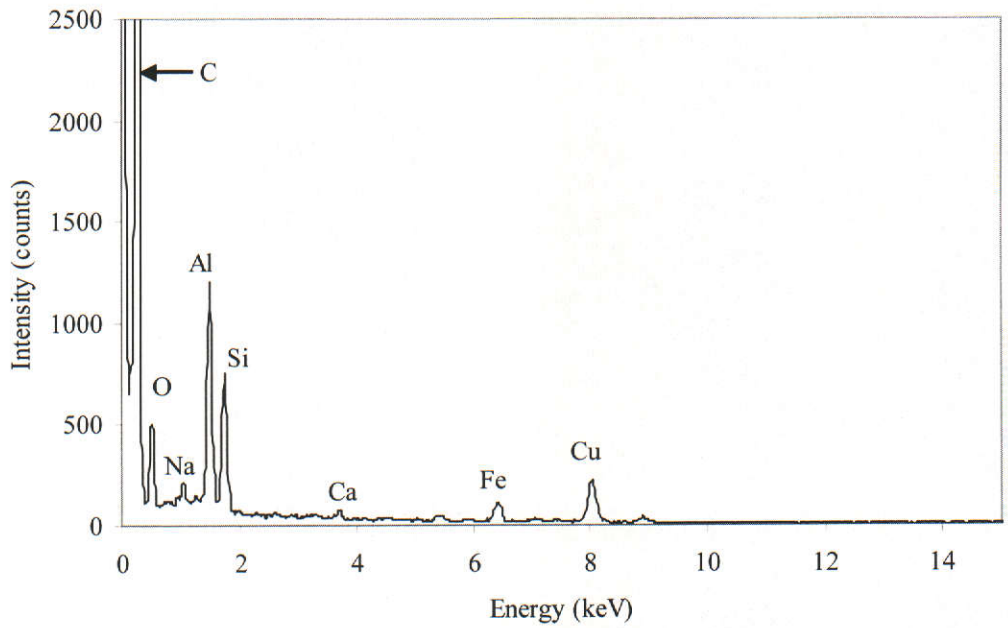

Figure 5.18 TEM-EDS spectrum in the circled area in figure 5.16 showing further evidence of unreacted metakaolinite. Ca and Fe are original constituents of kaolinite while Cu arises from the grid used to support the sample.

Figure 5.19 shows a higher magnification TEM image for geopolymer with Si:Al = 1.5, Na:Al = 0.6. The numbers indicates the spots where EDS analysis was performed (table 5.3).

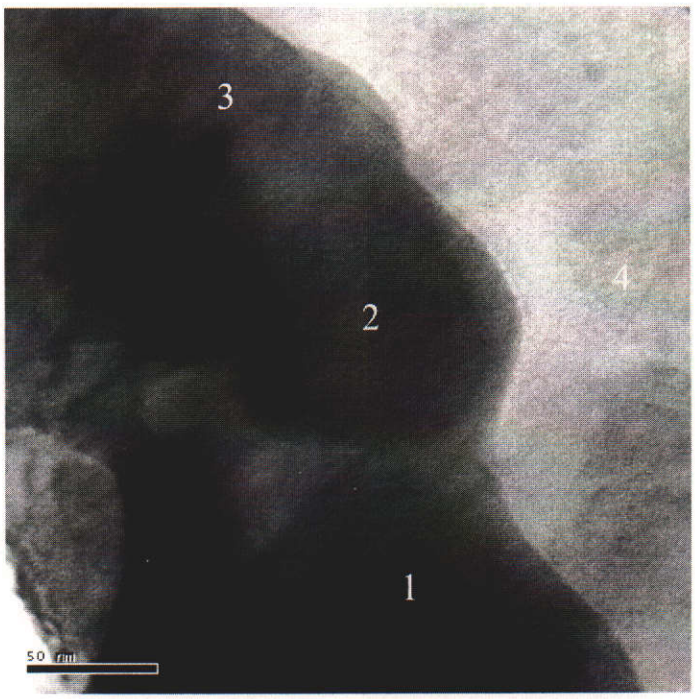

Figure 5.19 TEM image of geopolymer with Si:Al = 1.5, Na:Al = 0.6 at higher magnification. EDS analysis was performed on the spots shown.

Table 5.3 EDS results from spots shown in figure 5.19. All results in atomic percent and normalised to 100 %.

Spectrum	O	Na	Al	Si	K	Ca	Fe
1	63.09	1.22	16.67	18.48	0.12	0.05	0.35
2	63.25	0.95	16.49	18.72	0.06	0.07	0.44
3	63.20	0.96	16.59	18.53	0.10	0.10	0.47
4	62.58	3.44	12.19	20.94	0.35	0.24	0.24

The EDS results indicate that the bright area of figure 5.19 appears to be the geopolymer matrix while the dark area represents the unreacted metakaolinite. It should be mentioned that carbon in figure 5.18 originated from the araldite used to glue the specimen on the grid.

As mentioned in chapter 4 the Kingwhite kaolinite used in this study contains a small amount of halloysite as observed by SEM and TEM. It is worth mentioning that some of the halloysite retains its crystalline structure even after dehydroxylation at 750 °C as well as activation with sodium silicate solution (figure 5.20(a)). Figure 5.20(b) shows the SAED pattern from the circled area showing an electron diffraction typical of halloysite with d-spacings in good agreement with the value of halloysite d-spacings reported by Grim (1953, p.88-89).

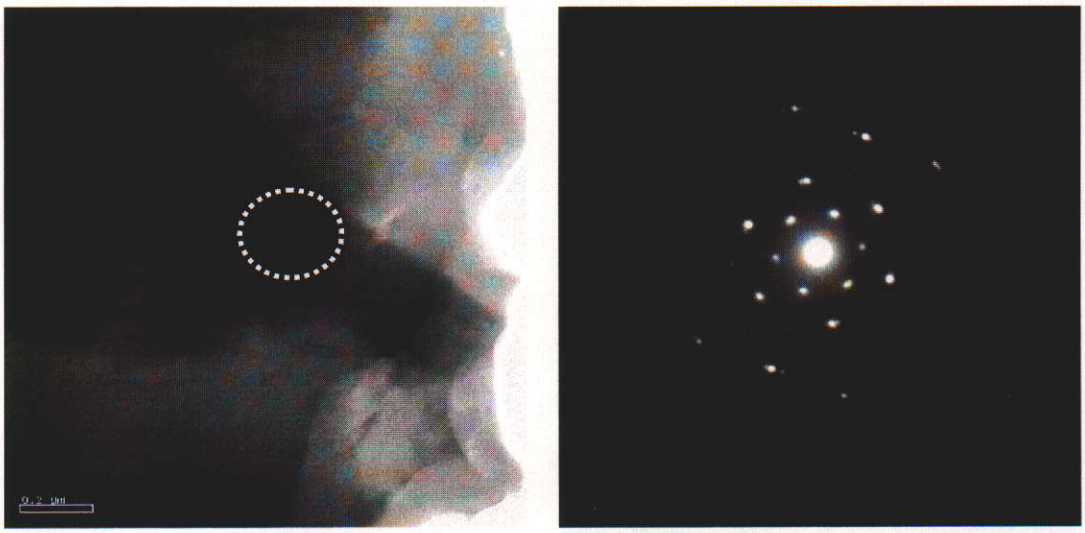

(a) (b)

Figure 5.20 (a) TEM image of a geopolymer (Si:Al = 1.5, Na:Al = 0.6) showing unreacted halloysite, (b) SAED from the circled area.

Na-PSS geopolymer with Si:Al = 2.0, Na:Al = 1.0

As shown in chapter 4, Na-PSS geopolymers prepared with nominal atomic ratios of Si:Al = 2.0, Na:Al = 1.0 have marginally lower compressive strength and hardness compared to those prepared with Si:Al = 1.5, Na:Al = 0.6. However, the workability of these samples was higher as there was more reaction water in the mixture. The water content within the structure of ordinary cements and geopolymers also influences the strength as well as the hardness of the resulting materials (Barbosa, MacKenzie & Thaumaturgo 2000).

Figure 5.21and 5.22 show SEM images of a geopolymer sample prepared with Si:Al = 2.0, Na:Al = 1.0. The images show that the sample still contains unreacted metakaolinite within a geopolymer matrix, pores and microcracks. The image clearly shows that the unreacted metakaolinite acts like aggregate in stopping or deflecting the propagation of microcracks. Figure 5.21 also shows that this sample is more homogeneous (less unreacted metakaolinite) than the sample prepared with Si:Al = 1.5, Na:Al = 0.6.

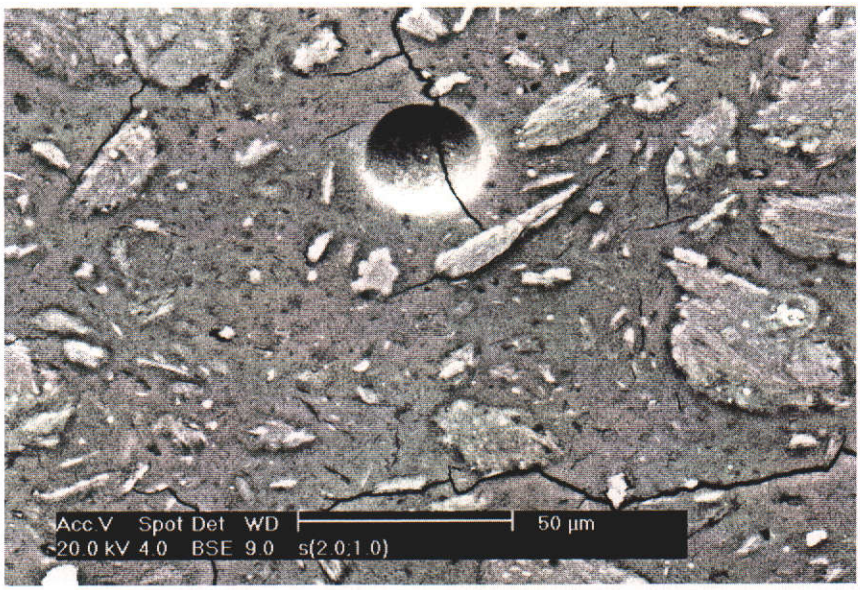

Figure 5.21 SEM image of geopolymer sample with Si:Al = 2.0, Na:Al = 1.0 showing unreacted metakaolinite, a pore (air bubble) and microcracks.

Figure 5.22 clearly shows that geopolymer prepared with Si:Al = 2.0, Na:Al = 1.0 has high homogeneity. This indicates that there was adequate sodium silicate solution to be able to dissolve most of the metakaolinite resulting in hardened geopolymer paste after curing. Rowles and O'Connor (2003) also produced highly homogeneous Na-PSS geopolymer samples with atomic ratios of Si:Al = 2.59, Na:Al = 1.29. They reported a maximum strength of 64±3 MPa for geopolymers prepared with this chemical composition. Their geopolymer samples prepared with Si:Al = 1.5, Na:Al = 0.72 showed the lowest compressive strength. The microstructure of this sample also contained unreacted metakaolinite, which led them to conclude that the presence of unreacted metakaolinite might be responsible for weakening the

microstructure of geopolymers. The sodium silicate solution used to prepare their geopolymers was synthesised from silica fume and sodium hydroxide.

Figure 5.22 SEM image of geopolymer sample with Si:Al = 2.0, Na:Al = 1.0 showing high homogeneity of the geopolymer matrix.

In this study technical grade sodium silicate solution was used as an activation solution (see section 3.1.1) and its SiO_2 content did not allow production of geopolymers with an atomic ratio of Si:Al higher than 2. However, geopolymer samples prepared with Si:Al = 2.0, Na:Al = 1.0 were found to have compressive strength of 59±2 MPa, comparable to the highest strength reported by Rowles & O'Connor (2002). In this study, the highest compressive strength 86±8 MPa was achieved for geopolymers with an atomic ratio of Si:Al = 1.5, Na:Al = 0.6. As shown in figures 5.6 and 5.11 these samples also contain considerable amounts of unreacted metakaolinite. It should be noted that the dehydroxylation of kaolinite and curing temperature of geopolymers as well as the size of the samples used in this study were similar to those used by Rowles and O'Connor. The difference in the strength of geopolymers observed in this study and those reported by Rowles & O'Connor (2003) is likely to be due to the difference in the type and range of the activator solution.

Figures 5.23 and 5.24 show representative EDS spectra from the grains and the geopolymer matrix for a sample with a nominal atomic ratio of Si:Al = 2.0 Na:Al = 1.0.

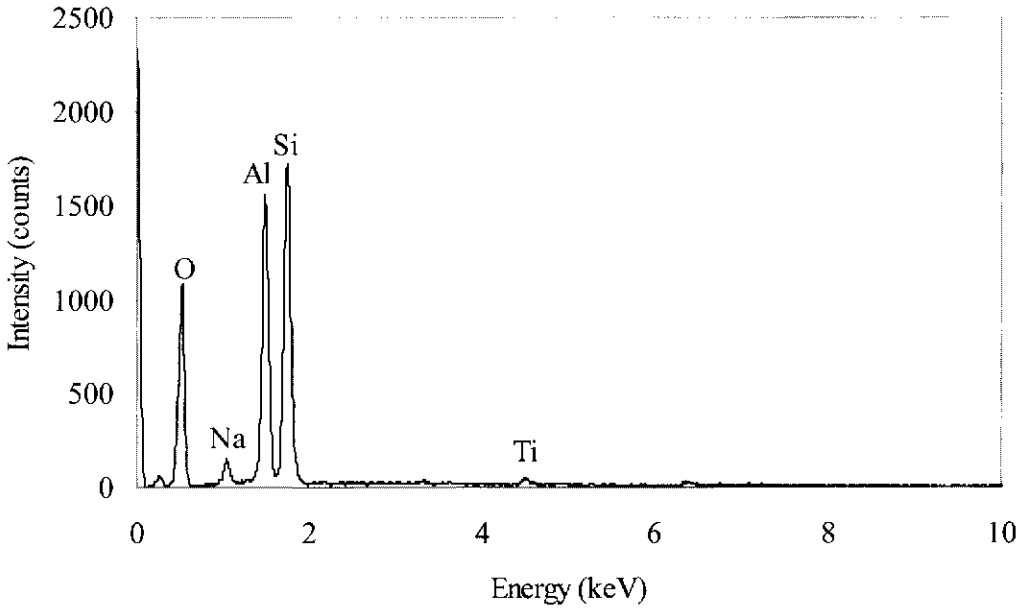

Figure 5.23 A representative SEM-EDS spectrum from a grain in geopolymer with Si:Al = 2.0, Na:Al = 1.0. Spectrum collected at 25 kV.

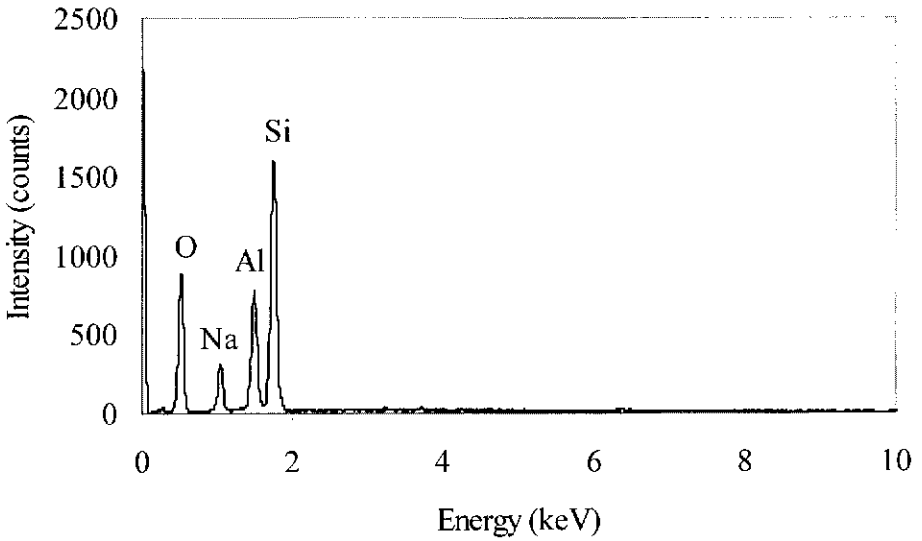

Figure 5.24 A representative SEM-EDS spectrum from the matrix of geopolymer sample with Si:Al = 2.0, Na:Al = 1.0. Spectrum collected at 25 kV.

The average atomic ratios of Si:Al and Na:Al of the grains and the geopolymer matrix for the sample with nominal atomic ratios of Si:Al = 2.0, Na:Al = 1.0 as obtained from elemental analysis are shown in table 5.4.

Table 5.4 Average atomic ratios of Si:Al and Na:Al for a geopolymer sample prepared with Si:Al = 2.0, Na:Al = 1.0. Standard deviations (SD) are shown in parentheses.

Phase	Si:Al	Na:Al
grain	1.51 (0.04)	0.27 (0.03)
matrix	2.38 (0.02)	0.69 (0.04)

As with the samples prepared with Si:Al = 1.50, Na:Al = 0.6, there is a significant difference in the atomic ratios of Si:Al and Na:Al measured from the grains and the matrix of geopolymer for samples with Si:Al = 2.0, Na:Al = 1.0. Again, the Na:Al measured from the matrix of geoplymer is significantly lower than its nominal value. According to Rowles & O'Connor (2003) some Na exists in an unreacted state and is either leached away from the polymer in the form of crystalline Na_2CO_3, or lost during the SEM sample preparation process.

The measured atomic ratios of Si:Al and Na:Al from the grains (Table 5.3) also indicates an incomplete reaction between the activation solution and metakaolinite. The atomic ratio of Si:Al measured on the grain (1.51) is much higher than that of metakaolinite (1.04) as well as the presence of sodium indicate that the reaction had commenced but did not go to completion. It is possible that some particles of metakaolinite used in this study were lacking of IV-V coordinated Al and therefore did not react properly with the sodium silicate solution to produce aluminosilicate gel as pointed out by Davidovits (1999). Also, not all kaolinite particles have been transformed into metakaolinite as observed by TEM.

The microstructure of the geopolymers was also investigated at higher resolution by TEM. Figure 5.25 shows a representative TEM image of the sample with Si:Al = 2.0, Na:Al = 1.0. The sample, prepared by ion beam milling, suffered extensive cracking when it was heated to 75 °C to soften the adhesive so it could be removed from the holder.

The TEM image verifies the presence of unreacted metakaolinite supporting SEM observations. However, SAED examination on every grain shown in figure 5.25 as well as on other images from different sites of the sample did not show any indication of crystallinity.

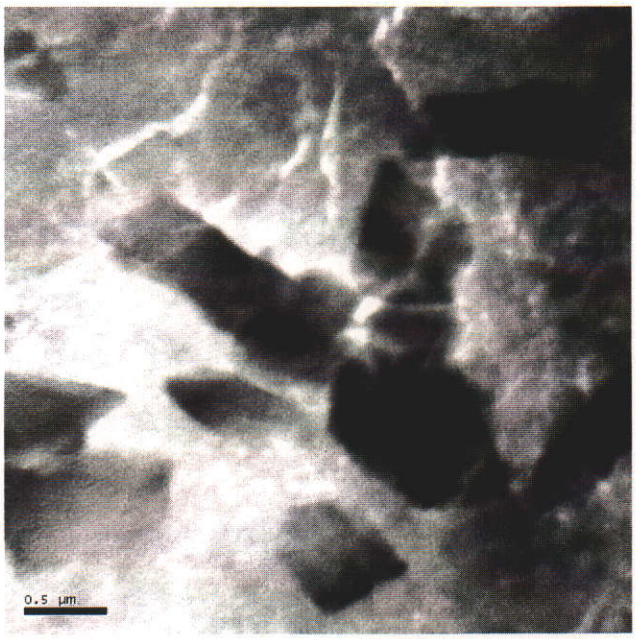

Figure 5.25 A representative TEM image for a geopolymer sample with Si:Al = 2.0, Na:Al =1.0 showing unreacted metakaolinite (dark grains) surrounded by geopolymer matrix.

Figure 5.26 (a) shows an SEM image of a specimen (Si:Al = 2.0, Na:Al = 1.0) for which X-ray mapping was also undertaken. Figure 5.26 (b), (c) and (d) shows X-ray elemental map for sodium, aluminium, and silicon, respectively. As with the sample shown in figure 5.15, the elemental maps of this sample also indicate that the grains are characterised as aluminium-rich regions and sodium-deficient regions, corresponding to the original composition of metakaolinite. The metakaolinite regions are visible as the bright phase bonded within the geopolymer matrix.

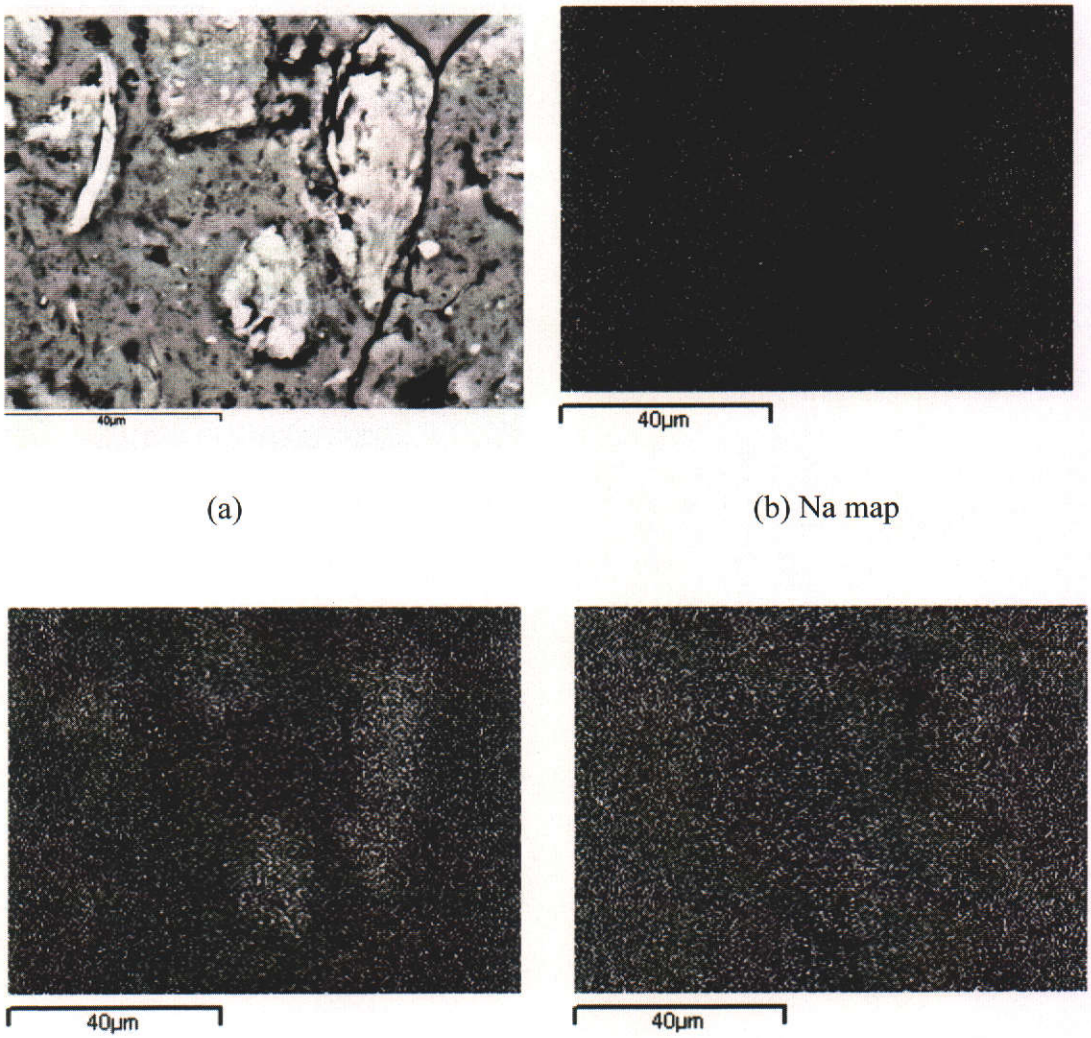

(a) (b) Na map

(c) Al map (d) Si map

Figure 5.26 (a) SEM image of geopolymer sample (Si:Al = 2.0, Na:Al = 1.0) and corresponding X-ray elemental maps: (b) sodium, (c) aluminium, (d) silicon.

5.3 The Influence of aggregate on the microstructure of Na-PSS geopolymers

The incorporation of aggregate (quartz and granite) on Na-PSS was expected to increase the strength of geopolymer through the reduction of pores, prevention of cracks as well as the contribution from the strength of the aggregate itself. The strength of cement-based materials has been found to be related to porosity (Rahier *et* al. 1996; Neville 2000 p. 277 – 284). The strength of the interfacial bond between the aggregate and the matrix as well the physical properties of aggregate particles (such

as porosity) also affect the overall strength of the geopolymeric system. Therefore, the microstructural examination of the geopolymer-aggregate composite is important in order to gain insight into the nature of the aluminosilicate gel as a binder as well as the interaction between the binder and the aggregate.

5.3.1 Crack development in geopolymers containing aggregate

Optical microscopy examination was performed particularly to observe the development of microcracks on as-prepared (polished) samples as well as after it was evacuated in a vacuum chamber for gold or carbon coating prior to SEM imaging. Figure 5.27 shows an optical image of a geopolymer sample with Si:Al = 1.5, Na:Al = 0.6 with α-quartz aggregate.

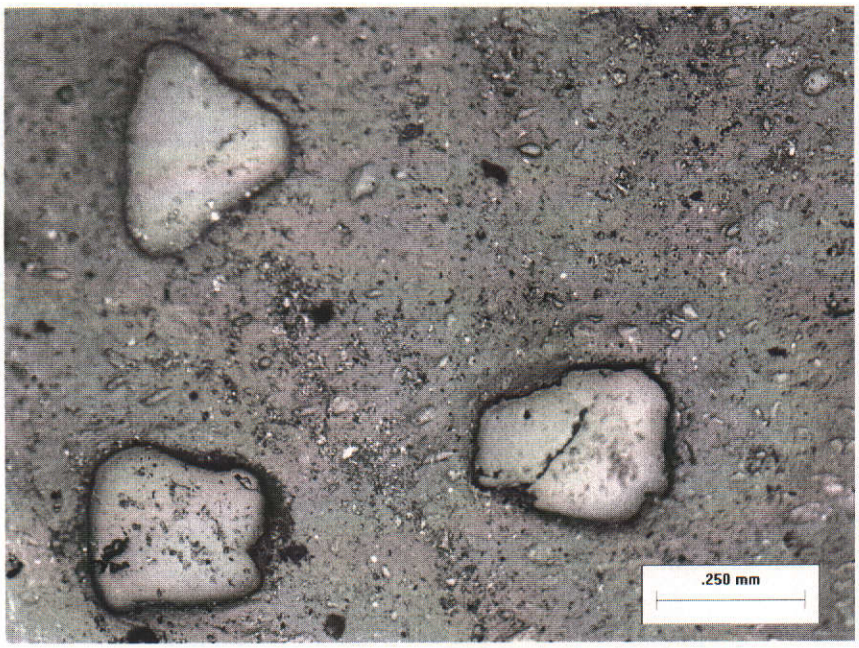

Figure 5.27 An optical image of a geopolymer sample (Si:Al = 1.5, Na:Al = 0.6) containing quartz aggregate.

The presence of aggregate prevents the polishing achieving the same surface finish as attained for samples without aggregate. No cracks were observed on the surface of the polished sample.

Figure 5.28 shows the image of the sample taken immediately after it was evacuated in a vacuum chamber with a pressure of about 0.1 Torr for 30 minutes. The image clearly shows the development of cracks due to moisture loss. Similar crack development was also observed in a geopolymer sample containing granite aggregate (figure 5.29).

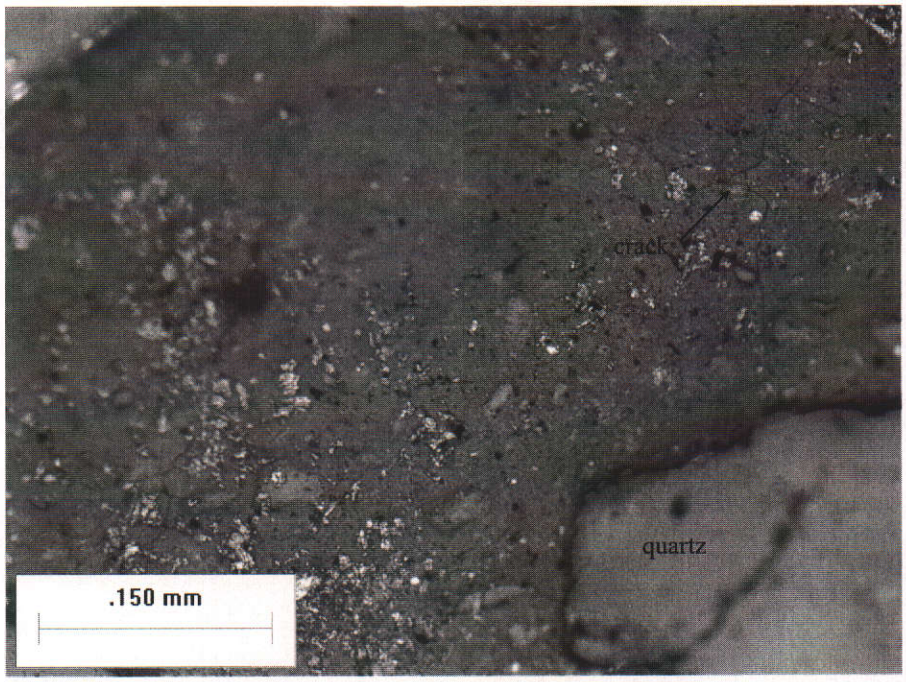

Figure 5.28 A magnified image of the geopolymer sample shown in figure 5.27. Note that the magnification and the field of view have been adjusted to enhance the position of the crack.

The development of microcracks in samples containing aggregate can be explained as follows. The aggregate, which has higher stiffness than the geopolymer paste, restrains the matrix shrinkage. This restraining effect causes radial and tangential stresses around the aggregate particle (Merchant *et* al. 2001; Bisschop & van Mier 2002). The shrinkage resulting from moisture loss will enhance these stresses leading to the development of extensive cracks.

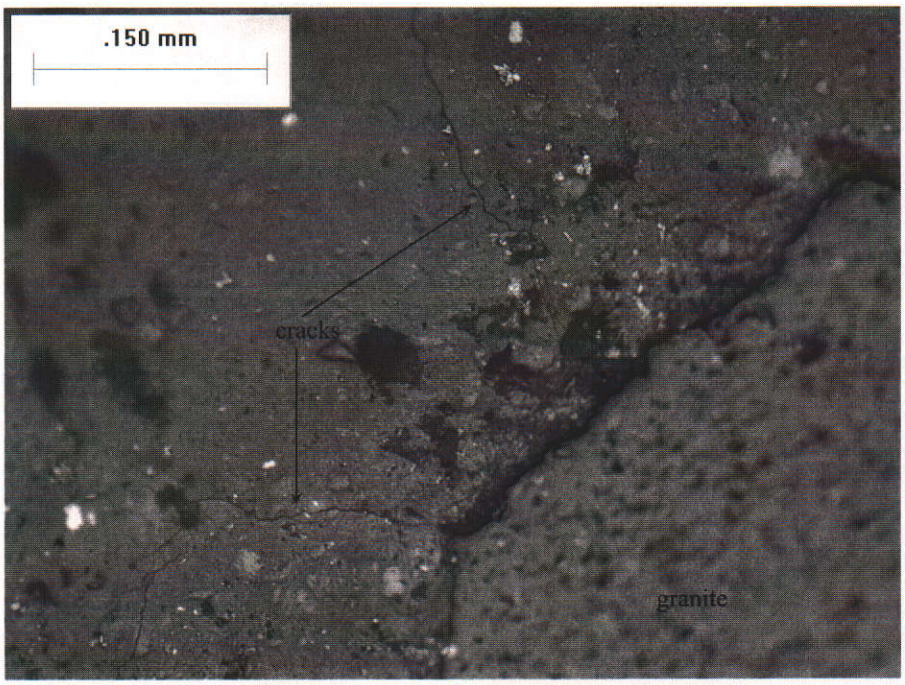

Figure 5.29 An optical image of a geopolymer sample (Si:Al = 1.5, Na:Al = 0.6) containing 20 wt % granite aggregate.

5.3.2 Interfacial transition zone (ITZ) and the strength of geopolymers containing aggregate

As a cement-based material, geopolymer has been recognised as a potential binder for mortar and concrete applications. In Portland cement, the interaction between mineral aggregates and cement binder (known as the interfacial transition zone, ITZ) has been studied intensively (Zang & Gjorv 1990; Tasong, Lynsdale, Cripps 1998; Shi & Xie 1998; Brough & Atkinson 2000; Diamond & Huang 2001; Zhou, Wagner & Nutt 2001; Rao & Prasad 2002; Elsharief, Cohen & Olek 2003). In contrast, to the present date, very little research has been conducted on examining the interaction between aggregate and hardened-geopolymer paste (Barbosa & MacKenzie 2003; Lee & van Deventer 2004).

In this study, the microstructural characterisation by means of SEM and TEM was performed in order to gain insight into the characteristics of the interface between aggregate and geopolymer paste. It was assumed that the concept of ITZ is also applicable to geopolymers containing natural aggregates such as quartz and granite.

The images of the samples taken by optical microscopy (figure 5.28 and 5.29) suggest that the geopolymers act like an inorganic binder similar to Portland cement. Figure 5.30 shows an image of geopolymer (Si:Al = 1.5, Na:Al = 0.6) containing 20 wt % quartz aggregate with a grain size of < 500 μm. The image shows a crack coming in from the left and being deflected by a quartz grain.

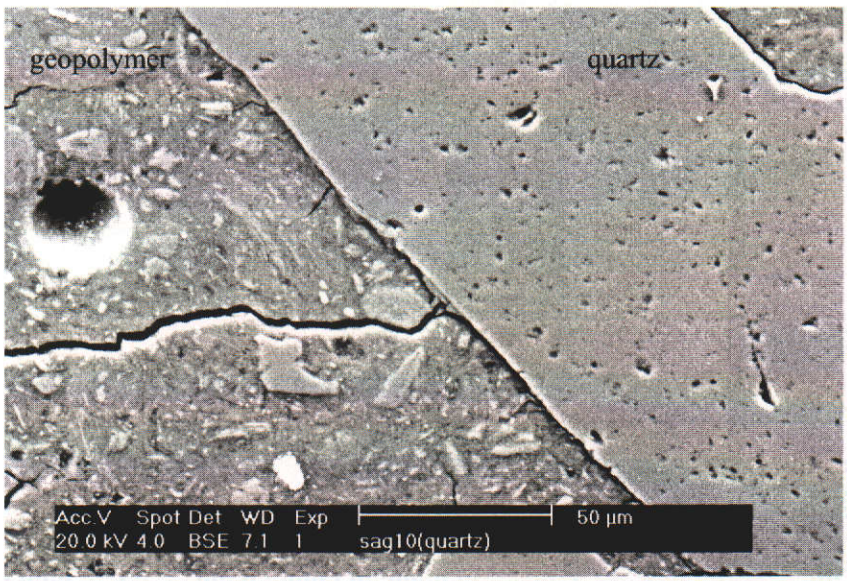

Figure 5.30 SEM image of geopolymer (Si:Al = 1.5, Na:Al = 0.6) containing 20 wt% quartz aggregate.

Figure 5.31 shows a higher magnification image of figure 5.30 to enable closer examination of the morphology of the interfacial zone. The crack development at the aggregate-matrix interface can be explained as follows. In a geopolymer-aggregate composite system, the interfacial bond between the matrix and aggregate restrains expansion or shrinkage of the matrix. The development of microcracking at the aggregate-matrix interface is enhanced by a large incompatibility between the moduli of elasticity of the aggregate and the hardened-geopolymer paste. The image also shows that the grain of unreacted metakaolinite acts like an aggregate particle in deflecting the propagation of a microcrack. From numerous micrographs it appears that the sample also contains pores (air bubbles) although not as extensive as in the sample without aggregate.

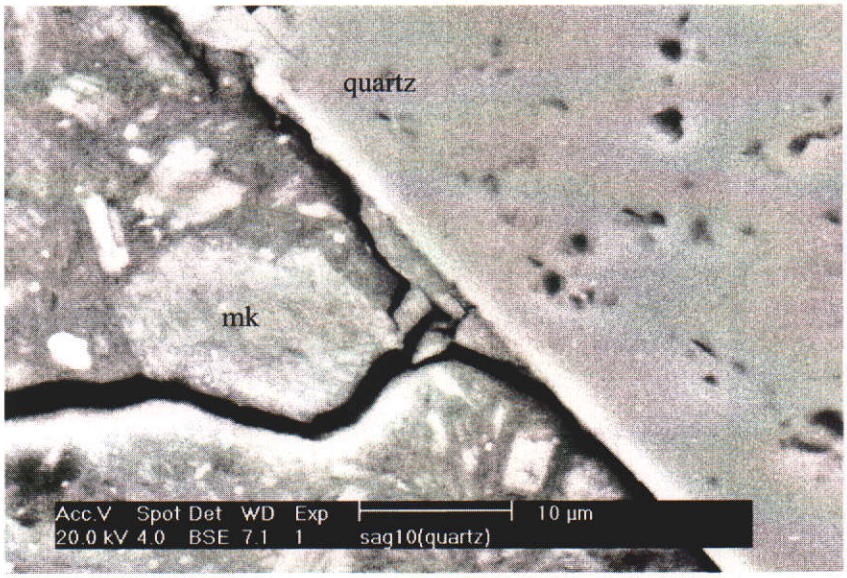

Figure 5.31 SEM image of the sample shown in figure 5.30 at higher magnification (mk = unreacted metakaolinite).

Further examination of the ITZ between the aggregate and the geopolymer matrix for the sample with Si:Al = 1.5, Na:Al = 0.6 was performed using the TEM. The sample for these observations contained crushed quartz with a particle size of less than 50 µm. The sample was sectioned into a 1 mm thick slab of 25 mm diameter. Both sides of the sample were then polished to a finish of 1 µm. The polished sample was coated and examined using SEM to identify areas of interest, before it was sectioned into several 3 mm discs. Further thinning was performed using TEM sample preparation techniques as described in chapter 3. The most crucial step in the preparation of the sample was during dimple grinding as the aggregate could easily detach itself from the sample when the sample thickness was less than 40 µm.

Figure 5.32 shows an image of geopolymer sample (Na:Al = 1.5, Na:Al = 0.6) containing crushed quartz prepared for TEM inspection. The image shows the presence of microcracks around the aggregate, which is believed to occur due to shrinkage during the evacuation in the gold coating unit. Closer inspection of this sample (figure 5.33) was performed in order to investigate the interfacial transition zone (ITZ) between the aggregate and the geopolymer matrix.

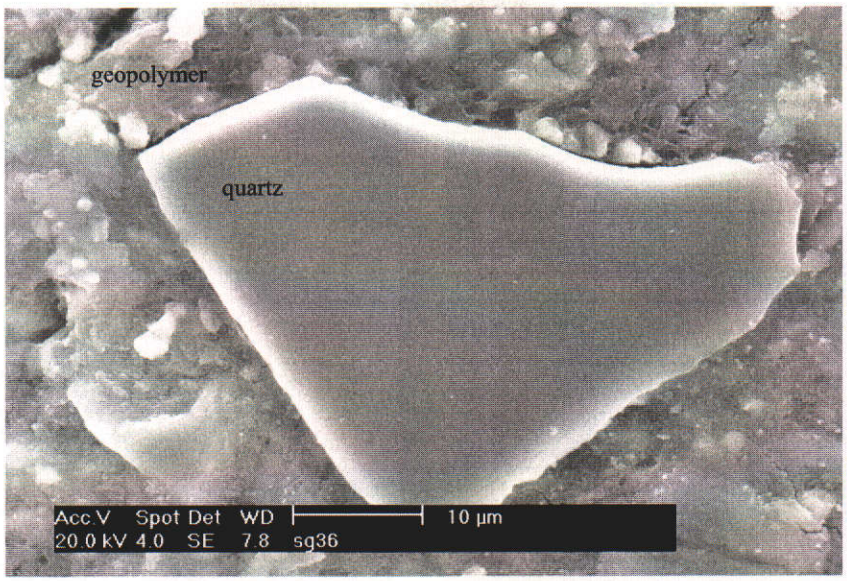

Figure 5.32 SEM image of a thin section of geopolymer (Si:Al = 1.5, Na:Al = 0.6) prepared for TEM inspection.

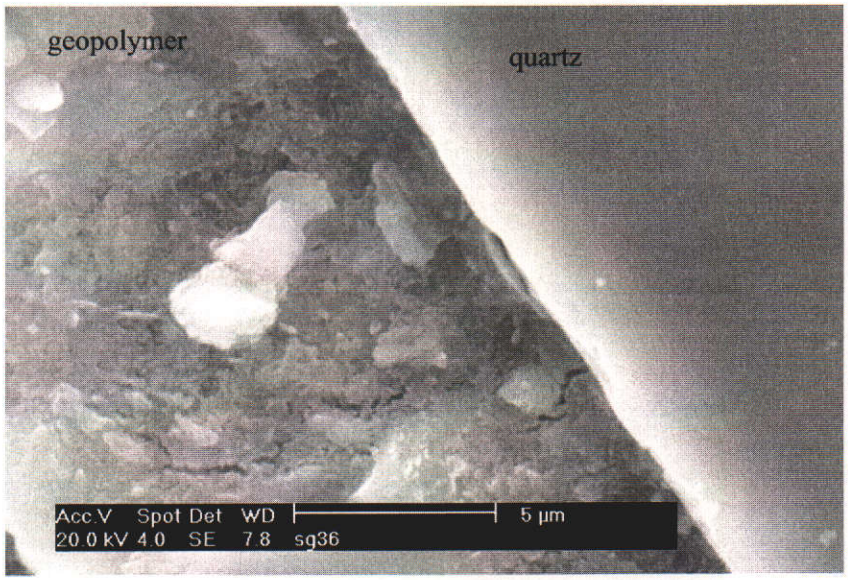

Figure 5.33 SEM image of the sample shown in figure 5.32 at higher magnification.

The image shows that the aggregate is fully bonded to the geopolymer matrix. There is no distinct difference in morphology or chemical composition between the matrix near the aggregate and the rest of the geopolymer paste.

Figure 5.34 shows a TEM image of geopolymer prepared from the same section of the sample shown in figure 5.32. The image shows that the ITZ appears to be very thin. The difference in hardness and density between the aggregate and the geopolymer matrix results in non-uniform thickness during mechanical polishing and

ion beam milling. Elemental analysis results indicated that spot A is quartz while spots B and C are geopolymer paste with similar chemical composition, except that the amount of Na in spot C was lower than that in spot B (Table 5.5).

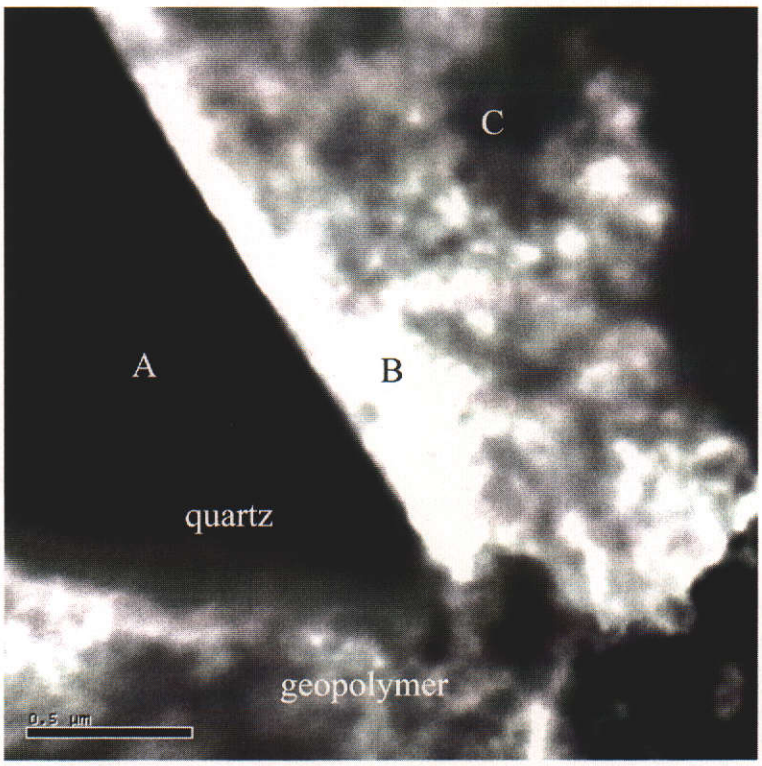

Figure 5.34 A TEM image of geopolymer (Si:Al = 1.5, Na:Al = 0.6) containing quartz aggregate. A, B and C are spots where elemental analysis was performed.

Table 5.5 Elemental analysis results from spots A, B and C shown in figure 5.34. Oxygen determined by stoichiometry (normalised to 100%). All results in atomic Percent.

Spectrum Label	Na	Al	Si	S	K	Fe	O
A			33.33				66.67
B	4.37	8.07	22.40	0.95	1.52		62.69
C	1.57	9.56	23.03	0.20	1.44	0.83	63.36

Figure 5.35(a) and 5.35(b) show TEM images taken from a different site of the same sample. The image shows that the geopolymer provides a strong enough bond to prevent the aggregate from being dislodged during the sample preparation.

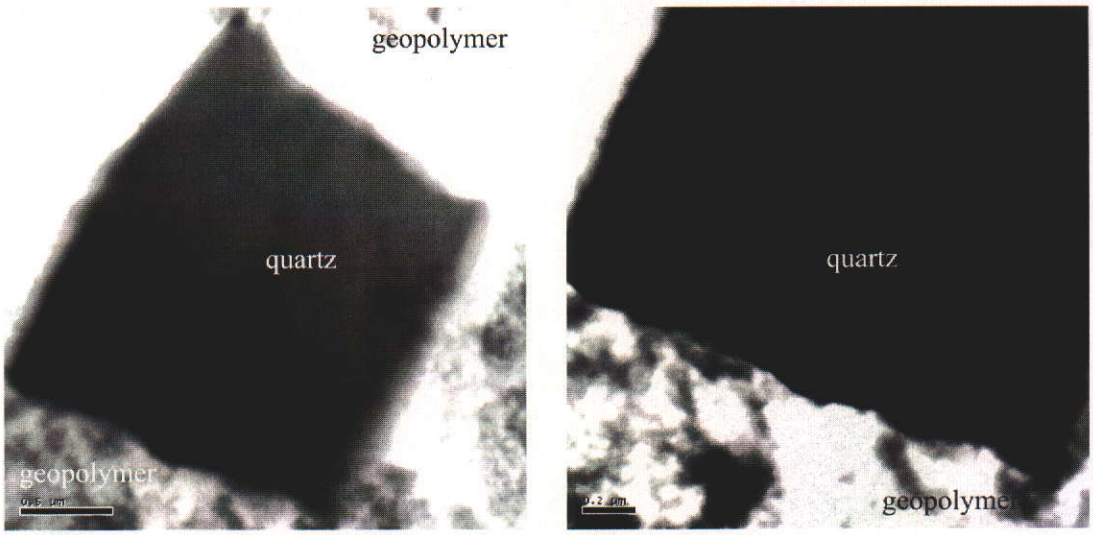

(a) (b)

Figure 5.35 (a) and (b) TEM image of geoplymer (Si:Al = 1.5, Na:Al = 0.6) showing quartz aggregate surrounded by geopolymer matrix.

Numerous SEM and TEM images were used to examine the morphology and chemical compositions of the ITZ (10 – 30 μm). Elemental analysis showed that the chemical composition of the geopolymer matrix and ITZ is relatively homogeneous. No evidence was found of higher density of pores in the ITZ compared to the "bulk" of the geopolymer paste as is the case in mortar or concrete made from Portland cement.

Based on SEM observation, Shi & Xie (1998) reported a very porous transition zone with a thickness of 40 to 60 μm, filled with well-formed $Ca(OH)_2$, between Portland cement and sand grains. They also reported that no porous zone was observed in the transition zone between alkali activated slag paste and sand grains.

It is known that the aluminosilicate gel network has a capacity to incorporate calcium resulting in calcium-aluminosilicate which can act as a binding phase in geopolymeric systems if the starting material is rich with calcium or calcium from another source is intentionally incorporated into the geopolymer starting materials (Davidovits 1994a; Lee & van Deventer 2004).

As observed by Lee and van Deventer (2004) and confirmed by this study no CH crystals could be identified in any of geopolymeric products prepared from low calcium-content fly ash and kaolinite. There is also no evidence that the area around the aggregate contained a higher density of pores compared to the bulk of the material. These results indicate that the notion of ITZ used in OPC mortar and concrete to characterise the area between aggregate and the cement binder, may not be applicable to the geopolymeric system prepared from aluminosilicate sources that contain very little or no calcium.

Diamond and Huang (2001) failed to observe any significant differences in the microstructure and chemical compositions of the ITZ in ordinary concrete from that of the bulk of cement paste. A different ITZ microstructure was also observed in concrete incorporated with lightweight aggregate (Zang & Gjorv 1990). Lightweight aggregate contains large numbers of pores at the outer layer, which encourages the migration of mobile ions towards it, leading to the formation of a more dense interface zone and also improved mechanical interlocking of the aggregate and the cement paste.

The major binding phase in a geopolymeric system prepared from calcium-poor aluminosilicate starting material, such as in the present study, is the aluminosilicate gel itself. Increasing amounts of sodium silicate solution in the starting material was observed to produce a stronger binding aluminosilicate gel and hence improve the overall strength of the geopolymeric system (Lee and van Deventer 2003).

The results of the present study, however, indicate that an increase of sodium silicate solution lowered the bond strength between aggregate and geopolymer paste. As mentioned in chapter 4 the compressive strength of geopolymer samples prepared with an atomic ratio of Si:Al = 2.0, Na:Al = 1.0 with and without the addition of aggregate is lower than geopolymer made with Si:Al = 1.5, Na:Al = 0.6. The amount of sodium silicate used in the present study is below those used by Rowles & O'Connor (2003), which might explain the lower compressive strength of their geopolymers.

Figure 5.36 shows an image of geopolymer with Si:Al = 2.0, Na:Al = 1.0 containing quartz aggregate. Cracks in quartz probably occurred during cutting and polishing of the specimen. The geopolymer matrix is more homogeneous than the sample prepared with Si:Al = 1.5, Na:Al = 0.6. Similar morphology was observed for the sample prepared with Si:Al = 2.0, Na:Al = 1.0 containing granite aggregate (figure 5.37).

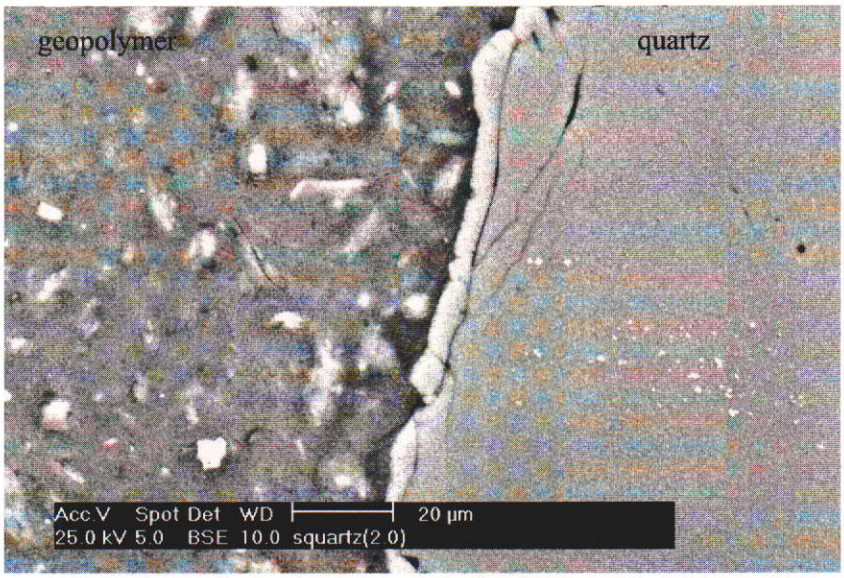

Figure 5.36 SEM image of geopolymer (Si:Al = 2.0, Na:Al = 1.0) with quartz aggregate.

As already mentioned, the strength of geopolymers depends on the cohesion of the geopolymer paste, the interfacial bond between the aggregate and the geopolymer paste and to a certain extent on the strength of the aggregate itself. The quartz and granite used as an aggregate in this study are similar to those used in the production of mortar and concrete. The strength of aggregate should be greater than that of the composite because the actual stresses at the interface of the individual aggregate particles within the concrete may be far in excess of the nominal applied compressive stress. The average compressive strength of quartz and granite commonly used in mortar and concrete is 252 MPa and 181 MPa, respectively (Neville 2000 p. 120-121).

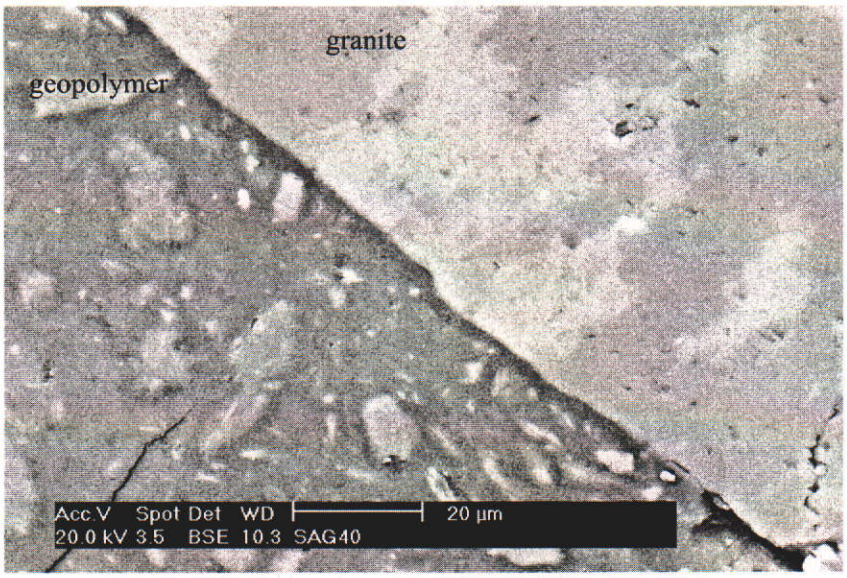

Figure 5.37 SEM image of geopolymer (Si:Al = 2.0, Na:Al = 1.0) with granite aggregate.

The results of compression tests showed that the strength of geopolymers with aggregate are similar, or slightly lower, than the strength of geopolymers without aggregate (see section 4.6 for details). The highest compressive strength measured for geopolymers prepared with an atomic ratio of Si:Al = 1.5, Na:Al = 0.6 was 85 ± 12 MPa for samples containing quartz aggregate and 72 ± 2 MPa for samples contained granite aggregate. In comparison, the highest compressive strength of geopolymer with Si:Al = 1.5, Na:Al = 0.6 without aggregate was 86±8 MPa. These results suggest that the interfacial bond between aggregate as well as the strength of the aggregate itself makes a negligible contribution to the overall strength of geopolymeric system. As cracks developed during the compression test, the aggregate particles did not have the ability to anchor the matrix on both sides of the crack so that the crack face separation was not inhibited.

Other researchers (Hos, MacCormick & Byrne 2002, Barbosa & McKenzie 2003, Lee & van Deventer 2004) also reported that incorporation of aggregate into geopolymer had a negligible effect on compressive strength. As with this study, all their geopolymers were prepared from a low calcium-content kaolinite or fly ash. It is assumed that the inclusion of calcium into the starting material will result in a stronger aluminosilicate binder and hence improve the strength of the interfacial

bond between the aggregate and the matrix. Lee & van Deventer (2004) pointed out that CSH can co-exist with calcium-aluminosilicate in a geopolymeric system if a high-calcium aluminosilicate solid is used.

It is well known that calcium in the form of CaO is the major constituent of Portland cement, which acts a major binder in the form of calcium silicate hydrate (CSH). The presence of calcium in the structure of geopolymer will resemble the structure of Portland cement. In fact, the term geopolymer cements (see section 2.5) refers to geopolymers prepared with calcium disilicates, $Ca(H_3SiO_4)$ or calcium from other sources. Davidovits (1994a, 1999) reported that the 28-day compressive strength of mortar prepared from geopolymer cement is in the range of 70 – 100 MPa.

SEM and TEM images of the aggregate-matrix interface indicate that to a certain extent the aluminosilicate gel act as a good binder. No conclusive evidence could be found that the interfacial zone between the aggregate and the matrix is the weakest area in the geopolymeric system. The compressive strength of quartz and granite categorises them as strong aggregates. Inspection of fractured surfaces after compression testing did not reveal any fractured aggregate as could occur with weak aggregate. Therefore, the strength of geopolymers made with aggregate is likely to depend on the nature of the interfacial bond between the aggregate and the matrix.

In compression tests, the fracture of geopolymer paste is initiated by the development and the propagation of extensive microcracks. As an increasing load is being applied, these microcracks remain stable up to about 30% of the ultimate load and they then begin to increase in length, width and number (Neville 2000 p. 298). The presence of aggregate will increase the strength of the material if the aggregate particle act as a bridge and is able to anchor the matrix as the cracks propagate (Merchant *et* al 2001). Generally, when the bond is strong, a crushed specimen of normal strength concrete should contain some fractured aggregate particles, in addition to more numerous ones pulled out from their sockets. An excess of fractured particles, however, might suggest that the aggregate is too weak (Neville, 2000 p. 119). Fractured surfaces resulting from compression tests were examined using SEM as shown in figure 5.38 and 5.39.

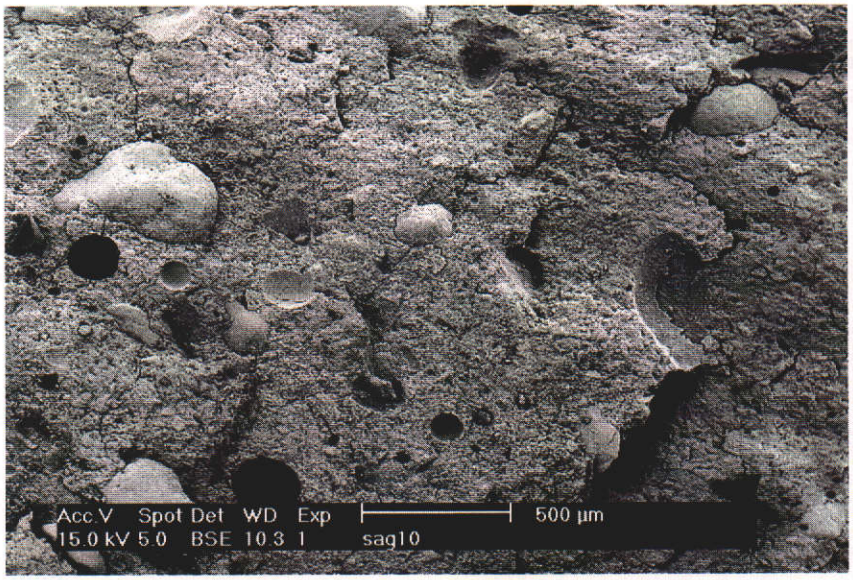

Figure 5.38 SEM image of a fractured geopolymer specimen (Si:Al = 1.5; Na:Al = 0.6) containing quartz aggregate. No broken quartz was observed.

Figure 5.38 shows that a number of aggregate particles have been detached from their sockets and no fractured aggregate was observed on the surface of the samples. It is possible that the aggregate particle was fully bonded to the matrix but the cracks, generated during the compression test, detached from the aggregate early not allowing the formation of a bridge. In this case, the aggregate acts as a filler reducing the overall strength of geopolymer.

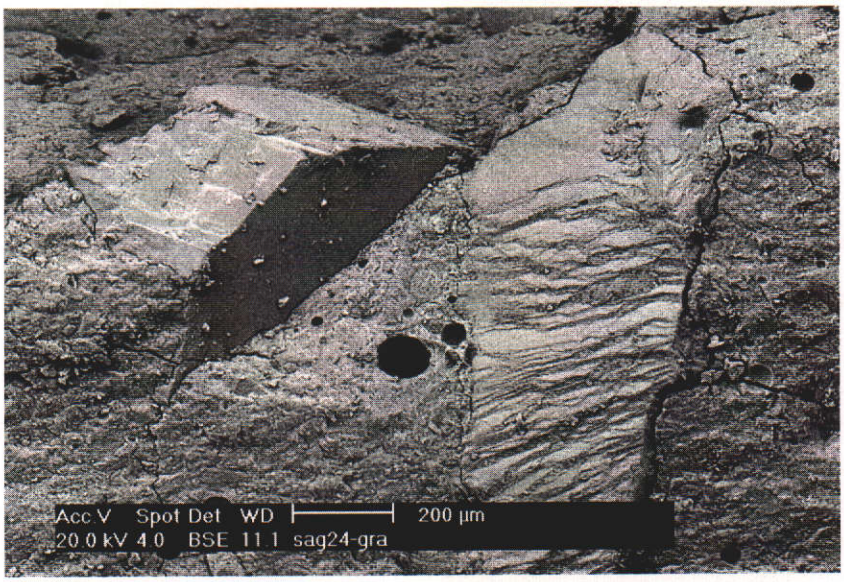

Figure 5.39 SEM image of a fractured geopolymer specimen (Si:Al = 1.5; Na:Al = 0.6) containing granite aggregate.

The granite aggregate in Figure 5.39 appears to be bonded more strongly to the geopolymer than the quartz aggregate which is consistent with the interfacial bond strength values presented in Table 4.8.

5.4 Summary

- SEM and TEM observations revealed that sodium-poly(sialate) (Na-PS) geopolymers have common morphology consisting of grains of crystalline zeolite, unreacted metakaolinite, substantial pores and microcracks.
- Microstructural characterisation by means of SEM and TEM revealed that sodium-poly(sialate-siloxo) (Na-PSS) geopolymers also contain unreacted metakaolinite, substantial pores and microcracks. The microcracks are categorised as secondary microcraks which formed as a result of cutting, polishing and vacuum evacuation in the coating unit. CT-Scan images on as prepared geopolymers with and without aggregate showed that the samples are free from any cracks.
- The presence of unreacted metakaolinite was confirmed by EDS microanalysis as well as X-ray mapping.
- SEM images revealed that the unreacted metakaolinite acts like aggregate in pinning and deflecting cracks.
- Crack development found on the surface of polished samples is believed to be mainly due to moisture loss during evacuation in the coating unit. These types of cracks were categorised as secondary cracks.
- Na-PSS geopolymers prepared with Si:Al = 2.0, Na:Al = 1.0 appear to be more homogeneous than those prepared with Si:Al = 1.5, Na:Al = 0.6.
- SEM and TEM observations showed that the microstructure of ITZ was the same as the adjacent geopolymer.
- No broken aggregate was found on fractured surfaces following compression testing suggesting that the aggregate failed to form a bridge between geopolymer paste and aggregate.

CHAPTER 6

CONCLUSIONS AND FUTURE WORK

6.1 Conclusions

This research was performed with the general aim of investigating the influence of aggregate on the microstructure of geopolymers synthesised from kaolinite. In relation to the objectives of this research, the following conclusions have been made.

6.1.1 Synthesis of geopolymers

The geopolymers in this experiment were synthesised from metakaolinite activated with sodium silicate solution at 70 °C. Variation of geopolymer compositions (Si:Al and Na:Al atomic ratios) were made based on the chemical compositions of metakaolinite and sodium silicate solutions. Two main types of aggregate were used in this experiment namely α-quartz and granite. Sandstone was also used as aggregate particularly to study the interfacial bond strength between geopolymer paste and aggregate. The major findings and conclusions from the synthesis of geopolymers can be summarised as follows:

- The metakaolinite was obtained through dehydroxylation of kaolinite at 750 °C for 6 hours in air. The XRD and TEM observations showed that dehydroxylation at this temperature has transformed kaolinite into the amorphous state of metakaolinite. The TG-DTA result confirmed that the dehydroxylation is essentially complete at 600 °C.
- Thermally assisted curing plays an important role in determining the rate of geopolymerisation (polycondensation). In this experiment the curing temperature was set at 70 °C for 2 hours. Lower curing temperatures will require a longer time for geopolymerisation. During the curing stage the mould was completely covered to avoid the loss of reaction water, which is essential for geopolymerisation as well as avoiding initiation of cracks on the surface of specimens.

- Geopolymers synthesised in this experiment were prepared by varying the atomic ratio of Si:Al (1.04, 1.25, 1.50, 1.75 and 2.0) and Na:Al (0.6, 0.8 and 1.0) while keeping the molar ratio of H_2O:Na_2O =10. The amount of water based on this molar ratio was found to be enough to facilitate the reaction although the workability was low for geopolymers prepared with Si:Al = 1.04 and 1.25.
- Geopolymers synthesised in this experiment were divided into two groups; *sodium-poly(sialate)* (Na-PS) (Si:Al = 1.04 and 1.25) and *sodium-poly(sialate-siloxo)* (Na-PSS) (Si:Al = 1.50, 1.75 and 2.00) geopolymers. The choice of NaOH and sodium silicate did not allow the production of geopolymers with higher Si:Al atomic ratios.
- α-quartz and granite of different sizes and proportions have been used as aggregate resulting in composite-like geopolymers. The main binder is aluminosilicate itself as no attempt was made to incorporate calcium disilicates, $Ca(H_3SiO_4)_2$, to produce geopolymer cements.
- The XRD patterns revealed that Na-PS geopolymer consists of zeolite-A or zeolite-X in conjunction with amorphous aluminosilicate, while Na-PSS geopolymers were amorphous with a broad hump in the region 20^o – 38^o (2θ). It was found that the amorphous hump shifts to higher values of 2θ as the Si:Al decreases. This has been attributed to the change of Al coordination to predominantly tetrahedral when metakaolinite is activated with sodium silicate solution as observed in ^{27}Al MAS-NMR (Rahier *et* al. 1997; Barbosa, MacKenzie & Thaumaturgo 2000).

6.1.2 Physical and mechanical properties of geopolymers

The major findings and conclusions from the physical and mechanical characterisation of the resulting geopolymers can be made as follows:

- Sodium-poly(sialate) (Na-PS) geopolymers were found to be brittle, with low bulk density, high apparent porosity, low Vickers hardness and low compressive strength.

- TG-DTA results on geopolymers with Si:Al = 1.5, Na:Al = 0.6 and Si:Al = 2.0, Na:Al = 1.0 showed a single endothermic peak at about 134 – 140 °C indicating the loss of reaction water from the geopolymer framework.
- Heating the geopolymers up to 950 °C results in shrinkage and extensive cracks. Severe cracking was observed for specimens containing quartz and granite. It was also found that geopolymer prepared with Si:Al = 1.5, Na:Al = 0.6 has significantly less cracks after heating up to 950 °C than geopolymer prepared with Si:Al = 2.0, Na:Al = 1.0.
- The shrinkage and extensive cracks after heating the geopolymer to 950 °C are associated with the mass loss of geopolymers. The mass loss of geopolymer prepared with Si:Al = 1.5, Na:Al = 0.6 is about 15% and about 19% for geopolymer prepared with Si:Al = 2.0, Na:Al = 1.0. The mass loss of geopolymers containing aggregate (quartz and granite) was predictably less than 15%.
- Dilatometer results show that geopolymers have negative thermal expansion. Geopolymer prepared with Si:Al = 1.5, Na:Al = 0.6 suffer about 2% shrinkage from RT to 300 °C. Between 300 and 800 °C geopolymer is essentially dimensionally stable.
- The coefficient of thermal expansion of geopolymers is comparable with the coefficient of thermal expansion of Portland cement paste.
- The inclusion of aggregate (quartz and granite) was found to reduce the shrinkage to below 1%. The useful working temperature range of geopolymers containing quartz was limited to 500 °C due to a sudden expansion of quartz at 570 °C. Geopolymer containing granite aggregate was found to stable up to 800 °C.
- Geopolymers with and without aggregate preheated at 125 °C for 1 hour significantly reduces the shrinkage for geopolymers with and without aggregate. The results indicate that geopolymers require a post-thermal treatment to minimise the shrinkage and thus cracking as a function of temperature before it can be put in service, particularly for fire-resistance applications.
- XRD examination of geopolymer after heating up to 950 °C (Si:Al = 2.0, Na:Al = 1.0) revealed the formation of sodium aluminium silicate ($Na_6Al_4Si_4O_{17}$) which is

likely to occur through solid-state transformation with excess sodium and unreacted metakaolinite.

- The hot wire method has been successfully used to measure the thermal conductivity of geopolymers. It was found that this method is sensitive to the specimen's size as the heat front will reach the edge of the specimen in a very short time deteriorating the linearity of temperature as a function of time. The optimum size of specimen used in this study is 25 cm x 5 cm. The thermal conductivity of geopolymers is comparable to thermal conductivity of Portland cement. The inclusion of aggregate increases the thermal conductivity by 40 %.
- The bulk density and the apparent porosity of geopolymers depend largely on the Si:Al and Na:Al ratio. The bulk density tends to increase with an associated decrease in apparent porosity with the increase of Si:Al ratio.
- The Vickers hardness was found to depend on the applied load and thus the same load of 1 kg was used for all subsequent testing. The value of Vickers hardness of geopolymers depends largely on Si:Al and Na:Al atomic ratios with Si:Al = 1.5, Na:Al = 0.6 having the highest hardness.
- The compressive strength of geopolymers is time dependent reaching a maximum after several days. The strength of geopolymers depends significantly on the Si:Al ratio as well as the apparent porosity. A Si:Al = 1.5, Na:Al = 0.6 without aggregate was found to produce the highest compressive strength (86±8 MPa) which is comparable or better that the strength of Portland cement paste. It was found that the inclusion of aggregate (quartz and granite) forming composite geopolymers has a negligible effect on the strength of geopolymers.
- The interfacial strength experiment revealed that sandstone provides the strongest bond with geopolymer paste followed by granite and quartz. A strong bond between sandstone and geopolymer paste is enhanced by mechanical interlocking and porosity of sandstone.

6.1.3 Microstructural character of geopolymers

The major findings and conclusions from the microstructural characterisation of the resulting geopolymers can be made as follows:

- The XRD investigation on sodium-poly(sialate) (Na-PS) geopolymers revealed that this material consists of amorphous aluminosilicate and cystalline zeolite-A or zeolite-X. SEM observations revealed that the morphology of Na-PS geopolymer consists of geopolymer matrix (amorphous aluminosilicate) in conjunction with grains of unreacted metakaolinite, pores and cracks.
- The XRD investigation of sodium-poly(sialate-siloxo) geopolymers showed that this material is essentially amorphous with a trace of ancillary minerals (quartz and anatase). SEM and TEM investigation revealed that the morphology of Na-PSS consists of geopolymer matrix (amorphous aluminosilicate) in conjunction with unreacted metakaolinite, pores and cracks.
- The CT-Scan results for as prepared Na-PSS geopolymers with and without aggregate did not reveal any resolvable cracks. These results indicate that the cracks observed by SEM and TEM are secondary cracks formed during cutting, polishing and vacuum evacuation in the coating unit.
- No broken aggregate was found on fracture surfaces following compression testing indicating that the aggregate detaches early, preventing the formation of a bridge between aggregate and geopolymer paste.

6.1.4 Overall Conclusion

Aluminosilicate geopolymers with different Si:Al and Na:Al atomic ratios have been produced from metakaolinite activated by sodium silicate solution at 70 °C. It was found the physical and mechanical properties as well as the microstructural character of geopolymers were largely determined by the Si:Al atomic ratio.

Geopolymers produced with Si:Al = 1.04 and Si:Al = 1.25 were categorised as *sodium-poly(sialate)* (Na-PS). These materials were soft, brittle, and porous and XRD patterns showed that these geopolymers were found to be composed of crystalline zeolite-A or zeolite-X in conjunction with amorphous aluminosilicate geopolymer paste.

Geopolymers produced with Si:Al = 1.50, 1.75 and 2.0 were categorised as *sodium-poly(sialate-siloxo)* (Na-PSS). The XRD patterns of Na-PSS showed that these materials are amorphous. Na-PSS geopolymers were hard and have high compressive strength. The strongest Na-PSS geopolymers resulted from Si:Al = 1.50, Na:Al = 0.6 atomic ratios. The inclusion of aggregate (quartz and granite) in the geopolymer paste unexpectedly has a negligible effect on the strength of Na-PSS geopolymers. Na-PSS geopolymers prepared with Si:Al = 1.50, Na:Al = 0.6 were also found to have the highest bulk density and Vicker's hardness.

The TG-DTA results showed that Na-PSS geopolymers retain about 15 wt% of the reaction water. Dilatometer measurements showed that the loss of water from the geopolymer framework was related to about 2% shrinkage of Na-PSS geopolymer between RT to 300 °C. Dilatometer results also showed that between 300 and 800 °C the Na-PSS geopolymers were dimensionally stable indicating that this may be the useful working temperature of geopolymer paste. The addition of aggregate (quartz and granite) significantly reduced the shrinkage of geopolymers by 50%. A phase change in quartz at 574 °C limits the upper working temperature of geopolymers with this aggregate to below 500 °C. It was also found that geopolymers with or without aggregate require a post-thermal treatment to minimise the shrinkage as a function of temperature before it can be put in service, particularly for fire-resistance applications.

Thermal conductivity of geopolymers was measured by using a hot wire method. It was found that the size of the sample significantly influences the accuracy of the thermal conductivity measurement. The results show that the thermal conductivity of geopolymer paste was comparable to those of Portland cement paste. The addition of quartz increases the thermal conductivity of geopolymers by 40 %.

The microstructural characterisations by SEM and TEM revealed that the morphology of geopolymers consists of geopolymer matrix (aluminosilicate paste), unreacted metakaolinite, pores and microcracks. The CT-Scan images revealed that the presence of microcracks were due to cutting, polishing and vacuum evacuation in the coating unit during sample preparation. No cracks were found in as prepared Na-PSS geopolymers with and without aggregate.

6.2 Future Work

This thesis has dealt with an investigation of the microstructure – property relationship for geopolymers synthesised from metakaolinite and sodium silicate solution. While much information regarding the characters and properties of these materials has been elucidated from this study, a number of issues could not be addressed due to equipment and time constraints. Therefore, future work should be undertaken to gain a better understanding of the relationship between the type of materials, the compositions, microstructural characters as well as the physical and mechanical properties of geopolymers. This is essential before geopolymers can be widely adopted as a material for industrial and commercial applications. The following recommendations are made for future work:

1. The synthesis and characterisation of geopolymers based on metakaolinite over a wider range of Si:Al and Na:Al atomic ratios incorporated with natural aggregates requires further study. Thus metakaolinite needs to be mixed with Si-rich material such as silica fume.
2. The inclusion of calcium from calcium disilicates, $Ca(H_3SiO_4)_2$, or other sources into geopolymer precursors in order to produce geopolymer cements deserves an in-depth study. This is expected to create calcium-aluminosilicate, which can act as a binding phase in geopolymeric systems. It is still not clear whether this binding phase will create stronger bonds between the aggregate and the geopolymer matrix.
3. Geopolymer concretes (geopolymer containing fine and coarse aggregate) with a size similar to those used in Portland cement concretes need to be considered. This is important to allow a direct comparison of the physical, mechanical, thermal, durability as well as economical standpoint between geopolymer concrete and Portland cement concrete.

References

Akcaoglu, T., Tokyay, M. & Celik, T. (2003), "Effect of coarse aggregate size and matrix quality on ITZ and failure behavior of concrete under uniaxial compression", *Cement & Concrete Composites,* [0nline], http://www.sciencedirect.com.dbgw.lis.curtin.edu.au, [11 June 2003]

Akolekar, D., Chaffee, A. & Howe, R. F. (1997), "The transformation of kaolin to low-silica X zeolite", *Zeolites,* **19**, 359 - 365.

Amparano, F. E., Xi, Y. & Roh, Y. (2000), "Experimental study on the effect of aggregate content on fracture behavior of concrete", *Engineering Fracture Mechanics,* **67**, 65-84.

Aparicia, P. & Galan, E. (1999), "Mineralogical interference of kaolinite crystallinity index measurements", *Clays and Clay Minerals,* **47**, (**1**), 12-27.

Aquino, M. J., Li, Z. & Shah, S., P (1995), "Mechanical properties of the aggregate and cement interface", *Advanced Cement Based Materials,* **2**, 211-223.

ASTM C20, A. (1992),"Standard test method for apparent porosity, water absorption, apparent specific gravity, and bulk density of burned refractory brick and shapes by boiling water".

ASTM C294 (1998), "Standard descriptive nomenclature for constituents of concrete aggregates".

ASTM C384, A. (1997),"Standard test method for microhardness of materials".

ASTM C773, A. (1994),"Standard test method for compressive (crushing) strength of fired whiteware".

ASTM D5930 (1997), "Standard test method for thermal conductivity of plastics by means of a transient line-source technique".

ASTM E92 (1997),"Standard test method for Vickers Hardness of Metallic materials".

Barbosa, V. F. F. & MacKenzie, K. J. D. (2002), "Synthesis and thermal behaviour of potassium sialate geopolymers", *Materials Letters,* **4012**, 1477-1482.

Barbosa, V. F. F. & MacKenzie, K. J. D. (2003), "Thermal behaviour of inorganic geopolymers and composites derived from sodium polysialate", *Materials Research Bulletin,* **38**, (**2**), 319 - 331.

Barbosa, V. F. F., MacKenzie, K. J. D. & Thaumaturgo, C. (2000), "Synthesis and characterisation of materials based on inorganic polymers of alumina and silica: sodium polysialate polymers", *International Journal of Inorganic Materials,* **2**, (**4**), 309-317.

Bell, A. T. (1999), "NMR applied to zeolite synthesis", *Colloids and Surfaces,* **158**, 221-234.

Bisschop, J. & van Mier, J. G. M. (2002), "How to study drying shrinkage microcracking in cement-based materials using optical and scanning electron microscopy?" *Cement & Concrete Research,* **32**, 279 - 287.

Bouguerra, A., Ledhem, A., de Barquin, F., Dheilly, R. M. & Queneudec, M. (1998), "Effect of microstructure on the mechanical and thermal properties of lightweight concrete prepared from clay, cement, and wood aggregates", *Cement and Concrete Research,* **28**, (**8**), 1179-1190.

Brindley, G. W. & Lemaitre, J. (1987) "Thermal, oxidation and reduction reactions of clay minerals" In *Chemistry of clays and clay minerals* (Ed, Newman, A. C. D.) Longman Scientific & Technical, New York.

Brough, A. R. & Atkinson, A. (2000), "Automated identification of the aggregate-paste interfacial transition zone in mortars of silica sand with Portland or alkali-activated slag cement paste", *Cement and Concrete Research,* **30**, 849-854.

Brough, A. R. & Atkinson, A. (2002), "Sodium silicate-based, alkali-activated slag mortars Part I. Strength, hydration and microstructure", *Cement and Concrete Research,* **32**, 1 - 15.

Caliskan, S. (2003), "Aggregate/mortar interface: influence of silica fume at the micro- and macro-level", *Cement & Concrete Composites,* **25**, (**4-5**), 557-564.

Callister, W. D. (1994) *Materials Science and Engineering An Introduction,* John Wiley & Sons, Inc., New York.

Campbell, D. H. & Folk, R. L.(1991) "The ancient Egyptian pyramids - concrete or rock?" *Concrete International,* August, 29-44.

Challa, G. (1993) *Polymer Chemistry An Introduction,* Ellis Horwood, New York.

Chandrasekhar, S. & Pramada, P. N. (2001), "Sintering behaviour of calcium exhanged low silica zeolites synthesised from kaolin", *Ceramics International,* **27**, 105 - 114.

Chandrasekhar, S., Raghavan, P., Sebastian, G. & Damodaran, A. D. (1997), "Brightness improvement studies on 'kaolin based' zeolite 4A", *Applied Clay Science,* **12**, 221 - 231.

Chen, P., Lin, M. & Zheng, Z. (1997), "On the origin of the name kaolin and the kaolin deposits of the Kauling and Dazhou areas, Kiangsi, China", *Applied Clay Science,* **12**, 1-25.

Cheng, T. W. & Chiu, J. P. (2003), "Fire-resistant geopolymer produced by granulated blast furnace slag", *Minerals Engineering,* **16**, 205 - 210.

Cioffi, R., Maffucci, L. & Santoro, L. (2003), "Optimisation of geopolymer synthesis by calcination and polycondensation of kaolinitic residue", *Resources, Conservation & Recycling,* **4**, (1), 27-38.

Davidovits, J. (1982), "Mineral polymers and methods of making them", 4,349,386 United States Patent.

Davidovits, J.(1987), "Properties of geopolymer cements", *Concrete International* **9** 23-35.

Davidovits, J. (1988), "Geopolymers of the first generation:SILIFACE-Process," *Geopolymer '88, First European Conference on Soft Mineralogy*, Compiegne, France,49-67.

Davidovits, J. (1989), "Waste solidification and disposal method", 4,859,367 United States Patent.

Davidovits, J. (1991), "Geopolymers:Inorganic Polymeric New Materials", *Journal of Thermal Analysis,* **37**, 1633-1656.

Davidovits, J. (1994a), "Properties of geopolymer cements", *Alkaline Cements and Concretes*,Kiev State Technical University, Ukraine,131-149.

Davidovits, J. (1994b), "Global Warning Impact on the cement and aggregate industries", *World Resource Review,* **6**, (**2**), 263-278.

Davidovits, J. (1999), "Chemistry of geopolymeric system, terminology" Geopolymere '99,Saint-Quentine, France, 9-39.

Davidovits, J.(2000), "*The dependence of geopolymer on Si:Al*", [online], http://www.geopolymer.org, [21 July 2001].

Davidovits, J. (2002), "*They have built the Pyramids*", Workshop Curtin University of Technology, Perth.

Davidovits, J. & Davidovits, F.(2001), "*The pyramids an anigma solved, 2nd revised edition based on the first edition (1998) by Joseph Davidovits and Margie Morris*", [online], http://www.geopolymer.org, 2001 [21 July 2001].

Davidovits, J. & James, C. (1988), "Low temperature geopolymeric setting (LTGS) and Archaeometry" Geopolymer '88, First European Conference on Soft Mineralogy, Compiegne, France, 69-78.

Davidovits, J. & Sawyer, J. L. (1985) "Early-high strength mineral polymer" 4,509.958 United States Patent.

Demiborga, R. (2003), "Thermo-mechanical properties of sand and high volume mineral admixtures", *Energy and Buildings,* **35**, 435 - 439.

Diamond, S. & Huang, J. (2001), "The ITZ in concrete - a different view based on image analysis and SEM observations", *Cement and Concrete Research,* **23**, 179-188.

Donza, H., Cabrera, O. & Irassar, E. F. (2002), "High-strength concrete with different fine aggregate", *Cement and Concrete Research,* **32**, 1755 - 1761.

Elias, H. (1997) *An introduction to polymer science,* VCH, Weinheim.

Elsharief, A., Cohen, M. D. & Olek, J. (2003), "Influence of aggregate size, water cement ratio and age on the microstructure of the interfacial transition zone", *Cement & Concrete Research,* **33**, 1873 - 1849.

Escalante-Garcia, J. I. & Sharp, J. H. (2001), "The microstructure and mechanical properties of blended cements hydrated at various temperatures", *Cement & Concrete Research,* **31**, 695-702.

Fitzgerald, J. J. & DePaul, S. M. (1999) "Solid-State NMR Spectroscopy of Inorganic Materials: An Overview" In *Solid-State NMR Spectroscopy of Inorganic Materials*(Ed, Fitzgerald, J. J.) American Chemical Society, Washington, DC.

Gard, J. A. (1976) "Interpretation of electron diffraction patterns" In *Electron Microscopy in Mineralogy* (Ed, Wenk, H. R.) Springer-Verlag, Berlin.

Glasser, F. P. (1995) "Advanced cementitious materials" In *Insight into speciality inorganic chemicals*(Ed, Thomson, D.) The Royal Society of Chemistry, pp. 369-389.

Glatzmaier, G. C. & Ramirez, W. F. (1988), "Use of volume averaging for the modelling of thermal properties of porous materials", *Chemical Engineering Science,* **43**, (**12**), 3157-3169.

Granizo, M. L., Blanco-Varela, M. T. & Palomo, A. (2000), "Influence of the starting kaolin on alkali-activated materials based on metakaolin. Study of the reaction parameters by isothermal conduction calorimetry", *Journal of Materials Science,* **35**, 6309-6315.

Griesinger, A., Heidermann, W. & Hahne, E. (1999), "Investigation on measurement accuracy of the periodic hot-wire method by means of numerical temperature filed calculations", *International Community Heat Mass Transfer,* **26**, (**4**), 451-465.

Grim, R. E. (1953) *Clay Mineralogy,* McGraw-Hill Book Company, Inc, New York.

Grutzeck, M., Kwan, S. & DiCola, M. (2004), "Zeolite formation in alkali-activated cementitious systems", *Cement & Concrete Research,* **32**, 949-955.

Guinea, G. V., El-Sayed, K., Rocco, C. G., Elices, M. & Planas, J. (2002), "The effect of the bond between the matrix and the aggregates on the cracking mechanism and fracture parameters of concrete", *Cement & Concrete Composites,* **32**, (**12**), 1961-1970.

Hermann, E., Kunze, C., Gatzweiler, R., Kiesig, G. & Davidovits, J. (1999) "Solidification of various radioactive residues by geopolymere with special emphasis on long-term-stability" Geopolymere '99, Saint-Quentine, France,211-228.

Hinckley, D. N. (1963), "Variability in "crystallinity" values among the kaolin deposits of the coastal plain of Georgia and South Carolina", *Clays and Clay Minerals,* **11**, 229 - 235.

Hos, J. P. (2000) "Synthetic aluminosilicates for geopolymer precursors". Final Year Thesis. The University of Western Australia.

Hos, J. P., McCormick, P. G. & Byrne, L. T. (2002), "Investigation of a synthetic aluminosilicate inorganic polymer", *Journal of Materials Science,* **37**, 2311-2316.

Husem, M. (2003), "The effect of bond strengths between lightweight and ordinary aggregate-mortar, aggregate-cement paste", *Materials Science & Engineering A,* **A363**, 152 -158.

Igarashi, S., Bentur, A. & Mindess, S. (1998), "Microhardness testing of cementitious materials", *Advanced Cement Based Materials,* **4**, 48-57.

Jiang, L. & Guan, Y. (1999), "Pore structure and its effect on strength of high-volume fly ash paste", *Cement and Concrete Research,* **29**, 631-633.

Jiang, W. (1997) "Alkali Activated Cementitious Materials:Mechanism, Microstructure and Properties". Doctor of Philosophy Thesis. The Pennsylvania State University.

Kakali, G., Perraki, T., Tsivilis, S. & Badogiannis, E. (2001), "Thermal treatment of kaolinite: the effect of mineralogy on the pozzolanic activity", *Applied Clay Science,* **20**, 73-80.

Kumar, R. & Bhattacharjee, B. (2003), "Porosity, pore size distribution and in situ strength of concrete", *Cement and Concrete Research,* **33**, 155 - 164.

Lee, W. K. W. & van Deventer, J. S. J. (2002), "The effects of inorganic salt contamination on the strength and durability of geopolymers", *Colloids and Surfaces A: Physicochem. Eng. Aspects,* **211**, 115-126.

Lee, W. K. W. & van Deventer, J. S. J. (2004), "The interface between natural siliceous aggregates and geopolymers", *Cement & Concrete Research,* **34**, **(2)**, 195-206.

Liefke, E. (1999) "Industrial applications of foamed inorganic polymers" Geopolymere '99, Saint-Quentine, France,189-199.

Lucksanasombool, P., Higgs, W. A. J., Higgs, R. J. E. D. & Swain, M. V. (2003), "Interfacial fracture toughness between bovine costical bone and cements", *Biomaterials,* **24**, 1159 - 1166.

Lutz, M. P., Monteiro, P. J. M. & Zimmerman, W. (1997), "Inhomogeneous interfacial transition model for the bulk modulus of mortar", *Cement and Concrete Research,* **27**, (7), 1113-1122.

Lyon, R. E., Balaguru, P. N., Foden, A., Sorathia, U., Davidovits, J. & Davidovics, M. (1997), "Fire resistant aluminosilicate composites", *Fire and Materials,* **21**, 67-73.

Martinez-Ramirez, S. & Palomo, A. (2001), "Microstructure studies on Portland cement pastes obtained in highly alkaline environments", *Cement and Concrete Research,* **31**, 1581 - 1585.

Matusinovic, T., Sipusic, J. & Vrbos, N. (2003), "Porosity-strength relation in calcium aluminate cement paste", *Cement and Concrete Research,* **33**, 1801-1806.

Merchant, I. J., Macphee, D. E., Chandler, H. W. & Henderson, R. J. (2001), "Toughening cement-based materials through the control of interfacial bonding", *Cement and Concrete Research,* **31**, 1873-1880.

Mladenovic, A., Suput, J. S., Ducman, V. & Skapin, A. S. (2004), "Alkali-silica reactivity of some frequently used lightweight aggregates", *Cement & Concrete Research,* **In Press**,

Mosquera, M. J., Benitez, D. & Perry, S. H. (2002), "Pore structure in mortars applied on restoration effect on properties relevant to decay of granite buildings", *Cement & Concrete Research,* **32**, 1883 - 1888.

Mozgowa, W., Fojud, Z., Handke, M. & Jurga, S. (2002), "MAS NMR and FTIR spectra of framework aluminosilicates", *Journal of Molecular Structure,* **614**, 281-287.

Neville, A. M. (2000) *Properties of concrete,* Prentice Hall, Harlow.

Owsiak, Z. (2004), "Alkali-aggregate relation in concrete containing high-alkali cement and granite aggregate", *Cement & Concrete Research,* **34**, 7-11.

Palomo, A., Blanco-Varela, M. T., Granizo, M. L., Puertas, F., Vasquez, T. & Grutzeck, M. W. (1999), "Chemical stability of cementitious materials based on metakaolin", *Cement and Concrete Research,* **29**, 997-1004.

Palomo, A., Grutzeck, M. W. & Blanco, M. T. (1999), "Alkali-activated fly ashes A cement for the future", *Cement and Concrete Research,* **29**, 1323-1329.

Parrott, J. E. & Stuckes, A. D. (1975) *Thermal conductivity of solids,* Pion Limited, London.

Phair, J. W., Smith, J. D. & van Deventer, J. S. J. (2003), "Characteristics of aluminosilicate hydrogels related to commercial "Geopolymers", *Materials Letters,* **57**, (**28**), 4356-4367.

Phair, J. W. & van Deventer, J. S. J. (2001), "Effect of silicate activator pH on the leaching and materials characteristics of waste-based inorganic polymers", *Minerals Engineering,* **14, (3)**, 289-304.

Phair, J. W. & van Deventer, J. S. J. (2002), "Effect of silicate activator pH on the microstructural characterics of waste-based geopolymers", *International Journal of Mineral Processing,* **66**, 121-143.

Plancon, A., Giese, R. F. & Snyder, R. (1988), "The Hinckley index for kaolinites", *Clay Minerals,* **23**, 249-260.

Pozarnsky, G. A. & McCormick, A. V. (1995), "Multinuclear NMR study of aluminosilicate sol-gel synthesis using the prehydrolysis method", *Journal of Non-Crystalline Solids,* **190**, 212-225.

Quinn, J. B. & Quinn, G. D. (1997), "Indentation brittleness of ceramics: A fresh approach", *Journal of Materials Science,* **32**, 4331-4346.

Rahier, H., Simons, W., Van Melle, B. & Biesemans, M. (1997), "Low-temperature synthesized aluminosilicate glasses Part III *Influence of composition of the silica solution on production, structure and properties*", *Journal of Materials Science,* **32**, 2237-2247.

Rahier, H., Van Melle, B., Biesemans, M., Wastiels, J. & Wu, X. (1996), "Low-temperature synthesized aluminosilicate glasses Part I Low-temperature reaction stoichiometry and structure of a model compound", *Journal of Materials Science,* **31**, 71-79.

Rahier, H., Wullaert, B. & Van Melle, B. (2000), "Influence of the degree of dehydroxylation of kaolinite on the properties of aluminosilicate glasses", *Journal of Thermal Analysis and Calorimetry,* **62**, 417-427.

Rao, G. A. (2001), "Influence of silica fume on long-term strength of mortars containing different aggregate fractions", *Cement and Concrete Research,* **31**, 7-12.

Rao, G. A. & Prasad, R. B. K. (2002), "Influence of the roughness of aggregate surface on the interface bond strength", *Cement & Concrete Composites,* **32**, 253-257.

Ray, A., Cantrill, E. R., Stevens, M. G. & Aldridge, L. (1995), "Use of DTA to determine the effect of mineralizers on the cement-quartz hydrothermal reactions", *Thermochimia Acta,* **250**, 189-195.

Ray, N. H. (1978) *Inorganic Polymers,* Academic Press, London.

Raz, U., Girsperger, S. & Thomson, A. B.(2004) "Thermal expansion, compressibility and volumetric changes of quartz obtained by single crystal dilatometry to 700 °C and 3.5 kilobars (0.35 GPa)", [online], http://e-collection.ethbib.ethz.ch/cgi-bin/, [12 May 2004].

Rocco, C. G., Guinea, G. V., Planas, J. & Elices, M. (2001), "Review of the splitting-test standards from a fracture mechanics", *Cement & Concrete Composites,* **31**, 73-82.

Rowles, M. & O'Connor, B. H. (2003), "Chemical optimisation of the compressive strength of aluminosilicate geopolymers synthesised by sodium silicate activation of metakaolinite", *Journal of materials chemistry,* **13**, (**13**), 1-6.

Rudolph, S.(2003) "The structure of kaolinite", [online], http://www.a-m.de/englisch/lexikon/kaolinit-bild.htm, 2003 [16 April 2003].

Salgueiro, W., Somoza, A., Cabrera, O. & Consolati, G. (2004), "Porosity study on free mineral addition cement paste", *Cement & Concrete Research,* **34**, 91-97.

Sangwal, K. (2000), "On the reverse indentation size effect and microhardness measurement of solids", *Materials Chemistry and Physics,* **63**, 145-152.

Santoyo, E., Garcia, A., Morales, J. M., Conteras, E. & Espinosa-Paredes, G. (2001), "Effective thermal conductivity of Mexican geothermal cementing systems in the temperature range from 28 °C to 200 °C." *Applied Thermal Engineering,* **21**, 1799 - 1812.

Shi, C. & Xie, P. (1998), "Interface between cement paste and quartz sand in alkali-activated slag mortars", *Cement & Concrete Composites,* **28**, (**6**), 887-896.

Shvarzman, A., Kovler, K., Grader, G. S. & Shter, G. E. (2003), "The effect of the dehydroxylation/amorphization degree on pozzolanic activity of kaolinite", *Cement & Concrete Research,* **33**, 405 - 416.

Silva, F. J., Mathias, A. F. & Thaumaturgo, C. (1999) "Evaluation of the fracture toughness in poly(sialate-siloxo) composite matrix" Geopolymere '99, Saint-Quentine, France,97-106.

Sinko, K. & Mezei, R. (1998), "Preparation effect on sol-gel aluminosilicate gels", *Journal of Non-Crystalline Solids,* **231**, 1-9.

Sridhar, M. R. & Yovanovich, M. M. (1996), "Empirical methods to predict Vickers microhardness", *Wear,* **193**, 91-98.

Swanepoel, J. C. & Strydom, C. A. (2002), "Utilisation of fly ash in a geopolymeric material", *Applied Geochemistry,* **17**, (**8**), 1143 - 1148.

Tasong, W. A., Lynsdale, C. J. & Cripps, J. C. (1998), "Aggregate-cement paste interface. II: Influence of aggregate physical properties", *Cement & Concrete Composites,* **28**, 1453-1465.

Tavman, I. H. (1996), "Effective thermal conductivity of granular porous materials", *International Community Heat Mass Transfer,* **21**, (**2**), 169-176.

Temuujin, J., Okada, K., MacKenzie, K. J. D. & Jadambaa, T. (1998), "The effect of water vapour atmospheres on the thermal transformation of kaolinite investigated by XRD, FTIR and solid state MAS NMR", *Journal of the European Ceramic Society,* **19**, 105 -112.

van Jaarsveld, J. G. S. & van Deventer, J. S. J. (1999), "The effect of metal contaminants on the formation and properties of waste-based geopolymers", *Cement and Concrete Research,* **29**, 1189-1200.

van Jaarsveld, J. G. S., van Deventer, J. S. J. & Lorenzen, L. (1997), "The potential use of geopolymeric materials to immobilise toxic metals: Part I. Theory and applications", *Minerals Engineering,* **10**, (**7**), 659-669.

van Jaarsveld, J. G. S., van Deventer, J. S. J. & Lukey, G. C. (2002), "The effect of composition and temperature on the properties of fly ash- and kaolinite-based geopolymers", *Chemical Engineering Journal,* **89**, (**1-3**), 63-73.

van Jaarsveld, J. G. S., van Deventer, J. S. J. & Schwartzman, A. (1999), "The potential use of geopolymeric materials to immobilise toxic metals: Part II. Materials and leaching characteristics", *Minerals Engineering,* **12**, (**1**), 75-91.

Vedalakshmi, R., Raj, A. S., Srinivasan, S. & Babu, K. G. (2003), "Quantification of hydrated cement product of blended cements in low medium strength concrete using TG and DTA technique", *Thermochimia acta,* **407**, (**1-2**), 49-60.

Wasserman, A. & Bentur, A. (1996), "Interfacial interactions in lightweight Aggregate Concretes and their influence on the concrete strength", *Cement & Concrete Composites,* **18**, 67-76.

Wei, S., Yun-sheng, Z., Wei, L. & Zhi-yong, L. (2003), "In situ monitoring of the hydration process of K-PS geopolymer cement with ESEM", *Cement & Concrete Research,* **34**, (**6**), 935-940.

Wong, Y. L., Lam, L., Poon, C. S. & Zhou, F. P. (1999), "Properties of fly ash-modified cement mortar-aggregate interfaces", *Cement & Concrete Composites,* **29**, 1905-1913.

Xie, Z. & Xi, Y. (2001), "Hardening mechanisms of an alkali-activated class F fly ash", *Cement & Concrete Research,* **31**, 1245-1249.

Xu, H. & van Deventer, J. S. J. (2000), "The geopolymerisation of alumino-silicate minerals", *International Journal of Mineral Processing,* **59**, 247-266.

Xu, H. & van Deventer, J. S. J. (2002), "Microstructural characterisation of geopolymers synthesised from kaolinite/stibite mixture using XRD, MAS-NMR, SEM/EDX, TEM/EDX, and HREM", *Cement and Concrete Research,* **32**, (**11**), 1705-1716.

Xu, Y. & Chung, D. D. L. (2000), "Effect of sand addition on the specific heat and thermal conductivity of cement", *Cement & Concrete Research,* **30**, 59-61.

Zang, M. H. & Gjorv, O. E. (1990), "Microstructure of the interfacial zone between lightweight aggregate and cement paste", *Cement & Concrete Research,* **24**, (**4**), 610 - 618.

Zarzycki, J. (1988) "The sol-gel methods of synthesis of glasses, ceramics and composites" Geopolymer '88, France, 287-302.

Zhandarov, S. F. & Pisanova, E. V. (1997), "The local bond strength and its determination by fragmentation and full-out test", *Composites Science and Technology,* **57**, 957-964.

Zhang, M. H. (1995), "Microstructure, crack propagation, and mechanical properties of cement pastes containing high volumes of fly ashes", *Cement and Concrete Research,* **25**, (**6**), 1165-1178.

Zhang, M. H. & Malhotra, V. M. (1995), "Characteristics of a thermally activated alumino-silicate pozzolanic materials and its use in concrete", *Cement and Concrete Research,* **25**, (**8**), 1713-1725.

Zhou, X.-F., Wagner, H. D. & Nutt, S. R. (2001), "Interfacial properties of polymer composites measured by push-out and fragmentation tests", *Composites: Part A: applied science and manufacturing,* **32**, 1543-1551.

LIST OF PUBLICATIONS

Refereed Publications

Subaer, Arie van Riessen, Brian O'Connor & Craig Buckley, (2002), "Compressive Strength and Microstructural Character of Aluminosilicate Geopolymer", *Journal of the Australasian Ceramic Society*, 38 (1), 83 – 86.

Subaer & Arie van Riessen, "Thermo-mechanical and microstructural characterisation of sodium-poly(sialate-siloxo) (Na-PSS) geopolymer", to be submitted to the *Journal of Materials Science.*

Conference Proceedings

Subaer, Arie van Riessen, Brian O'Connor and Craig Buckley, "Influence of aggregate on the microstructure of geopolymer ceramics", *Proceedings of the 2001 Joint AXAA (WA) and WASEM Conference*, 21 – 23 September 2001, The Atrium Hotel, Mandurah, WA. P99.

Subaer, Arie van Riessen, Brian O'Connor and Craig Buckley, "Physical properties of Aluminosilicate geopolymer", *Austceram 2002 Proceedings, International ceramic conference and exhibition of the Australasian ceramics society (incorporating IMCA)*, Central Tafe, Perth, WA. 30 September – 4 October 2002, p.43-44.

Subaer, Arie van Riessen and Robert Hart, "SEM/TEM study of matrix homogeneity and interfaces in aluminosilicate geopolymers", *Proceedings of the 2003 Joint AXAA (WA) and WASEM conference*, 19 – 21 September 2003, El Caballo Golf Resort, Wooroolo, WA.

APPENDICES

Appendix A – Kingwhite 65 Kaolinite

UNIMIN Australia Limited

PAINT/FILLER GRADE KAOLIN CLAY - KINGWHITE 65

Water washed high quality Kaolin Clay with controlled particle size distribution and colour. Kingwhite 65 is a high brightness filler clay suitable for many industrial applications where good surface properties, fine particle size and low yellowness factors are required.

Physical Form

Lump, pellet or powder

Typical Physical Properties

Colour	
Brightness (ISO)	84.0
Yellowness	5.0
Particle Size Distribution	
Plus 53 micron screen residue (%)	0.05
Plus 10 micron (%)	8.0
Minus 2 micron (%)	68.0
Moisture Content (%)	
Lump	15
Pellet	10
Powder	1 at packing
Loss of ignition (1000 °C)	13.8
pH (20% suspension)	7.0
Specific gravity	2.6

Typical Chemical Analysis (by X-ray fluorescence - %)

SiO_2	46.4
Al_2O_3	37.8
Fe_2O_3	0.8
CaO	0.08
MgO	0.15
TiO_2	0.8
Na_2O	0.01
K_2O	0.21

Mineralogical Analysis (by X-ray diffraction - %)

Kaolinite	99
Quartz	trace

Appendix B – Crystallographic Data

B1. PDF#14-0164: QM=Indexed(I); d=Other/Unknown; I=Film/Visual

Kaolinite-1A
Al2 Si2 O5 (O H)4 (White)

Radiation=CuKa	Lambda=1.5418	Filter=
Calibration=	d-Cutoff=	I/Ic(RIR)=

Ref: Goodyear, Duffin.
Mineral. Mag., 32 902 (1961)

Triclinic - Powder Diffraction, C1 (1)	Z=2	mp=	
CELL: 5.155 x 8.959 x 7.407 <91.68 x 104.9 x 89.94>			P.S=aP17 (?)
Density(c)=2.594	Density(m)=2.645	Mwt=258.16	Vol=165.22

F(30)=35.3(0.022,38)
Ref: Ibid.

Strong Line: 7.17/X 1.49/9 3.58/8 1.62/7 4.37/6 1.59/6 4.19/5 2.50/5 3.85/4 2.35/4

NOTE: Specimen from Scalby, Yorkshire, England, UK.Validated by calculated pattern Borg and Smith, GSA Memoir, 122.To replace 5-143 and 12-447.See ICSD 20593 (PDF 72-2300); ICSD 27713 (PDF 74-1784); ICSD 27715 (PDF 74-1786); ICSD 68698 (PDF 80-886); ICSD 31135 (PDF 75-1593); ICSD 63192 (PDF 78-1996); ICSD 68697 (PDF 80-885); ICSD 66571 (PDF 79-1570); ICSD 63315 (PDF 78-2109); ICSD 80082 (PDF 83-971).

2-Theta	d(A)	I(f)	(h k l)	Theta	1/(2d)	2pi/d	n^2
12.334	7.1700	100.0	(0 0 1)	6.167	0.0697	0.8763	
19.810	4.4780	35.0	(0 2 0)	9.905	0.1117	1.4031	
20.323	4.3660	60.0	(-1 1 0)	10.162	0.1145	1.4391	
21.207	4.1860	45.0	(-1-1 1)	10.604	0.1194	1.5010	
21.451	4.1390	35.0	(-1 1 1)	10.725	0.1208	1.5180	
23.101	3.8470	40.0	(0-2 1)	11.550	0.1300	1.6333	
23.739	3.7450	25.0	(0 2 1)	11.869	0.1335	1.6778	
24.857	3.5790	80.0	(0 0 2)	12.429	0.1397	1.7556	
26.033	3.4200	5.0	(1-1 1)	13.016	0.1462	1.8372	
26.378	3.3760	35.0	(1 1 1)	13.189	0.1481	1.8611	
28.263	3.1550	20.0	(-1-1 2)	14.131	0.1585	1.9915	
28.709	3.1070	20.0	(-1 1 2)	14.354	0.1609	2.0223	
32.484	2.7540	20.0	(0 2 2)	16.242	0.1816	2.2815	
34.938	2.5660	35.0	(-2 0 1)	17.469	0.1949	2.4486	
35.121	2.5530	25.0	(1 3 0)	17.561	0.1958	2.4611	
35.379	2.5350	35.0	(-1-3 1)	17.689	0.1972	2.4786	
35.611	2.5190	10.0	(1-1 2)	17.806	0.1985	2.4943	
35.965	2.4950	45.0	(2 0 0)	17.983	0.2004	2.5183	
37.685	2.3850	25.0	(0 0 3)	18.843	0.2096	2.6345	
38.319	2.3470	40.0	(-2 0 2)	19.159	0.2130	2.6771	
38.472	2.3380	40.0	(1-3 1)	19.236	0.2139	2.6874	

2-Theta	d(A)	I(f)	(h k l)	Theta	1/(2d)	2pi/d	n^2
39.045	2.3050	5.0	(-1 1 3)	19.523	0.2169	2.7259	
39.258	2.2930	35.0	(1 3 1)	19.629	0.2181	2.7402	
39.984	2.2530	20.0	(-1-3 2)	19.992	0.2219	2.7888	
40.283	2.2370	5.0	(0 4 0)	20.141	0.2235	2.8088	
40.643	2.2180	10.0	(-2 2 1)	20.321	0.2254	2.8328	
41.049	2.1970	20.0	(-1 3 2)	20.524	0.2276	2.8599	
41.265	2.1860	20.0	(2 0 1)	20.632	0.2287	2.8743	
41.523	2.1730	5.0	(2 2 0)	20.761	0.2301	2.8915	
41.968	2.1510	10.0	(0-4 1)	20.984	0.2325	2.9211	
42.339	2.1330	20.0	(0-2 3)	21.169	0.2344	2.9457	
42.695	2.1160	10.0	(0 4 1)	21.348	0.2363	2.9694	
43.188	2.0930	10.0	(-2-2 2)	21.594	0.2389	3.0020	
43.472	2.0800	5.0	(0 2 3)	21.736	0.2404	3.0208	
43.826	2.0640	20.0	(-2 2 2)	21.913	0.2422	3.0442	
45.377	1.9970	35.0	(-2 0 3)	22.688	0.2504	3.1463	
45.618	1.9870	35.0	(1-3 2)	22.809	0.2516	3.1621	
45.935	1.9740	20.0	(2-2 1)	22.968	0.2533	3.1830	
46.483	1.9520	20.0	(2 2 1)	23.242	0.2561	3.2188	
46.814	1.9390	35.0	(1 3 2)	23.407	0.2579	3.2404	
47.279	1.9210	20.0	(0-4 2)	23.639	0.2603	3.2708	
47.674	1.9060	5.0	(1 1 3)	23.837	0.2623	3.2965	
47.914	1.8970	25.0	(-1-3 3)	23.957	0.2636	3.3122	
48.650	1.8700	20.0	(0 4 2)	24.325	0.2674	3.3600	
49.353	1.8450	25.0	(-1 3 3)	24.677	0.2710	3.4055	
49.554	1.8380	35.0	(-2-2 3)	24.777	0.2720	3.4185	
50.373	1.8100	20.0	(-2 2 3)	25.187	0.2762	3.4714	
51.007	1.7890	25.0	(0 0 4)	25.503	0.2795	3.5121	
53.546	1.7100	25.0	(2-2 2)	26.773	0.2924	3.6744	
54.266	1.6890	25.0	(-1 5 0)	27.133	0.2960	3.7201	
54.546	1.6810	25.0	(-1-5 1)	27.273	0.2974	3.7378	
54.971	1.6690	40.0	(-2 4 0)	27.485	0.2996	3.7646	
55.294	1.6600	40.0	(2 4 0)	27.647	0.3012	3.7851	
55.439	1.6560	10.0	(0-4 3)	27.720	0.3019	3.7942	
55.695	1.6490	40.0	(-3 1 2)	27.847	0.3032	3.8103	
56.289	1.6330	30.0	(-3 1 0)	28.144	0.3062	3.8476	
56.781	1.6200	70.0	(1 3 3)	28.391	0.3086	3.8785	
57.283	1.6070	30.0	(0 4 3)	28.642	0.3111	3.9099	
57.794	1.5940	10.0	(-1-5 2)	28.897	0.3137	3.9418	
58.113	1.5860	60.0	(-1-3 4)	29.057	0.3153	3.9617	
58.681	1.5720	10.0	(2-4 1)	29.341	0.3181	3.9969	
59.471	1.5530	30.0	(-2 2 4)	29.735	0.3220	4.0458	
59.810	1.5450	40.0	(1-1 4)	29.905	0.3236	4.0668	
60.153	1.5370	40.0	(2 0 3)	30.077	0.3253	4.0880	
61.164	1.5140	5.0	(3-1 1)	30.582	0.3303	4.1501	
61.569	1.5050	5.0	(-2-4 3)	30.785	0.3322	4.1749	
62.304	1.4890	90.0	(-3-3 1)	31.152	0.3358	4.2197	

B2. PDF#46-1045: QM=Star(S); d=Diffractometer; I=Diffractometer

Quartz, syn
Si O2 (White)

Radiation=CuKa1 Lambda=1.5405981 Filter=Ge
Calibration=Internal(Si) d-Cutoff= I/Ic(RIR)=3.41
Ref: Kern, A., Eysel, W., Mineralogisch-Petrograph. Inst., Univ. Heidelberg, Germany.
ICDD Grant-in-Aid (1993)

Hexagonal - Powder Diffraction, P3221 (154) Z=3 mp=
CELL: 4.91344 x 4.91344 x 5.40524 <90.0 x 90.0 x 120.0>P.S=hP9 (O2 Si)
Density(c)=2.650 Density(m)=2.660 Mwt=60.08 Vol=113.01 F(30)=538.7(.0018,31)
Ref: Z. Kristallogr., 198 177 (1992)

Strong Line: 3.34/X 4.26/2 1.82/1 2.46/1 1.54/1 2.28/1 1.38/1 2.13/1 1.38/1 2.24/1

NOTE: Pattern taken at 23(1) C. Low temperature quartz. 2$GU determination based on profile fit method. To replace 33-1161.

2-Theta	d(A)	I(f)	(h k l)	Theta	1/(2d)	2pi/d	n^2
20.859	4.2550	16.0	(1 0 0)	10.430	0.1175	1.4767	
26.639	3.3435	100.0	(1 0 1)	13.320	0.1495	1.8792	
36.543	2.4569	9.0	(1 1 0)	18.272	0.2035	2.5574	
39.464	2.2815	8.0	(1 0 2)	19.732	0.2192	2.7540	
40.299	2.2361	4.0	(1 1 1)	20.149	0.2236	2.8098	
42.449	2.1277	6.0	(2 0 0)	21.224	0.2350	2.9530	
45.792	1.9799	4.0	(2 0 1)	22.896	0.2525	3.1736	
50.138	1.8180	13.0	(1 1 2)	25.069	0.2750	3.4562	
50.621	1.8017	1.0	(0 0 3)	25.310	0.2775	3.4873	
54.873	1.6717	4.0	(2 0 2)	27.437	0.2991	3.7585	
55.323	1.6592	2.0	(1 0 3)	27.662	0.3014	3.7869	
57.234	1.6083	1.0	(2 1 0)	28.617	0.3109	3.9068	
59.958	1.5415	9.0	(2 1 1)	29.979	0.3244	4.0759	
64.034	1.4529	2.0	(1 1 3)	32.017	0.3441	4.3246	
65.784	1.4184	1.0	(3 0 0)	32.892	0.3525	4.4297	
67.742	1.3821	6.0	(2 1 2)	33.871	0.3618	4.5461	
68.142	1.3750	7.0	(2 0 3)	34.071	0.3636	4.5697	
68.316	1.3719	5.0	(3 0 1)	34.158	0.3645	4.5800	
73.466	1.2879	2.0	(1 0 4)	36.733	0.3882	4.8786	
75.658	1.2559	3.0	(3 0 2)	37.829	0.3981	5.0027	
77.673	1.2283	1.0	(2 2 0)	38.837	0.4071	5.1153	
79.882	1.1998	2.0	(2 1 3)	39.941	0.4167	5.2368	

2-Theta	d(A)	I(f)	(h k l)	Theta	1/(2d)	2pi/d	n^2
80.044	1.1978	1.0	(2 2 1)	40.022	0.4174	5.2456	
81.171	1.1840	2.0	(1 1 4)	40.585	0.4223	5.3068	
81.489	1.1802	2.0	(3 1 0)	40.744	0.4237	5.3240	
83.838	1.1530	1.0	(3 1 1)	41.919	0.4337	5.4495	
84.955	1.1407	1.0	(2 0 4)	42.477	0.4383	5.5084	
87.437	1.1145	1.0	(3 0 3)	43.718	0.4486	5.6374	
90.828	1.0816	2.0	(3 1 2)	45.414	0.4623	5.8094	
92.785	1.0638	1.0	(4 0 0)	46.393	0.4700	5.9064	
94.648	1.0477	1.0	(1 0 5)	47.324	0.4772	5.9970	
95.115	1.0438	1.0	(4 0 1)	47.558	0.4790	6.0195	
96.234	1.0346	1.0	(2 1 4)	48.117	0.4833	6.0730	
98.747	1.0149	1.0	(2 2 3)	49.374	0.4927	6.1909	
102.228	0.9896	1.0	(1 1 5)	51.114	0.5053	6.3494	
102.563	0.9872	1.0	(3 1 3)	51.282	0.5065	6.3644	
103.873	0.9783	1.0	(3 0 4)	51.937	0.5111	6.4223	
104.199	0.9762	1.0	(3 2 0)	52.100	0.5122	6.4365	
106.589	0.9608	1.0	(3 2 1)	53.295	0.5204	6.5396	
112.110	0.9285	1.0	(4 1 0)	56.055	0.5385	6.7668	
114.057	0.9182	1.0	(3 2 2)	57.028	0.5446	6.8432	
114.462	0.9161	2.0	(4 0 3)	57.231	0.5458	6.8589	
114.635	0.9152	2.0	(4 1 1)	57.317	0.5463	6.8655	
115.881	0.9089	1.0	(2 2 4)	57.940	0.5501	6.9130	
117.532	0.9009	1.0	(0 0 6)	58.766	0.5550	6.9747	
118.308	0.8972	1.0	(2 1 5)	59.154	0.5573	7.0032	
120.119	0.8889	1.0	(3 1 4)	60.060	0.5625	7.0684	
121.848	0.8814	1.0	(1 0 6)	60.924	0.5673	7.1290	
122.600	0.8782	1.0	(4 1 2)	61.300	0.5694	7.1549	
127.245	0.8598	1.0	(3 0 5)	63.623	0.5815	7.3078	
131.197	0.8458	1.0	(1 1 6)	65.598	0.5911	7.4284	
132.750	0.8407	1.0	(5 0 1)	66.375	0.5947	7.4733	
134.286	0.8359	1.0	(4 0 4)	67.143	0.5981	7.5165	
136.417	0.8296	1.0	(2 0 6)	68.208	0.6027	7.5741	
137.887	0.8254	2.0	(4 1 3)	68.944	0.6058	7.6124	
140.310	0.8189	1.0	(3 3 0)	70.155	0.6106	7.6726	
143.242	0.8117	3.0	(5 0 2)	71.621	0.6160	7.7409	
144.110	0.8097	1.0	(3 3 1)	72.055	0.6175	7.7602	

B3. PDF#21-1272: QM=Star(S); d=(Unknown); I=(Unknown)

Anatase, syn
Ti O2 (Colorless)

Radiation=CuKa1 Lambda=1.5406 Filter=
Calibration= d-Cutoff= I/Ic(RIR)=3.3
Ref: Natl. Bur. Stand. (U.S.) Monogr. 25, 7 82 (1969)

Tetragonal - Powder Diffraction, I41/amd (141) Z=4 mp=
CELL: 3.7852 x 3.7852 x 9.5139 <90.0 x 90.0 x 90.0> P.S=tI12 (O2 Ti)
Density(c)=3.893 Density(m)=5.01A Mwt=79.90 Vol=136.31
F(30)=74.2(.0116,35)
Ref: Ibid.

Strong Line: 3.52/X 1.89/4 2.38/2 1.70/2 1.67/2 1.48/1 2.43/1 2.33/1 1.26/1 1.36/1

NOTE: Sample obtained from National Lead Co., South Amboy, New Jersey, USA. Anatase and another polymorph, brookite (orthorhombic), are converted to rutile (tetragonal) by heating above 700 C. Pattern reviewed by Holzer, J., McCarthy, G., North Dakota State Univ, Fargo, North Dakota, USA, ICDD Grant-in-Aid (1990). Agrees well with experimental and calculated patterns. Validated by calculated pattern. Pattern taken at 25 C. See ICSD 9852 (PDF 71-1166).

2-Theta	d(A)	I(f)	(h k l)	Theta	1/(2d)	2pi/d	n^2
25.281	3.5200	100.0	(1 0 1)	12.640	0.1420	1.7850	
36.946	2.4310	10.0	(1 0 3)	18.473	0.2057	2.5846	
37.800	2.3780	20.0	(0 0 4)	18.900	0.2103	2.6422	
38.575	2.3320	10.0	(1 1 2)	19.288	0.2144	2.6943	
48.049	1.8920	35.0	(2 0 0)	24.024	0.2643	3.3209	
53.890	1.6999	20.0	(1 0 5)	26.945	0.2941	3.6962	
55.060	1.6665	20.0	(2 1 1)	27.530	0.3000	3.7703	
62.119	1.4930	4.0	(2 1 3)	31.059	0.3349	4.2084	
62.688	1.4808	14.0	(2 0 4)	31.344	0.3377	4.2431	
68.760	1.3641	6.0	(1 1 6)	34.380	0.3665	4.6061	
70.309	1.3378	6.0	(2 2 0)	35.154	0.3737	4.6967	
74.029	1.2795	2.0	(1 0 7)	37.014	0.3908	4.9107	
75.029	1.2649	10.0	(2 1 5)	37.515	0.3953	4.9673	
76.017	1.2509	4.0	(3 0 1)	38.009	0.3997	5.0229	
80.725	1.1894	2.0	(0 0 8)	40.362	0.4204	5.2827	
82.136	1.1725	2.0	(3 0 3)	41.068	0.4264	5.3588	
82.659	1.1664	6.0	(2 2 4)	41.330	0.4287	5.3868	
83.146	1.1608	4.0	(3 1 2)	41.573	0.4307	5.4128	
93.217	1.0600	2.0	(2 1 7)	46.609	0.4717	5.9275	
94.178	1.0517	4.0	(3 0 5)	47.089	0.4754	5.9743	
95.139	1.0436	4.0	(3 2 1)	47.570	0.4791	6.0207	

2-Theta	d(A)	I(f)	(h k l)	Theta	1/(2d)	2pi/d	n^2
98.315	1.0182	2.0	(1 0 9)	49.158	0.4911	6.1709	
99.801	1.0070	2.0	(2 0 8)	49.900	0.4965	6.2395	
101.217	0.9967	2.0	(3 2 3)	50.609	0.5017	6.3040	
107.444	0.9555	4.0	(3 1 6)	53.722	0.5233	6.5758	
108.959	0.9464	4.0	(4 0 0)	54.479	0.5283	6.6390	
112.836	0.9246	2.0	(3 0 7)	56.418	0.5408	6.7956	
113.857	0.9192	2.0	(3 2 5)	56.928	0.5440	6.8355	
114.904	0.9138	2.0	(4 1 1)	57.452	0.5472	6.8759	
118.434	0.8966	4.0	(2 1 9)	59.217	0.5577	7.0078	
120.099	0.8890	2.0	(2 2 8)	60.049	0.5624	7.0677	
121.720	0.8819	2.0	(4 1 3)	60.860	0.5670	7.1246	
122.331	0.8793	2.0	(4 0 4)	61.165	0.5686	7.1457	
131.029	0.8464	2.0	(4 2 0)	65.514	0.5907	7.4234	
135.991	0.8308	2.0	(3 2 7)	67.996	0.6018	7.5628	
137.384	0.8268	4.0	(4 1 5)	68.692	0.6047	7.5994	
143.878	0.8102	2.0	(3 0 9)	71.939	0.6171	7.7551	
150.028	0.7974	4.0	(4 2 4)	75.014	0.6270	7.8796	
152.622	0.7928	2.0	(0 0 12)	76.311	0.6307	7.9253	

B4. PDF#38-0241: QM=Star(S); d=Diffractometer; I=Diffractometer

Sodium Aluminum Silicate Hydrate
Na2 Al2 Si1.85 O7.7 !5.1 H2 O

Radiation=CuKa Lambda=1.5418 Filter=
Calibration= d-Cutoff= I/Ic(RIR)=
Ref: Milton, R., 2,882,243.
U.S. Patent (1959)

Cubic - (Unknown) Z= mp=
CELL: 12.32 x 12.32 x 12.32 <90.0 x 90.0 x 90.0> P.S=c?0 (?)
Density(c)=0.326 Density(m)=1.990 Mwt=366.97 Vol=1869.96
F(30)=88.4(.0081,42)
Ref: Ibid.

Strong Line: 12.3/X 8.71/7 2.99/6 3.71/5 3.29/5 4.11/4 7.11/4 5.51/3 2.63/2 3.42/2

NOTE: To replace 11-590.

2-Theta	d(A)	I(f)	(h k l)	Theta	1/(2d)	2pi/d	n^2
7.187	12.2900	100.0	(1 0 0)	3.593	0.0407	0.5112	1
10.147	8.7100	69.0	(1 1 0)	5.074	0.0574	0.7214	2
12.439	7.1100	35.0	(1 1 1)	6.219	0.0703	0.8837	3
16.072	5.5100	25.0	(2 1 0)	8.036	0.0907	1.1403	5
17.618	5.0300	2.0	(2 1 1)	8.809	0.0994	1.2491	6
20.352	4.3600	6.0	(2 2 0)	10.176	0.1147	1.4411	8
21.620	4.1070	36.0	(3 0 0)	10.810	0.1217	1.5299	9
23.940	3.7140	53.0	(3 1 1)	11.970	0.1346	1.6918	11
26.056	3.4170	16.0	(3 2 0)	13.028	0.1463	1.8388	13
27.055	3.2930	47.0	(3 2 1)	13.528	0.1518	1.9080	14
29.888	2.9870	55.0	(4 1 0)	14.944	0.1674	2.1035	17
30.763	2.9040	9.0	(3 3 0)	15.382	0.1722	2.1636	18
32.484	2.7540	12.0	(4 2 0)	16.242	0.1816	2.2815	20
33.305	2.6880	4.0	(4 2 1)	16.652	0.1860	2.3375	21
34.115	2.6260	22.0	(3 3 2)	17.057	0.1904	2.3927	22
35.670	2.5150	5.0	(4 2 2)	17.835	0.1988	2.4983	24
36.434	2.4640	4.0	(4 3 0)	18.217	0.2029	2.5500	25
37.916	2.3710	3.0	(5 1 1)	18.958	0.2109	2.6500	27
39.329	2.2890	1.0	(5 2 0)	19.665	0.2184	2.7449	29
40.058	2.2490	3.0	(5 2 1)	20.029	0.2223	2.7938	30
41.443	2.1770	7.0	(4 4 0)	20.722	0.2297	2.8862	32
42.111	2.1440	10.0	(4 4 1)	21.056	0.2332	2.9306	33
42.759	2.1130	3.0	(5 3 0)	21.379	0.2366	2.9736	34

2-Theta	d(A)	I(f)	(h k l)	Theta	1/(2d)	2pi/d	n^2
43.406	2.0830	4.0	(5 3 1)	21.703	0.2400	3.0164	35
44.073	2.0530	9.0	(6 0 0)	22.037	0.2435	3.0605	36
47.201	1.9240	7.0	(5 4 0)	23.600	0.2599	3.2657	41
47.807	1.9010	4.0	(5 4 1)	23.903	0.2630	3.3052	42
48.985	1.8580	2.0	(6 2 2)	24.493	0.2691	3.3817	44
49.583	1.8370	3.0	(6 3 0)	24.791	0.2722	3.4204	45
51.941	1.7590	2.0	(7 0 0)	25.970	0.2843	3.5720	49
52.454	1.7430	13.0	(5 5 0)	26.227	0.2869	3.6048	50
54.162	1.6920	6.0	(7 2 0)	27.081	0.2955	3.7135	53
54.722	1.6760	2.0	(7 2 1)	27.361	0.2983	3.7489	54
56.326	1.6320	4.0	(7 2 2)	28.163	0.3064	3.8500	57
57.400	1.6040	6.0	(7 3 1)	28.700	0.3117	3.9172	59
58.477	1.5770	4.0	(6 5 0)	29.239	0.3171	3.9843	61
60.545	1.5280	2.0	(7 4 0)	30.272	0.3272	4.1120	65
61.075	1.5160	1.0	(7 4 1)	30.537	0.3298	4.1446	66
62.585	1.4830	3.0	(8 2 1)	31.292	0.3372	4.2368	69
63.058	1.4730	2.0	(6 5 3)	31.529	0.3394	4.2656	70
65.082	1.4320	3.0	(7 5 0)	32.541	0.3492	4.3877	74
65.597	1.4220	2.0	(7 5 1)	32.799	0.3516	4.4186	75
66.546	1.4040	5.0	(8 3 2)	33.273	0.3561	4.4752	77
68.480	1.3690	2.0	(9 0 0)	34.240	0.3652	4.5896	81
68.997	1.3600	8.0	(9 1 0)	34.498	0.3676	4.6200	82

B5. PDF#38-0237: QM=Star(S); d=Diffractometer; I=Diffractometer

Sodium Aluminum Silicate Hydrate
Na2 Al2 Si2.5 O9 !6.2 H2 O

Radiation=CuKa Lambda=1.5418 Filter=
Calibration= d-Cutoff= I/Ic(RIR)=
Ref: Milton, R., 2,882,244.
U.S. Patent (1959)

Cubic - (Unknown), F Z= mp=
CELL: 24.99 x 24.99 x 24.99 <90.0 x 90.0 x 90.0> P.S=cF0 (?)
Density(c)=0.045 Density(m)=1.930 Mwt=425.85
Vol=15606.26 F(30)=41.9(.0128,56)
Ref: Ibid.

Strong Line: 14.5/X 3.81/2 2.89/2 8.85/2 5.73/2 3.34/2 7.54/1 4.42/1 2.94/1 2.79/1

NOTE: Na2 O = 0.90.2, Si O2 = 2.50.2.

2-Theta	d(A)	I(f)	(h k l)	Theta	1/(2d)	2pi/d	n^2
6.103	14.4700	100.0	(1 1 1)	3.051	0.0346	0.4342	3
9.986	8.8500	18.0	(2 2 0)	4.993	0.0565	0.7100	8
11.727	7.5400	12.0	(3 1 1)	5.864	0.0663	0.8333	11
15.451	5.7300	18.0	(3 3 1)	7.726	0.0873	1.0965	19
18.430	4.8100	5.0	(5 1 1)	9.215	0.1040	1.3063	27
20.073	4.4200	9.0	(4 4 0)	10.036	0.1131	1.4215	32
20.984	4.2300	1.0	(5 3 1)	10.492	0.1182	1.4854	35
22.513	3.9460	4.0	(6 2 0)	11.257	0.1267	1.5923	40
23.341	3.8080	21.0	(5 3 3)	11.670	0.1313	1.6500	43
23.611	3.7650	3.0	(6 2 2)	11.805	0.1328	1.6688	44
24.647	3.6090	1.0	(4 4 4)	12.324	0.1385	1.7410	48
25.427	3.5000	1.0	(7 1 1)	12.714	0.1429	1.7952	51
26.684	3.3380	18.0	(6 4 2)	13.342	0.1498	1.8823	56
27.394	3.2530	1.0	(7 3 1)	13.697	0.1537	1.9315	59
29.247	3.0510	4.0	(7 3 3)	14.624	0.1639	2.0594	67
30.335	2.9440	9.0	(6 6 0)	15.168	0.1698	2.1342	72
30.971	2.8850	19.0	(7 5 1)	15.486	0.1733	2.1779	75
32.006	2.7940	8.0	(8 4 0)	16.003	0.1790	2.2488	80
32.618	2.7430	2.0	(9 1 1)	16.309	0.1823	2.2906	83
33.626	2.6630	8.0	(6 6 4)	16.813	0.1878	2.3594	88
34.195	2.6200	3.0	(9 3 1)	17.098	0.1908	2.3982	91
35.164	2.5500	1.0	(8 4 4)	17.582	0.1961	2.4640	96
37.376	2.4040	5.0	(10 2 2)	18.688	0.2080	2.6136	108

2-Theta	d(A)	I(f)	(h k l)	Theta	1/(2d)	2pi/d	n^2
39.966	2.2540	1.0	(11 1 1)	19.983	0.2218	2.7876	123
40.816	2.2090	3.0	(8 8 0)	20.408	0.2263	2.8444	128
41.344	2.1820	3.0	(9 7 1)	20.672	0.2291	2.8796	131
42.173	2.1410	2.0	(10 6 0)	21.086	0.2335	2.9347	136
42.611	2.1200	2.0	(9 7 3)	21.305	0.2358	2.9638	139
43.406	2.0830	1.0	(12 0 0)	21.703	0.2400	3.0164	144
46.483	1.9520	1.0	(10 8 0)	23.242	0.2561	3.2188	164
47.097	1.9280	1.0	(10 8 2)	23.548	0.2593	3.2589	168
49.439	1.8420	1.0	(12 6 2)	24.719	0.2714	3.4111	184
51.007	1.7890	1.0	(13 5 1)	25.503	0.2795	3.5121	195
51.688	1.7670	2.0	(14 2 0)	25.844	0.2830	3.5558	200
53.177	1.7210	3.0	(11 9 3)	26.588	0.2905	3.6509	211
57.439	1.6030	3.0	(11 11 1)	28.720	0.3119	3.9196	243

B6. PDF#10-0033: QM=Blank(B); d=Debye-Scherrer; I=Densitometer

Sodium Aluminum Silicate
Na6 Al4 Si4 O17

Radiation=CuKa1	Lambda=1.5405	Filter=Ni
Calibration=	d-Cutoff=	I/Ic(RIR)=

Ref: Borchert, Keidel.
Beitr. Mineral. Petrogr., 1 17 (1949)
Cubic - Powder Diffraction, F-43m (216) Z=1 mp=
CELL: 7.296 x 7.296 x 7.296 <90.0 x 90.0 x 90.0> P.S=cF31 (?)
Density(c)=2.720 Density(m)=2.630 Mwt=630.20 Vol=388.38
F(12)=4.8(0.103,24)
Ref: Ibid.

Strong Line: 4.21/X 2.58/X 1.49/3 1.82/2 1.29/1 1.15/1 2.10/1 0.98/1 1.67/1 1.40/1

NOTE: 1 Visual estimate.
Synthetic material prepared by heating 3NaOH with 1 mol kaolin at 600 C.
Shows slightly different intensities from Na8 Al4 Si4 O18.
Cell parameter generated by least squares refinement.
Reference reports: a=7.273.

2-Theta	d(A)	I(f)	(h k l)	Theta	1/(2d)	2pi/d	n^2
21.085	4.2100	100.0	(1 1 1)	10.542	0.1188	1.4924	3
34.742	2.5800	95.0	(2 2 0)	17.371	0.1938	2.4353	8
42.972	2.1030	8.0	(2 2 2)	21.486	0.2378	2.9877	12
50.048	1.8210	16.0	(4 0 0)	25.024	0.2746	3.4504	16
54.971	1.6690	4.0	(3 3 1)	27.485	0.2996	3.7646	19
62.444	1.4860	30.0	(4 2 2)	31.222	0.3365	4.2283	24
66.546	1.4040	4.0	(5 1 1)	33.273	0.3561	4.4752	27
73.526	1.2870	10.0	(4 4 0)	36.763	0.3885	4.8820	32
77.398	1.2320	4.0	(5 3 1)	38.699	0.4058	5.1000	35
83.925	1.1520	10.0	(6 2 0)	41.963	0.4340	5.4542	40
104.377	0.9750	6.0	(6 4 2)	52.188	0.5128	6.4443	56
126.923	0.8610	2.0	(6 6 0)	63.461	0.5807	7.2975	72

Appendix C. SEM images and EDS results

C1. Geopolymer, Si:Al = 1.04, Na:Al = 0.6

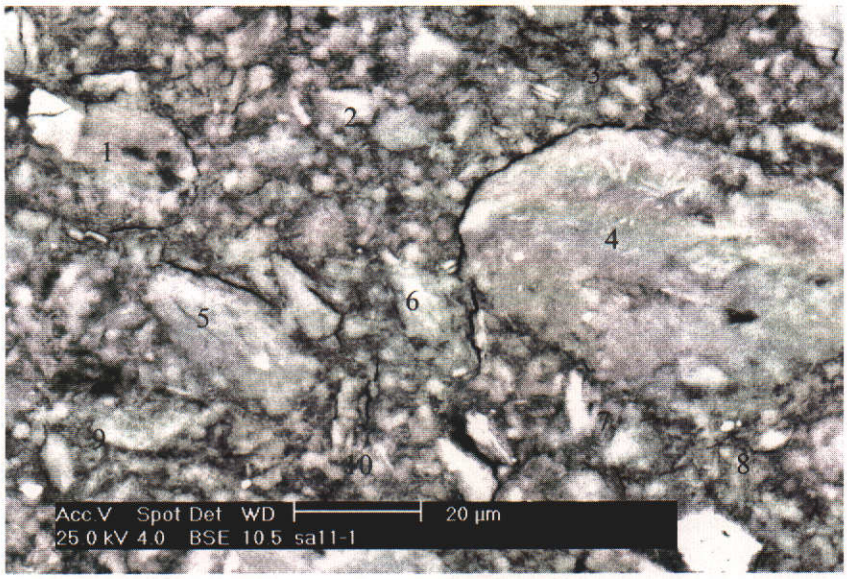

Figure C1. SEM image of geopolymer with Si:Al = 1.04, Na:Al = 0.6.

Table C1. EDS Results from the spots shown in figure C1. Results in an atomic percent and normalised to 100%. EDS was performed at 25 kV.

Spectrum	O	Na	Al	Si	K	Ca	Ti	Fe
1	66.22	7.64	10.38	14.73	0.15	0.31	0.20	0.37
2	64.21	6.74	12.90	15.13		0.26	0.19	0.25
3	62.24	9.22	12.46	15.26		0.32	0.27	0.23
4	64.22	6.65	13.20	15.59				0.35
5	65.14	7.08	12.16	14.61		0.35	0.18	0.49
6	63.72	8.87	12.23	14.16		0.37		0.25
7	57.72	8.82	14.13	17.6	0.17	0.37		0.45
8	58.18	8.42	14.61	18.12		0.35		0.31
9	58.19	9.35	13.79	17.41		0.52	0.24	0.49
10	64.95	7.42	12.49	14.49		0.18		

C2. Geopolymer with Si:Al = 1.25, Na:Al = 0.6

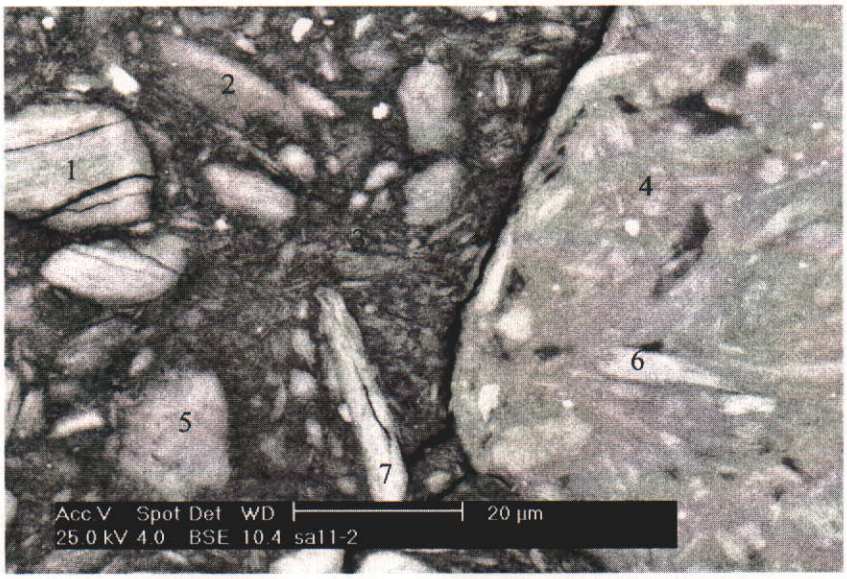

Figure C2. SEM image of geopolymer with Si:Al = 1.25, Na:Al = 0.6.

Table C2. EDS Results from the spots shown in figure C2. Results in an atomic percent and normalised to 100%. EDS was performed at 25 kV.

Spectrum	O	Na	Al	Si	K	Ca	Ti	Fe
1	64.86	2.87	14.69	17.37				0.21
2	62.50	4.24	14.34	18.49		0.15		0.29
3	56.25	6.83	14.17	21.45		0.71	0.21	0.39
4	64.84	5.34	12.47	17.04				0.32
5	66.01	2.46	14.19	16.6				0.73
6	64.83	4.71	12.92	17.24				0.31
7	65.25	3.62	13.59	17.25		0.12		0.17

C3. Geopolymer with Si:Al = 1.5, Na:Al = 0.6

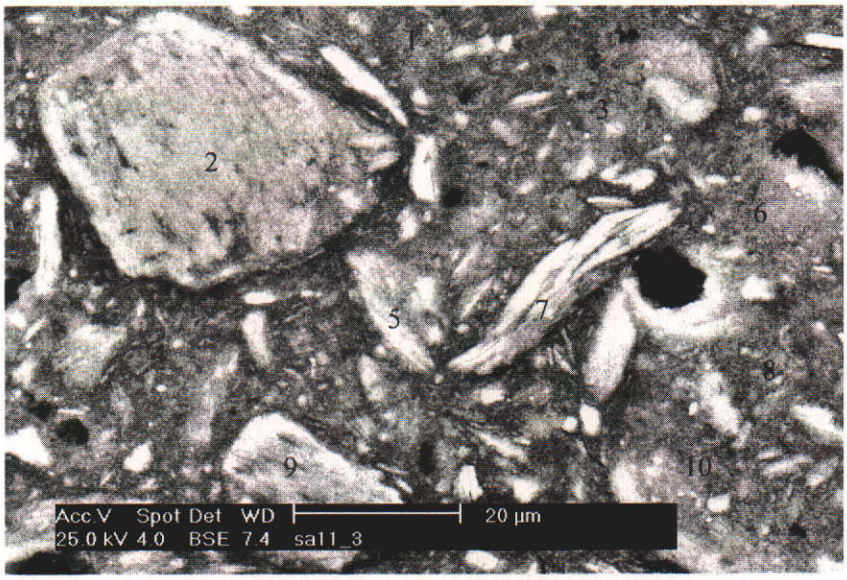

Figure C3. SEM image of geopolymer with Si:Al = 1.50, Na:Al = 0.6.

Table C3. EDS Results from the spots shown in figure C3. Results in an atomic percent and normalised to 100%. EDS was performed at 25 kV.

Spectrum	O	Na	Al	Si	K	Ca	Ti	Fe
1	70.60	4.80	8.33	15.93		0.33		
2	67.70	2.15	13.47	16.39				0.29
3	68.51	4.00	10.94	16.02		0.35		0.18
4	70.83	5.06	8.61	15.10		0.42		
5	70.35	4.70	9.12	15.36		0.29		0.19
6	68.36	3.63	11.23	16.29		0.32	0.17	
7	69.13	2.74	11.82	15.94				0.37
8	69.33	4.77	9.18	16.12		0.61		
9	70.34	4.12	10.03	14.94		0.19	0.19	0.18
10	69.67	4.93	8.90	15.64		0.52		0.35

C4. Geopolymer with Si:Al = 1.04, Na:Al = 0.8

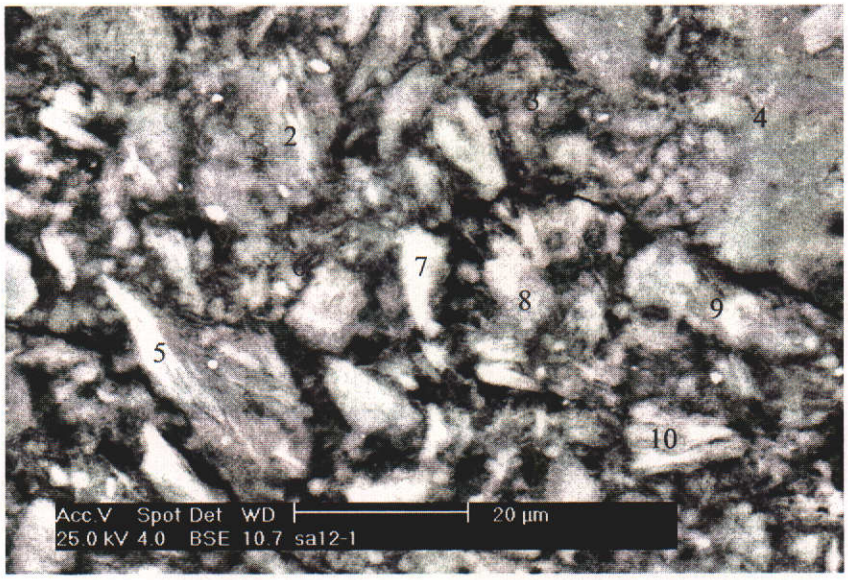

Figure C4. SEM image of geopolymer with Si:Al = 1.04, Na:Al = 0.8.

Table C4. EDS Results from the spots shown in figure C4. Results in an atomic percent and normalised to 100%. EDS was performed at 25 kV.

Spectrum	O	Na	Al	Si	K	Ca	Ti	Fe
1	63.56	6.93	12.14	16.85			0.16	0.36
2	64.43	5.23	13.13	16.70	0.23			0.28
3	63.86	6.2	11.88	17.48		0.29		0.29
4	64.68	5.07	12.97	16.73		0.16		0.39
5	63.02	3.93	14.19	17.85				1.02
6	64.48	6.50	12.21	16.18		0.17	0.22	0.24
7	65.65	5.17	12.62	15.68		0.25		0.64
8	64.46	7.26	11.78	15.80		0.22	0.16	0.32
9	65.08	6.10	12.29	15.90			0.28	0.35
10	65.98	5.62	12.56	15.36		0.20	0.10	0.17

C5. Geopolymer with Si:Al = 1.25, Na:Al = 0.8

Figure C5. SEM image of geopolymer with Si:Al = 1.25, Na:Al = 0.8.

Table C5. EDS Results from the spots shown in figure C5. Results in an atomic percent and normalised to 100%. EDS was performed at 25 kV.

Spectrum	O	Na	Al	Si	K	Ca	Ti	Fe
1	62.61	7.20	12.20	14.34		2.26	0.12	0.23
2	59.91	7.59	13.36	15.66		0.37	2.62	0.49
3	66.72	7.92	11.12	13.55	0.15	0.20		0.34
4	60.59	9.01	13.46	16.45		0.29		0.19
5	60.97	6.73	13.62	16.93	0.24	0.84	0.26	0.41
6	64.18	4.31	14.53	16.75				0.23
7	53.55	9.53	15.24	19.72		0.51	0.38	0.56
8	57.90	8.25	14.21	18.68	0.15	0.41	0.17	0.24
9	60.77	8.50	13.23	16.72		0.18	0.22	0.38
10	60.40	8.40	13.39	17.03		0.32		0.46

C6. Geopolymer with Si:Al = 1.04, Na:Al = 1.0

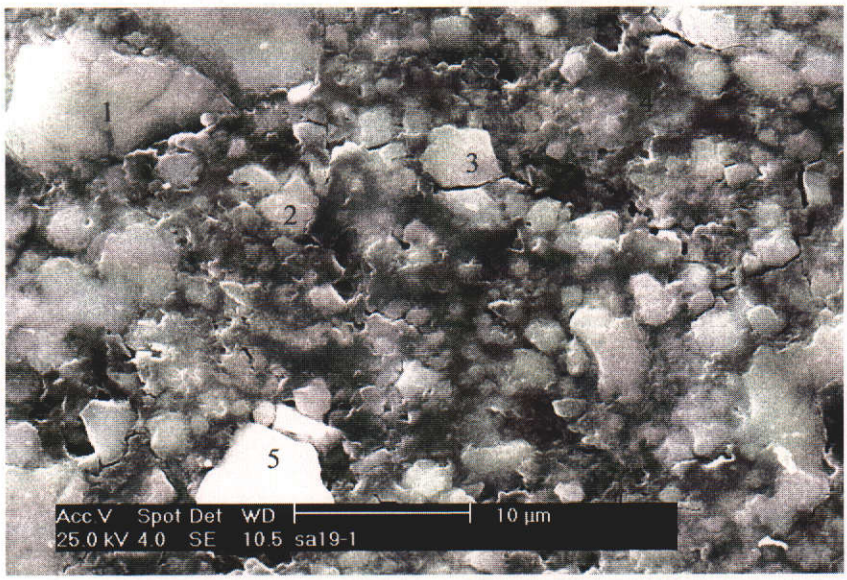

Figure C6. SEM image of geopolymer with Si:Al = 1.04, Na:Al = 1.0.

Table C5. EDS Results from the spots shown in figure C5. Results in an atomic percent and normalised to 100%. EDS was performed at 25 kV.

Spectrum	O	Na	Al	Si	K	Ca	Ti	Fe
1	51.61	8.86	16.59	21.05		0.54	0.49	0.86
2	50.97	8.26	17.24	21.59	0.37	0.86		0.71
3	47.18	8.93	18.38	23.75		0.91		0.85
4	39.70	10.50	19.58	27.78				1.45
5	54.52	2.13	2.92	40.43				

C7. Geopolymer with Si:Al = 1.25, Na:Al = 1.0.

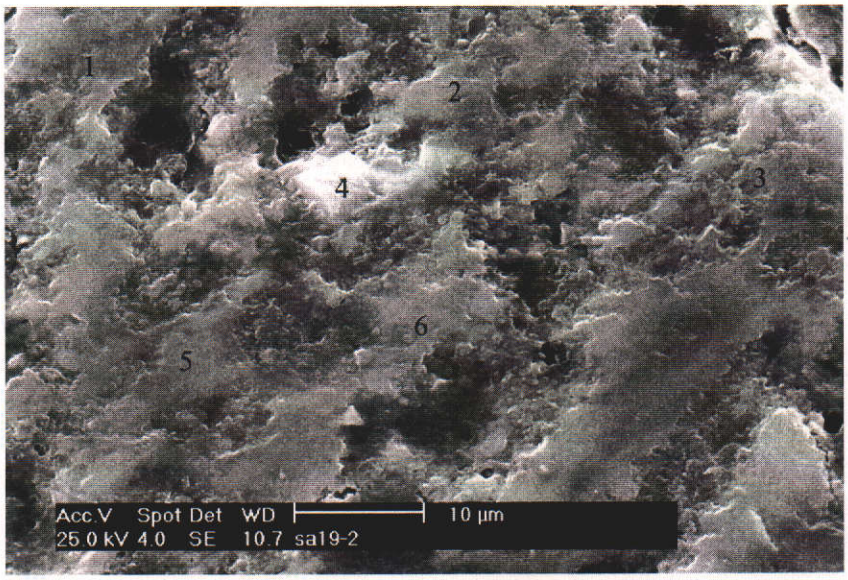

Figure C7. SEM image of geopolymer with Si:Al = 1.25, Na:Al = 1.0.

Table C7. EDS Results from the spots shown in figure C7. Results in an atomic percent and normalised to 100%. EDS was performed at 25 kV.

Spectrum	O	Na	Al	Si	K	Ca	Ti	Fe
1	64.53	6.59	11.65	16.75		16.75		0.35
2	65.25	7.10	11.33	15.78		15.78	0.18	0.23
3	64.04	8.15	11.67	15.86		15.86	0.10	0.17
4	68.80	2.13	1.61	27.46		27.46		
5	62.40	7.95	12.05	16.67		16.67	0.25	0.48
6	65.29	7.77	11.07	15.20		15.20		0.24

C8. Geopolymer with Si:Al = 1.50, Na:Al = 1.0

Figure C8. SEM image of geopolymer with Si:Al = 1.50, Na:Al = 1.0.

Table C8. EDS Results from the spots shown in figure C8. Results in an atomic percent and normalised to 100%. EDS was performed at 25 kV.

Spectrum	O	Na	Al	Si	K	Ca	Ti	Fe
1	65.67	9.31	8.99	15.55			0.22	0.26
2	66.44	6.87	9.69	16.65			0.12	0.23
3	68.22	7.03	9.36	15.15		0.09		0.15
4	67.66	7.10	9.28	15.46		0.12	0.18	0.20
5	67.48	7.19	9.32	15.74	0.11			0.15
6	67.71	6.83	9.23	15.67		0.18	0.12	0.25
7	68.73	6.86	8.96	15.22				0.22

C9. Geopolymer with Si:Al = 1.75, Na:Al = 1.0

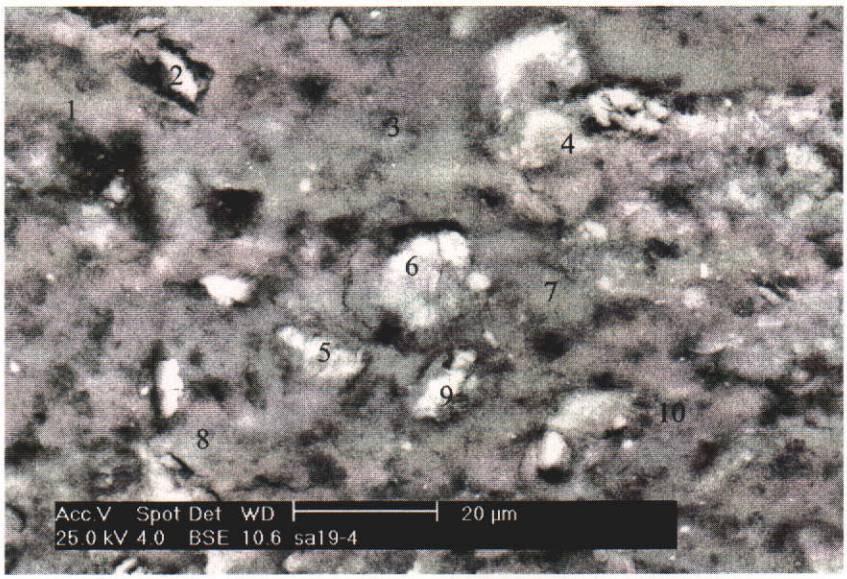

Figure C9. SEM image of geopolymer with Si:Al = 1.75, Na:Al = 1.0.

Table C9. EDS Results from the spots shown in figure C9. Results in an atomic percent and normalised to 100%. EDS was performed at 25 kV.

Spectrum	O	Na	Al	Si	K	Ca	Ti	Fe
1	67.92	6.31	8.31	16.47		0.18	0.6	0.21
2	67.72	4.75	10.63	16.71				0.18
3	65.63	6.44	9.25	18.00	0.14	0.19	0.16	0.19
4	65.37	2.90	12.97	18.22			0.37	0.18
5	65.81	4.30	11.95	17.74				0.2
6	66.09	3.74	11.94	17.72				0.51
7	66.47	6.29	8.88	17.6		0.25	0.26	0.24
8	62.85	7.12	9.99	19.12		0.54		0.38
9	67.13	3.59	12.57	16.49	0.11			0.11
10	65.26	6.59	9.08	18.64		0.23		0.19

C10. Geopolymer with Si:Al = 2.0, Na:Al = 1.0

Figure C10. SEM image of geopolymer with Si:Al = 2.0, Na:Al = 1.0.

Table C10. EDS Results from the spots shown in figure C10. Results in an atomic percent and normalised to 100%. EDS was performed at 25 kV.

Spectrum	O	Na	Al	Si	K	Ca	Ti	Fe
1	66.81	3.96	11.25	17.71				0.27
2	64.89	6.78	8.14	19.83		0.16		0.21
3	65.78	2.87	12.13	18.97				0.26
4	65.48	3.78	12.07	18.23				0.44
5	63.98	5.94	7.27	22.60				0.21
6	66.83	2.38	12.56	17.62	0.14		0.28	0.20
7	65.19	6.32	8.44	19.67		0.16		0.22
8	65.17	6.90	8.16	19.62				0.14
9	65.53	6.79	8.26	19.26			0.16	
10	64.51	6.67	8.39	20.25				0.18